Springer Theses

Recognizing Outstanding Ph.D. Research

For further volumes:
http://www.springer.com/series/8790

Aims and Scope

The series "Springer Theses" brings together a selection of the very best Ph.D. theses from around the world and across the physical sciences. Nominated and endorsed by two recognized specialists, each published volume has been selected for its scientific excellence and the high impact of its contents for the pertinent field of research. For greater accessibility to non-specialists, the published versions include an extended introduction, as well as a foreword by the student's supervisor explaining the special relevance of the work for the field. As a whole, the series will provide a valuable resource both for newcomers to the research fields described, and for other scientists seeking detailed background information on special questions. Finally, it provides an accredited documentation of the valuable contributions made by today's younger generation of scientists.

Theses are accepted into the series by invited nomination only and must fulfill all of the following criteria

- They must be written in good English.
- The topic should fall within the confines of Chemistry, Physics, Earth Sciences and related interdisciplinary fields such as Materials, Nanoscience, Chemical Engineering, Complex Systems and Biophysics.
- The work reported in the thesis must represent a significant scientific advance.
- If the thesis includes previously published material, permission to reproduce this must be gained from the respective copyright holder.
- They must have been examined and passed during the 12 months prior to nomination.
- Each thesis should include a foreword by the supervisor outlining the significance of its content.
- The theses should have a clearly defined structure including an introduction accessible to scientists not expert in that particular field.

Benni Thiebes

Landslide Analysis and Early Warning Systems

Local and Regional Case Study in the Swabian Alb, Germany

Doctoral Thesis accepted by
The University of Vienna, Austria

Springer

Author
Dr. Benni Thiebes
Department of Geography and Regional Research
University of Vienna
Universitaetsstrasse 7
1010 Vienna
Austria

Supervisor
Prof. Dr. Thomas Glade
Department of Geography and Regional Research
University of Vienna
Universitaetsstrasse 7
1010 Vienna
Austria

ISSN 2190-5053
ISBN 978-3-642-27525-8
DOI 10.1007/978-3-642-27526-5
Springer Heidelberg New York Dordrecht London

e-ISSN 2190-5061
e-ISBN 978-3-642-27526-5

Library of Congress Control Number: 2011945689

Printed on acid-free paper

Springer is part of Springer Science+Business Media (www.springer.com)

Parts of this thesis have been published in the following book chapters and articles:

Mayer J, Glade T, Thiebes B, Bell R (2010) Integrative Frühwarnsysteme. In: Bell R, Glade T, Greiving S, Mayer J, Pohl J (eds) *Integrative Frühwarnsysteme für gravitative Massenbewegungen (ILEWS)—Monitoring, Modellierung, Implementierung*, pp 17–31.

Bell R, Greiving S, Pohl J, Röhrs M, Glade T, Thiebes B, Mayer J (2010) Untersuchungsgebiete. In: Bell R, Glade T, Greiving S, Mayer J, Pohl J (eds) *Integrative Frühwarnsysteme für gravitative Massenbewegungen (ILEWS)—Monitoring, Modellierung, Implementierung*, pp 32–45.

Bell R, Wiebe H, Krummel H, Camek T, Becker R, Öhl S, Aslan AM, Burghaus S, Li L, Schauerte W, Kuhlmann H, Thiebes B (2010) Monitoring. In: Bell R, Glade T, Greiving S, Mayer J, Pohl J (eds) *Integrative Frühwarnsysteme für gravitative Massenbewegungen (ILEWS)—Monitoring, Modellierung, Implementierung*, pp 62–129.

Thiebes B, Bell R, Glade T, Aslan AM, Schauerte W, Kuhlmann H (2010) Frühwarnmodellierung. In: Bell R, Glade T, Greiving S, Mayer J, Pohl J (eds) Integrative Frühwarnsysteme für gravitative Massenbewegungen (ILEWS)—*Monitoring, Modellierung, Implementierung*, pp 130–154.

Bell R, Mayer J, Pohl J, Greiving S, Paulsen H, Röhrs M, Jäger S, Wiebe H, Thiebes B (2010) Erfahrungen aus dem integrativen Projekt. In: Bell R, Glade T, Greiving S, Mayer J, Pohl J (eds) *Integrative Frühwarnsysteme für gravitative Massenbewegungen (ILEWS)—Monitoring, Modellierung, Implementierung*, pp 231–237.

Bell R, Mayer J, Pohl J, Greiving S, Paulsen H, Röhrs M, Jäger S, Wiebe H, Thiebes B, Aslan AM (2010) Transferierbarkeit des integrativen Frühwarnsystems. In: Bell R, Glade T, Greiving S, Mayer J, Pohl J (eds) *Integrative Frühwarnsysteme für gravitative Massenbewegungen (ILEWS)—Monitoring, Modellierung, Implementierung*, pp 238–243.

Bell R, Becker R, Burghaus S, Dix A, Flex F, Glade T, Greiving S, Greve K, Jäger S, Janik M, Kuhlmann H, Krummel H, Lang A, Li L, Mayer C, Mayer J, Padberg A, Paulsen H, Pohl J, Röhrs M, Schauerte W, Thiebes B, Wiebe H (2009) ILEWS—Integrative landslides early warning systems. In: Stroink L (ed) *Geotechnologien Science Report* (conference proceeding), early warning systems in Earth management, No 13, Technical University Munich, Germany, pp 16–32.

Bell R, Glade T, Thiebes B, Jäger S, Krummel H, Janik M Holland R (2009) Modelling and web processing of early warning. In: Malet J-P, Remaître A,

Bogaard T (eds) *Landslide processes—from geomorphic mapping to dynamic modelling* (conference proceeding), CERG Editions, Strasbourg, France, pp 249–252.

Bell R, Thiebes B, Glade T, Becker R, Kuhlmann H, Schauerte W, Burghaus S, Krummel H, Janik M, Paulsen H (2008) The technical concept within the integrative landslide early warning systems (ILEWS) project. *10th international symposium on landslides and engineered slopes* (conference proceeding). Xi'an, China, pp 293–298.

I dedicate this work to my family

Supervisor's Foreword

Landslide early warning systems are most important throughout the world. These systems are always installed when the socio-economic consequences have either been experienced or are expected to be significant. Commonly, landslide early warning systems are based on either spatial warnings with respect to triggers, and herein specifically to hydro-meteorological events, or on locally installed monitoring devices. In most cases, these systems focus on the technical aspects of early warning—and do not take into consideration the whole chain of early warning including monitoring, analysis, establishing alert thresholds, issuing warnings and up to the societal responses including responsibilities, management options and decision making.

In this research, both local and regional early warning systems are investigated and potential applications are given. Specific research questions included the topic on how slope hydrology contributes to the reactivation of landslide movements and how physically-based slope stability models can be applied in local landslide early warning. On the regional scale, the research focused on the question if landslide triggering rainfall thresholds are applicable to regional early warning. All these questions are explored in a case study in the Swabian Alb, Germany. Innovative concepts and solutions are suggested, in particular the online web-based physically-based slope stability model has never been developed and installed. However, also the continuous monitoring of geoelectric profiles to determine the spatiotemporal water percolation, the data transfer in the field using wireless network technology or the development, implementation and application of a web-based online landslide early warning deserves wide international attention.

I am confident, that numerous of the explored research topics are of highest interest and relevance to the landslide community as well as to the stakeholders having to deal with the landslide problems. The knowledge and conceptual ideas of landslide early warning systems enhanced significantly by this research work.

Vienna, November 2011 Prof. Dr. Thomas Glade

Preface

Recent landslide events demonstrate the need to improve landslide forecasting and early warning capabilities in order to reduce related risks and protect human lives. In this thesis, local and regional investigations were carried out to analyse landslide characteristics in the Swabian Alb region, and to develop prototypic landslide early warning systems.

In the local study area, an extensive hydrological and slope movement monitoring system was installed on a seasonally reactivated landslide body located in Lichtenstein-Unterhausen. Monitoring data was analysed to assess the influence of rainfall and snow-melt on groundwater conditions, and the initiation of slope movements. The coupled hydrology-slope stability model CHASM was applied to detect areas most prone to slope failures, and to simulate slope stability using a variety of input data. Subsequently, CHASM was refined and two web-based applications were developed: a technical early warning system to constantly simulate slope stability integrating rainfall measurements, hydrological monitoring data and weather forecasts; and a decision-support system allowing for quick calculation of stability for freely selectable slope profiles.

On the regional scale, available landslide inventory data were analysed for their use in evaluation of rainfall thresholds proposed in other studies. Adequate landslide events were selected and their triggering rainfall and snow-melting conditions were compared to intensity-duration and cumulative thresholds. Based on the results, a regional landslide early warning system was developed and implemented as a web-based application.

Both, the local and the regional landslide early warning systems are part of a holistic and integrative early warning chain developed by the ILEWS project, and could easily be transferred to other landslide prone areas.

Acknowledgments

First of all I want to thank my supervisor Prof. Dr. Thomas Glade, who encouraged me to write a Ph.D. thesis and who kindly offered me the chance to work in his new working group established at the University of Vienna. Thank you for your support and guidance! I would like to thank my colleague and friend Dr. Rainer Bell for the great cooperation over the last few years; it has always been a great pleasure to work with you, and our discussions have helped immensely to improve my thesis.

I am grateful to the entire ENGAGE working group at the Institute of Geography and Regional Research in Vienna for comments and discussion. My special thanks go out to my office colleagues. Your support and friendship helped me a lot on my way. I also would like to thank the entire ILEWS project. These have been exciting and challenging years and I enjoyed working with you very much. Thank you for the wonderful colleagueship. I would especially like to thank Stefan, Raik and Bernd from the company Geomer for great cooperation in creating the technical early warning systems.

For help with bureaucracy and organisation I want to acknowledge the support technical staff at the institute, especially Helmut Slawik and Rudi Voit. Laboratory analysis of soil samples could not have been carried out without the kind help of Christa Hermann and Robert Petizka. I would also like to thank all the helping hands during field work, in particular Berndl Groiss. Another person acknowledged here is Mr. Siegler; without his appreciation of our work the entire project would not have been possible. Furthermore, the local administration of Lichtenstein-Unterhausen was very supportive which is highly acknowledged.

Many thanks to Malcolm Anderson and Liz Holcombe from the University of Bristol for providing the CHASM software and the helpful tips on how to use it most effectively. Significant rainfall data was kindly provided by Prof. Dr. Clemens Simmer (Uni Bonn), Dr. Armin Mathes (Uni Bonn), Dr. Antje Claussnitzer (Uni Berlin) and Walter Koelschtzky (DWD). Additional data was kindly provided by the LUBW and LGL. Many thanks also to Jean-Christophe Kohn for the landslide inventory data. The financial support granted by the

German Ministry of Education and Research (BMBF) and the Geotechnologien Consortium is highly acknowledged.

For proof-reading of this thesis, I am grateful towards Rainer, Emma, Ronny, Catrin, Helene and Melanie. I want to express my deepest thanks to all my friends in Vienna. Thank you for the great times!

Last but not least, thank you fide for your love and support over the past challenging years. I think now there are some new adventures waiting for us!

To all of you and to all the people I might have forgotten to mention, thank you!

Contents

Acronyms

ALS	Airborne laser scanning
AMSL	Above mean sea level
BOTDR	Brillouin optical time-domain reflectometry
CAD	Computer aided design
CHASM	Combined hydrology and stability model
DOGAMI	Oregon department of geology and mineral industry
DSM	Digital surface model
DTM	Digital terrain model
DWD	Deutscher wetterdienst
FLaIR	Forecasting of landslides induced by rainfall
FoS	Factor of safety
FVA	Forstliche versuchs- und forschungsanstalt
GEO	Geotechnical engineering office
GIS	Geographic information system
GPR	Ground penetrating radar
GPS	Global positioning system
ILEWS	Integrative landslide early warning systems
(D)InSAR	(Differential) Interferential synthetic aperture radar
KOSTRA	Koordinierte Starkniederschlags-Regionalisierungs-Auswertungen
LGL	Landesamt für Geoinformation und Landentwicklung Baden-Württemberg
LGRB	Landesamt für Geologie, Rohstoffe und Bergbau Baden-Württemberg
LiDAR	Light detection and ranging
LUBW	Landesanstalt für Messung, Umwelt und Naturschutz Baden-Württemberg
LV BW	Landesvermessungsamt Baden-Württemberg
NOAA	National oceanic and atmospheric administration
ODF	Oregon department of forestry

ODOT	Oregon department of transportation
OEM	Oregon emergency management
SAR	Synthetic aperture radar
TDR	Time domain reflectometry
TIN	Triangulated irregular network
TLS	Terrestrial laser scanning
UM BW	Umweltministerium Baden-Württemberg
USGS	United States geological survey
WPS	Web-processing service

Symbols

m	Mass
g	Gravity
τ	Shear stress
β	Slope angle
c	Cohesion with respect effective normal stress
c'_{max}	Maximum effective cohesion
c'_{min}	Minimum effective cohesion
u	Pore water pressure
σ	Total normal stress
σ'	Effective stress ($\sigma - u$)
φ'	Effective angle of internal friction
φ'_{max}	Maximum effective internal angle of friction
φ'_{min}	Minimum effective internal angle of friction
W	Weight of the material (γ * V)
B	Angle of shear surface
$\wedge$	Reciprocal velocity (1/v)
v	Velocity
t	Time
H	Slope height
α	Slope angle
C	Slope convergence/divergence
w, b, d	Mesh resolution
t	Iteration period
x/y	Coordinates of shear surface search
p	Rainfall intensity
K_{sat}	Hydraulic conductivity
Ψ	Initial surface suction
wt	Initial water table height

θ_{sat}	Saturated moisture content
$\Psi - \theta$	Suction-moisture curve
γ_{unsat}	Unsaturated bulk density
γ_{sat}	Saturated bulk density
c'	Effective cohesion
I	Rainfall intensity
D	Rainfall duration

Chapter 1
Introduction

1.1 Problem Statement

On the 8th of August 2010 a devastating mudslide occurred in the Chinese Gansu Province after floods and torrential rainfall (BBC News 2010). Several landslides were triggered by intense rainfall, transported gravel and mud into the river and built up a temporary dam. The lake behind the dam grew to a length of 3 km before it finally broke (BBC News 2010). An estimated 1.8 million cubic meter of debris swept through three towns in Zhouqu county destroying homes and burying the area in mud several meters deep (Bloomberg 2010). More than 10,000 soldiers and rescue staff members were send to aid (Boston Globe 2010). According to Xinhua News Agency (2010) the total death toll of the mudslide event was 1,471 with several hundreds of people still missing.

Disasters like the one in Gansu Province demonstrate the devastating effects that mass movements can have on society. However, the impacts of landslides are often underestimated and damage is not accounted for. This is also due to the effect that landslides are rarely sole events but mostly accompanying other natural hazards like storms with intense rainfall or earthquakes which trigger mass movements. In these cases damage is often accounted for the triggering event and not for the landslides. An illustrative example is the 2008 Wenchuan earthquake in Sichuan Province, China, which caused approximately 70,000 fatalities and was one of the worst natural disasters in this year (MunichRe 2010b). Remarkably, 20,000 of those fatalities resulted from more than 15,000 mass movements (Yin et al. 2009). A closer look at the 50 worst disasters in 2008 listed by MunichRe (2010a) reveals that landslides processes are in no case the sole cause of a disasters but accompany 20% of all catastrophic events.

Turner (1996) estimated the annual losses and fatalities from landslides and other mass movement processes in the USA to US $ 1–2 billion and 25–50 deaths. Krauter (1992) calculates the yearly economic damage for Germany alone as US $ 150 million. According to Yin (2009) the damage due to landslides cause

B. Thiebes, *Landslide Analysis and Early Warning Systems*, Springer Theses,
DOI: 10.1007/978-3-642-27526-5_1, © Springer-Verlag Berlin Heidelberg 2012

property losses in China which add up to 10 billion RMB (approximately 1 billion EUR) and a death toll of 700–900 each year.

The occurrence of landslides is not only bound to the high-alpine regions of the world but also many lower mountain ranges suffer from landslides if steep terrain, unfavourable geological conditions and triggering factors are present (Dikau and Schmidt 2004; Van Den Eeckhaut et al. 2007). Moreover, it is not only fast landslide processes that pose a problem for societies. Generally, slow moving landslides do not require emergency actions like for example evacuation, but continuous displacement calls for ongoing maintenance, adopted building codes and stabilisation works. Further on, even if observed displacement rates are small there is still the imminent danger of sudden acceleration which could lead to a catastrophic slope failure.

In general, there are four approaches to counter risk from landslides (Schuster and Highland 2007): (1) avoiding hazards and restricting development in landslide-prone areas; (2) securing potentially dangerous slopes by grading and excavation, and enforcement of adopted building codes; (3) protecting existing infrastructure by technical mitigation measures; and (4) implementing monitoring and early warning systems. Avoidance is in most cases the easiest and cheapest option to prevent damage from mass movements, but is not possible in the case of already existing infrastructure. Excavation and protective measures are expensive and may not be technically or economically possible or feasible for large landslides. Badoux et al. (2009) note that communities threatened by mass movements are often also subject to other natural hazards like floods which also need sufficient protective measures. Landslide monitoring and early warning systems have been developed in many parts of the world but most cases consist of prototypic approaches as damage due to landslides is often perceived as private losses which led to poor investments by the public sector and only minor standardisation (Baum and Godt 2009).

Despite the fact, that predictive landslide simulation models are very common methods to forecast future behaviour, or as Janbu (1996) notes, one of the three general tasks of slope stability practice along with investigative subsurface exploration and experience driven safety assessment, this is only poorly reflected in recent landslide early warning systems. Most technical systems rely on monitoring of external and internal factors and utilise thresholds which are either based on expert experience or model results. However, only very few examples exist where full advantage is taken of the predictive possibilities of landslide simulation and prediction models.

Moreover, many regions which exhibit occurrences of mass movements are not equipped with early warning systems, even though the necessary input data like quantitative rainfall forecasts are widely available, and the technical advances in computers and internet make basic warning service feasible.

1.2 Research Objectives

This thesis deals with landslide analysis and the subsequent development and implementation of local and regional early warning systems in the Swabian Alb. The local study area in Lichtenstein-Unterhausen comprises a extremely-slow

reactivated deep-seated landslide, for which a relation between hydrological processes and displacement reactivation was assumed in earlier studies (Kruse 2006; Bell 2007); however, no detailed monitoring data was available to verify this. In this study, it is tried to get deeper insights into slope hydrology by the installation of an extensive monitoring system. The application of landslide simulation software aims to simulate and forecast landslide behaviour and consequently allow for early warning. On a regional scale, it is tried to assess the potential for regional landslide early warning based on rainfall thresholds.

In the following, research questions and the respective objectives for local and regional investigations are summarised.

Local scale
How does slope hydrology contribute to the reactivation of landslide movements?

- Installation of a monitoring system for hydrology and slope movement
- Combined analysis of hydrological and slope movement monitoring data

How can physically-based slope stability models be applied in landslide early warning?

- Simulation of landslide behaviour with a physically-based slope stability model
- Development and implementation of a decision-support and early warning model

Regional scale
Are landslide triggering rainfall thresholds applicable to regional early warning in the Swabian Alb?

- Analysis of available landslide inventories
- Comparison of landslide events to landslide triggering rainfall thresholds
- Implementation of a regional landslide early warning model

The work presented is embedded into the ILEWS project in which a holistic approach is pursuit. The overall goal is to develop and implement an integrative landslide early warning system starting with the sensor in the field and ending with user-optimised warning messages and action advice. Additional information on the ILEWS project is provided in Sect. 2.5. More detailed description of the results can be found in Chap. 7 and in Bell et al. (2010).

1.3 Thesis Outline

The thesis is designed to provide a systematic understanding of landslide early warning. Chapter 2 summarises the principles of landslides and the instability of slopes. Further on, a comprehensive review on landslide detection and monitoring methods, as well as applied landslide early warning systems is presented. The study area Swabian Alb, its natural characteristics and previous research on

landslides are presented in Chap. 3. The data used within this study and their properties are described in Chap. 4. Chapter 5 presents the methodologies applied in this study. Therein, the procedure of data analysis and the subsequent development and implementation of early warning models on the local and regional scale are explained. Results of this research are illustrated in Chap. 6. Due to great diversity of the results, initial discussions are already provided in the respective subchapters. Some additional information on the incorporation of the developed early warning models into an integrative early warning system is given in Chap. 7. Chapter 8 contains a concluding discussion in which the research questions are addressed. Perspectives for further research and possible advancement of the developed early warning models, as well as the potential for a transfer to other study areas are summarized in Chap. 9. The thesis ends with a summary given in Chap. 10. Some additional information are provided in the appendix.

References

Badoux A, Graf C, Rhyner J, Kuntner R, McArdell BW (2009) A debris-flow alarm system for the Alpine Illgraben catchment: design and performance. Nat Hazards 49(3):517–539

Baum RL, Godt JW (2009) Early warning of rainfall-induced shallow landslides and debris flows in the USA. Landslides 7(3):259–272

BBC News (2010) BBC news—dozens killed in landslides in China's Gansu province

Bell R (2007) Lokale und regionale Gefahren- und Risikoanalyse gravitativer Massenbewegungen an der Schwäbischen Alb. University of Bonn, Germany

Bell R, Mayer J, Pohl J, Greiving S, Glade T (eds) (2010) Integrative Frühwarnsysteme für Gravitative Massenbewegungen (ILEWS)—Monitoring. Klartext Modellierung, Implementierung, Essen

Bloomberg (2010) Death toll of China's Gansu mudslide may rise, disaster relief chief says—Bloomberg [Online]. Available at: http://www.bloomberg.com/news/2010-08-11/death-toll-of-china-s-gansu-mudslide-may-rise-disaster-relief-chief-says.html. Accessed 23 Sep 2010

Boston Globe (2010) Landslides strike Zhouqu County, China—the big picture—Boston.com [Online]. Available at: http://www.boston.com/bigpicture/2010/08/landslides_strike_zhouqu_count.html. Accessed 23 Sep 2010

Dikau R, Schmidt J (2004) Modeling historical climate variability and slope stability. Geomorphology 60(3–4):433–447 Accessed 4 Oct 2010

Janbu N (1996) Slope stability evaluations in engineering practice. In: Senneset K (ed) Landslides. Seventh international symposium on landslides. Trondheim, Norway, Balkema, Rotterdam, pp 17–34

Krauter E (1992) Hangrutschungen—ein Umweltproblem. In: Ingenieurvermessung. XI. Internationaler Kurs für Ingenieurvermessung. Zürich, Switzerland, pp 1–12

Kruse JE (2006) Untergrunderkundung und Monitoring von gravitativen Massenbewegungen mit Gleichstromgeoelektrik und Radiomagnetotellurik. University of Bonn, Germany

MunichRe (2010a) Great natural catastrophes 1950–2009. MunichRe NatCatService

MunichRe (2010b) Topics geo-natural catastrophes 2008. MunichRe NatCatService

Schuster RL, Highland LM (2007) The third Hans Cloos lecture. Urban landslides: socioeconomic impacts and overview of mitigative strategies. Bull Eng Geol Environ 66(1):1–27

Turner AK (1996) Socioeconomic significance of landslides. In: Turner AK, Schuster RL (eds) Landslides: investigation and mitigation (special report). Transportation Research Board, pp 12–35

Van Den Eeckhaut M, Poesen J, Dewitte O, Demoulin A, Bo De H, Vanmaercke-Gottigny MC (2007) Reactivation of old landslides: lessons learned from a case-study in the Flemish Ardennes (Belgium). Soil Use Manag 23(2):200–211

Xinhua News Agency (2010) Death toll from NW China mudslides rises to 1,471; 294 still missing [Online]. Available at: http://news.xinhuanet.com/english2010/china/2010-09/02/c_13474994.htm. Accessed 23 Sep 2010

Yin Y (2009) Landslide mitigation strategy and implementation in China. In: Sassa K, Canuti P (eds) Landslides-disaster risk reduction. Springer, Berlin Germany, pp 482–484

Yin Y, Wang F, Sun P (2009) Landslide hazards triggered by the 2008 Wenchuan earthquake, Sichuan, China. Landslides 6(2):139–152

Chapter 2
Theoretical Background

2.1 Landslide Processes

2.1.1 Definitions and Classifications

A very basic but widely accepted and used definition for landslide was established by Cruden (1991) and Cruden and Varnes (1996) and defines a landslide as "*the movement of a mass of rock, debris or earth down a slope*". However, the term can be confusing if the parts of the word are considered. Cruden and Varnes (1996) note that it describes all kinds of mass movements and is not limited to granular soil (as land might suggest) or a sliding movement process. The term landslide is well established in the research community and will therefore also be used in this thesis as an overarching term referring to all movement types and material properties. Further on, the term mass movement is used interchangeably with landslide.

The most common classification for landslides is based on material properties and process types (Table 2.1). Besides the main types of movement processes there is one complex class which contains movement processes with two or more different processes acting together along with downslope movement of the landslide mass.

A second widely acknowledged classification of landslides is based on movement velocity (Cruden and Varnes 1996), which ranges from extremely fast to extremely slow (Table 2.2). Moreover, landslides can be distinguished regarding their state of activity. Cruden and Varnes (1996) established eight groups, namely active, suspended, reactivated, inactive, dormant, abandoned, stabilized and relict mass movements. Further on, single, multiple and successive movements are distinguished. Other differentiations can be based on, for example, the water content of involved materials (Cruden and Varnes 1996).

The term creep, which was used to describe continuous and imperceptible slow movements of the ground (e.g., Terzaghi 1950, 1961) was omitted due to various definitions and interpretations. Cruden and Varnes (1996) propose to not use the

B. Thiebes, *Landslide Analysis and Early Warning Systems*, Springer Theses,
DOI: 10.1007/978-3-642-27526-5_2, © Springer-Verlag Berlin Heidelberg 2012

Table 2.1 Mass movement classification based on process type and material (Cruden and Varnes 1996; Dikau et al. 1996)

Process type		Type of material		
		Rock	Debris	Earth
Topple		Rock topple	Debris topple	Earth topple
Fall		Rock fall	Debris fall	Earth fall
Slide	Translational	Rock slide	Debris slide	Earth slide
	Rotational			
Flow		Rock flow	Debris flow	Earth flow
Spread		Rock spread	Debris spread	Earth spread
Complex		e.g., rock avalanche	e.g., flow slide	e.g., slump-earthflow

Table 2.2 Mass movement classification based on velocity of displacement (Australian Geomechanics Society 2002 after Cruden and Varnes 1996)

Class	Description	Typical velocity	Expected damages and population reaction
1	Extremely rapid	>5 m/sec	Disaster of major violence; buildings destroyed by impact of displaced material; many deaths; escape unlikely
2	Very rapid	>3 m/min	Some lives lost; velocity too great to permit all persons to escape
3	Rapid	>1.8 m/h	Escape evacuation possible; structures destroyed
4	Moderate	>13 m/month	Some temporary and insensitive structures can be temporarily maintained
5	Slow	>1.6 m/year	Remedial constructions can be undertaken during movement; insensitive structures can be maintained with frequent maintenance work if total movement is not large during a particular acceleration phase
6	Very slow	>15 mm/year	Some permanent structures undamaged by movement
7	Extremely slow	<15 mm/year	Imperceptible without instruments; construction possible with precautions

term creep and to replace it with the appropriate descriptors of their classification. However, the term creep may still be applied in a simple mechanical way to describe deformation that continues under constant stress (Cruden and Varnes 1996; Terzaghi et al. 1996).

2.1.2 Principles of Slope Stability

Landslides are a sign of slope instability which is defined as the "*propensity for a slope to undergo morphologically and structurally disruptive landslide processes*" (Glade and Crozier 2005b, p. 43). Glade and Crozier (2005b) visualise slope stability as a dynamic spectrum (Fig. 2.1). On one end, there is a stable slope

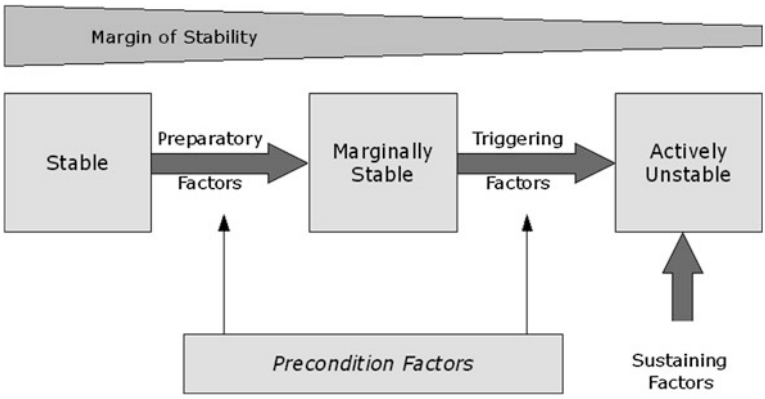

Fig. 2.1 Stability states and destabilising factors (after Crozier 1989; Glade and Crozier 2005b)

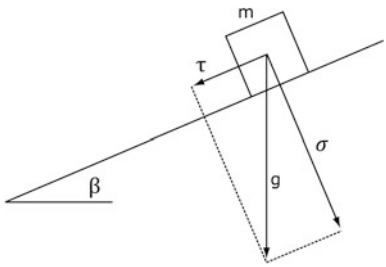

Fig. 2.2 Stress vectors within a slope (after Ahnert 2003)

which is subject to preparatory factors which convert the slope to a marginally stable state. At this point, dynamic triggering factors exceeding certain thresholds can alter the state of the slope to actively unstable which leads to continuous or intermittent movement. During the described transformation from stable to actively unstable slope conditions the margin of stability is continuously decreasing. Precondition or pre-disposing factors are thought as static factors that influence the margin of stability and allow dynamic factors. Preparatory factors are dynamic which change the stability margin over time without initiating slope failure. Typical examples for preparatory factors are weathering, deforestation, tectonic uplift or environmental change. Triggering factors actively shift the state of stability to an unstable condition. Common triggers for landslides are intense rainstorms, seismic shaking or slope undercutting (Glade and Crozier 2005b). Inherent in this concept is the theory of extrinsic and intrinsic thresholds (Schumm 1979). Sustaining factors control the behaviour of the actively unstable state and therefore dictate the duration of movement, form and run out distance of slope failure.

A similar concept is described by Leroueil (2004) who distinguishes four stages of landslide movement: a pre-failure stage including deformation process leading

to failure, the onset of failure characterized by the formation of a continuous shear surface through the entire soil mass, a post-failure stage starting from failure until the mass stops, and a reactivation phase when sliding occurs on a pre-existing shear surface.

Stresses acting within a slope can be illustrated by vectors (Fig. 2.2), where a mass (m) is subject to acceleration of gravity (g) which can be differentiated into a downslope component (τ) and a force acting perpendicular to slope surface (σ). Distribution of stresses depends on slope angle (β) and downslope force increases with higher slope angles.

The potentially destructive effects of slope instability led to early research in prediction of slope failures. Calculation of slope stability dates back to Coulomb (1776) and his work on stability of retaining walls and determination of the most likely shear surfaces with a wedge method, which are still valuable today (Ahnert 2003). Another important advance of slope stability calculation was made by Terzaghi (1925), who established the fundamental concept of effective stress. Therein, the effects of pore water pressure in slope stability are acknowledged. Pore water pressure is the pressure of water in the voids between solid particles of the soil (Casagli et al. 1999). As water cannot sustain shear stress, only the skeleton of solid particles at their contact points can, slope stability decreases with a higher pore water pressure. The stability of slope can be assessed by calculating the Factor of Safety (FoS), which is the ratio of driving and resisting forces within a slope (Crozier 1989):

$$FoS = \frac{shear\ strength}{shear\ stress} = \frac{c + (\sigma - u)\tan\varphi'}{\tau} = c + \left(\frac{\frac{W}{A}\cos B - u\tan\varphi'}{\frac{W}{A}\sin B}\right) \quad (2.1)$$

where

	τ	=	shear stress
	c	=	cohesion with respect effective normal stress
	σ	=	total normal stress
	u	=	pore water pressure
	σ	=	total normal stress
	σ'	=	$\sigma - u$
	φ'	=	angle of internal friction with respect to effective normal stress
	W	=	weight of the material; that is γ = bulk density multiplied by V
	B	=	angle of shear surface

In theory, a slope is stable as long as the FoS is greater than one and slope movement commences if the FoS is 1.0 or smaller. However, Glade and Crozier (2005b) stress the point that the FoS is only a relative measure of stability as it gives no information on the magnitude of destabilisation that is needed until slope failure occurs. Moreover, some authors describe the onset of movements even before the FoS becomes lower than 1.0 (Petley et al. 2002, 2005b, c) which they

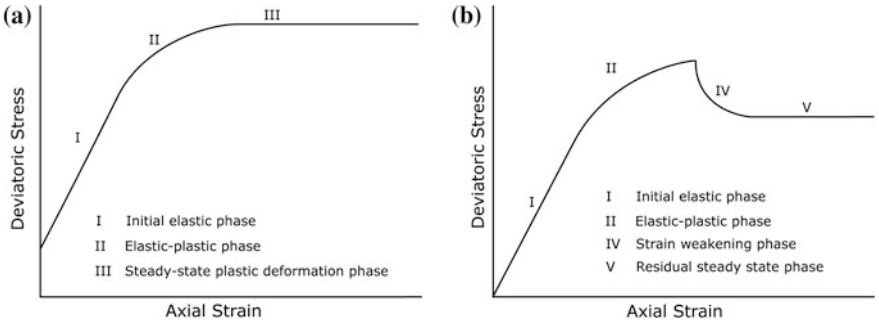

Fig. 2.3 Idealized stress–strain curves for brittle (**a**) and ductile (**b**) deformation (Petley and Allison 1997)

attribute to the development of micro-cracks which progressively form a complete shear surface.

The Mohr-Coulomb equation given above is the basis for limit equilibrium analyses and has been widely applied to calculate the stability of potential slip surfaces. However, in this form it applies to drained failures, where no excess pore pressure is generated during shearing. However, undrained conditions can involve the development of significant excess pore pressure and cause liquefaction, like in the case of low density, fine-grained, saturated soils (e.g., quick-clay) (Bovis 2004). Moreover, shear strength of rock is largely affected by geological bedding and stratification, the properties of involved materials, and the morphology and complex interactions along discontinuities like cracks and joints during shearing (Prinz and Strauß 2006).

Examination of shear parameters and the stress–strain behaviour of materials are primarily experimental, because of the technical difficulties to study the processes in nature. Shear parameters are generally determined in the laboratory by undertaking uniaxial or triaxial shear tests (Wu 1996). A relatively undisturbed soil sample is placed into a shear box and stress is applied until the material fails. Applied loads and subsequent strains are recorded. Idealized stress-strain curves for brittle and ductile failure regimes are given in Fig. 2.3.

Most geological materials and engineering soils can display both brittle and ductile failure modes depending on their confining pressure (Cristescu 1989). However, brittle failure is dominant at low confining pressures representative for shallow failures (Petley and Allison 1997). As stress or load is applied soil materials generally display an initial phase of elastic and recoverable strain. The applied stress is loaded on the grain-bonds within the material which deform but do not break. An increase of stress causes the material's weakest bonds to break and an elastic–plastic phase can be observed which is characterised by increasing strain rates. As more and more bonds break, peak strength is exceeded and shear strength is significantly reduced. The shear surface fully develops in the strain weakening phase in which shear strength steadily reduces to a residual value.

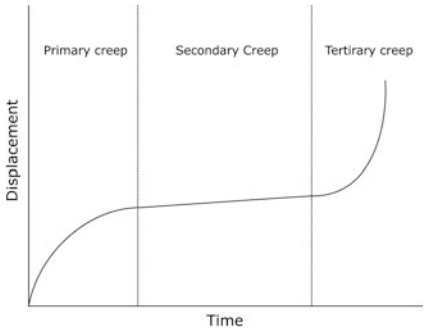

Fig. 2.4 Idealized strain curves for the three stages of creep (after Petley et al. 2008)

During this phase shear zone contraction or dilation may occur which affects pore pressures and therefore strain rates (Iverson 2005). Thereafter, strains primarily occur as displacement along the shear surface.

Ductile behaviour can be observed at high effective stresses prevalent in very deep-seated landslides and in materials with little or no inter-particle bonding like weathered clays (Petley and Allison 1997). The initial phases of elastic and elastic–plastic strain are similar to the brittle failure regime. However, due to the high confining stress no shear surface can develop. Increased load results in purely plastic deformation at constant stresses as the material reforms. Moreover, a transition between ductile and brittle behaviour was observed by Petley and Allison (1997) at very high pressures, which are present in very deep-seated landslides.

As mentioned above the term creep does not describe a certain landslide type but refers to the mechanical behaviour of geological materials to constant stress. Some creep takes place in almost all steep earth and rock slopes and may concentrate along pre-existing or potential slip surfaces or distribute evenly across the landslide profile (Fang 1990). Creep movements in landslide can be continuous or may vary seasonally with hydrological conditions (Petley and Allison 1997). Creep can be maintained for long periods, however, creep gradually decreases shear strength and a slope's margin of stability (Fang 1990) and eventually the slope may fail.

A widely acknowledged concept of creep distinguishes between the phases of creep movement (Okamoto et al. 2004; Petley et al. 2005b, c, 2008). When constant stress lower than peak strength is applied to a soil mass subsequent strains are time-dependant and can be visualised as displacement versus time plot (Fig. 2.4). In the primary creep stage strains are initially high due to elastic deformation but decrease with time. During the secondary creep phase the material suffers diffuse damage but strains are generally slow or almost steady (Okamoto et al. 2004), or may even stop altogether (Petley et al. 2008). When diffuse micro-cracks start to interact to form a shear surface, the critical point into the tertiary phase is reached (Reches and Lockner 1994; Main 2000). This phase is characterized by a rapid acceleration of displacement until final failure.

The increasing displacement rates associated with rupture growth and micro-crack interactions during the tertiary creep stage have been subject to research for

a long time in order to predict final failure (Saito 1965; Bjerrum 1967; Saito 1969; Voight 1989; Fukuzono 1990) and volcanic eruptions (Voight 1988). The concept is frequently termed progressive failure analysis and usually employs examination of movement patterns by plotting movement in $\Lambda - t$ space, where $\Lambda = 1/v$ (v is velocity and t is time) (Petley et al. 2002).

It has been observed in many shear experiments and real landslides that linear trends in acceleration occur if failure is imminent. This was the case for first-time failures and for failures in which brittle behaviour was dominant in the basal shear zone. However, reactivated landslides and failures where ductile deformation is dominant display asymptotic trend in $\Lambda - t$ space which has been observed in several landslides, e.g., in Italy, New Zealand, California, Japan and the UK (Petley et al. 2002; Carey et al. 2007).

The potential for prediction and early warning of landslide failures has been showed by several case studies. Kilburn and Petley (2003) and Petley and Petley (2006) analysed displacement data from the famous Vaiont reservoir rockslide in Northern Italy, which caused a flood wave that killed around 2000 people in 1963. The result of the analysis was that at 30 days before final failure a transition to a linear trend in movement acceleration was visible and final failure was therefore predictable. Moreover, in the case of the artificial landslide experiment at the Selford slide (Selford Cutting Slope Experiment) final failure could be predicted 50 days in advance (Petley et al. 2002).

Despite its potential, progressive failure analysis has not been integrated into an early warning system yet. A test application to the slope under investigation in this study failed because of slow movement rates and insufficient acceleration phases (Thiebes et al. 2010).

Slow active landslides are widespread in many geomorphological contexts and materials, and can display steady movements over long periods of time, often along completely developed shear zones (Picarelli and Russo 2004). Changes in displacement rates of slow or extremely slow landslides is in many cases related to varying pore water pressures (Leroueil 2004) and movements can be continuous or intermittent. Especially in landslides of moderate depths pore pressures primarily drive displacements, while in deeper landslides creep and erosion, as other phenomena of stress relief, are the main influential factors (Picarelli and Russo 2004). While pore pressures control landslide movement on short and medium time-scales, erosion, weathering, progressive weakening due to strain are influencing on a larger time-scale (Picarelli and Russo 2004).

Seasonal variations of pore pressures close to surface are not necessarily reflected by deeper layers if materials are rich in clay (Leroueil 2004). Moreover, clays also influence infiltration and slope stability by their swelling and drying behaviour. Very dry clay may develop cracks which allow for quick percolation into depth along preferential flow paths. Preferential flow paths can have a positive effect on slope stability by allowing quick drainage of potentially unstable areas, but can also have an adverse effect by contributing additional water to areas where shear surfaces may develop (Uchida et al. 2001). Infiltration in unsaturated materials is a complex process (Leroueil 2004) and strongly

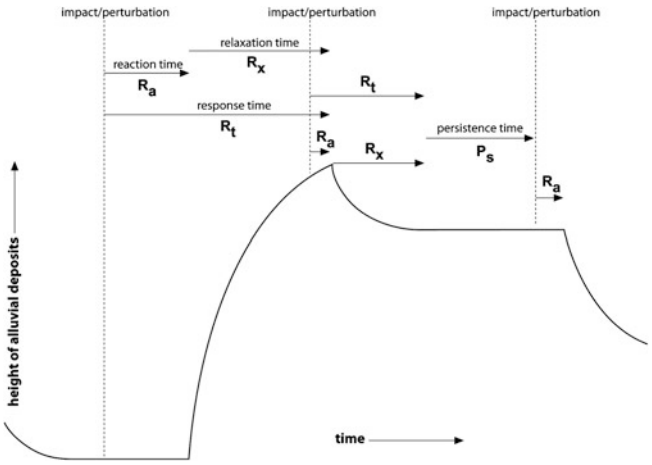

Fig. 2.5 Effects of external perturbations on a geomorphological system (after Bull 1991)

dependant on initial conditions such as antecedent soil water conditions, degree of saturation, pore pressure field, hydraulic conductivity and amount of water required for saturation. As a result, it is extremely difficult to relate rainfall conditions to pore water pressures and to the occurrence of landslides. Moreover, transferring one threshold to an entire landslide is extremely difficult (Picarelli and Russo 2004).

Slow moving slopes often interact with infrastructure as movement rates are generally low, so that permanent avoidance or evacuation is not necessary (Picarelli and Russo 2004). Still there is a danger of acceleration, as many catastrophic slope failures are preceded by long periods of slow creep (Petley and Allison 1997). Geotechnical stabilisation on the other hand would in many cases be too expensive or non-effective.

2.1.3 Systems Theory Considerations

Landslides are the results of complex interaction within the natural environment, and if human intervention is present, the interactions and feedbacks become even more complex (Bell 2007). A widely acknowledged approach in physical geography was laid out by Chorley and Kennedy (1971) and aimed to provide a theoretical framework which allows for analysis of form, material, and processes, as well as interaction and feedbacks (Dikau 2005). Moreover, the conceptual approach comprises variable space and time-scales of system evolution and external system control, as well as early approaches to non-linear system response (Slaymaker 1991). Four types of systems can be distinguished: morphological systems, cascading systems, process-response systems and control systems (Chorley and Kennedy 1971). Following Glade

(1997) morphological systems can be used to describe the interaction between landslide-prone regions and potentially landslide-triggering rainfall events. Bell (2007) notes, that if research focuses on, for example, landsliding of periglacial strata cascading systems may be more appropriate. Research on factors controlling landslide behaviour can benefit from a process-response system point of view, while control systems are important in geomorphological hazard research where direct human manipulation of material parameters aims to decrease risks (Dikau 2005). The effects of external perturbation on a geomorphological system are exemplified for alluvial deposits in Fig. 2.5.

Reaction time is important within landslide research and illustrates how fast a slope reacts to external perturbation, such as rainfall, snow melting or earthquakes. Relaxation time describes the velocity of movement until all energy is depleted and may range from slow creeping movements to sudden failure. During persistence time a slope is stable until further perturbation impacts trigger further system response.

The classic systems approach by Chorley and Kennedy (1971) is essentially based on the concept of thermo-dynamic equilibrium which means that a system will return to a steady-state by negative feeback effects after external perturbations (Dikau 2006). In recent years, however, research shifted more to the analyis of non-equilibrium systems and non-linear relationships (Dikau 2005). Nonlinearity implies that "*outputs or responses of a system are not proportional to inputs or forcings across the entire range of the latter*" (Phillips 2006, p. 110), which is dominant in geomorphic systems. Sources of nonlinearity in nature are summarized by Phillips (2003) and comprise thresholds, storage effects, saturation and depletion, self-reinforcing positive feedbacks, self-limitation, competitive relationships, multiple modes of adjustment, self-organisation and hysteresis. Nonlinear system analysis provides, according to Dearing (2004), new insights and aids to understand system behaviour. Novel concepts developed in this area of research include complexity, self-organisation, deterministic chaos and are reviewed and discussed in detail elsewhere (Phillips 1992a, b, 2003; Richards 2002; Favis-Mortlock and De Boer 2003; Dikau 2006).

There is no single, precise definition of complexity (Favis-Mortlock and De Boer 2003). However, complexity may loosely be delineated as the fact that systems cannot be described by the properties of its parts (Gallagher and Appenzeller 1999). According to Phillips (1992a) complexity can arise from cumulative process-response mechanisms which are far too numerous to be accounted for in individual details, or due to multiple controls over process–response relationships that operate over a range of spatial and temporal scales.

The studies of Bak et al. (1988) on sand-pile models provided some insights on complex systems. In these models grains were dropped onto a sand pyramid. This resulted either in no changes, or in landslides of various sizes. The landslide sizes were found to follow a power-law distribution, but it was, however, not possible to predict the size of the next landslide. The fact that the system drove itself to a critical state was referred to as self-organised criticality, a concept that has been

been widely applied to geomorphological processes (Favis-Mortlock 1998; Phillips et al. 1999; Fonstad and Marcus 2003; Favis-Mortlock 2004).

Deterministic chaos describes the sensitivity of a system to initial conditions and small perturbations, whereby initial differences or effects of minor perturbations tend to persist and grow over time and may have unpredictable and apparently random consequences (Phillips 2003). The basic principle of deterministic chaos has popularly been described by the butterfly effect, where the flap of butterfly wings in one part of the world may cause a hurricane at another place. Chaotic behavior was first described by Lorenz (1963) who simulated meteorological processes and found drastically differing model results depending on minimal changes to small decimal places. Prediction of model states was only possible for short time-spans.

These aspects of nonlinearity have drastic consequences for the predictability of natural phenomena such as landslides (Von Elverfeldt 2010). However, this does not mean that prediction is not possible as Dikau (2005) notes: nonlinear systems can be simple and predictable, but this is not necessarily the case for complex systems. Most landslide simulation programs, such as the models presented in Sect 1.3, cannot accomodate nonlinear system behaviour, such as complexity, self-organisation or deterministic chaos. Some landslide related research projects, however, exploited for example self-organised criticality for prediction of landslides and forest fires (Turcotte and Malamud 2004), characterisation of landslide evolution (Huang et al. 2008) or analyis of triggering conditions (Stähli and Bartelt 2007). Moreover cellular automata have widely been used to simulate self-organising complex systems in geomorphic research (Smith 1991; Avolio et al. 2000; D'Ambrosio et al. 2003; Iovine et al. 2005; Fonstad 2006).

2.1.4 Landslide Triggering

Even though landslides can occur without the impact of external factors, generally their occurrence is connected to some kind of triggering event. Many factors can act as triggers for landslides. The most common natural triggers are either related to geological events, such as seismic shaking due to volcanic eruptions or earthquakes, or hydrological events such as intense rainfall, rapid snow melt or water level changes in rivers or lakes at the foot of slopes (Wieczorek 1996). Moreover, human interaction in the form of loading or slope cutting can trigger landslide events. The most important trigger, however, in both shallow and deep-seated landslides is intense rainfall (Crosta and Frattini 2008). Infiltrating rain percolates within the soil, thus increasing pore pressures at hydrologic boundaries, which subsequently decreases shear strength. Positive pore water pressure may occur directly caused by infiltration and percolation (saturation from above), or may be the result of perched groundwater tables (saturation from below) (Terlien 1998). Important factors determining the evolution of saturation are soil permeability and

stratification, preferential flow paths, as well as mechanical characteristics (Berardi et al. 2005).

In the following landslide triggering, the efforts made to predict landslide occurrences with respect to hydrological thresholds will briefly be described. More general reviews on landslide triggering (Wieczorek 1996; Schuster and Wieczorek 2002; Wieczorek and Glade 2005) and rainfall threshold determination (Terlien 1998; Wieczorek and Guzzetti 1999; Polemio and Petrucci 2000; Aleotti 2004; Wieczorek and Glade 2005; Guzzetti et al. 2007; Guzzetti et al. 2008; Brunetti et al. 2010) can be found in the respective literature.

Prediction of landslide triggering thresholds is one of the key issues in landslide research (Berardi et al. 2005), and established thresholds have an important role in early warning (Terlien 1998). One of the most influential works in this field was published by Caine (1980) who worked on landslide triggering rainfall thresholds based on rainfall intensity and duration analyses. Since then, many research projects worked on defining rainfall thresholds which trigger landslides. Triggering thresholds are predominantly expressed as rainfall intensity and duration, or cumulative and antecedent rainfall, and can be defined as the line fitting the minimum intensity of rainfall associated with the occurrence of landslide in different areas (Caine 1980). However, Terlien (1998) notes that rainfall events that did not cause landslides also should be recognised. Therefore, minimum and maximum thresholds should be acquired, where rainstorms below the minimum threshold never cause landslides, and storms above maximum threshold always lead to landslides (Glade 1998; Crozier 1999). Between these thresholds landslides may occur under certain conditions.

Landslide triggering thresholds differ from one region to another based on hydro-climatological and geophysical properties, such as regional and local rainfall characteristics and patterns, slope morphometry, soil characteristics, lithology, morphology, climate and geological history (Crosta 1998). Further on, landslide triggering thresholds may also vary with time (Crozier 1999), for example due to seasonal changes of vegetation (Wieczorek and Glade 2005). Moreover, Crozier and Preston (1999) note that after movements have occurred resistance to further events may occur, if for example., all material for future debris flows has already been transported.

Guzzetti et al. (2007) distinguish between rainfall thresholds on three spatial scales, for example, global, regional and local scale. A further distinction between landslide triggering rainfall thresholds can be made between statistical or empirical and deterministic thresholds (Guzzetti et al. 2007). When sufficient data on landslide occurrences and rainfall conditions are available, thresholds can be determined in a statistical way. With limited data deterministic models have to be applied to predict landslide behaviour under certain hydrological conditions (Terlien 1998).

Most case studies of rainfall thresholds relate to shallow landslides or debris flows. Triggering of these landslide types generally refers to short and intense rain storms, while the occurrence of deep-seated landslides is more affected by long-term rainfall trends (Terranova et al. 2007). Deep-seated landslides share a more

complex hydrology compared to shallow landslides and simple correlations between rainfall and deep-seated landslide triggering cannot be determined (Terlien 1998). To establish triggering rainfall thresholds in deep-seated landslides it is necessary to include rainfall, water infiltration and percolation, generally by means of modelling subsurface hydrology (Ekanayake and Phillips 1999), and to determine the location of shear surface, as well as the hydrological triggering mechanism (Terlien 1998).

The intensity-duration method first proposed by Caine (1980) has been applied in many other studies (Pasuto and Silvano 1998; Jakob et al. 2006; Matsushi and Matsukura 2007; Crosta and Frattini 2008; Guzzetti et al. 2008; Capparelli et al. 2009; Saito et al. 2010). Rainfall duration generally refers to periods between 10 min and 35 days (Guzzetti et al. 2008), but some authors extended the time span analysed to several months (Terranova et al. 2007; Marques et al. 2008). Long-term rainfall trends have been integrated into threshold determination by relating intensity and duration of rainstorms to mean annual precipitation (MAP) (Giannecchini 2006; Giannecchini et al. 2007; Guzzetti et al. 2007; Sengupta et al. 2009).

Crozier and Eyles (1980) developed the Antecedent Daily Rainfall method to determine rainfall thresholds based on antecedent and daily rainfall. A decay factor derived from discharge hydrographs controls the influence of antecedent soil water. Several other case studies applied this methodology as well (e.g., Crozier 1999; Glade 2000; Glade et al. 2000; Strenger 2009).

Although rain is regarded as the prime factor of landslides triggering, infiltration and the development of positive pore water pressures at potential shear surfaces are initiating landslide processes (Reichenbach et al. 1998; Ekanayake and Phillips 1999; Leroueil 2004). There is, however, no established standard procedure for calculation of pore pressure in relation to rainfall events (Persson et al. 2007). A common procedure is to calculate pore pressures conditions required for slope instability which are then compared to observed pore pressures and checked for reasonability. Based on multiple regression analysis of piezometric measurements Matsushi and Matsukura (2007) established rainfall intensity duration thresholds. Godt et al. (2006) applied a similar approach and derived rainfall thresholds by comparing rainfall data with measurements of volumetric water content. Other authors utilise models to predict pore pressure in response to rainfall events. Wilson (1989) presented a simple numerical model to investigate the build up of saturation and establish rainfall thresholds. The model represents soils as leaky barrels, where additional water is added at one rate, while water is lost by another rate. Wilson and Wieczorek (1995) combined the model with measurements of piezometric levels and data on antecedent rainfall to derive rainfall thresholds. A related approach has been performed by Terranova et al. (2007) who derive critical rainfall situation for landslide triggering based on modelled infiltration and comparison with piezometer data. Moreover, several other case studies also applied hydrological models to predict pore pressure evolution in response to rainfall events to establish landslide triggering rainfall

thresholds (Reid 1994; Crosta 1998; Terlien 1998; Ekanayake and Phillips 1999; Iverson 2000; Frattini et al. 2009).

Coupled hydrology and stability models have been widely applied to predict the effects of rain storms, and to define critical situations. Examples for local scale (Buma 2000; Brooks et al. 2004; Berardi et al. 2005; Pagano et al. 2008), and regional scale (Dhakal et al. 2002; Crosta and Frattini 2003) approaches can be found in the respective literature.

2.2 Landslide Investigation and Monitoring

The occurrence of landslides is sometimes surprising for humans as they seem to occur without previous warning signs. However, (Terzaghi 1950) noted that if a landslide comes as a surprise to eyewitnesses, it would be more accurate to say that the observers failed to detect the phenomena which preceded the slide. Therefore, dedicated landslide analyses and monitoring methods have to be applied to be able to recognise potential slope failures.

Many methodological approaches have been developed to reveal the occurrence of landslides in space and time, to investigate processes acting within mass movements and to monitor ground displacements. The wide range of possible methodological approaches for landslide research stretch from field or desk-based mapping, to measurements of surface and subsurface movement in field or by remotely acquired data sources, recordings of triggering factors like rainfall or hydrological parameters, and the use of simulation models.

Landslides can be assessed on various spatial scales (Glade and Crozier 2005a), but a general distinction between local and regional approaches can be made. The initial step of regional approaches is to define the spatial occurrence of landslides, commonly by preparing landslide inventories (Wieczorek et al. 2005). For local analyses Nakamura (2004) argues that one of the first steps to understand the landslides under investigation are field investigation s and boreholes to define the slip surface. Regarding rockslides, but also applicable to other landslide phenomena, Glawe and Lotter (1996) stated that when instabilities can be expected geotechnical investigation s, displacement monitoring and modelling techniques are generally applied. Following Cornforth and Mikkelsen (1996) ideal features of a landslide monitoring system are continuous measurements of pore water pressure in the shear zone by automated sensors in order to correlate these with rainfall data.

In the following a review of methods for landslide detection, surface and subsurface investigations and monitoring techniques is given. The aim of this chapter is not to provide a complete summary of all methods available for landslide research, but rather to give a comprehensive overview on the methods most used in research practice and to highlight their advantages and disadvantages for monitoring. More information on the methodological approaches to landslide investigation and monitoring methods can be found in the sources given or in the general

reviews (Franklin 1984; Keaton and DeGraff 1996; McGuffey et al. 1996; Mikkelsen 1996; Soeters and Van Westen 1996; Turner and McGuffey 1996; Olalla 2004; Van Westen 2007; Liu and Wang 2008). No self-contained review on existing monitoring systems will be given as many examples of monitoring systems are presented in the review on early warning systems (Sect 1.4). It is however important to mention that many landslide monitoring systems employ several different techniques, such as methods for measuring landslide movement and hydrology.

Regarding monitoring it should be made clear, that there is no obvious threshold that determines what time intervals between repeated measurements are necessary for it to be classed as monitoring. Olalla (2004) points out that monitoring can range from, for example, inclinometer measurements carried out once in a year, or automatic measurements in intervals of seconds. Therefore, every repeated measurement could be defined as monitoring. Automatic monitoring systems are however more convenient than manual measurements as they do not require humans to regularly go to study sites which may be remote or difficult to access. Another advantage of automated monitoring systems is the ability to control measures by time intervals, thresholds or user input. Besides this, questions of data storage, transmission and security arise with such automatic systems. Moreover, data should automatically be processed and checked to prevent inconsistencies (Olalla 2004). However, issues of managing automatic monitoring systems will not be discussed here.

2.2.1 Mapping and Inventory Approaches

A basic method to detect landslides in space and to prepare landslide inventories is geomorphological mapping in the field. Geomorphological mapping requires expert knowledge and experience of landslides and the study area. Results can vary drastically depending on the specialists who prepared the map, the knowledge on the study area and the processes present (Guzzetti et al. 2000; Ardizzone et al. 2002). Repeated mapping campaigns in the field without further measurements give rather qualitative information on how processes have evolved over time but are essential for process understanding. Important information could include cracks that open up due to ground displacements, or damage to existing infrastructure.

Landslide maps and inventories are frequently prepared based on the analysis of remote sensing data like stereographic aerial or space-borne images, and digital terrain models (DTM) from, for example, LiDAR (Light Detection And Ranging) data. General reviews on landslide mapping and inventories can be found in various literature sources (e.g., Soeters and Van Westen 1996; Malamud et al. 2004; Guzzetti et al. 2006; Van Westen 2007).

The use of aerial photography is well established in landslide research (Soeters and Van Westen 1996). Interpretation of aerial images is primarily qualitative;

however photogrammetric methods can be used to extract quantitative information. While qualitative interpretation is common, quantitative studies are more rare, probably due to limited availability of good quality photographs, adequately fixed control points and cost (Morgenstern and Martin 2008). However, several landslide related quantitative photogrammetric studies have been described (Maria et al. 2004; Mills et al. 2005; Hu et al. 2008; Liu and Wang 2008; Smith et al. 2009).

Medium resolution satellite imagery, such as LANDSAT, SPOT, ASTER, IRIS-D etc., is today used routinely to create landuse maps and inventories of landslides (Van Westen 2007). He also notes that Google Earth and other providers of high resolution satellite data greatly facilitate mapping by offering capabilities of creating polygons and exporting them to Geographic Information Systems (GIS). In several case studies landslide inventories were created based on satellite imagery (Mondini et al. 2009; Fiorucci et al. 2010; Santurri et al. 2010; Yang and Chen 2010) or Google Earth (Sato and Harp 2009; Chigira et al. 2010).

In recent years the interpretation of Airborne Laser Scanning (ALS) DTM data has been frequently applied for creation of landslide inventories (Van Westen 2007). By removing vegetation and other objects from the DTM, Digital Surface Models (DSM) can be created (Schulz 2004). This together with different modifiable angles of shading enable very detailed mapping of landslides and other geomorphological features (Haneberg 2004; Thiebes 2006). Examples of ALS-based landslide maps are provided by several authors (Chigira et al. 2004; Sekiguchi and Sato 2004; Ardizzone et al. 2007; Eeckhaut et al. 2007).

By using multi-temporal remote sensing data sets landslides can be dated, and activity and evolution quantitatively investigated. Examples for multi-temporal landslide inventories are provided by several authors (e.g., Cardinali et al. 2002; Dai and Lee 2003; Brennecke 2006; Imaizumi et al. 2008; Chiang and Chang 2009).

Several automatic landslide detection and mapping approaches have been developed and are comprehensively reviewed by Van Westen (2007). These approaches utilise DTM subtraction analysis or multi-spectral analysis of satellite imagery. Fairly recent applications of an automated landslide mapping system are presented by Tarantino et al. (2004) and Booth et al. (2009).

Another remote-sensing method for mapping landslides and for detection rates and extents of ground deformations is Synthetic Aperture Radar (SAR). SAR and the related methods of Interferometric SAR (InSAR), and their use for landslide research are extensively reviewed by Rosen et al. (2002), Froese et al. (2004) and Morgenstern and Martin (2008). SAR is based on microwave signals which are emitted by a satellite or airplane and the back-scattered signals, which represent distance measurements, are recorded. By processing two slightly offset images from the same flight paths InSAR images can be created which can be used to create pixel-based images which form a DTM. The benefits of this method are that radar measurements can be performed at almost every weather condition and at day and night. Furthermore, large areas can be analysed in a short period of time. Determination of displacements can be achieved by analysing images from different flights. To further increase the accuracy of displacement measurements Permanent or Persistent Scatterer Interferometric Synthetic Aperture Radar

(PS-InSAR) was introduced to landslide research (Morgenstern and Martin 2008). Permanently fixed ground-points, in many cases buildings or other constructions, are determined in multiple InSAR images and relative movements of these points can be measured. Best results, with accuracy of measurements in the sub-centimetre range, can be obtained for movements along the line of sight (Rosen et al. 2002; Luzi et al. 2005). Several case studies have been performed utilising satellite-based InSAR technology to detect and monitor ground movements (Colesanti and Wasowski 2004; Ferretti et al. 2005; Meisina et al. 2006; Calcaterra et al. 2008; Vallone et al. 2008; Yin et al. 2010b).

Also historic data such as newspaper articles, eyewitness records, road construction office reports, city archives, old photographs and many more sources can be utilised for landslide mapping. In many cases spatial and temporal information regarding landslide occurrence can be found which are exceptionally useful for understanding the magnitude-frequency characteristics of mass movements (Glade 2001). Examples of landslide inventories based on historic data can be found in, for example, Calcaterra et al. (2003), Carrara et al. (2003), Tropeano and Turconi (2004) and Kohn (2006).

2.2.2 Displacement Measurements

Many field methods exist to measure ground displacements due to landslide movements. A simple but convenient field method is the use of quadrilaterals (Keaton and DeGraff 1996) which consist of four stakes that are fixed inside and outside the landslide body. Distances between the stakes can then be measured manually by tape. Quadrilaterals have been applied within several research applications (Baum and Fleming 1991; Bogaard 2000; Giraud 2002; Fernandez Merodo et al. 2004; Keaton and Gailing 2004).

Standard theodolite geodetic measurements are frequently applied to measure and monitor ground displacements (Reyes and Fernandez 1996; Walstra et al. 2004; Wasowski et al. 2004; Burghaus et al. 2009) and available automatic systems have often been used (Oboni 2005; Heincke et al. 2010). However, theodolite measurements require pre-defined ground points or prisms. Manual measurements are also cost and time intensive.

The Global Positioning System (GPS) is another method that is often used to monitor landslide movements (Bonnard et al. 1996; Wasowski et al. 2004; Mills et al. 2005; Webster and Dias 2006; Yin et al. 2008; Zhang et al. 2008). Precision of measurements is in the range of cm to mm. However, the applicability of this method depends on the visibility of satellites which may not be the case in narrow valleys, densely forested areas or on steep cliffs.

The methods described above are applicable to measure and monitor ground deformation at the surface. In order to understand landslide behaviour subsurface measurements are necessary. Basic approaches are pits and trenches which can be used to investigate e.g., the depth of a landslide and the position of shear surfaces

or to take undisturbed material samples. Generally, pits and trenches can only be established on shallow movements. Examples are given by Bromhead et al. (2000), Clark et al. (2000) and Topal and Akin (2008). Penetration tests can also be performed to investigate stiffness of subsurface materials. More often, drillings are utilised to investigate landslide bodies. An ample variety of drilling devices is available on the market from simple handheld sounding poles to truck-sized rotary drilling machines. Besides the advantage of directly probing the landslide body and having the opportunity to take core samples, sensors can be applied within the boreholes to further investigate subsurface movement and hydrological processes.

In many cases inclinometers are used to determine subsurface movement of landslides (Borgatti et al. 2006; Bonnard et al. 2008; Bressani et al. 2008; Jongmans et al. 2008; Mihalinec and Ortolan 2008; Yin et al. 2008). General remarks on the use of inclinometers for landslides research are provided by Stark and Choi (2008). Inclinometers consist of a flexible drilled pipe which is placed vertically into a drilled borehole. A high-precision probe is inserted and the inclination of the pipe is measured in even distances, for example, every e.g., 50 cm. Repeated measurements give information of the occurred inclination changes in downslope and horizontal direction for the entire length of the pipe. However, it is important that inclinometers are fixed into the stable ground beneath the shear surface to prevent data bias. Automated inclinometer s are commercially available and usually consist of several inclinometer probes connected to each other to a chain, or automatic systems where the probe automatically moves within the pipe. Within landslide monitoring the use of automatic inclinometer and inclinometer chains has been described by for example, Lollino et al. (2002) and Olalla (2004), Volkmann and Schubert (2005) and Wienhöfer and Lindenmaier (2009). However, inclinometers can only withstand a certain amount of displacement before pipes break. This makes them especially applicable for monitoring of slow moving landslides, but also for detection of shear processes in faster moving landslides.

A more recent method for the detection of subsurface movements and deformation is Time Domain Reflectometry (TDR). Barendse and Machan (2009) note that inclinometers can determine the magnitude and direction of ground deformation, while TDR is primarily used to identify depths of active shearing. The TDR method has initially been developed in the 1950s for locating discontinuities in power transmission cables (Pasuto et al. 2000). TDR has first been used within landslide research in the 1980s in underground coal mine monitoring (Olalla 2004) and since then applied to several other case studies (Pasuto et al. 2000; Barendse and Machan 2009; Singer et al. 2009; Yin et al. 2010a). The principle of TDR is based on an electric signal sent through a coaxial cable. Shear movements deform the cable which creates a spike in cable signature and depth can be detected from the signal. Laboratory tests of TDR method for detection of shear processes have been performed by Baek et al. (2004) and Blackburn and Dowding (2004). Pasuto et al. (2000) compared TDR cables to inclinometer measurements and extensometers. Their result was that TDR cables are less sensitive to deformations but can withstand a larger displacement than usual inclinometers. The higher stability of

TDR cables make them a good choice for monitoring faster moving processes like the Gschliefgraben flowslide in Austria (Marschallinger et al. 2009).

Wire or rod extensometers are used to monitor the distance between two points and are frequently utilised in surface movement investigations (Furuya et al. 2000; Angerer et al. 2004; Barla et al. 2004; Willenberg et al. 2004; Wu et al. 2008). Extensometers are in most cases applied to investigate surface movements but can also be installed within boreholes (Bloyet et al. 1989; Krauter et al. 2007). Accuracy of extensometers depends on the length measured and usually is in the sub-mm range.

Tiltmeters are able to give high resolution information on inclination and have been applied to several landslide monitoring systems (Clark et al. 1996; Meidal and Moore 1996; Barton and McCosker 2000; Blikra 2008; García et al. 2010).

Crackmeters are used to monitor displacements in the sub-mm range at joints and cracks in rocks, buildings and other structures. The application of crackmeters has been described by several authors (e.g., Keaton and DeGraff 1996; Greif et al. 2004; Olalla 2004; Vlcko 2004; Moore et al. 2010).

The mentioned field based methods only give information on ground displacements for points or along lines. However, spatial methods are also available that give information on displacement for entire slopes.

In recent years many studies utilised Terrestrial Laser Scanning (TLS) for monitoring of geomorphological processes. The technique is similar to LiDAR, but ground-based. In contrast to LiDAR it is appropriate for steep cliffs and rock faces as the scanner can be placed in front of it. TLS scans are used to create three dimensional DTM which can further be analysed quantitatively within GIS or CAD environments to assess e.g., the volume of displaced material between measurements. Precision of TLS is heavily dependent on distance to the target and ranges from centimetres to mm, as well as environmental conditions such as rain or vegetation. General remarks on TLS and its usage for monitoring geomorphological processes are provided by Prokop and Panholzer (2009) and Schaefer and Inkpen (2010). Many case studies applied TLS for landslide monitoring (e.g., Mikoš et al. 2005; Rosser et al. 2005; Rosser and Petley 2008; Avian et al. 2009; Baldo et al. 2009; Oppikofer et al. 2009; Abellán et al. 2010).

SAR methods can also be applied in ground-based studies, which are frequently termed Slope Stability Radar (SSR) (Van Westen 2007). The major advantages of this method are that they provide high precision data in sub-millimetre range without being affected by weather conditions and without the need to install reflectors or ground marks. However, vegetation drastically decreases accuracy. Luzi et al. (2005) used a ground-based DinSAR system to monitor displacement on the Italian Tessina landslide and compared the measurements to regular theodolite surveys. Based on comparable displacement results by both methods they conclude that InSAR is also applicable for landslide early warning systems. Several other research projects installed SSR systems to monitor displacements of landslides (Canuti et al. 2002; Antonello et al. 2004; Casagali et al. 2004; Eberhardt et al. 2008; Bozzano et al. 2010; Casagli et al. 2010).

Another method that has increasingly been used in recent years is Brillouin Optical Time-Domain Reflectometry (BOTDR). These optical fibres can be used for measurement of ground deformations along profiles. The principle of this method is based on an interaction of pulsed beam and photons that are thermally excited within the light propagation medium (Wang et al. 2008a), which are affected by temperature and strains. Laboratory simulations to test the applicability of BOTDR (Dai et al. 2008; Wang et al. 2008a), as well as field applications (Higuchi et al. 2007; Dai et al. 2008; Shi et al. 2008a, b; Moore et al. 2010) have been described.

2.2.3 Hydrological Measurements

Given the great importance of rainfall and slope hydrology for landslide triggering, these factors are frequently analysed and monitored within landslide research. Climatic factors such as rain, snowfall, temperature and wind are usually measured at climate stations, which are commercially available or in many cases provided by meteorological agencies. Measurement of ground-water conditions such as pore pressures and soil water suction is usually accomplished by using piezometers and tensiometers. An overview on different types of these sensors can be found in Kneale (1987). Piezometers are probably the most common hydrological sensor utilised for landslide research (e.g., Wu et al. 2008; Yin et al. 2008; Calvello et al. 2008; Ching-Chuan et al. 2009; Yin et al. 2010a) and come as simple standpipe or more advanced vibrating wire piezometers. Piezometers measure the pressure of water in saturated soils and therefore give information on the height of the groundwater table within a soil. Tensiometers measure matrix potentials and are frequently utilised to assess the soil suction in the vadose zone (Li et al. 2004; Rinaldi et al. 2004; Montrasio and Valentino 2007; Greco et al. 2010). Piezometers and tensiometers are usually installed within boreholes or directly into the soil at trenches.

In recent years Time Domain Reflectometry (TDR) has also been applied to measure volumetric soil water contents. Greco et al. (2010) compared TDR sensors with tensiometers and concluded that TDR might be more useful for landslide monitoring and early warning since TDR measurements of soil water content change smoothly, while soil suction showed abrupt steep fronts. More examples of TDR application for assessing soil water are presented by e.g., Hennrich (2000), Tohari et al. (2004) and Kim (2008).

The chemical properties of ground and pore water have a widely acknowledged effect on shear strength and affect slope stability (Di Maio and Onorati 2000; Angeli et al. 2004) by for example, influencing the mechanical behaviour of clays (Leroueil 2004). However, monitoring of ground water composition is only rarely included in landslide monitoring systems (Sakai and Tarumi 2000; Montety et al. 2007; Sakai 2008).

2.2.4 Geophysical Measurements

Several methods from geophysics have been utilised for landslide research, mainly for prospection of landslide bodies and for investigation of hydrological processes acting within landslides. However, wider application of geophysics in landslide research have been hindered for two reasons (Jongmans and Garambois 2007): geophysical methods provide images of geophysical parameters which are not directly linked to geological parameters required by geotechnical engineers and geomorphologists; and the overestimation of the quality and reliability of results among some geophysicists. The main advantages of geophysical methods compared to standard geotechnical approaches are that they are non-invasive and can be applied to large areas for a low cost. However, the main disadvantages are the decrease of resolution with depth, the non-uniqueness of solutions for data inversion and interpretation, and the in-direct information (Jongmans and Garambois 2007). Generally, geophysical methods are used for prospection of landslide bodies, detection of discontinuities and shear surfaces, as well as for investigation of hydrological regimes. Measurements are usually short-term and only a few long-term monitoring exist (Supper and Römer 2003; Lebourg et al. 2005). Geophysical methods will only briefly be presented here, more detailed reviews on geophysical application are provided by many introductive textbooks (Telford et al. 1990; McGuffey et al. 1996; Parasnis 1997; Reynolds 1997; Kearey et al. 2002; Milsom 2003; Schrott et al. 2003; Knödel et al. 2005).

Seismic methods are based on the velocity measurements of seismic waves in subsurface materials. Generally, denser material causes faster wave propagation. At layer interfaces waves are partly reflected, but also partly transferred into depth due to refraction. In geomorphological applications seismic signal is usually induced by a sledge hammer that is pounded on a steel plate. Penetration depths of more than 30 m can be reached by more powerful sources e.g., drop weights or explosives) (Schrott and Sass 2008). Measurements are taken by geophones which are located at even distances along a profile. A number of different seismic techniques have been established, of which seismic reflection, seismic refraction and seismic tomography are the most common. Although seismic methods proved to be suitable for many geomorphological studies which require definition of subsurface properties (Hecht 2001), such as determination of active layer in permafrost or volumes of sediment bodies, problems may occur if low velocity layers are sandwiched in high velocity layers (Schrott and Sass 2008). Examples of dedicated landslide subsurface characterisation applying seismic methods are provided by several authors (Schmutz et al. 2000; Willenberg et al. 2002; Meric et al. 2004; Meric et al. 2005; Heincke et al. 2006, 2010).

A variation of seismic method is applied to record fracture signals produced by deformation within landslides, and to locate fracture both in space and time. These methods can be distinguished as micro-seismic, nano-seismic and passive seismic (Joswig 2008). Instead of creating a seismic signal by e.g., a sledge hammer, these methods use the acoustic signals emitted by deformation processes by “listening”

to ruptures. This method yields information on depth and mode of slope deformation (Bláha 1996). An increasing number of studies employ such approaches in laboratory tests (Dixon and Spriggs 2007; Ishida et al. 2010) and field applications (Merrien-Soukatchoff et al. 2005; Amitrano et al. 2007; Meric et al. 2007; Häge and Joswig 2009; Walter and Joswig 2009).

Ground penetrating radar (GPR) has increasingly been used in recent years in many geomorphological research projects to investigate subsurface (Sass and Krautblatter 2007; Gomez et al. 2009). Advantages of the method include high resolution and wide range of penetration depth (Jongmans and Garambois 2007). In landslide research, GPR is generally used to determine landslide boundaries and discontinuities, such as shear surfaces and cracks in rock, but GPR is also sensitive to groundwater. High-frequency electromagnetic waves are emitted by an antenna and wave propagation is determined by dielectric properties of the subsurface materials (Schrott and Sass 2008). Emitted pulses are reflected by inhomogeneities and received by a second antenna. The antennas are usually moved along a profile, and travel times of pulses are measured and subsequently inverted into 2D images. Penetration depth depends on material properties and frequencies used, but can be up to 60 m if conditions are favourable (Schrott and Sass 2008). Landslide related research applying GPR are provided by (Bichler et al. 2004; Avila-Olivera and Garduño-Monroy 2008; Sass et al. 2008; Willenberg et al. 2008; Pueyo-Anchuela et al. 2009). However, GPR is generally only applied for short-term measurement campaigns, and has not been employed in monitoring projects. Still, Roch et al. (2006) propose repeated GPR monitoring for rockfall monitoring.

Electrical resistivity and spontaneous potential are both geoelectrical methods. Self-potential measurements investigate natural electrical potential by assessing potential differences between pairs of electrodes. If electrochemical processes are absent within a slope changes reflect changes of fluid flows, i.e. ground water. Spontaneous potential measure can more easily be deployed and monitored compared to the resistivity method (Jongmans and Garambois 2007); however, electrical resistivity measurements are more common (Telford et al. 1990). This method is based on the measurement of electrical potentials between an electrode pair while a direct current is transmitted by another electrode pair (Schrott and Sass 2008). Several different procedures and array setups exist for electrical resistivity measurements which have to be chosen depending on the research question, study site properties and desired penetration depth. Electrical resistivity is affected by the nature of material, in particular clay content, water content, as well as rock weathering and fracturing (Jongmans and Garambois 2007). Geoelectric geophysical methods have frequently been used for landslide prospection and determination of internal structure, such as the location of shear surfaces and boundaries of landslide bodies (Jomard et al. 2007; Deparis et al. 2008; Sass et al. 2008; Heincke et al. 2010). However, sensitivity of resistivity to water content also allows detection of groundwater tables or preferential flow (Hiura et al. 2000; Kusumi et al. 2000; Lebourg et al. 2005). Geoelectrical methods are usually applied for short-term measurement campaigns, and only a few case studies describe continuous monitoring (Supper and Römer 2003; Lebourg et al. 2004).

2.3 Landslide Modelling

Landslide modelling is, along with experimental subsoil exploration and experience driven safety assessment, one of the main tasks of slope stability practice (Janbu 1996). Models are applied to analyse current stability status and to predict slope behaviour under certain conditions such as rainfall events or scenarios for environmental change. Moreover, models are used for the back-analyses of already failed slopes and for assessment of effectiveness of geotechnical stabilisation measures (Barla et al. 2004). However, when dealing with modelling it is important to keep in mind, that all models are necessarily simplified generalisation and approximations of processes which are occurring in nature (Favis-Mortlock and De Boer 2003).

Modelling of landslide failures can be either qualitative or quantitative (Carrara et al. 1999). Qualitative approaches integrate descriptive prediction and the opinion of experts, while quantitative applications are based on numerical simulations. Landslide modelling approaches can broadly be separated into models that are focussing on single landslide processes (i.e. local models), and models with greater spatial extent (i.e. regional models) (Crozier and Glade 2005).

Local approaches to landslides have a long tradition within geotechnical engineering slope stability practice, while regional applications have increasingly emerged since the wide availability of powerful computers and GIS. A brief summary on regional and local approaches to model landslides in order to predict slope failures is given in the following sub-chapters.

2.3.1 Regional Models

Regional landslide modelling methods generally focus on either landslide susceptibility or hazard, or eventually landslide risk. Landslide susceptibility is defined as the "*probability of spatial occurrence of slope failures, given a set of geo-environmental conditions*" (Guzzetti et al. 2005, p. 113). Therefore landslide susceptibility modelling seeks to delineate the terrains' potential for landslide processes. In contrast, landslide hazard is defined as "*the probability of occurrence within a specified period of time and within a given area of potentially damaging phenomenon*" (Varnes 1984). The term hazard therefore also requires definition of magnitude of potential events, that is, affected area, volume and velocity of expected landslide events (Reichenbach et al. 2005). The term landslide risk refers to the outcomes of landslide events and is defined as "*the expected degree of loss due to a landslides and the expected number of lives lost, people injured, damage to property and disruption of economic activity*" (Varnes 1984). While landslide susceptibility and hazard concentrate on the causes and properties of landslides, risk also refers to the consequences and outcomes of such processes, which are strongly dependant on the vulnerability of the effected people and infrastructure.

Soeters and Van Westen (1996) distinguish between four distinct approaches for regional landslide hazard analysis, i.e. inventory-based, heuristic, statistic and deterministic approaches.

Landslide inventories allow for detailed analyses of landslide distribution and in case of multi-temporal inventories activity patterns and form the basis for regional modelling of landslide susceptibility, hazard and risk.

Heuristic methods integrate the knowledge and experience of geomorphological and geotechnical experts to derive a regional map of landslide susceptibility and hazard. Soeters and Van Westen (1996) distinguish between geomorphological analysis (Kienholz et al. 1984; Cardinali et al. 2002; Reichenbach et al. 2005) and weighted combination of thematic maps (Pachauri et al. 1998; Nagarajan et al. 2000; Dikau and Glade 2003; Moreiras 2005; Petley et al. 2005a).

Statistical methods are the most frequently applied method to model regional landslide susceptibility and hazard, and to predict future slope failures (Bell 2007). Herein, a statistical relationship between possible landslide causative factors and the presence of existing landslides is established, and used for prediction of future landslide by spatial interpolation. A vast range of different methods has been developed. Bell (2007) provides a extensive list of statistical methods, of which the most frequently applied are bivariate regression (Ayalew et al. 2004; Süzen and Doyuran 2004), multiple regression (Carrara 1983; Chung et al. 1995), discriminant analyses (Ardizzone et al. 2002; Carrara et al. 2003; Guzzetti et al. 2006), logistic regression (Atkinson et al. 1998; Ohlmacher and Davis 2003; Süzen and Doyuran 2004; Brenning 2005), neural networks (Fernández-Steeger et al. 2002; Lee et al. 2003; Catani et al. 2005), support vector (Brenning 2005), bayesian statistic (Chung and Fabbri 1999; Lee et al. 2002; Neuhäuser 2005), fuzzy logic (Tangestani 2003; Dewitte et al. 2006; Lee 2006) and likelihood ratio (Chung et al. 1995; Chung 2006; Demoulin and Chung 2007).

Regional deterministic models apply physically-based simulations to assess landslide susceptibility expressed chiefly as FoS, and provide useful insights into landslide causes (Carrara et al. 1992). The most frequently applied methodology for regional deterministic modelling is based on distributed hydrological modelling and stability calculation using a simplified approach, i.e. the infinite-slope model. Hydrological modelling is essentially based on topographical flow routing and the simulated development of soil saturation above an impermeable layer (O'Callaghan and Mark 1984; Fairfield and Leymarie 1991; Freeman 1991; Quinn et al. 1991; Lea 1992; Costa-Cabral and Burges 1994; Terlien et al. 1995; Tarboton 1997). Calculation of slope stability utilises geotechnical parameters such as cohesion and internal friction, which can be measured in the field or laboratory (Soeters and Van Westen 1996; van Westen et al. 1997). The infinite-slope model estimates stability for single grid-cells of a DTM and neglects any effects of neighbouring areas. Moreover, deterministic methods are only applicable when geomorphic and geologic conditions are fairly homogenous over the entire study area and landslide types are simple (Soeters and Van Westen 1996). Due to these limitations, regional deterministic models are only suitable for simple landslide processes, such as shallow translational landslides. The most widely used models for regional deterministic analyses are

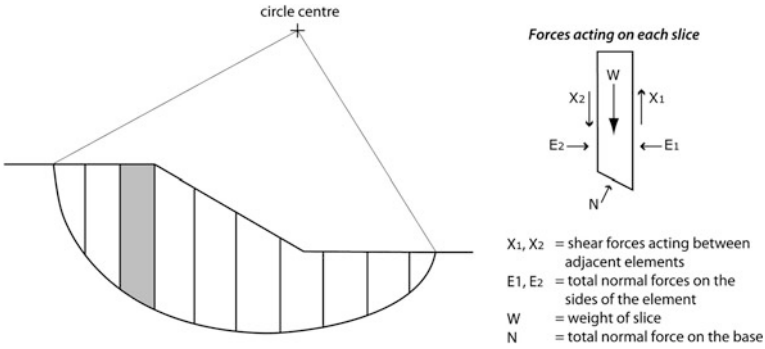

Fig. 2.6 Simplified illustration of method of slices (after Conolly 1997)

TOPMODEL (Montgomery and Dietrich 1994; Casadei et al. 2003; Meisina and Scarabelli 2007), SHALSTAB (Dietrich et al. 1998; Morrissey et al. 2001; Huang Jr et al. 2006), and SINMAP (Pack et al. 1998, 2001, 2005; Zaitchik and van Es 2003; Pack and Tarboton 2004; Kreja and Terhorst 2005; Thiebes 2006; Deb and El-Kadi 2009), but similar studies have also been performed by other authors (Hammond et al. 1992; Terlien et al. 1995; Wu and Sidle 1995; van Westen et al. 1997; Wu and Sidle 1997; Sidle and Wu 1999; Xie et al. 2004; Claessens et al. 2005).

2.3.2 Local Models

Models for the analysis of single slope failures, i.e. local models, have a long tradition in geotechnical slope stability practice. These models have frequently been applied to assess the stability of human-made or natural slopes, and the design of slopes, such as embankments, road cuts, open-pit mines etc. Moreover, physically-based models for single slopes allow detailed investigation of failure processes, assessment effects of triggering events, and assessment of the effectiveness of remedial measures and stabilisation works.

Today, a wide range of computer calculation programs are available for numerical slope stability assessment. Despite the development of more sophisticated numerical models, limit-equilibrium methodology is still widely applied (Abramson 2002). In the following a short overview of local landslide modelling methods and techniques is presented. It is beyond the scope to review the theoretical background and mathematical and mechanical derivation of local stability calculation. These can be found in the literature sources provided or in various textbooks (Chandler 1991; Bromhead 1998; Abramson 2002; Aysen 2002; Eberhardt 2003a; Ortigão and Sayao 2004; Duncan and Wright 2005; Gitirana Jr 2005; Cheng and Lau 2008).

Limit-equilibrium methods provide a mathematical procedure to determine the forces within a slope that drive and resist movement. The factors included in the

calculation have been presented in Sect. 2.1.2. Limit-equilibrium analysis usually calculates stability for discrete two-dimensional slices of a slope and for assumed or known potential shear surfaces (Fig. 2.6), but three-dimensional approaches have also been developed. Shear strength of materials along shear surface is assumed to be governed by linear or nonlinear relationship between shear strength and normal stress (US Army Corps of Engineers 2003). The result of limit-equilibrium analysis is a global FoS for shear surface, which provides a snapshot on stresses and resisting forces relationship.

Several numerical methods are available today which assist in locating critical shear surfaces, this is, where the lowest FoS is prevalent. The most widely applied methods are Bishop's simplified approach, which accounts for circular slip surfaces, and Janbu's method for con-circular, i.e. polygonal shear surfaces. Other methods like the infinite-slope wedge method, ordinary slice method, general slice method, Spencer's method, Morgenstern and Price's method, and some others are reviewed elsewhere (Graham 1984; Anderson and Richards 1987; Nash 1987). Given the wide use of numerical limit-equilibrium methods for slope stability analysis in geotechnical practice, most available models allow assessment of effects of e.g., external loads or remedial stabilisation structures, such as soil nails or other reinforcements.

However, limit-equilibrium methods also comprise some drawbacks. The resulting FoS represents a global value for a two-dimensional slope profile, where movement occurs if the FoS < 1.0. However, (Bonnard 2008, p. 46) notes that limit-equilibrium methods only provide an approximation of force balance within landslides and that in reality displacements may occur with a FoS between 1.0 and 1.1–1.15. Moreover, the FoS is an average value for an assumed critical failure surface and provides no information about the actual distributions of stresses or the progressive development of unstable state (Eberhardt et al. 2004).

A second family of stability models on a local scale is concerned with continuum modelling. The entire slope mass is divided into a finite number of elements and represented as a mesh. Continuum approaches include finite-difference and finite-element methods. Finite-difference methods provide numerical approximations of differential equations of equilibrium, strain–displacement relations or the stress–strain equations (Eberhardt 2003a). In contrast, finite-element procedures exploit approximations to the connectivity of elements, and continuity of displacements and stresses between elements (Eberhardt 2003a). However, in both methods the problem domain is discretised into a set of subdomains or elements. In contrast to limit-equilibrium analysis, continuum modelling software allows for complex time-dependant landslide analysis by including constitutive models such as elasticity, elasto-plasticity and strain softening.

A third family of local landslides models are discontinuum methods, where slopes are represented by distinct blocks which dynamically interact during movement or deformation. The underlying concept of these methods is that limit-equilibrium is repeatedly computed for each block, so that complex non-linear interaction can be accounted for (Eberhardt 2003a).

Three variations of discrete-element variation can be distinguished. Distinct-element methods are based on a force–displacement law to describe interaction between deformable elements, and a law of motion to numerically simulate displacements. Discrete element methods are computationally intensive as many case studies involve a very high number of interacting discrete objects. More detailed information is provided by (Hart 1993) and (Jing 1998). Discontinuous deformation analysis simulates interaction of independent blocks along discontinuities, such as fractures and joints. In contrast to distinct-elements methods, discontinuous deformation analysis accounts for displacement instead of simulating forces (Cundall and Strack 1979). Particle flow methods represent slopes with spherical particles that interact through frictional sliding contacts (Eberhardt 2003a).

Below, an overview of commercially available local landslide analysis and simulation models is presented. This is, however, only a selection of models frequently applied in landslide research as a complete summary is far beyond the scope of this study.

GGU is a CAD-based (Computer Aided Design) stability model which allows for predicting stability based on Bishop's and Janbu's, as well as general wedge and vertical slice method. Moreover, stabilising factors such as anchors, soil nails and geosynthetics can be included in the modelling process. However, the GGU stability software does not account for dynamic hydrological modelling. Several applications utilising the GGU stability software are available (Chok et al. 2004; Schneider-Muntau and Zangerl 2005; Kupka et al. 2009; Hu et al. 2010).

Galena is another numerical software solution available which includes limit-equilibrium analysis. It includes Bishop's and Spencer-Wright method and Sarma method, which utilises non-vertical slices for slope stability analysis. However, the Galena software was developed mainly for slope design in open-pit mines, and only few project applied it to analyse landslides (Kumar and Sanoujam 2006).

The program Xslope is capable of calculating slope stability based on Bishop's or Morgenstern and Price's method, and is available through University of Sydney. It does not include hydrological modelling, but pore water pressure from an external finite element steady-state seepage model can be integrated. Several case studies are available that describe the application of Xslope (Lee et al. 2001; Hubble 2004; Cássia de Brito Galvão et al. 2007).

Another model for limit-equilibrium analysis of soil and rock slopes is provided by SLOPE/W which includes several methods (Morgenstern-Price, Spencer, Bishop, Ordinary, Janbu and more). Also, several soil strength models are available. Stability analysis may be performed using deterministic or probabilistic input parameters. However, dynamic hydrological modelling of pore pressures is not included in SLOPE/W, but can be imported from SEEP/W, a finite-element software by the same company. Moreover, external stresses by earthquakes for example, and also the effects of reinforcements can be analysed. The use of SLOPE/W, also in combination with SEEP/W is fairly widely acknowledged in recent landslide research (Anderson et al. 2000; Rahardjo et al. 2007; Cascini et al. 2008; Heng 2008; Yagoda-Biran et al. 2010; Rahimi et al. 2010; Navarro et al. 2010).

SVSlope is a slope stability software with a similar complexity and range of available methods as SLOPE/W. However, three-dimensional limit-equilibrium analyses can also be performed for which slopes are represented as columns to analyse stability by a series of two-dimensional calculations. Moreover, a finite-element stability analysis tools have been added to compute stresses and strains.

Several authors presented case studies applying SVSlope (Gitirana Jr 2005; Fredlund 2007; Gitirana Jr. et al. 2008).

A similar program is Clara-W, which performs two and three-dimensional stability limit-equilibrium analysis (Eberhardt 2003b; Stead et al. 2006; Cotza 2009; Montgomery et al. 2009).

CHASM (Combined Hydrology And Stability Model) is a coupled hydrology and slope stability model for limit-equilibrium analysis. The software program integrates simulation of saturated and unsaturated hydrological processes to calculate pore water pressures, which are then incorporated into stability computation. CHASM is essentially two-dimensional but hydrological simulations can be extended to account for flow concentration at topographic hollows. Moreover, vegetation and stabilisation measures can be integrated into Janbu and Bishop stability simulations. Furthermore, a simple empirical-based run-out simulation is integrated into the model. CHASM was also employed within this study and a more detailed review on CHASM methodology is presented in Sect. 5.1.3.2.

The CHASM model has been applied by several research projects, for example in New Zealand (Wilkinson et al. 2000), Malaysia (Collison and Anderson 1996; Lateh et al. 2008), Hong Kong (Wilkinson et al. 2002b), the Caribbean (Anderson et al. 2008), Kuala Lumpur (Wilkinson et al. 2000; Wilkinson et al. 2002a), and Greece (Matziaris et al. 2005; Ferentinou et al. 2006; Sakellariou et al. 2006). Common applications of CHASM include investigations of effects of rainfall on slope hydrology and subsequently on slope stability (Matziaris et al. 2005; Ferentinou et al. 2006). Other studies compared CHASM to other slope stability model and carried out sensitivity analyses for rainfall, groundwater conditions and slope geometry (Lloyd et al. 2004).

Sensitivity analysis of CHASM has been carried out for geotechnical and hydrological parameters (Hamm et al. 2006), hydraulic conductivity (Ibraim and Anderson 2003), vegetation (Wilkinson et al. 2002b) and slope stability methods (Wilkinson et al. 2000). Comparisons of field measurements of pore water pressures with modelled results are provided by Anderson and Thallapally (1996) and Hennrich (2000). Other applications of CHASM include studies to improve criteria for geotechnical slope design (Anderson et al. 1996), and validation of rainfall thresholds to enhance the performance of a landslide early warning system in Kuala Lumpur (Lloyd et al. 2001). Later works of Wilkinson et al. (2002a) implemented a slope information system in which pre-defined slopes can be modelled in CHASM using a variety of input parameter constellations. Recent applications of CHASM include the work of Karnawati et al. (2005) in which the aim was to provide guidance to local population in Java, Indonesia on how to judge stability and hazardousness of slopes. Back analysis of recent landslides within CHASM was applied by Anderson

et al. (2008) in the Caribbean. Based on modelling results critical hydrological situations were determined and an effective slope drainage system was designed.

Several models are available from RocScience for calculation of stability, stresses and displacement for rock and soil. Phase^2 offers two-dimensional elasto-plastic finite-element stress analysis for underground or surface excavations with integrated groundwater seepage modelling (Hammah et al. 2008, 2009). The program Slide utilises two-dimensional limit-equilibrium analysis with built-in finite-element hydrological modelling. Generally, capabilities of Slide are similar to other limit-equilibrium programs described above. Case studies utilising Slide are described by several authors (Kjelland et al. 2004; Hadjigeorgiou et al. 2006; Hammah et al. 2006; Brandon et al. 2008; Topal and Akin 2008).

Plaxis is a collection of finite-element methods for numerical analysis of deformation and stability in geotechnical engineering in two and three dimensions. Moreover, unsaturated groundwater flow and pore pressures, as well as their effects on slope stability can be simulated. Static loads and dynamic loads and stability in response to earthquakes, as well as non-linear, time-dependent and anisotropic behaviour of soils and/or rock are more features of this complex software. Plaxis-aided research concerned with landslides has been provided by several authors (e.g., Spickermann et al. 2003; Ausilio et al. 2004; Comegna et al. 2004; Kellezi et al. 2005; Keersmaekers et al. 2008; Majidi and Choobbasti 2008; Chang et al. 2010).

FLAC (Fast Lagrangian Analysis of Continua) is a two-dimensional explicit finite difference program widely acknowledged in analysis of plastic deformation (Cala et al. 2004; Maffei et al. 2004; Chugh and Stark 2005; Petley et al. 2005d; Jian et al. 2009). Slopes are represented by elements which form a grid and behave according to a prescribed linear or nonlinear stress and strain law. Deformation of the grid allows for flowing and plastic-deformation, and large strain can be simulated. A simplified of this model is FLAC/Slope, which is sold by the same company. Moreover, a three-dimensional version, FLAC3D, is available and has frequently been applied within research (Teoman et al. 2004; Pasculli and Sciarra 2006; Sitharam et al. 2007; Poisel et al. 2009).

DAN, and its related version DAN-W and DAN3D, are software tools used for dynamic run-out analysis of rapid landslides processes such as rock avalanches (Hungr 1995). The core of the models is a Lagrangian solution of the integrated equations of motion which is implemented for thin elements of the flowing mass. The model simulates travel distance, velocity and flow depth and volumes in iterative time-steps. Many case studies acknowledge the use of DAN codes (Hungr 1995; Sosio et al. 2008; Hungr and McDougall 2009; Pirulli 2009).

UDEC (Universal Distinct Element Code) simulates the response of discontinuous media such as jointed rock which subject to loading. The two-dimensional analysis allows for rigid or deformable blocks. However, the related 3DEC model offers similar modelling capabilities but in three dimensions. Several case studies applied UDEC on rock slopes (Bandis et al. 2000; Bozzano et al. 2000; Chen et al. 2000; Gunzberger et al. 2004; Watson et al. 2004; Gong et al. 2005; Zhao et al.

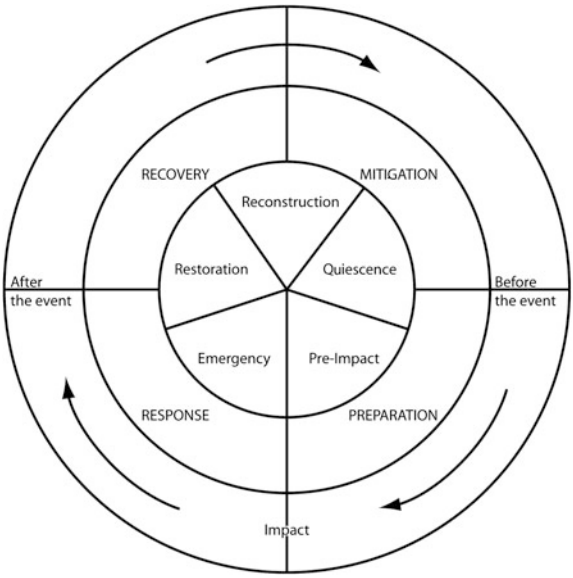

Fig. 2.7 General risk management cycle (after Alexander 2000, 2002)

2008), and 3DEC (Cheng et al. 2006; Ming-Gao et al. 2006; Lato et al. 2007; Bai et al. 2008).

2.4 Landslide Early Warning Systems

In the following an introduction to early warning and the challenges of early warning systems is presented. Therein, general aspects on social and technical aspects of early warning are demonstrated. The focus, however, is put on landslide early warning. More information regarding early warning systems for natural hazards in general is provided by several other authors (e.g., Zschau et al. 2001; Zschau and Küppers 2003; Dikau and Weichselgärtner 2005; Hall 2007; Schuster and Highland 2007; Felgentreff and Glade 2007; Glantz 2009). In addition, a review of existing landslide early warning systems worldwide is presented. It is beyond the scope to give a complete summary of all existent systems, but to illustrate a wide range of technical applications and to highlight integration of social components into early warning process.

Early warning can broadly be defined as the timely advice before a potentially hazardous phenomenon occurs. Dikau and Weichselgärtner (2005) add that the effective use of information for early warning is an important element of general risk management which includes activities such as hazard zoning and prediction, warning communication, disaster prevention and evacuation planning (Fig. 2.7). Good early warning systems therefore comprise identification and estimation of hazardous processes, communication of warnings and adapted reaction of local

population. Moreover, early warning systems have to be embedded into local communities to ensure effectiveness of the entire system.

A more pin-pointed definition is used by UNISDR (2009) where early warning system are described as "*the set of capacities needed to generate and disseminate timely and meaningful warning information to enable individuals, communities and organizations threatened by a hazard to prepare and to act appropriately and in sufficient time to reduce the possibility of harm or loss*".

Early warning systems have been developed for a wide range of natural hazards of which extreme weather events, floods and tsunamis are maybe the best known. However, also for processes such as volcanic eruptions, droughts, snow avalanches, earthquakes and landslides early warning systems have been installed. Extensive information on applied early warning systems is presented by several publications in the United Nations International Strategy for Disaster Reduction (UNISDR 2004a, b, 2006a, b). However, specialized landslide early warning systems are not described therein.

Within the UNISDR a Platform for the Promotion of Early Warning Systems (UNISDR-PPEW) has been founded to stimulate the advance of early warning. UNISDR puts an emphasis on social aspects of early warning and promotes the development of people-centred early warning systems (UNISDR 2006b). Four essential key parts for effective early warning can be defined (UNISDR 2006b):

1. Knowledge about the risks that threaten a community
2. Monitoring and warning service for these risks
3. Dissemination and communication of warning messages in a way that is understood by the local population
4. Response capability of involved people, who need to know how to react appropriately in case of a warning.

These four segments are also reflected in a general distinction of early warning proposed by Zschau et al. (2001), who distinguish the elements of prediction, warning and reaction. These components constitute the early warning chain. The segments of this chain have to be tightly connected and interlinked in order to provide an effective measure for risk reduction.

Prediction is strongly influenced by a natural science and technological perspective and aims to improve knowledge on the hazardous process itself and its timing, size, extent, severity, duration etc. The time-span between warning and the occurrence of the hazardous event is another important issue of prediction, and can last from seconds (for e.g. earthquakes) to months (for e.g., droughts) (Zschau et al. 2001).

The second element, warning, can be regarded as the critical element within the early warning chain (Dikau and Weichselgärtner 2005). Prediction has to be transferred into an adequate warning message and distributed to the target population. Several communication channels (e.g., SMS, Fax, Email, sirens) can be used to distribute warning messages. However, effective warning is not only a technical problem, but is also dependant on the social and political decisions and the legal framework (Zschau et al. 2001). Moreover, it is important that communication

of warning is carefully planned (Mayer and Pohl 2010). According to Kunz-Plapp (2007) warning messages should be believable, clearly formulated, adapted to the context of the target group, and should contain clear instructions on appropriate protection action.

Reaction is the third component of early warning, in which warning messages should lead to appropriate action such as evacuation of hazardous areas. Decision makers have to initiate protection actions based on the warning message. Effective reaction to warning messages primarily depends on the administrative and organisational circumstances (Zschau et al. 2001).

Given the complex conditions of early warning it is obvious that purely technical approaches cannot provide effective early warning. It has already been noted by the fathers of hazard research that it is important to know how technological advances in early warning systems can be used to more efficiently trigger appropriate reactions of populations to prevent losses from natural hazards (White and Haas 1975). Still, for a long time advances in early warning systems were primarily related to the use of more sophisticated monitoring equipment while social aspects of early warning were neglected (Zschau et al. 2001). This is problematic, as many communities cannot afford expensive high-tech warning systems. Sorensen (2000, p. 214) states that "*better local management and decision making about the warning process are more critical than promoting more advanced technologies*, *although both would help*". Many important social aspects are not accounted for in technical approaches to early warning. However, the importance of the hazard awareness can be illustrated by recent disaster events, such as devastating the tsunami in the Indian Ocean in 2004 which caused more than 200,000 fatalities. Even though no early warning system was installed, this disaster illustrates a major problem in early warning. As many people did not know that a sudden decrease in sea-level precedes the occurrence of a tsunami, no appropriate reaction could be initialised. If a threatened population is not informed about potential hazards, their consequences and suitable protective actions, early warning cannot be effective.

Although an early warning system could have enabled many people to evacuate coastal areas, early warning systems cannot provide full security from hazardous events. An example of this took place in April 2010, when a train derailed in the Etsch Valley, South Tyrol, Italy, because of a rockfall occurring above the track. Even though an automatic early warning system existed to close the track in case of blockages, it failed in this event because the rockfall took place right above the passing train (Murmelter 2010).

Moreover, it is important to keep in mind that only people and moveable objects can benefit from early warnings and not stationary objects such as infrastructure. An alarm can motivate people to escape from potentially dangerous situations, but it does not stop the hazardous event itself (Hübl 2000). Therefore, early warning systems do not substantially decrease property damage (National Research Council 2004).

Although early warning systems can be an effective tool for risk reduction (Dikau and Weichselgärtner 2005) they can also increase the risk. Increased risk

may be due to a false sense of security and building of higher value infrastructure in potentially hazardous areas.

Uncertainties always prevail in hazard prediction and are also a major challenge for early warning (UNISDR 2004b). Storms may change their track, or lose their strength over time, earthquakes may be expected for a large area, but no exact location can be determined. For many hazard events, only statistical forecasts, such as an El Niño event probability for the next year of 60% can be made. In addition, uncertainties within the social components complicate the prediction of the hazard consequences. These include the reaction of the population to warnings and hazardous events, and the functioning of evacuation plans and general disaster management. Baum and Godt (2009) provide interesting examples where people were moving into warning areas on purpose to secure their homes or save pets. Others misunderstand the warning and believe that if a warning is issued by for example the Department of Forestry it only relates to areas with actual logging activities.

Moreover, the costs of unnecessary evacuations due to false alarms are a major concern for decision makers. False alarms are a problem of early warning systems as they can substantially compromise the credibility of early warning systems (Larsen 2008). In 1982 the United States Geological Survey (USGS) issued a warning for the Mammoth Lakes Area because of an expected volcanic eruption potentially threatening a ski resort on the slopes of the volcano. After the eruption did not occur the USGS was mocked as the US Guessing Society (Die Zeit 2010). However, Sorensen (2000) argues, that false alarms do not necessarily diminish the trust in early warning systems if the reason for the false alarm is understood. The number of false alarms can be reduced by pursuing a conservative strategy and by issuing generalised warnings. However, the use of generalised warnings decreases with the size of the geographic area (Larsen 2008).

An interesting example of consequences of false warning took place in Italy in 2009 were a scientist had been measuring the emissions of radon gases which are associated with earthquakes. Based on his measurements he was expecting a major earthquake for the city of Sulmona two days before the devastating L'Aquila earthquake (5.8 magnitude on Richter scale) which is located 70 km north-west. As his prediction did not turn out to be accurate he was accused for creating panic but later absolved (Die Zeit 2010).

On the other hand a group of seven Italian earthquake scientists who were assessing the seismic activity in the L'Aquila region were accused of gross negligent manslaughter as they failed to predict the disaster. Only days before the earthquake they had stated at a meeting with city officials that there were no grounds for believing a major quake was on the way despite some smaller quakes in the previous days (Cartlidge 2010). The allegations gained much attention in the scientific community as well as from general public, and a petition to end the investigations had been signed by over 5000 scientists. In this open letter it was stated that at the moment there are no scientific method to predict earthquake timing and that therefore, there is no ground for the allegations (Die Zeit 2010). Warner Marzocchi, chief scientist at the Italian National Institute for Geophysics

and Vulcanology commented that "*as scientists, we have to focus on giving the best kind of scientific information*" and that the decisions of what actions need to be taken "*is down to others to decide*" (Cartlidge 2010). Thomas Jordan, earth scientists who had also been working in the L'Aquila region added that the costs of false alarms are too high compared to the low probabilities of an earthquake occurring, so that there was no basis to initiate actions such as mass evacuations (Cartlidge 2010).

A similar case happened in the Italian community of Sarno, which was hit by devastating landslides and a debris flood in 1998. Before the disaster event the mayor had told the people to stay calm and to stay at home even though there were already heavy rainfall and landslides occurring in the vicinity of the town (Die Zeit 2010). After the event he was accused for negligent manslaughter but later absolved because the event could not have been foreseen.

The previous examples clearly illustrate some of the problems and challenges of early warning systems, arising from both natural and social components. Besides technical difficulties of natural hazard prediction, legal, social and political dimensions add to the complexity of early warning. Effective early warning systems must therefore be carefully planned. Resulting from the work of the Integrative Landslide Early Warning Systems (ILEWS) project, issues have been identified that need to be addressed when early warning systems are to be installed (Bell et al. 2010). Important factors to be accounted for include the process (flood, volcanic eruptions, landslides), time (slowly developing or rapidly initiating hazards), forewarn time needed to provide useful warning, financial aspects (private or public investments), communication of warning (unidirectional, bidirectional), threatened human lives and infrastructure (cost-effectiveness) and stakeholders to be warned (governmental agencies, emergency services). Thus, early warning systems have to be demand-orientated and adapted to local conditions (Twigg 2003). In addition, it is important that early warning systems are embedded into the local community to increase acceptance of warnings (Mileti 1999; Greiving and Glade 2011).

Given the variety of hazards for which early warning systems have been installed it is difficult to define clear categories. Some basic distinction, however, can be made (Bell et al. 2010):

- Monitoring systems are primarily installed to increase the understanding of natural processes but can also be utilised to plan further actions. These monitoring systems differ by technologies applied, time intervals between measurements and degree of automation.
- Expert- or control systems provide information on potentially hazardous events and are chiefly implemented to gain information on critical developments and with the aim to guide scientists and decision makers.
- Alarm systems are based on monitoring systems and provoke an automatic warning if, for example, a predefined threshold is exceeded. Further differentiation of alarm systems can be made between pre- and post event systems and the forewarn time provided by the system. Moreover, these systems differ in

their degree of integration of social aspects between purely technical applications and integrative early warning systems.

Early warning systems have also been applied for landslide processes, e.g. rotational and translational slides, debris flows and rock slides. Landslide early warning systems can be installed for single slopes, but also for entire regions. Also global landslide early warning systems have been proposed by applying methods such as rainfall intensity and duration thresholds (Guzzetti et al. 2008) or satellite-based InSAR monitoring and progressive failure analysis (Petley et al. 2002).

Regional landslide early warning systems can only issue warnings, such as a 70% probability of debris occurrence for a certain region; single slopes cannot be identified (Wieczorek and Glade 2005). However, local or site-specific landslide early warning systems provide another quality of information. Exceedance of critical thresholds may automatically lead to protective actions, such as alarms, road and bridge closures, evacuation and further disaster management actions. Local landslide early warning systems have been frequently applied, partly because they can sometimes replace structural measures of slope stabilisation while providing sufficient protection (Palm et al. 2003). Site-specific systems generally apply monitoring systems for slope movement or landslide triggering factors such as rainfall and pore water pressure (see Sect. 2.2) as the early basis of warning.

One of the first modern landslide early warning systems was installed in 1984 in Utah, USA, after significant damage by debris flows initiated by snow melt (Baum 2007). Initially, monitoring of precipitation, temperature and slope movement on potential landslides were used to alert local officials and issue a regional debris flow early warning. Later works of (Ashland 2003) established groundwater thresholds for instrumented potential landslides. Regional thresholds were determined based on annual cumulative rainfall. Recent developments include snow monitoring to account for landslide triggering by snow-melt (Baum 2007).

Based on the works of Campbell (1975), who established landslide and debris flow triggering rainfall thresholds by intensity and duration analysis, a regional debris flow early warning system was set up for the San Francisco Bay Area, USA in 1986 (Keefer et al. 1987; Wilson 2005). The system was developed and implemented as cooperation between USGS and National Weather Service (NWS). Quantitative weather forecasts issued by NWS two times a day for the upcoming 24 h were provided to the Landslide Initiation and Warning Project of USGS. Rainfall forecasts were combined with data from automatic rainfall gauges and consequently checked against pre-defined thresholds. Estimation of hazard level and final decision upon warning was assessed cooperatively by experts from USGS and NWS. Initially, triggering thresholds based on rainfall intensity in relation to annual rainfall (Cannon and Ellen 1988) were utilised. Later thresholds were adjusted to account for water storage capacity (Wieczorek 1987) and minimum thresholds for debris initiation (Wilson et al. 1993). Below the minimum rainfall threshold debris flow occurrences are unlikely while above the upper threshold significant debris initiation in the region can be expected. In 1992 it was attempted to integrate radar data into the early warning system to improve the spatial

resolution of rainfall measurement. However, integration failed because no reliable relations between radar reflectivity and ground based measurement could be established. Along with technical problems the social aspects were a major challenge for the early warning system. For instance, NWS and USGS had different expectations to the technical system. While USGS interpreted the system as an experimental prototype of which warnings are by-products, NWS demanded reliable predictions and warnings. Warning communication was another challenge for the early warning system. USGS considered early warning as an entirely technical system which ended with issuing an alarm. The population was expected to react appropriately by avoiding dangerous areas. Yet, the population and also emergency services were mostly unaware of debris hazards and their damage potential. In reality, many people intentionally drove into hazardous areas in severe storm conditions trying to get home to save the house or feed a pet (Wilson 2005). Eventually, the system was shut down in 1995 because USGS could not afford to continue the service.

Based on the experiences in the San Francisco Bay Area, USGS and National Oceanic and Atmospheric Administration (NOAA) cooperatively initiated a regional landslide early warning system for burned areas in south California, which are prone to debris flow initiation (NOAA-USGS Debris Flow Task Force 2005). An assessment of potential end-users and their demands towards landslide early warning were clarified before the system was set-up. Alert level terminology was overtaken from NWS severe weather forecasts to increase the acceptance of the population. Dissemination of information and warning communication were adjusted to end-users needs. USGS also developed an education program for involved meteorologists and interested public to explain hydrological characteristics of debris flow initiation in areas with burned vegetation (e.g., California Geological Survey 2003). Technical advances compared to the previous system comprise improved quantitative rainfall forecasts, and implementation of test areas to improve the understanding of triggering groundwater conditions. In addition, empirical and physically-based models were applied to assess susceptibility to debris flows, their potential volume and run-out distance (NOAA-USGS Debris Flow Task Force 2005).

Another regional debris flow early warning system for Oregon, USA, was developed and implemented as a cooperation between Oregon Departments of Forestry (ODF), Transportation (ODOT) and Geology and Mineral Industry (DOGAMI) with Oregon Emergency Management (OEM) (Baum 2007). During periods of intense rainfall meteorologists of ODF monitor measured rainfall and forecasts and assess current hazard level together with geotechnicians which are available 24 h a day. Warning messages are issued if thresholds are almost reached or exceeded. Thresholds used within the system account for rainfall intensity and duration, but are modified in case of significant antecedent rainfall or snow melting. Warning is spread via the emergency channel of the National Weather Service. Within the developed system information and education on debris flow hazards and early warning are also addressed by for example, warning signs along the highway, advise to homeowners and information on websites (Burns et al. 2008; Oregon Department of Geology and Mineral Industry 2010).

A regional early warning system for shallow landslides is implemented for the Seattle Area, USA since 2002 (Baum et al. 2005a; Baum and Godt 2009) and is jointly managed by NWS, USGS and the city of Seattle. The technical system comprises a total number of 17 automatic rain gauges with an average distance of 2–5 km between them and quantitative weather forecasts. In addition, a test slope was instrumented to improve understanding of pore water pressure development and landslide triggering. Furthermore, landslide mapping and probabilistic regional hazard modelling were performed (Baum et al. 2005b). Detailed examination of rainfall data led to the establishment of a minimum threshold for landslide triggering based on intensity and duration analysis and an antecedent water index calculated from cumulative rainfall of 3 days, and rain within the previous 15 days (Chleborad 2000, 2003, 2006). For the assignment of alert levels thresholds are used for both, intensity-duration and antecedent water index. Rainfall exceeding intensity-duration thresholds triggers a warning status at high antecedent water status. Watch level is issued, in the occurrence of medium antecedent rainfall index values and observed or forecasted rainfalls above thresholds. Outlook level is activated if any of the rainfall threshold is exceeded. In other cases the alert is null. In addition, warnings are only provided if thresholds are exceeded for at least three gauges relating to an expected number of three or more landslide events (Baum and Godt 2009). Warning thresholds performed satisfactory in back-analysis with data from the 1978 to 2003 period; only eight storms caused landslides without previous threshold exceedance (Godt et al. 2006). Forty per cent of all warnings were followed by landslides events and 85% off all landslides were triggered by rainfall above thresholds values. To increase the acceptance of the early warning system and improve risk awareness of the local residents, USGS provides educational material and information (USGS 2006).

In the USA, USGS is responsible for allocation of warnings related to geological events, including landslides. To increase interoperability of warning systems and ensure smooth warning communication a common alerting protocol (CAP) was created (Highland and Gori 2008). This data format is the same for many different kinds of warnings including also man-made hazards and terrorism. Today it is widely used by state agencies in the USA. Landslide related CAP warning have been adopted for all study areas, for which reliable rainfall thresholds have been established, i.e. Seattle, San Francisco Bay Area and burned areas and parts of the Appalachian mountain areas of the eastern US. All alerts, including archived warnings, are presented on USGS website. To increase the populations' awareness of landslide hazards and the potential outcomes of landslide events, a documentary movie was produced, which is also planned for school education (Highland and Gori 2008). Moreover, a wide range of fact sheets, reports and other information on landslide hazards, consequences and warnings is produced by USGS.

The most advanced and successful landslide early warning system may be that installed in Hong Kong, China (Schuster and Highland 2007). Hong Kong is densely populated by seven million inhabitants and very prone to landslides occurrences and damage consequences. The terrain is rugged, with hills rising up

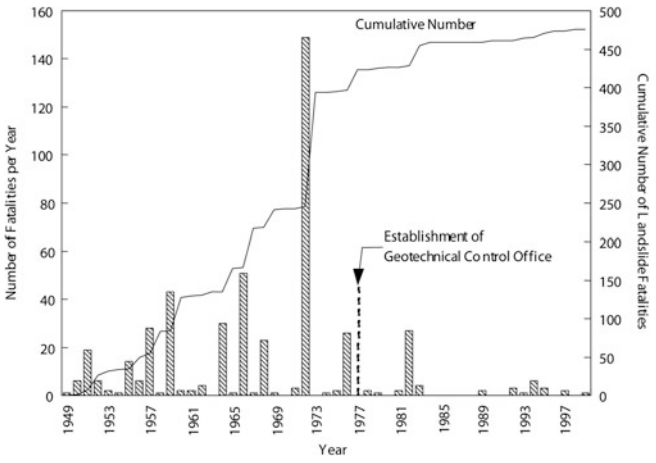

Fig. 2.8 Number of landslide fatalities in Hong Kong (after Wong and Ho 2000)

steeply, and less than 30% of the densely populated areas are flat (0–5°) (Brand et al. 1984). The limited availability of favourable land means that geotechnical slope construction works including design of cut and fill slopes and slope stabilisation are frequently required. Moreover, strong rainfalls with hourly intensities exceeding 150 mm occur along with tropical cyclones and low pressure. After two catastrophic landslide events in 1972 and 1976 which together caused more than 100 fatalities, the Geotechnical Control Office was established to reduce landslide consequences (Malone 1997). Later, the agency was renamed the Geotechnical Engineering Office (GEO). GEO has many responsibilities, such as establishing instructions and guidelines for slope design, slope stabilisation, quantitative risk management and early warning (Chan 2007). Moreover, education programs for the general population and homeowners aim to raise awareness of landslides and related risks. Radio and television features, a telephone hotline and a website provide a wide range of information and advice to local residents (Massey et al. 2001). Detailed information on integrative landslide risk management strategies in Hong Kong and the efforts and experiences of GEO is available in a collection of scientific papers published for the 30th anniversary of GEO (Geotechnical Engineering Office 2007). The great success of slope safety in Hong Kong is also illustrated by significantly lower fatalities due to landslides after the establishment of GEO's predecessor in 1977 (Fig. 2.8).

The Hong Kong regional landslide early warning system was launched in 1977 and is managed cooperatively by GEO and Hong Kong Observatory. More than 100 automatic rain gauges built the technical base for early warning. Rainfall thresholds triggering landslides in Hong Kong were first established by Lumb (1975), but were modified several times afterwards when improved real time rainfall and landslide data became available. Initially, warning thresholds accounted for cumulative 24 h rainfall in relation to rainfall of the preceding

15 days. Warnings were issued if measured rainfall of the last 20 h and the forecasted rain for the next 4 h exceed 175 mm (Chan et al. 2003). In the 1980s an hourly rainfall threshold of 70 mm was added to the warning scheme. Progressive analysis of landslide initiation and related rainfall events led to prediction of the number of landslides expected for certain storm events. Warnings were only issued if 15 or more landslides were expected to occur (Chan et al. 2003). Since 2003 a GIS-based approach has been used for landslide prediction (Yu et al. 2004). Therein, the entire area of Hong Kong is represented as grid cells accounting for number of properties contained on the slopes. The number of expected landslides is then modelled according to a spatially variable susceptibility to slope failure. A recent development of the landslide early warning system includes the integration of radar data from the SWIRLS system (Short-range Warning of Intense Rainstorms in Localised Systems) to track storm cells and improve quantitative prediction of localised storms (Cheung et al. 2006). Warning dissemination utilises TV, radio and internet to inform the public. In addition, emergency forces and hospitals are contacted if large numbers of landslide are expected. In early years warning messages were mostly aimed at slum dwellers because they lived in most hazardous areas. However, social and geotechnical developments since the 1980s changed the focus. Today, the intention of early warning is to inform the entire population about potentially hazardous events, thus to provoke cautious behaviour.

Mainland China is probably experiencing the highest landslide damage and number of fatalities in the world (Tianchi 1994). China has begun to address the landslide problem in the 1990s by starting a nationwide investigation program including landslide mapping, susceptibility zoning, risk analysis, rainfall threshold analysis, prevention planning and engineering counter measures (Yin 2009) and early warning (Zhou and Chen 2005). Since 2003 landslide warning based on rainfall forecasts are issued after general weather reports on prime time TV shows (Yin 2009).

A regional landslide early warning system based on susceptibility maps and rainfall thresholds was installed for Zhejiang Province (Kunlong et al. 2007; Eng et al. 2009). The system is based on rainfall forecasts and works as a WebGIS. Warnings are issued if rainfall predictions exceed one of the two defined thresholds and near real-time warnings are spread through various communication channels (internet, telephone, etc.). The warning system is also combined with an assessment of economical risks which aim to extend the system to landslide risk warning (Wu et al. 2009).

Zhong et al. (2009) provide detailed information of the precipitation based early warning system for Hubei Province. The landslide early warning system was installed in 2006 and represents a WebGIS. Critical rainfall thresholds have been determined by analysing the statistic relationship between spatial distribution of occurred landslides and rainfall data. Warning generation is based on 2 and 15 day antecedent rainfall, which is compared to 24 h rainfall forecast. If thresholds are exceeded in any of the 82 divisions in which Hubei is differentiated, the Meteorological Survey of Hubei Province issues a warning on the internet. More information on the current situation is freely accessible in the form of maps on the

internet. In three years of operation the system issued 11 warnings, of which 6 were followed by landslide events (Zhong et al. 2009).

The Geotechnical Engineering Office of Rio de Janeiro, Brazil, implemented a regional landslide early warning based on rainfall thresholds and rainfall monitoring in 1996 (Ortigao et al. 2002; Ortigao and Justi 2004). In early years the early warning system was not entirely automated which resulted in a lack of warnings on for example, weekends and holidays, as no experts were available (D'Orsi et al. 2004). Instead, automated fax messages were sent without proper data analysis. However, due to wide acceptance of the early warning system it was expanded in 1998, and since then provides continuous service. At the same time a rainfall radar was included into the technical input to increase forewarn time. In addition, a test slope was equipped with piezometers and inclinometers to gain more insights into the failure processes. However, it was decided not to establish more site-specific monitoring systems as the costs were too high. Two critical rainfall thresholds were determined which relate hourly rainfall intensity to accumulated rainfall for 24 and 96 h (D'Orsi 2006). Four warning levels are used, e.g., low (landslides could happen), medium (occasional landslides), high (scattered landslides) and very high (generalized landsliding). Current information on warning levels is broadcasted by media and is also available online. In addition, emergency services are informed by fax to prepare for potential landslide events. In addition to the landslide early warning system, flash floods were later integrated into forecasting activities (D'Orsi 2006).

A regional debris flow early warning system was installed in Combeima-Tolima Region in Colombia (Huggel et al. 2008; Huggel et al. 2009). The project was initiated by the Swiss Agency for Development and Cooperation (SDC) which promoted investment into early warning, risk awareness education and disaster prevention training instead of solely focussing on reconstruction. The automatic technical monitoring system includes three rainfall stations and a series of geophones. At the Regional Emergency Committee Centre data is collected and analysed 24 h a day and is available online. Rainfall thresholds initiating debris flows were calculated based on intensity and duration, and with respect to antecedent rainfall up to 30 days. If thresholds are exceeded an emergency plan determines actions to be taken. Interestingly, Huggel et al. (2009) analyse the performance of the developed system by a cost-effectiveness calculation based on historic records. Therein, the costs of false alarms are compared to losses in case of hazard events which can be used to adjust rainfall thresholds. However, this approach is ethically questionable as it requires definition of monetary costs of lost human lives.

The combined hydrology and slope stability model CHASM, which is applied within this study, has also been used in another landslide early warning system. However, instead of applying CHASM for continuous modelling of slope stability, rainfall thresholds previously calculated were validated by detailed analyses for single slopes. The system is located along the Kuala Lumpur Highway, Malaysia, and is in service since 1996 (Lloyd et al. 2001). An automated monitoring system measures rainfall intensity which is compared to pre-defined threshold values also

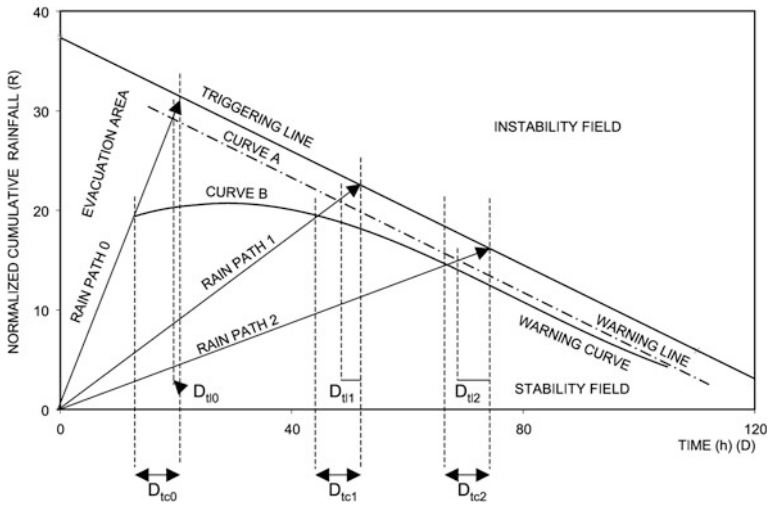

Fig. 2.9 Comparison of warning curve and warning line thresholds and subsequent time spans for evacuation (after Aleotti 2004)

accounting for antecedent rainfall conditions. A series of single slope CHASM simulations illustrated the effect of high soil permeability on slope stability. In conclusion, rainfall longer than 6 days ago did not significantly influence slope stability and could be neglected in rainfall threshold determination in the study area.

An extensive early warning system for debris flows in Indonesia is presented by Apip et al. (2009, 2010). Based on local rainfall threshold analyses accounting for rainfall intensity and duration, as well as antecedent rainfall, design charts were created which provide three warning levels (safe, watch, danger). Moreover, it is tried to widen predictive power of the warning system by integrating spatially distributed modelling of slope stability with physically-based hydrology and stability model. Therein, quantitative rainfall forecasts by National Oceanic and Atmospheric Administration (NOAA) are utilised for real-time modelling of potential landslide initiation. In addition, the model is planned to be further developed to provide forecasts of river flows, sediment transport and debris flow run out.

A similar approach to early warning is provided by Liao et al. (2010), who also worked on regional landslide early warning in Indonesia. The proposed system includes a physically-based hydrology and slope stability model, as well as integration of quantitative rainfall forecasts. Modelling is performed in two steps. Initial calculations provide hot spots, which can then be modelled using data with higher resolution. However, the technical system represents a prototype development and further research has to be accomplished in order to increase its predictive capacities.

Schmidt et al. (2008) present an innovative landslide early warning system for New Zealand. Therein, probability of landslide failures is computed by combination of a regional physical-based hydrology and stability model with quantitative weather forecasts. However, landslide prediction is subject to large uncertainties which are assessed by probabilistic methods. Unfortunately, the early warning system was only a prototypic development and is currently not active.

Aleotti (2004) presents a prototype of a regional landslide early warning system for shallow landslides in the Piedmont Region of north-western Italy. Rainfall thresholds were determined by analysing intensity-duration, antecedent rainfall and mean annual precipitation. Warning thresholds, however, were established lower than triggering thresholds to provide more safety. Instead of a warning threshold parallel to the triggering threshold (Aleotti 2004) applied a curve to account for different rain paths (Fig. 2.9). By doing so time spans until landslide triggering threshold exceedance are integrated, which are important for initiation of evacuations. The technical warning system includes rainfall forecasts and station measurements. The system remains in an ordinary attention state until thresholds are exceeded by rainfall forecasts. A preceding warning procedure is launched if landslide prone areas are affected by threshold exceedance. Rainfall paths are then plotted according to antecedent and real-time rainfall and an alert is issued according to the pre-defined thresholds.

Recent developments of the regional landslide early warning system concentrated on the improvement of thresholds by including local properties, such as topography and geological properties (Tiranti and Rabuffetti 2010). Consequently, three thresholds were established, i.e. regional, sub-regional and a pragmatic threshold, which accounts for multiple occurrences of landslide in single rain events. All thresholds were tested for their performance in a back-analysis in terms of correct, false and missed alarms. In addition, a technical system named SMART was developed which analyses rainfall time series for each rain gauge in real time and identifies where thresholds are exceeded. The current early warning system utilises rainfall forecast and real-time measurements and applies the pragmatic threshold (Tiranti and Rabuffetti 2010).

The Åknes rockslide in Norway is one of the most intensely investigated and monitored landslides worldwide (e.g., Derron et al. 2005; Ganerød et al. 2008; Kveldsvik et al. 2008, 2009; Eidsvig et al. 2011; Heincke et al. 2010; Grøneng et al. 2010). The rockslide itself does not pose direct threat to a community, however, slope failure is supposed to trigger a tsunami affecting ships and towns along the fjord. The rockslide mass has a volume of 30–40 million m^3 and displacements vary with seasons and reach 3–10 cm/year with daily movements up to 1 mm (Blikra 2008). The technical monitoring system includes extensometers, inclinometers, crackmeters, tiltmeters, geophones, piezometers, automated measurements by theodolites, laser and GPS and ground based radar, and a climate station. All data is available in a web-based database and supervised by experts 24 h a day. Threshold values for displacement velocity have been established which relate to five alert levels colour-coded from green to red. In case of imminent slope failure sirens warn the population in potentially affected towns.

Fig. 2.10 Early warning system at Winkelgrat landslide equipped with automatic extensometers (*left*) and traffic light for road closure (*right*)

Other topics of the project include development and implementation of warning routines and evacuation planning (Blikra 2008).

Another example of an intensely monitored rock slide is the Frank Slide at Turtle Mountain, Canada, which exhibited a catastrophic failure in 1903 causing 70 fatalities (Froese et al. 2005). A landslide monitoring and early warning program was launched in 2003 and commenced with detailed site investigations using InSAR, microseismic surveys, ground penetrating radar, drilling and core sample analysis. Within the actual early warning system tiltmeters, extensometers and crack meters are used as primary sensors as they provide high detail displacement data (Froese et al. 2006). Secondary sensors include differential GPS and automatic theodolite measurements which have higher fluctuations but improve understanding of the overall situation. Background information is gained by tertiary sensors, i.e. climate station data and microseismic monitoring. The early warning system comprises four elements (Froese et al. 2005). A monitoring procedure was established to determine responsibilities for measurements and their frequencies, which might change in response to trends and anomalies in the data. Within the threshold development procedure value-based and velocity-based thresholds two standard deviations above noise level were established. Development of alert levels and notification protocols comprise the third element of the early warning system. A standardised terminology and appropriate response to trends in monitoring data were determined. Moreover, action advice was developed for emergencies including procedures for communication and evacuation. The current alert level is accessible on the internet and is presented in four colours. The green alert level indicates normal situations where measurements are in the range of background noise but may exhibit seasonal fluctuation. The watch level is active if multiple sensors display unusual trends and leads to direct communication between technical experts and local decision makers and municipal officials). The warning level is initiated if multiple sensors demonstrate acceleration trends exceeding pre-defined thresholds. If several sensors indicate accelerations and final failure is imminent (one to three days to failure) then the alarm level is issued and

the emergency response procedure is executed. More detailed information on monitoring (Read et al. 2005), modelling (Froese et al. 2009) and the information platform (Froese et al. 2006) is given in the respective literature.

An early warning system for rockfall is installed at the Winkelgrat, also located at the Swabian Alb in Germany (Fig. 2.10). The technical system consists of nine automatic extensometers installed in 2002 (Ruch 2009). An automatic alarm message is sent to the local emergency service if pre-defined thresholds are exceeded. The road below the unstable rock mass is then closed by setting two traffic lights to red to prevent cars from entering the hazardous area. At the same time road maintenance service, police, rescue forces and the regional geological department are informed via SMS and fax. Following field investigations by experts of the regional geological department it is decided to initiate further protective measures, or in case of false alarms, to reopen the road (GEOSENS 2009; Krause 2009).

Another landslide early warning system in Germany is described by Lauterbach et al. (2002) and Krauter et al. (2007). This system relies primarily on technical solutions, for example, GPS displacement measurements, and is installed at an autobahn in south-west Germany. The slope under investigation is known to cause deformations to the road surface since the 1960s. The landslide mass is calculated to be 700,000 m^3 with average annual movement rates of 1–2 cm. As structural measures were considered uneconomical a GPS based warning system was installed. The system consists of 5 measured points of which the main station is based outside the landslide mass. Accuracy of the system is about 1 mm in location, and 2–3 mm in height. Two kinds of alarms are implemented: one occurs when obviously false measurements are being taken or maintenance works are necessary, the other if pre-defined thresholds of movement rates are exceeded. If warning thresholds are exceeded the experts operating the system are informed via automatic telephone calls and immediately check the situation in the field, which then can lead to emergency actions like, for example, road closure.

Several slope monitoring and early warning systems have been installed in the United Kingdom. An extensive technical monitoring and early warning was installed for the coastal landslides on the Isle of Wight (Clark et al. 1996) where the first tiltmeter slope early warning started in 1981 (Barton and McCosker 2000). Today, the technical system comprises monitoring of surface and subsurface movements by theodolites, GPS, inclinometers, tiltmeters and crackmeters. Weather stations and piezometers record also rainfall and its effect on landslide triggering. Automatic alarms are issued if pre-defined displacement thresholds are exceeded. Automatic monitoring systems were preferred over manual systems even though initial costs are considerably higher. Similar technical monitoring systems have also been installed in Lyme Regis, Scarborough and Cromer (Clark et al. 1996).

In Lyme Regis a series of inclinometers, piezometers and GPS ground markers are continuously monitored and provide an alarm to experts and decision makers if an imminent threat is given (Clark et al. 2000). In addition, an increased monitoring frequency can be initiated and emergency response is prepared.

At Cromer, automatic readings of field sensors activate an alarm by sending a message by pager. Warning thresholds are based on a pre-determined movement velocity of 3 mm per hour or 10 mm in 6 h.

Landslide early warning on the Isle of Wight is part of an extensive general coastal management scheme by the Isle of Wight Centre for Coastal Environment which promotes a holistic approach. Coastal management comprises for example, allocation of planning guidance maps, building codes, engineering measures, monitoring, forecasting and early warning. A wide range of information is available on the websites (Isle of Wight Centre for the Coastal Environment 2010), such as a best practice guide (McInnes 2000) providing detailed descriptions of monitoring and warning schemes, as well as advice to homeowners on how to reduce risk of coastal erosion and instability. In addition, the local management and information centre arranges workshops and educational field trips.

An extensive technical monitoring system is installed along the slopes of Clyde Dam Reservoir, New Zealand (Macfarlane et al. 1996). More than 5,500 theodolite observation points were installed to monitor displacements during dam construction and reservoir filling. After filling was accomplished the number of observation points was reduced. Further monitoring equipment includes borehole extensometers and inclinometers for subsurface movements and piezometers for slope hydrology. All data is automatically stored in a database and alarms are raised automatically if pre-defined thresholds are exceeded.

Given the great number of engineering works in China many applications of monitoring and early warning systems are described in the literature. Since the 1990s much attention has been paid to the landslide hazards along the Three Gorges Dam Reservoir, China, and many investigations have been performed by researchers on this emerging topic (Fourniadis et al. 2007a, b; Li et al. 2008; Wang et al. 2008c; Jian et al. 2009; Li et al. 2009a, b; Yin 2009). Several landslide monitoring and early warning systems are located along the lake created by the Three Gorges Dam. One of these was installed for the Shuping landslide, a reactivated mass movement which accelerated after the impoundment of the lake. Several extensometers are used to measure the landslide (Wang et al. 2008b; Wang et al. 2009). Dai et al. (2008) describe a monitoring and warning system based on high resolution optical fibres for the Yuhuangge landslide in the Three Gorges Area. Four alert levels were determined which account for changes in velocity and pore water pressure. Local decision makers are informed about current alert levels and are obliged to issue final warnings and initiate evacuation. Since 2004 the alert level was once set to yellow level due to significant acceleration and damage on infrastructure (Yin et al. 2010a). Later however, displacement rates decreased to former values and the alert level was subsequently lowered.

Moreover, several more interesting papers on applied landslide early warning systems in China have been published, unfortunately, many are only available in Chinese language with English abstracts (Jiang et al. 2009; Xu and Zeng 2009; Ye et al. 2009).

The Illgraben catchment (9.5 km^2) in Switzerland has some one of the highest debris-flow activity in the Alps. A monitoring and early warning system for debris

flows was installed and described in detail by Badoux et al. (2009). The overarching early warning concepts includes ongoing education and allocation of information for the local population regarding debris flows and possible consequences, a monitoring system, repeated field surveys to assess changes in the catchment, and integration of meteorological measurements to increase forewarn time (Graf et al. 2006). Several education campaigns were performed to inform local population about potential hazards and the early warning systems. In addition, children at elementary level learn about debris flows in school. Tourists are provided information at local tourist information centre. Along the debris flow channel warning signs were put up every 200 m explaining the threat of debris flow occurrences in five languages. Moreover, warning lights and loud speakers were installed at three spots where hiking trails cross the debris flow channel. The early warning system is managed and maintained by Illgraben Security Commission and contacts local emergency task forces if potentially dangerous situations emerge. The technical system includes several geophones located at check dams, which can automatically trigger warning lights and speakers further down the debris channel if a seismic signal lasts for more than five seconds. At the same time SMS and emails are sent to local decision makers. A forewarn time of 5 to 15 min between measurement of debris flow by geophones and a debris flow reaching settlement areas in the valley is provided by the system. Alarms can be cancelled if geophones further downslope do not detect seismic signals 10 min after the first signal. This is done to decrease chances of false alarms due to other potential geophone triggers, e.g., rock fall, thunderstorms or earthquakes. Further technical equipment of the Illgraben monitoring systems includes measurement of discharge by ultrasonic sensors, laser and radar. Based on their experiences Badoux et al. (2009) propose radar as the most suitable method for early warning, as it provides smooth and reliable data on discharge even in situations of rapidly fluctuating discharge amounts. The catchment is visited and mapped regularly to detect changes in the debris flow source area, such as landslides that provide material for further debris flow occurrences. Including meteorological forecasts into the early warning systems and defining rainfall thresholds was also trialled. However, integration failed because local thunderstorms in alpine areas are difficult to predict. The debris flow early warning system at the Illgraben can be regarded successful. Since its implementation 20 alarms were issued, of which only one was a false alarms, and in only three cases a warning was cancelled even though the debris flow had not stopped. The Illgraben catchment is also part of the national IFKIS-Hydro early warning and information platform, which provides monitoring data and event documentation (Romang et al. 2010).

In the North Italian community of Nals a local debris flow early warning system was installed after devastating debris flow events in 2000 (Egger and Mair 2009). The aim of the early warning system was to be an addition to structural protection measures. Debris flow material is supplied by landslide processes in the upper catchment. However, due to the high activity it was decided not to install an automatic system there, but to place a series of geophones into the debris flow channel to detect already initiated events. Still, a forewarn time of 20 to 60 min

between a geophone alarm and the debris reaching settled areas is accomplished. Further technical equipment includes a piezometer, rainfall stations and a remote controlled video camera with flood lights.

Another Italian case study on a debris flow warning system utilising geophones is presented by Arattano (1999), however, it only was active for one summer.

A prototype of a mudflow early warning system for the Italian city Sarno is described by Sirangelo and Braca (2004). Therein, the probabilistic hydrology model FLaIR (Forecasting of Landslides Induced by Rainfall) was applied, which correlates rainfalls with landslide occurrence. Warning thresholds were established by back analysis and included the large 1998 event. According to these thresholds three warning levels were determined, i.e. attention, alert and alarm.

The same model has been applied to Lanzo Valley of the Piedmont, Italy (Capparelli and Tiranti 2010). Promising performance led to the current implementation of an automatic early warning system.

Hübl (2000) describes the application of a prototypic early warning system for the Wartschenbach catchment in Austria, which frequently experiences debris flows and flash flood events. The developed early warning system is thought as a passive protection measure. The technical system is based on measurement of rainfall and flow discharge by ultrasonic sensors in the upper catchment. If measurements exceed pre-defined thresholds it is up to experts to decide whether to close lower lying roads to prevent cars being hit by debris flows. By developing adequate response plans for hazardous events they have tried to address the response of the local community. The implemented system was planned and implemented as a prototype and should be installed in other catchments which could potentially produce debris flows after a test period.

A novel a landslide early warning system is described by Sakai (2008). Earlier research (Sakai and Tarumi 2000) indicated that concentrations of sodium, calcium and, sulphate ions in groundwater changed before phases of landslide activity. Landslide failures could be predicted up to 90 days in advance. Therefore, a prototypic landslide early warning system was set up which utilises automated ion-selective electrodes to provide early warning to railroads in Japan. Data is transmitted from the sensors in the field to train dispatchers and track maintenance engineers via mobile phone networks. Measurements are taken every 1 to 3 days, but frequency can be increased in the case of unusual sensor readings.

Another example of an early warning system in Japan is presented by Chiba (2009). The warning system strongly emphasises warning communication and is regarded as an integral element of the local disaster prevention program against sediment-related processes (debris flows and debris floods). Earlier research on local hazards provided information on potential hazardous zones and return periods, which was utilised to allocate warning and evacuation zones in the occurrence of debris flow events. Several people were employed to carry out education programs in which local residents were informed about potential hazards and appropriate reactions in case of a warning. If exceedance of pre-defined river flow thresholds occurs a disaster management headquarter is assigned in which all information about the current hazard status is collected. Information is gathered

primarily by the employees by calling local residents by cell phone. Moreover, all data is updated to a GIS platform which is available online. Chiba (2009) illustrates the effectiveness of the warning system by comparing its performance to a neighbouring town, in which no early warning system was installed, and no detailed hazard maps and evacuation plans were available. During a debris flow event local disaster managers were overwhelmed by incoming information and no efficient evacuation could be initialised. In contrast, disaster managers of the town with a warning system were able to quickly determine where debris flows had occurred and to initialise evacuation according to the pre-determined schemes.

Flentje et al. (2005) present a real-time monitoring network for time pore water pressure, slope movement and rainfall in Wollongong, Australia, which aims to enhance understanding of landslide triggering process and improve quantitative assessment of landslide hazards. All data is automatically sent via a cell phone network to a web-based database available online. Threshold values have been determined and current measurements are colour-coded to allow for easy interpretation. However, the described system is essentially technical and does not aim to provide warning messages or initiate counter measures or evacuation.

Besides the ILEWS project several other research programs focussing on early warning systems for natural hazards were funded within the Geotechnologien framework. Three of these projects also concentrated on landslide processes, and will briefly be described in the following.

The SLEWS (Sensor-based Early Warning System) project focused on three sensor types measuring acceleration, inclination and pressure to monitor landslide initiation (Fernandez-Steeger et al. 2009). The project emphasized technological developments accounted for sensor development and laboratory testing. A large proportion of the accomplished work concentrated on wireless sensor networks to ensure smooth data transmission. Developed sensors were applied to several real case studies on the Barcolonette earthflow in France, and rockfall warning in Rathen, Germany. However, besides the technical research, the integration of early warning in social decision making process was another topic of the SLEWS project.

The main goal of the alpEWAS project was sensor-based monitoring and early warning in the Bavarian Alps (Singer et al. 2009; Thuro et al. 2009). Thereto, three main methods were utilised to detect displacements, i.e. TDR measurements, prism-less tachymetrie and low-cost GPS measurements. In addition, an information platform was set up to collect all data and inform involved experts by email and SMS if pre-defined thresholds were exceeded.

The EGIFF project adopted a technical approach and concentrated on the development of new methods applicable within landslide early warning. A wide range of geotechnical data for a test slope south of Munich, Germany, was compiled and modelled by a finite element model (Breunig et al. 2009). In addition, 3D/4 D databases were developed for effective data visualisation. Moreover, the project implemented an automated system to interpret media news and extract landslide related information.

From the examples of landslide early warning systems illustrated above some conclusions can be drawn. Regional landslide early warning systems that focus on shallow landslides or debris flows generally rely on rainfall thresholds derived by

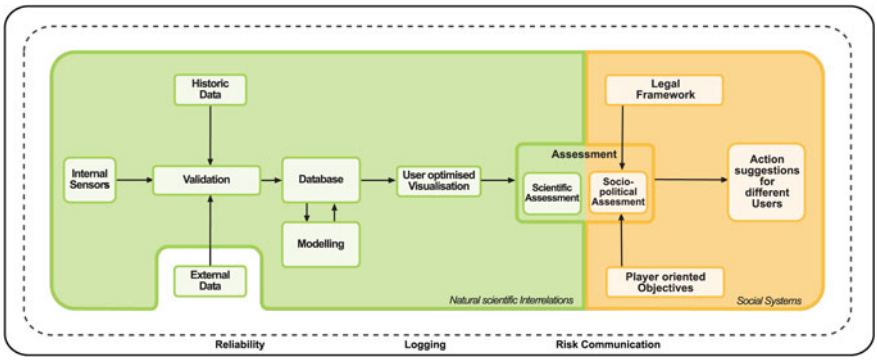

Fig. 2.11 General structure of ILEWS project (Bell et al. 2009)

empirical or physically-based methods. In some cases local test slopes are equipped with monitoring systems to improve understanding of landslide triggering and consequently modify rainfall thresholds. Innovative approaches try to integrate sophisticated slope stability models and real time modelling of landslide initiation Local landslide early warning systems however are installed for a wider range of processes. For debris flows technical early warning systems can be fairly simple because it may take several minutes until an initiated debris flow reaches settled areas. Forewarn time for other landslide processes is often shorter and early warnings are more complex. For deep-seated landslides and failures in rock more complex monitoring is applied to measure displacements and processes related to movement triggering. Warning thresholds may account for displacement or critical parameter values of triggering factors. Modelling of slope behaviour by complex slope stability models is an important part of landslide prediction and is frequently applied for landslide early warning. Most landslide early warning system are not fully automated but leave judgment of the current situation and final warning to experts. Existing landslide early warning systems differ substantially regarding the integration of social aspects. In some cases landslide early warning is integrated into larger schemes for slope safety, risk management, disaster prevention and hazard awareness, while other systems constitute simple technical approaches.

2.5 The ILEWS Project

The work described within this thesis is embedded into the ILEWS project (Integrative Landslide Early Warning Systems) which will be briefly introduced in the following. Integrativity therein does not only refer to a strong interdisciplinary and cooperative work between the project partners, but also to involvement of social sciences aiming to cooperatively embed early warning into the prevalent political

structures. Some results are presented in Chap. 7; more detailed information is provided in Bell et al. (2010). The ILEWS project was funded by the German Federal Ministry of Education and Research (BMBF) and integrated into the Geotechnologien research program. The project started in 2007 and ran for three years.

It is important to note that the research carried out in the ILEWS project partly overlaps with the topics of this thesis; however, several aspects are investigated in more detail in this work while other aspects are not covered. While the analysis of slope movement and hydrological monitoring data, and subsequent development of landslide early warning models are main goals of this thesis, the ILEWS project had a wider scope. The overall goal of the ILEWS project was to develop and implement a transferable early warning concept starting with sensors in the field and modelling of early warning, and ending with user-optimized action advice embedded in a holistic risk management strategy. To address the multiple issues arising from such a comprehensive approach project partners from various scientific backgrounds participated in the project, i.e. sensor technology, geoinformation, geomorphology, geodesy, history, social geography and spatial planning. Altogether, 10 research partners cooperated within the ILEWS project, of which five were private companies, and five university research groups. The general structure of the ILEWS project is illustrated in Fig. 2.11.

The project can be distinguished in three clusters, i.e. monitoring, modelling and implementation. However, due to the complex mission of developing and implementing integrative landslide early warning systems and the interlinked workflow of the involved project partners, several tasks were carried out cooperatively.

Within the monitoring cluster the main goals were the prospection, and installation and operation of an adapted monitoring system for hydrology and slope movement on a landslide at the Swabian Alb, South-West Germany. Important milestones of the monitoring cluster include:

- geophysical prospection and development of a technical monitoring system accounting for local geomorphology
- installation of hydrological sensors, inclinometers and geodetic network
- continuous and periodic measurements of hydrology and slope movement
- automated data storage, transmission and web-based visualisation
- development of web-based data management platform allowing for analysis and interpretation
- archival research for analysis of magnitude -frequency characteristics of landslides in the study areas.

The overall goal of the modelling cluster was to analyse the data, and provide reliable information on future slope behaviour based on a range of modelling approaches. Some of the main aims of this cluster were:

- data analysis and validation
- application of empirical-based, physically-based and movement-based models
- integration of models into an early warning system
- modelling of early warning in real-time for both local and regional study areas.

Within the cluster implementation cooperative risk management and end-user optimised warning communication were the main objectives. Other goals include:

- clarification of local and regional demands towards landslide early warning
- integration of warning into the respective social processes of decision making
- cooperative definition of protection goals
- development of alternative risk management strategies.

The objective of ILEWS, to develop and implement an adaptive and integrative landslide early warning concept, was examined by a transfer to two studies of which one is already equipped with a technical system.

References

Abellán A, Calvet J, Vilaplana JM, Blanchard J (2010) Detection and spatial prediction of rock falls by means of terrestrial laser scanner monitoring. Geomorphology 119(3–4):162–171

Abramson LW (2002) Slope stability and stabilization methods. Wiley, New York

Ahnert F (2003) Einführung in die Geomorphologie. Ulmer, Stuttgart

Aleotti P (2004) A warning system for rainfall-induced shallow failures. Eng Geol 73(3–4):247–265

Alexander DE (2000) Confronting catastrophe: new perspectives on natural disasters. Oxford University Press, Oxford

Alexander D (2002) Principles of emergency planning and management, 1st edn. Oxford University Press, Oxford

Amitrano D, Gaffet S, Malet J.-P, Maquaire O (2007) Understanding mudslides through micro-seismic monitoring: the Super-Sauze (South French Alps) case study. Bulletin de la Société Géologique de France 178(2):149–157. Accessed 15 Oct 2010

Anderson MG, Richards K (1987) Modelling slope stability: the complementary nature of geotechnical and geomorphological approaches. In: Anderson MG (ed) Slope stability: geotechnical engineering and geomorphology. Wiley, New York, pp 1–9

Anderson SA, Thallapally LK (1996) Hydrologic response of a steep tropical slope to heavy rainfall. In: Senneset K (ed) Landslides. Seventh international symposium on landslides. Balkema, Rotterdam, pp 1489–1495

Anderson MG, Lloyd DM, Park A, Hartshorne J, Hargraves S, Othman A (1996) Establishing new design dynamic modelling criteria for tropical cut slopes. In: Senneset K (ed) Landslides. Seventh international symposium on landslides. Balkema, Rotterdam, pp 1067–1072

Anderson H, Bengtsson P-E, Berglund C, Larsson C, Larsson R, Sällfors G, Öberg-Högsta A-L (2000) The landslide at Vagnharad in Sweden. In: Bromhead E, Dixon N, Ibsen M-L (eds) Landslides in research, theory and practice. Eighth international symposium on landslides. T. Telford, London, pp 65–70

Anderson M, Holcombe L, Flory R, Renaud J-P (2008) Implementing low-cost landslide risk reduction: a pilot study in unplanned housing areas of the Caribbean. Nat Hazards 47(3):297–315

Angeli M-G, Gasparetto P, Bromhead E (2004) Strength-regain mechanisms in intermittently moving slides. In: Lacerda W, Ehrlich M, Fontoura SAB, Sayao AS (eds) Landslides: evaluation and stabilization. Ninth international symposium on landslides. A.A. Balkema Publishers, Leiden, pp 689–696

Angerer H, Hermann SW, Kittl H, Poisel R, Roth W (2004) Monitoring, mechanics and risk assessrnent of the landslide Lärchberg Galgenwald (Austria). In: Lacerda W, Ehrlich M,

Fontoura SAB, Sayao AS (eds) Landslides: evaluation and stabilization. Ninth international symposium on landslides. A.A. Balkema Publishers, Leiden, pp 821–826
Antonello G, Casagli N, Farina P, Leva D, Nico G, Sieber AJ, Tarchi D (2004) Ground-based SAR interferometry for monitoring mass movements. Landslides 1(1):21–28
Apip K, Takara K, Yamashina S, Ibrahim AB (2009) Study on early warning systems for shallow landslide in the upper Citarum River catchment, Indonesia. In: Annuals of disaster prevention research institute, Kyoto University, Japan (52B), pp 9–17
Apip K, Takara K, Yamashiki Y, Sassa K, Ibrahim AB, Fukuoka H (2010) A distributed hydrological–geotechnical model using satellite-derived rainfall estimates for shallow landslide prediction system at a catchment scale. Landslides 7(3):237–258
Arattano M (1999) On the use of seismic detectors as monitoring and warning systems for debris flows. Nat Hazards 20(2):197–213
Ardizzone F, Cardinali M, Carrara A, Guzzetti F, Reichenbach P (2002) Impact of mapping errors on the reliability of landslide hazard maps. Nat Hazards Earth Syst Sci 2:3–14
Ardizzone F, Cardinali M, Galli M, Guzzetti F, Reichenbach P (2007) Identification and mapping of recent rainfall-induced landslides using elevation data collected by airborne Lidar. Nat Hazards Earth Syst Sci 7:637–650
Ashland FX (2003) Characteristics, causes, and implications of the 1998 Wasatch Front landslides. Utah Geological Survey Special Study, Utah, p 105
Atkinson P, Jiskoot H, Massari R, Murray T (1998) Generalized linear modelling in geomorphology. Earth Surf Proc Land 23(13):1185–1195
Ausilio E, Cairo R, Dente G (2004) Role of viscous soil properties on landslide movement triggered by pore water fluctuations. In: Lacerda W, Ehrlich M, Fontoura SAB, Sayao AS (eds) Landslides: evaluation and stabilization. Ninth international symposium on landslides. A.A. Balkema Publishers, Leiden, pp 1195–1200
Australian Geomechanics Society (2002) Landslide risk management concepts and guidelines. Australian Geomechanics Society sub-committee on landslide risk management, pp 51–70
Avian M, Kellerer-Pirklbauer A, Bauer A (2009) LiDAR for monitoring mass movements in permafrost environments at the cirque Hinteres Langtal, Austria, between 2000 and 2008. Nat Hazards Earth Syst Sci 9:1087–1094
Avila-Olivera JA, Garduño-Monroy VH (2008) A GPR study of subsidence-creep-fault processes in Morelia, Michoacán, Mexico. Eng Geol 100(1–2):69–81
Avolio MV, Di Gregorio S, Mantovani F, Pasuto A, Rongo R, Silvano S, Spataro W (2000) Simulation of the 1992 Tessina landslide by a cellular automata model and future hazard scenarios. Int J Appl Earth Observ Geoinform 2(1):41–50
Ayalew L, Yamagishi H, Ugawa N (2004) Landslide susceptibility mapping using GIS-based weighted linear combination, the case in Tsugawa area of Agano River, Niigata Prefecture, Japan. Landslides 1(1):73–81
Aysen A (2002) Soil mechanics: basic concepts and engineering applications. Taylor & Francis, Vancouver
Badoux A, Graf C, Rhyner J, Kuntner R, McArdell BW (2009) A debris-flow alarm system for the Alpine Illgraben catchment: design and performance. Nat Hazards 49(3):517–539
Baek Y, Koo H, Bae GJ (2004) Study on development monitoring system of slope using the optical fibre sensor. In: Lacerda W, Ehrlich M, Fontoura SAB, Sayao AS (eds) Landslides: evaluation and stabilization. Ninth international symposium on landslides. A.A. Balkema Publishers, Leiden, pp 755–758
Bai Y, Huang R, Ju N, Zhao J, Huo Y (2008) 3DEC stability analysis of high and steep rock slope. J Eng Geol 16(5):592–597
Bak P, Tang C, Wiesenfeld K (1988) Self-organized criticality. Phys Rev A 38(1):364. Accessed 2 Nov 2010
Baldo M, Bicocchi C, Chiocchini U, Giordan D, Lollino G (2009) LIDAR monitoring of mass wasting processes: The Radicofani landslide, Province of Siena, Central Italy. Geomorphology 105(3–4):193–201

Bandis S, Colombini V, Delmonaco G, Margottini C (2000) New typology of low environmental impact consolidation for rockfall prone cliffs through interventions from the underground. In: Bromhead E, Dixon N, Ibsen M-L (eds) Landslides in research, theory and practice. Eighth international symposium on landslides. T. Telford, London, p 107

Barendse MB, Machan G (2009) In-place microelectromechanical system inclinometer strings: evaluation of an evolving technology—Publications index. In: TRB 88th annual meeting compendium of papers DVD. Washington, p 12

Barla G, Amici R, Vai L, Vanni A (2004) Investigation, monitoring and modelling of a landslide in porphyry in a public safety perspective. In: Lacerda W, Ehrlich M, Fontoura SAB, Sayao AS (eds) Landslides: evaluation and stabilization. Ninth international symposium on landslides. A.A. Balkema Publishers, Leiden, pp 623–628

Barton ME, McCosker M (2000) Inclinometer and tiltmeter monitoring of a high chalk cliff. In: Bromhead E, Dixon N, Ibsen M-L (eds) Landslides in research, theory and practice. Eighth international symposium on landslides. T. Telford, London, pp 127–132

Baum RL (2007) Landslide warning capabilities in the United States—2006. In: Proceedings of the first North America landslide conference. Association of Engineering Geologists Special Publication, Vail Colorado, USA, vol 23, pp 1–14

Baum RL, Fleming RW (1991) Use of longitudinal strain in identifying driving and resisting elements of landslides. Geol Soc Amer Bullet 103(8):1121–1132. Accessed 20 Sep 2010

Baum RL, Godt JW (2009) Early warning of rainfall-induced shallow landslides and debris flows in the USA. Landslides 7(3):259–272

Baum RL, Coe JA, Godt JW, Harp EL, Reid ME, Savage WZ, Schulz WH, Brien DL, Chleborad AF, McKenna JP, Michael JA (2005a) Regional landslide-hazard assessment for Seattle, Washington, USA. Landslides 2(4):266–279

Baum RL, Godt JW, Harp EL, McKenna JP, McMullen SR (2005b) Early warning of landslide for rail traffic between Seattle and Washington. In: Hungr O, Fell R, Couture R, Eberhardt E (eds) International conference on landslide risk management. Taylor & Francis Ltd, Vancouver, p 731

Bell R (2007) Lokale und regionale Gefahren- und Risikoanalyse gravitativer Massenbewegungen an der Schwäbischen Alb. University of Bonn, Germany

Bell R, Glade T, Thiebes B, Jäger S, Krummel H, Janik M, Holland R (2009) Modelling and web processing of early warning. In: Malet J-P, Remaître A, Bogaard T (eds) Landslide processes, From geomorphic mapping to dynamic modelling. CERG Editions, Strasbourg, pp 249–252

Bell R, Mayer J, Pohl J, Greiving S, Glade T (2010) Integrative Frühwarnsysteme für Gravitative Massenbewegungen (ILEWS)—Monitoring, Modellierung, Implementierung. Klartext, Essen

Berardi R, Mercurio G, Bartolini P, Cordano E (2005) Dynamics of saturation phenomena and landslide triggering by rain infiltration in a slope. In: Hungr O, Fell R, Couture R, Eberhardt E (eds) International conference on landslide risk management. Taylor & Francis Ltd., Vancouver, pp 212–219

Bichler A, Bobrowsky P, Best M, Douma M, Hunter J, Calvert T, Burns R (2004) Three-dimensional mapping of a landslide using a multi-geophysical approach: the Quesnel Forks landslide. Landslides 1(1):29–40

Bjerrum L (1967) Progressive failure in slopes of over consolidated plastic clay and clay shales. J Soil Mech Found Div Amer Soc Civil Eng 93:1–49

Blackburn JT, Dowding CH (2004) Finite-element analysis of time domain reflectometry cable-grout-soil interaction. J Geotech Geoenviron Eng 130(3):231–239

Bláha P (1996) Geoacoustic method and slope deformations. In: Senneset K (ed) Landslides. Seventh international symposium on landslides. Balkema, Rotterdam, pp 1521–1524

Blikra LH (2008) The Aknes rockslide; monitoring, threshold values and early-warning. In: Landslides and engineered slopes. From the past to the future proceedings of the tenth international symposium on landslides and engineered slopes. pp 1089–1094

Bloyet J, Beghoul N, Ricard Y, Froidevaux C (1989) In situ test of a borehole extensometer. Rock Mech Rock Eng 22(4):289–297. Accessed 11 Oct 2010

Bogaard T (2000) The slope movements within the Mondorès graben (Drôme, France); the interaction between geology, hydrology and typology. Eng Geol 55(4):297–312. Accessed 20 Sep 2010

Bonnard C (2008) Introduction to Lanslide: mechanisms of landslides and specificities of large landslides. Presentation at laram summer school, Ravello, Italy, 2008

Bonnard C, Noverraz F, Dupraz H (1996) Long-term movement of substabilized versants and climatic changes in the Swiss Alps. In: Senneset K (ed) Landslides. Seventh international symposium on landslides. Balkema, Rotterdam, pp 1525–1530

Bonnard C, Tacher L, Beniston M (2008) Prediction of landslide movements caused by climate change: modelling the behaviour of a mean elevation large slide in the Alps and assessing its uncertainties. In: Proceedings of the tenth international symposium on landslides and engineered slopes (Volume 1)

Booth AM, Roering JJ, Perron JT (2009) Automated landslide mapping using spectral analysis and high-resolution topographic data: Puget Sound lowlands, Washington, and Portland Hills, Oregon. Geomorphology 109(3–4):132–147

Borgatti L, Corsini A, Barbieri M, Sartini G, Truffelli G, Caputo G, Puglisi C (2006) Large reactivated landslides in weak rock masses: a case study from the Northern Apennines (Italy). Landslides 3(2):115–124

Bovis MJ (2004) Failure. In: Goudie A (ed) Encyclopedia of geomorphology. Taylor & Francis, Routledge, pp 360–361

Bozzano F, Gaeta M, Scarascia GM, Valentini G (2000) Numerical modelling of slopes surrounding ignimbrite plateaux. In: Bromhead E, Dixon N, Ibsen M-L (eds) Landslides in research, theory and practice. Eighth international symposium on landslides. T. Telford, London, p 177

Bozzano F, Mazzanti P, Prestininzi A, Scarascia Mugnozza G (2010) Research and development of advanced technologies for landslide hazard analysis in Italy. Landslides 7(3):381–385

Brand EW, Premchitt J, Philipson HB (1984) Relationship between rainfall and landslides in Hong Kong. In: Proceedings of the fourth international symposium on landslides. Toronto, pp 377–384

Brandon TL, Wright SG, Duncan JM (2008) Analysis of the stability of I-Walls with Gaps between the I-Wall and the Levee Fill. J Geotech Geoenviron Eng 134(5):692

Brennecke M (2006) Erstellung einer Inventarkarte gravitativer Massenbewegungen an der Schwäbischen Alb—Kartierung aus Luftbildern und einem digitalen Höhenmodell. University of Bonn, Germany

Brenning A (2005) Spatial prediction models for landslide hazards: review, comparison and evaluation. Nat Hazards Earth Syst Sci 5(6):853–862

Bressani LA, Pinheiro RJB, Eisenberger CN, Soares JMD (2008) Movements of a large urban slope in the town of Santa Cruz do Sul (RGS), Brazil. Landslides Eng Slopes. From the Past to the Future 1:293–298

Breunig M, Schilberg B, Kupfer PV, Jahn M, Reinhardt W, Nuhn E, Boley C, Trauner F-X, Wiesel J, Richter D, Abecker A, Gallus D, Kazakos W, Bartels A (2009) EGIFF—Developing advanced GI methods for early warning in mass movement scenarios. In: Stroink L (ed) Geotechnologien science report 13. Early warning system in earth management. pp 49–72

Bromhead EN (1998) Stability of slopes. Taylor & Francis, Routledge

Bromhead E, Huggins M, Ibsen M-L (2000) Shallow landslides in Wadhurst clay at Robertsbridge, Sussex, UK. In: Bromhead E, Dixon N, Ibsen M-L (eds) Landslides in research, theory and practice. Eighth international symposium on landslides. T. Telford, London, pp 183–188

Brooks SM, Crozier MJ, Glade TW, Anderson MG (2004) Towards establishing climatic thresholds for slope instability: use of a physically-based combined soil hydrology-slope stability model. Pure Appl Geophys 161(4):881–905

Brunetti MT, Peruccacci S, Rossi M, Luciani S, Valigi D, Guzzetti F (2010) Rainfall thresholds for the possible occurrence of landslides in Italy. Nat Hazards Earth Syst Sci 10:447–458

Bull WB (1991) Geomorphic responses to climatic change. Oxford University Press, Oxford

Buma J (2000) Finding the most suitable slope stability model for the assessment of the impact of climate change on a landslide in southeast France. Earth Surf Proc Land 25(6):565–582
Burghaus S, Bell R, Kuhlmann H (2009) Improvement of a terrestric network for movement analysis of a complex landslide. Presentation at FIG conference, Eilat, Israel, 2009
Burns SF, Harden TM, Andrew CJ (eds) (2008) Homeowner's guide to landslides—Recognition, prevention, control and mitigation. Portland State University, Portland
Caine N (1980) The rainfall intensity: duration control of shallow landslides and debris flows. Geografiska Annaler. Series A, Phys Geog 62(1/2):23–27. Accessed 18 Oct 2010
Cala M, Flisiak J, Tajdus A (2004) Slopc stability analysis with modified shear strength reduction technique. In: Lacerda W, Ehrlich M, Fontoura SAB, Sayao AS (eds) Landslides: evaluation and stabilization. Ninth international symposium on landslides. A.A. Balkema Publishers, Leiden, pp 1085–1090
Calcaterra D, Parise M, Palma B (2003) Combining historical and geological data for the assessment of the landslide hazard: a case study from Campania, Italy. Nat Hazards Earth Syst Sci 3:3–16
Calcaterra D, Ramondini M, Calò F, Longobardi V, Parise M, Galzerano CM (2008) DInSAR techniques for monitoring slow moving-landslides. In: Chen Z, Zhang J-M, Ho K, Wu F-Q, Li Z-K (eds) Landslides and engineered slopes. From the Past to the Future Proceedings of the tenth international symposium on landslides and engineered slopes. pp 1089–1094
California Geological Survey (2003) Hazards from "Mudslides"…Debris Avalanches and Debris flows in Hillslide and Wildfire Areas. U.S. Geological Survey Open File Report 2006-1064
Calvello M, Cascini L, Sorbino G (2008) A numerical procedure for predicting rainfall-induced movements of active landslides along pre-existing slip surfaces. Int J Numer Anal Meth Geomech 32(4):327–351
Campbell RH (1975) Soil slips, debris flows, and rainstorms in the Santa Monica Mountains and vicinity, Southern California. US Geological Survey Professional Paper 851
Cannon SH, Ellen SD (1988) Rainfall that resulted in abundant debris flow activity during the storm. In: Ellen SD, Wieczorek GF (eds) Landslides, floods, and marine effects of the storm of January 3–5, 1982. US Geological Survey Professional Paper, San Francisco Bay region, California, pp 27–33
Canuti P, Casagali N, Moretti S, Leva D, Sieber AJ, Tarchi D (2002) Landslide monitoring by using ground-based radar differential interferometry. In: Rybár J, Stemberk J, Wagner P (eds) First European conference on landslides. Balkema Publishers, Czech Republic, pp 523–528
Capparelli G, Tiranti D (2010) Application of the MoniFLaIR early warning system for rainfall-induced landslides in Piedmont region (Italy). Landslides 4(7):401–410
Capparelli G, Biondi D, De Luca DL, Versace P (2009) Hydrological and complete models for forecasting landslides triggered by rainfalls. In: Rainfall–induced landslides. Mechanisms monitoring techniques and nowcasting models for early warning systems. Proceedings of the first Italian workshop on landslides. pp 8–10
Cardinali M, Reichenbach P, Guzzetti F, Ardizzone F, Antonini G, Galli M, Cacciano M, Castellani M, Salvati P (2002) A geomorphological approach to the estimation of landslide hazards and risks in Umbria, Central Italy. Nat Hazards Earth Syst Sci 2(1/2):57–72
Carey JM, Moore R, Petley DN, Siddle HJ (2007) Pre-failure behaviour of slope materials and their significance in the progressive failure of landslides. In: McInnes R, Jakeways J, Fairbank H, Mathie E (eds) Landslide and climate change—Challenges and solutions. Taylor & Francis, Routledge, pp 217–226
Carrara A (1983) Multivariate models for landslide hazard evaluation. Math Geol 15(3):403–426
Carrara A, Cardinali M, Guzzetti F (1992) Uncertainty in accessing landslide hazard risk. ITC J 2:172–183
Carrara A, Guzzetti F, Cardinali M, Reichenbach P (1999) Use of GIS technology in the prediction and monitoring of landslide hazard. Nat Hazards 20(2):117–135
Carrara A, Crosta G, Frattini P (2003) Geomorphological and historical data in assessing landslide hazard. Earth Surf Proc Land 28(10):1125–1142

Cartlidge E (2010) Scientists face trial over L'Aquila quake. http://physicsworld.com/cws/article/news/43001. Accessed 13 Sep 2010
Casadei M, Dietrich WE, Miller NL (2003) Testing a model for predicting the timing and location of shallow landslide initiation in soil-mantled landscapes. Earth Surf Proc Land 28(9):925–950
Casagali N, Farina P, Leva D, Tarchi D (2004) Landslide monitoring on the Stromboli volcano through SAR interferometry. In: Lacerda W, Ehrlich M, Fontoura SAB, Sayao AS (eds) Landslides: evaluation and stabilization. Ninth international symposium on landslides. A.A. Balkema Publishers, Leiden, pp 803–808
Casagli N, Rinaldi M, Gargini A, Curini A (1999) Pore water pressure and stream bank stability: results from a monitoring site on the Sieve River, Italy. Earth Surf Proc Land 24(12):1095–1114
Casagli N, Catani F, Del Ventisette C, Luzi G (2010) Monitoring, prediction, and early warning using ground-based radar interferometry. Landslides 7(3):291–301
Cascini L, Cuomo S, Pastor M (2008) The role played by mountain tracks on rainfall-induced shallow landslides: a case study. In: Proceedings of the iEMSs fourth biennial meeting: International congress on environmental modelling and software (iEMSs 2008). 7–10 July 2008, Barcelona, Spain, pp 1484–1491
Cássia de Brito Galvão T, Parizzi MG, Sobreira FG, Elmiro T, Beirigo EA (2007) Landslide in Belo Horizonte, Brazil
Catani F, Casagli N, Ermini L, Righini G, Menduni G (2005) Landslide hazard and risk mapping at catchment scale in the Arno River basin. Landslides 2(4):329–342
Chan RKS (2007) Challenges in slope engineering in Hong Kong. In: Proceedings of the sixteenth southeast Asian geotechnical conference, Southeast Asian Geotechnical Society, Malaysia. pp 137–151
Chan RKS, Pang PLR, Pun WK (2003) Recent developments in the landslip warning system in Hong Kong. In: Proceedings of the fourteenth Southeast Asian geotechnical conference, Southeast Asian Geotechnical Society, Hong Kong, pp 219–224
Chandler RJ (1991): Slope stability engineering: developments and applications? In: Proceedings of the international conference on slope stability. Thomas Telford, London
Chang K-T, Wan S, Lei T-C (2010) Development of a spatial decision-support system for monitoring earthquake-induced landslides based on aerial photographs and the finite element method. Int J Appl Earth Observ Geoinform 12(6):448–456. Accessed 27 Oct 2010
Chen SG, Cai JG, Zhao J, Zhou YX (2000) Discrete element modelling of an underground explosion in a jointed rock mass. Geotech Geol Eng 18(2):59–78
Cheng YM, Lau CK (2008) Slope stability analysis and stabilization: new methods and insight. Taylor & Francis, Routledge
Cheng DX, Pan W, Liu DA, Feng SR, Guo HF, Ding EB (2006) 3 DEC modeling of equivalent mechanical parameters in anchored jointed rock mass. Yantu Lixue (Rock and Soil Mechanics) 27(12):2127–2132
Cheung PY, Wong MC, Yeung HY (2006) Application of rainstorm nowcast to real-time warning of landslide hazards in Hong Kong. In: WMO PWS workshop on warnings of real-time hazards by using nowcasting technology. pp 9–13
Chiang S, Chang K (2009) Application of radar data to modeling rainfall-induced landslides. Geomorphology 103(3):299–309
Chiba M (2009) Warning and evacuation in response to sediment-related disasters. Nat Hazards 2(56):499–507
Chigira M, Duan F, Yagi H, Furuya T (2004) Using an airborne laser scanner for the identification of shallow landslides and susceptibility assessment in an area of ignimbrite overlain by permeable pyroclastics. Landslides 1(3):203–209
Chigira M, Wu X, Inokuchi T, Wang G (2010) Landslides induced by the 2008 Wenchuan earthquake, Sichuan, China. Geomorphology 3–4(118):225–238
Ching-Chuan H, Yih-Jang J, Lih-Kang H, Jin-Long L (2009) Internal soil moisture and piezometric responses to rainfall-induced shallow slope failures. J Hydrol 370(1–4):39–51

Chleborad AF (2000) Preliminary method for anticipating the occurrence of precipitation-induced landslides in Seattle, Washington. U.S. Geological Survey Open-File Report 03-463

Chleborad AF (2003) Preliminary evaluation of a precipitation threshold for anticipating the occurrence of landslides in the Seattle, Washington, area. U.S Department of the Interior, U.S. Geological Survey, Denver

Chleborad AF, Baum RL, Godt JW (2006) Rainfall thresholds for forecasting landslide in the seattle. Washington, Area—Exceedance and probability. U.S. Geological Survey Open File Report 2006-1064

Chok YH, Kaggwa W, Jaksa MB, Griffiths DV (2004) Modelling the effects of vegetation on stability of slopes. In: Proceedings of the ninth Australia New Zealand conference on geomechanics. Auckland, New Zealand, pp 391–397

Chorley RJ, Kennedy BA (1971) Physical geography—A systems approach. Prentice-Hall, London

Chugh AK, Stark TD (2005) Permanent seismic deformation analysis of a landslide. Landslides 3(1):2–12

Chung CJ (2006) Using likelihood ratio functions for modeling the conditional probability of occurrence of future landslides for risk assessment. Comput Geosci 32(8):1052–1068

Chung CJ, Fabbri AG (1999) Probabilistic prediction models for landslide hazard mapping. Photogrammetric Eng Remote Sensing 65(12):1389–1399

Chung C, Fabbri AG, Van Westen CJ (1995) Multivariate regression analysis for landslide hazard zonation. In: Carrara A, Guzzetti F (eds) Geographical information systems in assessing natural hazards. Kluwer Academic Publishers, Dordrecht, pp 107–134

Claessens L, Heuvelink GBM, Schoorl MJ, Veldkamp A (2005) DEM resolution effects on shallow landslide hazard and soil redistribution modelling. Earth Surf Proc Land 30:461–477

Clark AR, Moore R, Palmer JS (1996) Slope monitoring and early warning systems: Application to coastal landslide on the south and east coast of England, UK. In: Senneset K (ed) Landslides. Seventh international symposium on landslides. Balkema, Rotterdam, pp 1531–1538

Clark AR, Fort D, Davis GM (2000) The strategy, management and investigation of coastal landslides at Lyme Regis, Dorset. In: Bromhead E, Dixon N, Ibsen M-L (eds) Landslides in research, theory and practice. Eighth international symposium on landslides. T. Telford, London, pp 279–286

Colesanti C, Wasowski J (2004) Satellite SAR interferometry for wide-area slope hazard detection and site-specific monitoring of sloe landslides. In: Lacerda W, Ehrlich M, Fontoura SAB, Sayao AS (eds) Landslides: evaluation and stabilization. Ninth international symposium on landslides. A.A. Balkema Publishers, Leiden, pp 795–802

Collison AJC, Anderson MG (1996) Using a combined slope hydrology/stability model to identify suitable conditions for landslide prevention by vegetation in the humid tropics. Earth Surf Proc Land 21(8):737–747

Comegna L, Urciuoli G, Picarelli L (2004) The role of pore pressures on the mechanics of mudslides. In: Lacerda W, Ehrlich M, Fontoura SAB, Sayao AS (eds) Landslides: evaluation and stabilization. Ninth international symposium on landslides. A.A. Balkema Publishers, Leiden, pp 1183–1188

Conolly H (1997) World wide web pages for slope design. School of Engineering, University of Durham, UK

Cornforth DH, Mikkelsen PE (1996) Continuous monitoring of the slope above an excavation within a marginally stable landslide. In: Senneset K (ed) Landslides. Seventh international symposium on landslides. Balkema, Rotterdam, pp 1539–1544

Costa-Cabral MC, Burges SJ (1994) Digital elevation model networks (DEMON): a model of flow over hill slopes for computation of contributing and dispersal areas. Water Resour Res 30(6):1681–1692. Accessed 26 Oct 2010

Cotza G (2009) Geologische und geotechnische Verhältnisse der Massenbewegungen bei Pontives (Grödnertal, Südtirol). University of Vienna, Austria

Coulomb CA (1776) Essai sur une application des regles des maximis et minimis a quelques problemes de statique relatifs a l'architecture. Memoires de l'Academie Royale pres Divers Savants 7:343–387

Cristescu N (1989) Rock rheology. Springer, Berlin

Crosta G (1998) Regionalization of rainfall thresholds: an aid to landslide hazard evaluation. Env Geol 35(2):131–145

Crosta GB, Frattini P (2003) Distributed modelling of shallow landslides triggered by intense rainfall. Nat Hazards Earth Syst Sci 3:81–93

Crosta GB, Frattini P (2008) Rainfall-induced landslides and debris flows. Hydrol Process 22(4):473–477

Crozier MJ (1989) Landslides: causes, consequences and environment. Taylor & Francis, Routledge

Crozier MJ (1999) Prediction of rainfall-triggered landslides: a test of the antecedent water status model. Earth Surf Proc Land 24(9):825–833

Crozier MJ, Eyles RJ (1980) Assessing the probability of rapid mass movement. In: Proceedings of the third Australia and New Zealand conference on Geomechanics. New Zealand Institute of Engineers, pp 247–251

Crozier MJ, Glade T (2005) Landslide hazard and risk: issues, concepts, and approach. In: Glade T, Anderson M, Crozier MJ (eds) Landslide hazard and risk. Wiley, New York, pp 1–40

Crozier MJ, Preston NJ (1999) Modelling changes in terrain resistance as a component of landform evolution in unstable hill country. In: Hergarten S, Neugebauer HJ (eds) Process modelling and landform evolution. Springer, Berlin, pp 267–284

Cruden DM (1991) A very simple definition for a landslide. IAEG Bulletin, pp 27–29

Cruden DM, Varnes DJ (1996) Landslide types and processes. In: Turner AK, Schuster RL (eds) Landslides: investigation and mitigation (Special Report). Washington, DC, USA: National Research Council, Transportation and Research Board Special Report 247, pp 36–75

Cundall PA, Strack ODL (1979) A discrete numerical model for granular assemblies. Géotechnique 29(1):47–65

D'Ambrosio D, Di Gregorio S, Iovine G, Lupiano V, Rongo R, Spataro W (2003) First simulations of the Sarno debris flows through cellular automata modelling. Geomorphology 54(1–2):91–117

D'Orsi R (2006) Alerta Rio—The Rio de Janeiro warning system against severe weather and mass movements. Presentation at laram summer school, Ravello, Italy, 2006

D'Orsi R, Feijo RL, Paes NM (2004) 2,500 operational days of Alerta Rio System—History. In: Lacerda W, Ehrlich M, Fontoura SAB, Sayao AS (eds) Landslides: evaluation and stabilization. Ninth international symposium on landslides. A.A. Balkema Publishers, Leiden, pp 549–555

Dai FC, Lee CF (2003) A spatiotemporal probabilistic modelling of storm-induced shallow landsliding using aerial photographs and logistic regression. Earth Surf Proc Land 28(5):527–545

Dai Z-Y, Liu Y, Zhang L-X, Ou Z-H, Zhou C, Liu Y-Z (2008) Landslide monitoring based on high-resolution distributed fiber optic stress sensor. J Electron Sci Technol China 6(4):416–419

Dearing J (2004) Non-linear dynamics. In: Goudie A (ed) Encyclopedia of Geomorphology. Taylor & Francis, Routledge, pp 721–725

Deb SK, El-Kadi AI (2009) Susceptibility assessment of shallow landslides on Oahu, Hawaii, under extreme-rainfall events. Geomorphology 108(3–4):219–233. Accessed 10 Sep 2010

Demoulin A, Chung CJ (2007) Mapping landslide susceptibility from small datasets: A case study in the Pays de Herve (E Belgium). Geomorphology 89(3–4):391–404

Deparis J, Fricout B, Jongmans D, Villemin T, Effendiantz L, Mathy A (2008) Combined use of geophysical methods and remote techniques for characterizing the fracture network of a potentially unstable cliff site (the 'Roche du Midi', Vercors massif, France). J Geophys Eng 5:147

Derron MH, Blikra LH, Jaboyedoff M (2005) High resolution digital elevation model analysis for landslide hazard assessment (Åkerneset, Norway). In: Senneset K, Flaate K, Larsen JO (eds)

Landslide and Avalanches. ICFL 2005, Norway. Taylor & Francis Group, London, pp 101–106
Dewitte O, Chung C, Demoulin A (2006) Reactivation hazard mapping for ancient landslides in West Belgium. Nat Hazards Earth Syst Sci 6(4):653–662
Dhakal G, Yoneda T, Kato M, Kaneko K (2002) Slake durability and mineralogical properties of some pyroclastic and sedimentary rocks. Eng Geol 65(1):31–45
Di Maio C, Onorati R (2000) Influence of pore liquid composition on the shear strength of an active clay. In: Bromhead E, Dixon N, Ibsen M-L (eds) Landslides in research, theory and practice. Eighth international symposium on landslides. T. Telford, London, pp 463–468
Die Zeit H (2010) Erdbeben in Italien: "Trinken Sie lieber einen!". http://www.zeit.de/2010/37/T-Erdbeben. Accessed 13 Sep 2010
Dietrich WE, Real de Asua R, Coyle1 J, Orr B, Trso M (1998) A validation study of the shallow slope stability model, SHALSTAB, in forested lands of Northern California. Stillwater Ecosystem, Watershed & Riverine Sciences, Berkley, USA
Dikau R (2005) Geomorphologische Perspektiven integrativer Forschungsansätze in Physischer Geographie und Humangeographie. In: Wardenga U, Müller-Mahn D (eds) Möglichkeiten und Grenzen integrativer Forschungsansätze in Physischer Geographie und Humangeographie. forum ifl. Leibniz-Institut für Länderkunde, Leipzig, pp 91–108
Dikau R (2006) Komplexe Systeme in der Geomorphologie. Mitteilungen der Österreichischen Geographischen Gesellschaft 148:125–150
Dikau R, Glade T (2003) Nationale Gefahrenhinweiskarte gravitativer Massenbewegungen. In: Liedtke H, Mäusbacher R, Schmidt K-H (eds) Relief, Boden und Wasser. Nationalatlas Bundesrepublik Deutschland. Spektrum Akademischer Verlag, Heidelberg, pp 98–99
Dikau R, Weichselgärtner J (2005) Der unruhige Planet. Der Mensch und die Naturgewalten. 1st ed. Primus Verlag, Darmstadt
Dikau R, Brunsden D, Schrott L (1996) Landslide recognition: identification, movement and causes: identification, movement and courses. Wiley, New York
Dixon N, Spriggs M (2007) Quantification of slope displacement rates using acoustic emission monitoring. Canad Geotech J 44(8):966–976. Accessed 15 Oct 2010
Duncan JM, Wright SG (2005) Soil strength and slope stability. Wiley, New York
Eberhardt E (2003a) Rock slope stability analysis—Utilization of advanced numerical techniques. University of British Columbia, Vancouver
Eberhardt E (2003b) Rock slope stability analysis—Utilization of advanced numerical techniques. University of British Columbia, Vancouver
Eberhardt E, Spillmann T, Maurer H, Willenberg H, Loew S, Stead D (2004) The Randa Rockslide Laboratory: establishing brittle and ductile instability mechanisms using numerical modelling and microseismicity. In: Lacerda W, Ehrlich M, Fontoura SAB, Sayao AS (eds) Landslides: evaluation and stabilization. Ninth international symposium on landslides. A.A. Balkema Publishers, Leiden, pp 481–488
Eberhardt E, Watson AD, Loew S (2008) Improving the interpretation of slope monitoring and early warning data through better understanding of complex deep-seated landslide failure mechanisms. In: Chen Z, Zhang J-M, Ho K, Wu F-Q, Li Z-K (eds) Landslides and engineered slopes: From the past to the future. Proceedings of the tenth international symposium on landslides and engineered slopes. Taylor & Francis, Xi'an, pp 39–51
Eeckhaut MVD, Poesen J, Verstraeten G, Vanacker V, Nyssen J, Moeyersons J, Beek LPH, Vandekerckhove L (2007) Use of LIDAR-derived images for mapping old landslides under forest. Earth Surf Proc Land 32(5):754–769
Egger P, Mair V (2009) Innovative Maßnahmen zur gefahrenreducktion am beispiel Grissianerbach. J für Wildbach-, Lawinen-, Erosion- und Steinschlagschutz 161:1–15
Eidsvig UM, Medina-Cetina Z, Kveldsvik V, Glimsdal S, Harbitz CB, Sandersen F (2011) Risk assessment of a tsunamigenic rockslide at Åknes. Nat Hazards 56(2):529–545
Ekanayake JC, Phillips CJ (1999) A model for determining thresholds for initiation of shallow landslides under near-saturated conditions in the East Coast region, New Zealand. J Hydrol (NZ) 38(1):1–28

Eng HJ, Li W, Ma TH, Li CJ (2009) Geological disasters early warning and forecast information-releasing system: A new generation of releasing system based on ann and gis. J Nat Disasters 18(1):187–193

Fairfield J, Leymarie P (1991) Drainage networks from grid digital elevation models. Water Resour Res 27(5):709–717. Accessed 26 Oct 2010

Fang H-Y (1990) Foundation engineering handbook. Springer, Berlin

Favis-Mortlock D (1998) A self-organizing dynamic systems approach to the simulation of rill initiation and development on hill slopes. Comput Geosci 24(4):353–372

Favis-Mortlock D (2004) Self-organization and cellular automata models. In: Wainwright J, Mulligan M (eds) Environmental modelling: finding simplicity in complexity. Wiley, New York, pp 349–370

Favis-Mortlock D, De Boer D (2003) Simple at heart? Landscape as a self-organizing complex system. In: Trudgill S, Roy A (eds) Contemporary meanings in physical geography. Oxford University Press, Oxford, pp 127–172

Felgentreff C, Glade T (2007) Naturrisiken und Sozialkatastrophen. 1st ed. Spektrum Akademischer Verlag, Heidelberg

Ferentinou MD, Sakellariou M, Matziaris V, Charalambous S (2006) An introduced methodology for estimating landslide hazard for seismic and rainfall induced landslides in a geographical information system environment. In: Nadim F, Pöttler R, Einstein H, Klapperich H, Kramer S (eds) Geohazards Proceedings of the ECI Conference on Geohazards. Lillehammer, Norway, pp 1–8

Fernandez Merodo JA, Pastor M, Mira P, Tonni L, Herreros MI, Gonzalez E, Tamagnini R (2004) Modelling of diffuse failure mechanisms of catastrophic landslides. Comput Methods Appl Mech Eng 193(27–29):2911–2939

Fernandez-Steeger TM, Arnhardt C, Hass S, Niemayer F, Nakaten B, Homfeld SD, Asch K, Azzam R, Bill R, Ritter H (2009) SLEWS—A prototype system for flexible real time monitoring of landslide using on open spatial data infrastructure and wireless sensor networks. In: Geotechnologien Science Report 13. Early Warning System in Earth Management. pp 3–15

Fernández-Steeger TM, Rohn J, Czurda K (2002) Identification of landslide areas with neural nets for hazard analysis. In: Rybár J, Stemberk J, Wagner P (eds) Landslides: Proceedings of the first European conference on landslides, June 24–26, 2002. Taylor & Francis, Czech Republic, pp 163–168

Ferretti A, Prati C, Rocca F, Casagli N, Farina P, Young B (2005) Permanent Scatterers technology: a powerful state of the art tool for historic and future monitoring of landslides and other terrain instability phenomena. In: Hungr O, Fell R, Couture R, Eberhardt E (eds) International conference on landslide risk management. Taylor & Francis Ltd., Vancouver, pp 389–397

Fiorucci F, Cardinali M, Carlà R, Mondini A, Santurri L, Guzzetti F (2010) Comparison of event-based landslide inventory maps obtained interpreting satellite images and aerial photographs. Geophys Res Abstracts 12

Flentje PN, Chowdhury RN, Tobin P, Brizga V (2005) Towards real-time landslide risk management in an urban area. In: Hungr O, Fell R, Couture R, Eberhardt E (eds) International conference on landslide risk management. Taylor & Francis Ltd., Vancouver, pp 741–751

Fonstad MA (2006) Cellular automata as analysis and synthesis engines at the geomorphology-ecology interface. Geomorphology 77(3–4):217–234

Fonstad M, Marcus WA (2003) Self-organized criticality in riverbank systems. Ann Assoc Amer Geographers 93(2):281–296. Accessed 4 Nov 2010

Fourniadis IG, Liu JG, Mason PJ (2007a) Landslide hazard assessment in the Three Gorges area, China, using ASTER imagery: Wushan-Badong. Geomorphology 84(1–2):126–144

Fourniadis IG, Liu JG, Mason PJ (2007b) Regional assessment of landslide impact in the Three Gorges area, China, using ASTER data: Wushan-Zigui. Landslides 4(3):267–278

Franklin JA (1984) Slope instrumentation and monitoring. In: Brunsden D, Prior DB (eds) Slope instability. Wiley, New York, pp 143–170

Frattini P, Crosta G, Sosio R (2009) Approaches for defining thresholds and return periods for rainfall-triggered shallow landslides. Hydrol Process 23(10):1444–1460

Fredlund DG (2007) Slope stability hazard management systems. J Zhejiang Univ Sci A 8(11):1695–1711. Accessed 28 Oct 2010

Freeman T (1991) Calculating catchment area with divergent flow based on a regular grid. Comput Geosci 17(3):413–422

Froese CR, Van der Kooij M, Kosar K (2004) Advances in the application of inSAR to complex, slowly moving landslides in dry and vegetated terrain. In: Lacerda W, Ehrlich M, Fontoura SAB, Sayao AS (eds) Landslides: evaluation and stabilization. Ninth international symposium on landslides. A.A. Balkema Publishers, Leiden, pp 1255–1264

Froese CR, Murray C, Cavers DS, Anderson WS, Bidwell AK, Read RS, Cruden DM, Langenberg W (2005) Development and implementation of a warning system for the South Peak of Turtle Mountain. In: Hungr O, Fell R, Couture R, Eberhardt E (eds) International conference on landslide risk management. Taylor & Francis Ltd., Vancouver, pp 705–712

Froese CR, Carter G, Langenberg W, Morena F (2006) Emergency response planning for a second catastrophic rock slide at Turtle Mountain, Alberta. In: First specialty conference on Disaster Mitigation. Calgary, Canada, pp 1–10

Froese CR, Jaboyedoff M, Pedrazzini A, Hungr O, Moreno F (2009) Hazard mapping for the eastern face of Turtle Mountain, adjacent to the Frank Slide, Alberta, Canada. Landslide Processes, pp 283–289

Fukuzono T (1990) Recent studies on time prediction of slope failure. Landslide News 4:9–12

Furuya G, Sassa K, Fukuoka H, Hiura H, Wang J, Yang Q (2000) Monitoring of slope deformation in Lishan Landsiide, Xi'an, China. In: Bromhead E, Dixon N, Ibsen M-L (eds) Landslides in research, theory and practice. Eighth international symposium on landslides. T. Telford, London, pp 591–596

Gallagher R, Appenzeller T (1999) Beyond reductionism. Science 284(5411):79

Ganerød GV, Grøneng G, Rønning JS, Dalsegg E, Elvebakk H, Tønnesen JF, Kveldsvik V, Eiken T, Blikra LH, Braathen A (2008) Geological model of the Åknes rockslide, Western Norway. Eng Geol 102(1–2):1–18

García A, Hördt A, Fabian M (2010) Landslide monitoring with high resolution tilt measurements at the Dollendorfer Hardt landslide, Germany. Geomorphology 120(1–2):16–25

GEOSE NS (2009) Felsmonitor Winkelgrat. Alarm- und Überwachungssystem zur Sicherung der Kreisstraße 7145 gegen Felssturz. Messsystem- und Softwareentwicklung, Ebringen

Geotechnical Engineering Office ed. (2007) Thirty years of slope safety practice in Hong Kong. Hong Kong, China

Giannecchini R (2006) Relationship between rainfall and shallow landslides in the southern Apuan Alps (Italy). Nat Hazards Earth Syst Sci 6:357–364

Giannecchini R, Naldini D, D'Amato Avanzi G, Puccinelli A (2007) Modelling of the initiation of rainfall-induced debris flows in the Cardoso basin (Apuan Alps, Italy). Quaternary International 171-172, pp 108–117. Accessed 18 Oct 2010

Giraud RE (2002) Movement history and prelimanary hazard assessment of the Heather Drive Landslides, Layton, Davis County, Utah. Utah Geological Survey, Utah Department of Natural Resources, Utah

Gitirana Jr, G (2005) Weather-related geo-hazard assessment model for railway embankment stability. Department of Civil and Geological Engineering, University of Saskatchewan, Saskatoon

Gitirana Jr, G, Santos MA, Fredlund MD (2008) Three-dimensional analysis or the Lodalen Landslide. In: Geosustainability and geohazard mitigation. Proceedings of Geocongress 2008. New Orleans, Louisiana, USA, pp 1–5

Glade T (1997) The temporal and spatial occurrence of rainstorm-triggered landslide events in New Zealand. School of Earth Science Institute of Geography, Victoria University of Wellington, New Zealand

Glade T (1998) Establishing the frequency and magnitude of landslide-triggering rainstorm events in New Zealand. Env Geol 35(2):160–174

Glade T (2000) Modelling landslide-triggering rainfalls in different regions of New Zealand—the soil water status model. Zeitschrift für Geomorphologie Suppl.-Bd. 122:63–84

Glade T (2001) Landslide hazard assessment and historical landslide data—an inseparable couple? In: Glade T, Albini P, Francés F (eds) The use of historical data in natural hazard assessments. Springer, Berlin, pp 153–167

Glade T, Crozier MJ (2005a) A review of scale dependency in landslide hazard and risk analysis. In: Glade T, Anderson M, Crozier MJ (eds) Landslide hazard and risk. Wiley, New York, pp 75–138

Glade T, Crozier MJ (2005b) The nature of landslide hazard impact. In: Glade T, Anderson M, Crozier MJ (eds) Landslide hazard and risk. Wiley, New York, pp 43–74

Glade T, Crozier M, Smith P (2000) Applying probability determination to refine landslide-triggering rainfall thresholds using an empirical "Antecedent Daily Rainfall Model". Pure Appl Geophys 157(6):1059–1079

Glantz MH (2009) Heads Up!: Early Warning Systems for Climate-, Water- And Weather-Related Hazards. United Nations University Press, Tokyo

Glawe U, Lotter M (1996) Time prediction of rocl slope failures based on monitoring results. In: Senneset K (ed) Landslides. Seventh international symposium on landslides. Balkema, Rotterdam, pp 1551–1555

Godt JW, Baum RL, Chleborad AF (2006) Rainfall characteristics for shallow landsliding in Seattle, Washington, USA. Earth Surf Proc Land 31(1):97–110

Gomez C, Lavigne F, Hadmoko DS, Lespinasse N, Wassmer P (2009) Block-and-ash flow deposition: A conceptual model from a GPR survey on pyroclastic-flow deposits at Merapi Volcano, Indonesia. Geomorphology 110(3–4):118–127

Gong QM, Zhao J, Jiao YY (2005) Numerical modeling of the effects of joint orientation on rock fragmentation by TBM cutters. Tunn Undergr Space Technol 20(2):183–191

Graf C, Badoux A, MacArdell B, Dufour F, Rhyner J, Kuntner R (2006) A warning system for natural hazards in summer at the Illgraben. In: Proceedings of the fourth Swiss geoscience meeting. Bern, Switzerland

Graham J (1984) Methods of slope stability analysis. In: Brunsden D, Prior DB (eds) Slope instability. Wiley, New York, pp 171–215

Greco R, Guida A, Damiano E, Olivares L (2010) Soil water content and suction monitoring in model slopes for shallow flowslides early warning applications. Phys Chem Earth 35(3–5):127–136

Greif V, Sassa K, Fukuoka H (2004) Monitoring of rock displacement at Bitchu-Matsuyama Rock Slope in Japan using Linear Variable Differential Transformer (LVDT) Sensors. In: Lacerda W, Ehrlich M, Fontoura SAB, Sayao AS (eds) Landslides: evaluation and stabilization. Ninth international symposium on landslides. A.A. Balkema Publishers, Leiden, pp 773–779

Greiving S, Glade T (2011) Risk governance. In: Bobrowsky P (ed) Encyclopedia of natural hazards. Springer, Berlin

Grøneng G, Christiansen HH, Nilsen B, Blikra LH (2010) Meteorological effects on seasonal displacements of the Åknes rockslide, western Norway. Landslides 1(8):1–15

Gunzberger Y, Merrien-Soukatchoff V, Senfaute G, Piguet J-P (2004) Field investigations, monitoring and modeling in the identification of rock fall causes. In: Lacerda W, Ehrlich M, Fontoura SAB, Sayao AS (eds) Landslides: evaluation and stabilization. Ninth international symposium on landslides. A.A. Balkema Publishers, Leiden, pp 557–563

Guzzetti F, Cardinali M, Reichenbach P, Carrara A (2000) Comparing landslide maps: A case study in the Upper Tiber River Basin, Central Italy. Environ Manag 25(3):247–263. Accessed 7 Oct 2010

Guzzetti F, Reichenbach P, Cardinali M, Galli M, Ardizzone F (2005) Probabilistic landslide hazard assessment at the basin scale. Geomorphology 72(1–4):272–299. Accessed 25 Oct 2010

Guzzetti F, Reichenbach P, Ardizzone F, Cardinali M, Galli M (2006) Estimating the quality of landslide susceptibility models. Geomorphology 81(1–2):166–184

Guzzetti F, Peruccacci S, Rossi M, Stark CP (2007) Rainfall thresholds for the initiation of landslides in central and southern Europe. Meteorol Atmos Phys 98(3–4):239–267

Guzzetti F, Peruccacci S, Rossi M, Stark CP (2008) The rainfall intensity–duration control of shallow landslides and debris flows: an update. Landslides 5(1):3–17

Hadjigeorgiou J, Kyriakou E, Papanastasiou P (2006) A road embankment failure near Pentalia in southwest Cyprus. In: International conference on the stability of Rock Slopes in open pit mining and civil engineering. The South African Institute of Mining and Metallurgy, Cape Town, South Africa, pp 343–352

Häge M, Joswig M (2009) Microseismic study using small arrays in the swarm area of Nový Kostel: increased detectability during an inter-swarm period. Studia Geophysica et Geodaetica 52(4):651–660. Accessed 15 Oct 2010

Hall P (2007) Early warning systems: reframing the discussion. The Australian J Emerg Manag 22(2):32–36. Accessed 12 Oct 2010

Hamm NAS, Hall JW, Anderson MG (2006) Variance-based sensitivity analysis of the probability of hydrologically induced slope instability. Comput Geosci 32(6):803–817

Hammah R, Yacoub T, Curran J (2006) Investigating the performance of the shear strength reduction (SSR) method on the analysis of reinforced slopes. In: Proceedings of the 59th canadian geotechnical and seventh joint CGS/IAH-CNC groundwater specialty conference. Vancouver, British Columbia, Canada

Hammah RE, Yacoub TE, Curran JH (2008) Probabilistic slope analysis with the finite element method. In: Proceedings of the 41st U.S. symposium on rock mechanics and the fourth U.S.-Canada rock mechanics symposium. Asheville, North Carolina, USA

Hammah RE, Yacoub TE, Curran JH (2009) Numerical modelling of slope uncertainty due to rock mass jointing. In: Proceedings of the international conference on rock joints and jointed rock masses. pp 7–8

Hammond C, Hall D, Miller S, Swetik P (1992) Level I stability analysis (LISA). U.S. Department of Agriculture, Forest Service, Intermountain Research Station

Haneberg WC (2004) The ins and outs of airborne LIDAR: An introduction for practicing engineering geologists. AEG News 48(1):16–19

Hart RD (1993) An introduction to distinct element modelling for rock engineering. In: Proceedings of the seventh international congress on rock mechanics. Pergamon Press, Aachen, pp 1881–1892

Hecht S (2001) Anwendung refraktionsseismischer Methoden zur Erkundung des oberflächennahen Untergrundes: Mit acht Fallbeispielen aus Südwestdeutschland. University of Stuttgart, Germany

Heincke B, Maurer H, Green AG, Willenberg H, Spillmann T, Burlini L (2006) Characterizing an unstable mountain slope using shallow 2D and 3D seismic tomography. Geophysics 71(6):241–256

Heincke B, Günther T, Dalsegg E, Ronning JS, Ganerod GV, Elvebakk H (2010) Combined three-dimensional electric and seismic tomography study on the Aknes rockslide in western Norway. J Appl Geophys 70:292–306

Heng M (2008) Comparative study of rock slope stability analysis based on SLOPE/W and fuzzy evaluation. Express Information of Mining Industry 476(9):23–26

Hennrich K (2000) Modelling critical water contents for slope stability and associated rainfall thresholds using computer simulations. In: Bromhead E, Dixon N, Ibsen M-L (eds) Landslides in research, theory and practice. Eighth international symposium on landslides. T. Telford, London, pp 713–718

Highland LM, Gori PL (2008) Two approaches for public landslide awareness in the United States—U.S. geological survey warning system and a landslide film documentary. In: Chen Z, Zhang J-M, Ho K, Wu F-Q, Li Z-K (eds) Landslides and engineered slopes. From the past to the future. Proceedings of the tenth international symposium on landslides and engineered slopes. pp 1173–1176

Higuchi K, Fujisawa K, Asai K, Pasuto A, Marcato G (2007) Application of new landslide monitoring technique using optical fiber sensor at Takisaka Landslide, Japan. In: AEG Special

Publication. Proceedings of the first North American landslide conference. Vail, Colorado, pp 1074–1083
Hiura H, Furuya G, Fukuoka H, Sassa K (2000) Investigation of the groundwater distribution in a crystalline Schist Landslide Zentoku, Shikoku Island, Japan. In: Bromhead E, Dixon N, Ibsen M-L (eds) Landslides in research, theory and practice. Eighth international symposium on landslides. T. Telford, London, pp 719–724
Hu XW, Tang HM, Li JS (2008) General digital camera-based experiments for large-scale landslide physical model measurement. In: Chen Z, Zhang J-M, Ho K, Wu F-Q, Li Z-K (eds) Landslides and engineered slopes: from the past to the future proceedings of the tenth international symposium on landslides and engineered slopes, pp 249–255
Hu H, Fernandez-Steeger TM, Dong M, Nguyen HT, Azzam R (2010) 3D modeling using LiDAR data and its geological and geotechnical applications. In: Geoinformatics. 18th international conference on geoinformatics. Beijing, China, pp 1–6
Huang Jr C, Kao SJ, Hsu ML, Lin JC (2006) Stochastic procedure to extract and to integrate landslide susceptibility maps: an example of mountainous watershed in Taiwan. Nat Hazards Earth Syst Sci 6:803–815
Huang Z, Law KT, Liu H, Jiang T (2008) The chaotic characteristics of landslide evolution: a case study of Xintan landslide. Environ Geol, 56:1585–1591
Hubble TCT (2004) Slope stability analysis of potential bank failure as a result of toe erosion on weir-impounded lakes: an example from the Nepean River, New South Wales, Australia. Marine Freshwater Res 55(1):57–65. Accessed 27 Oct 2010
Hübl H (2000) Frühwarnsysteme als passive Schutzmaßnahmen in Wildbacheinzugsgebieten. In: Wildbach und Lawinenverbauung (ed) Jahresbericht 2000 des Bundesministeriums für Landwirtschaft, Forst, Wasser und Umwelt. p 46
Huggel C, Ramírez JM, Calvache M, González H, Gutierrez C, Krebs R (2008) A landslide early warning system within an integral risk management strategy for the Combeima-Tolima Region, Colombia. In: The international disaster and risk conferences. IDRC Davos, Switzerland, pp 273–276
Huggel C, Khabarov N, Obersteiner M, Ramírez JM (2009) Implementation and integrated numerical modeling of a landslide early warning system: a pilot study in Colombia. Nat Hazards 52(2):501–518
Hungr O (1995) A model for the run out analysis of rapid flow slides, debris flows and avalanches. Can Geotech J 32(4):610–623
Hungr O, McDougall S (2009) Two numerical models for landslide dynamic analysis. Comput Geosci 35(5):978–992
Ibraim I, Anderson MG (2003) A new approach to soil characterisation for hydrology-stability analysis models. Geomorphology 49(3–4):269–279
Imaizumi F, Sidle RC, Kamei R (2008) Effects of forest harvesting on the occurrence of landslides and debris flows in steep terrain of central Japan. Earth Surf Proc Land 33(6):827–840
Iovine G, D'Ambrosio D, Di Gregorio S (2005) Applying genetic algorithms for calibrating a hexagonal cellular automata model for the simulation of debris flows characterised by strong inertial effects. Geomorphology 66(1–4):287–303
Ishida T, Kanagawa T, Kanaori Y (2010) Source distribution of acoustic emissions during an in situ direct shear test: Implications for an analog model of seismogenic faulting in an inhomogeneous rock mass. Eng Geol 110(3–4):66–76
Isle of Wight Centre for the Coastal Environment (2010) Isle of Wight Centre for the Coastal Environment. http://www.coastalwight.gov.uk/index.html. Accessed 2 Dec 2010
Iverson RM (2000) Landslide triggering by rain infiltration. Water Resour Res 36(7):1897–1910
Iverson RM (2005) Regulation of landslide motion by dilatancy and pore pressure feedback. J Geophys Res 110:1–17
Jakob M, Holm K, Lange O, Schwab JW (2006) Hydrometeorological thresholds for landslide initiation and forest operation shutdowns on the north coast of British Columbia. Landslides 3(3):228–238

Janbu N (1996) Slope stability evaluations in engineering practice. In: Senneset K (ed) Landslides. Seventh international symposium on landslides. Balkema, Rotterdam, pp 17–34
Jian W, Wang Z, Yin K (2009) Mechanism of the Anlesi landslide in the Three Gorges Reservoir, China. Eng Geol 108(1–2):86–95
Jiang T, Wang W, Cui JL, Chen XT (2009) Landslide forecast based on state vector method. Yantu Lixue/Rock Soil Mech 30(6):1747–1752
Jing L (1998) Formulation of discontinuous deformation analysis (DDA)–an implicit discrete element model for block systems. Eng Geol 49(3–4):371–381
Jomard H, Lebourg T, Binet S, Tric E, Hernandez M (2007) Characterization of an internal slope movement structure by hydrogeophysical surveying. Terra Nova 19(1):48–57
Jongmans D, Garambois S (2007) Geophysical investigation of landslides: a review. Bulletin de la Société Géologique de France 178(2):101–112
Jongmans D, Renalier F, Kniess U, Bièvre G, Schwartz S, Pathier E, Orengo Y, Villemin T, Delacourt C (2008) Characterisation of the Avignonnet landslide (French Alps) using seismic techniques. In: Chen Z, Zhang J-M, Ho K, Wu F-Q, Li Z-K (eds) Landslides and engineered slopes: from the past to the future. Proceedings of the tenth international symposium on landslides and engineered slopes. Taylor & Francis, Xi'an, pp 395–401
Joswig M (2008) Nanoseismic monitoring fills the gap between microseismic networks and passive seismic. First Break 26:81–88
Karnawati D, Ibriam I, Anderson MG, Holcombe EA, Mummery GT, Renaud J-P, Wang Y (2005) An initial approach to identifying slope stability controls in Southern Java and to providing community-based landslide warning information. In: Glade T, Anderson M, Crozier MJ (eds) Landslide hazard and risk. Wiley, New York, pp 733–763
Kearey P, Brooks M, Hill I (2002) An introduction to geophysical exploration. Wiley, Blackwell
Keaton JR, and DeGraff JV (1996) Surface observation and geologic mapping. In: Turner AK, Schuster RL (eds) Landslides: investigation and mitigation (Special Report). Washington, DC, USA: National Research Council, Transportation and Research Board Special Report 247, pp 178–230
Keaton JR, Gailing RW (2004) Monitoring slope deformation with quadrilaterals for pipeline risk management. In: ASME conference proceedings. Proceedings of the 2004 international pipeline conference (IPC). Calgary, Canada, pp 269–274
Keefer DK, Wilson RC, Mark RK, Brabb EE, BROWN III WM, Ellen SD, Harp EL, Wieczorek GF, Alger CS, Zatkin RS (1987) Real-time landslide warning during heavy rainfall. Science 238(4829):921
Keersmaekers R, Maertens J, Van Gemert D, Haelterman K (2008) Modeling landslide triggering in layered soils. In: Chen Z-Y, Zhang J-M, Ho K (eds) Landslides and engineered slopes: From the past to the future. Proceedings of the 10th international symposium on landslides and engineered slopes. Taylor & Francis, Xi'an, pp 761–767
Kellezi L, Allkja S, Hansen PB (2005) Landslide FE stability analysis. In: Proceedings of the IACMAG. Italy, pp 545–553
Kienholz H, Hafner H, Schneider G, Zimmermann M (1984) Methods for the assessment of mountain hazards and slope stability in Nepal. Erdwissenschaftliche Forschung 18:147–160
Kilburn CR, Petley DN (2003) Forecasting giant, catastrophic slope collapse: lessons from Vajont, Northern Italy. Geomorphology 54(1–2):21–32
Kim HW (2008) Development of wireless sensor node for landslide detection. In: Chen Z, Zhang J-M, Ho K, Wu F-Q, Li Z-K (eds) Landslides and engineered slopes: from the past to the future. Proceedings of the 10th international symposium on landslides and engineered slopes. Taylor & Francis, Xi'an, pp 1183–1187
Kjelland NH, Hutchinson DJ, Diederichs MS, Lawrence MS, Harrap R (2004) Development of GIS-based decision-support systems for stability analysis of slow moving, active landslides using geotechnical modeling. In: Lacerda W, Ehrlich M, Fontoura SAB, Sayao AS (eds) Landslides: evaluation and stabilization. Ninth international symposium on landslides. A.A. Balkema Publishers, Leiden, pp 1299–1304

Kneale P (1987) Instrumentation of pore pressure and soil water suction. In: Anderson MG (ed) Slope stability: geotechnical engineering and geomorphology. Wiley, New York, pp 77–112

Knödel K, Krummel H, Lange G (2005) Handbuch zur Erkundung des Untergrundes von Deponien: Geophysik. Springer, Berlin

Kohn J-C (2006) Potenzial der Auswertung des Archivs der Straßenbauverwaltung für die Risikoforschung - Nutzung des Archivs der Baustoff und Bodenprüfstelle Ludwigsburg als historische Quelle. University of Bonn, Germany

Krause R (2009) Felsmonitor Winkelgrat - Erfahrungen mit einem sensorbasierten Frühwarnsystem zum Schutz vor Bergsturz. Presentation at SLEWS and ILEWS Workshop on Warn- und Risikomanagement bei Massenbewegungen, Hannover, Germany, 2009

Krauter E, Lauterbach M, Feuerbach J (2007) Hangdeformationen–Beobachtungsmethoden und Risikoanalyse. geo-international & Forschungsstelle Rutschungen, pp 1–6

Kreja R, Terhorst B (2005) GIS-gestützte Ermittlung rutschungsgefährdeter Gebiete am Schönberger Kapf bei Öschingen (Schwäbische Alb). Die Erde 136(4):395–412

Kumar A, Sanoujam M (2006) Landslide studies along the national highway (NH 39) in Manipur. Nat Hazards 40(3):603–614

Kunlong YIN, Lixia C, Guirong Z (2007) Regional landslide hazard warning and risk assessment. Earth Sci Frontiers 14(6):85–93

Kunz-Plapp T (2007) Vorwarnung, Vohersage und Frühwarnung. In: Felgentreff C, Glade T (eds) Naturrisiken und Sozialkatastrophen. 1st ed. Spektrum Akademischer Verlag, Heidelberg, pp 213–223

Kupka M, Herle I, Arnold M (2009) Advanced calculations of safety factors for slope stability. Int J Geotech Eng 3(4):509–515. Accessed 27 Oct 2010

Kusumi H, Nakamura M, Nishida K (2000) Monitoring of groundwater behaviour caused by rainfall in fracture zone of rock slope using electric resistivity method. In: Bromhead E, Dixon N, Ibsen M-L (eds) Landslides in research, theory and practice. Eighth international symposium on landslides. T. Telford, London, pp 871–876

Kveldsvik V, Einstein HH, Nilsen B, Blikra LH (2008) Numerical analysis of the 650,000 m2 Åknes rock slope based on measured displacements and geotechnical data. Rock Mech Rock Eng 42(5):689–728

Kveldsvik V, Kaynia AM, Nadim F, Bhasin R, Nilsen B, Einstein HH (2009) Dynamic distinct-element analysis of the 800 m high Aknes rock slope. Int J Rock Mech Mining Sci 46(4):686–698

Larsen MC (2008) Rainfall-triggered landslides, anthropogenic hazards, and mitigation strategies. Adv Geosci 14:147–153

Lateh H, Anderson MG, Ahmad F (2008) CHASM—The model to predict stability of Gully Walls along the East-West highway in Malaysia: A case study. In: Proceeding of the first world landslide forum. ISDR, Tokyo, pp 340–343

Lato M, Hutchinson J, Diederichs M, Kalenchuk K (2007) Evaluating block shape and block volume distributions of rock faces using LiDAR and 3DEC. In: Geophysical research abstracts

Lauterbach M, Krauter E, Feuerbach J (2002) Satellitengestütztes Monitoring einer Großrutschung im Bereich eines Autobahndammes bei Landstuhl/Pfalz. Geotechnik 25(2):97–100

Lea NL (1992) An aspect driven kinematic routine algorithm. In: Parsons AJ (ed) Overland flow: hydraulics and erosion mechanics. Taylor & Francis, Routledge, pp 374–388

Lebourg T, Binet S, Jomard HET, El Bedoui S (2004) 3D geophysical survey of the "La Clapiere" landslide, southeastern France. In: Lacerda W, Ehrlich M, Fontoura SAB, Sayao AS (eds) Landslides: evaluation and stabilization. Ninth international symposium on landslides. A.A. Balkema Publishers, Leiden, pp 851–856

Lebourg T, Binet S, Tric E, Jomard H, El Bedoui S (2005) Geophysical survey to estimate the 3D sliding surface and the 4D evolution of the water pressure on part of a deep seated landslide. Terra Nova 17(5):399–406. Accessed 15 Oct 2010

Lee S (2006) Application and verification of fuzzy algebraic operators to landslide susceptibility mapping. Environ Geol 52(4):615–623

Lee CF, Kwong AKL, Ghazavi M, Emami N (eds) (2001) Analysis of failed slope in saturated soft soils: A case study. In: Soft soil engineering. Taylor & Francis, Routledge, pp 11–116

Lee S, Choi J, Min K (2002) Landslide susceptibility analysis and verification using the Bayesian probability model. Environ Geol 43(1–2):120–131. Accessed 25 Oct 2010

Lee S, Ryu JH, Lee MJ, Won JS (2003) Use of an artificial neural network for analysis of the susceptibility to landslides at Boun, Korea. Environ Geol 44(7):820–833

Leroueil S (2004) Geotechnics of slopes before failure. In: Lacerda W, Ehrlich M, Fontoura SAB, Sayao AS (eds) Landslides: evaluation and stabilization. Ninth international symposium on landslides. A.A. Balkema Publishers, Leiden, pp 863–884

Li AG, Tham LG, Lee CF, Yue QZ, Law KT, Deng JH (2004) Field instrumentation for a saprolite cut slope. In: Lacerda W, Ehrlich M, Fontoura SAB, Sayao AS (eds) Landslides: evaluation and stabilization. Ninth international symposium on landslides. A.A. Balkema Publishers, Leiden, pp 571–576

Li C, Knappett J, Feng X (2008) Centrifuge modelling of reservoir landslides in three. In: Proceedings of the international conference on landslide risk management. Vancouver, Canada, pp 732–735

Li D, Yin K, Leo C (2009a) Analysis of Baishuihe landslide influenced by the effects of reservoir water and rainfall. Environ Earth Sci 60(4):677–687

Li D, Yin K, Gao H, Liu C (2009b) Design and application analysis of prediction system of geo-hazards based on GIS in the three gorges reservoir. In: Liu Y, Tang X (eds) International symposium on spatial analysis, spatial-temporal data modeling, and data mining. Proceedings of SPIE—The international society for optical engineering. Wuhan, Hubei, China

Liao Z, Hong Y, Wang J, Fukuoka H, Sassa K, Karnawati D, Fathani F (2010) Prototyping an experimental early warning system for rainfall-induced landslides in Indonesia using satellite remote sensing and geospatial datasets. Landslides 7(3):317–324

Liu S, Wang Z (2008) Choice of surveying methods for landslides monitoring. In: Chen Z, Zhang J-M, Ho K, Wu F-Q, Li Z-K (eds) Landslides and engineered slopes: from the past to the future. Proceedings of the tenth international symposium on landslides and engineered slopes. Taylor & Francis, Xi'an

Lloyd DM, Wilkinson PL, Othmann MA, Anderson MG (2001) Predicting landslides: assessment of an automated rainfall based landslide warnings systems. In: Ho KKS, Li KS (eds) Geotechnical engineering—Meeting society's needs. Taylor & Francis, Routledge, pp 135–139

Lloyd DM, Anderson MG, Renaud JP, Wilkinson P, Brooks SM (2004) On the need to determine appropriate domains for hydrology-slope stability models. Adv Environ Res 8(3–4):379–386

Lollino G, Arattano M, Cuccureddu M (2002) The use of the automatic inclinometric system for landslide early warning: the case of Cabella Ligure (North-Western Italy). Phys Chem Earth 27(36):1545–1550

Lorenz EN (1963) Deterministic non-periodic flow. J Atmos Sci 20:130–141

Lumb P (1975) Slope failures in Hong Kong. Quart J Eng Geol Hydrogeol 8(1):31

Luzi G, Pieraccini M, Macaluso G, Mecatti D, Noferini L, Atzeni C, Galgaro A, Teza G (2005) Ground based microwave interferometry for estimating the movement of landslides. In: Hungr O, Fell R, Couture R, Eberhardt E (eds) International conference on landslide risk management. Taylor & Francis Ltd, Vancouver, pp 309–314

Macfarlane DF, Silvester PK, Benck JM, Whiford ND (1996) Monitoring strategy and performance of instrumentation int the clyde power project landslide, New Zealand. In: Senneset K (ed) Landslides. Seventh international symposium on landslides. Balkema, Rotterdam, pp 1557–1564

Maffei A, Martino S, Prestininzi A, Scarascia Mugnozza G, Pellegriono A (2004) The impact of alteration on DSGSD in crystalline-metamorphic rocks: the case of Mt. Granieri-Salineriti (Calabria - Italy). In: Lacerda W, Ehrlich M, Fontoura SAB, Sayao AS (eds) Landslides: evaluation and stabilization. Ninth international symposium on landslides. A.A. Balkema Publishers, Leiden, pp 1247–1253

Main IG (2000) A damage mechanics model for power-law creep and earthquake aftershock and foreshock sequences. Geophys J Int 142(1):151–161. Accessed 6 Oct 2010

Majidi A, Choobbasti AJ (2008) Numerical analysis of Hollar landslide. Electron J Geotech Eng 13(B):1–10

Malamud BD, Turcotte DL, Guzzetti F, Reichenbach P (2004) Landslide inventories and their statistical properties. Earth Surf Proc Land 29(6):687–711

Malone AW (1997) Risk management and slope safety in Hong Kong. Trans Hong Kong Inst Eng 4(2–3):12–21

Maria FA, Gianfranco F, Hélène VI (2004) Rock slope stability analysis based on photogrammetric surveys. In: Lacerda W, Ehrlich M, Fontoura SAB, Sayao AS (eds) Landslides: evaluation and stabilization. Ninth international symposium on landslides. A.A. Balkema Publishers, Leiden, pp 789–794

Marques R, Zêzere J, Trigo R, Gaspar J, Trigo I (2008) Rainfall patterns and critical values associated with landslides in Povoação County (São Miguel Island, Azores): relationships with the North Atlantic Oscillation. Hydrol Process 22(4):478–494

Marschallinger R, Eichkitz C, Gruber H, Heibl K, Hofmann R, Schmid K (2009) The Gschliefgraben Landslide (Austria): A remediation approach involving Torrent and avalanche control, geology, geophysics, geotechnics and geoinformatics. Austrian J Earth Sci 102(2):36–51

Massey JB, Mak SH, Yim KP (2001) Community based approach to landslide risk reduction. In: Proceedings of the fourteenth Southeast Asian geotechnical conference. Hong Kong, China, pp 141–147

Matsushi Y, Matsukura Y (2007) Rainfall thresholds for shallow landsliding derived from pressure-head monitoring: cases with permeable and impermeable bedrocks in Boso Peninsula, Japan. Earth Surf Proc Land 32(9):1308–1322

Matziaris VG, Ferentinou M, Sakellariou MG (2005) Slope stability assessment in unsaturated soils under rainfall conditions In: Agioutantis Z, Komnitsas K (eds) Ovidius University Annals Series: Civil Engineering 1 (7), pp 103–110

Mayer J, Pohl W (2010) Risikokommunikation. In: Bell R, Pohl J, Glade T, Mayer J, Greiving S (eds) Integrative Frühwarnsysteme für gravitative Massenbewegungen (ILEWS) Monitoring, Modellierung, Implementierung. Klartext, Germany, pp 180–202

McGuffey V, Modeer J, Victor A, Turner AK (1996) Subsurface exploration. In: Turner AK, Schuster RL (eds) Landslides: investigation and mitigation (Special Report). National Research Council, Transportation and Research Board Special Report 247, Washington, DC, USA, pp 231–277

McInnes RG (2000) Managing ground instability in urban areas—A guide to best practice. Isle of Wight Centre for the Coastal Environment, UK

Meidal KM, Moore DP (1996) Long-term performance of instrumentation at Dutchman's Ridge. In: Senneset K (ed) Landslides. Seventh international symposium on landslides. Balkema, Rotterdam, pp 1565–1577

Meisina C, Scarabelli S (2007) A comparative analysis of terrain stability models for predicting shallow landslides in colluvial soils. Geomorphology 87(3):207–223

Meisina C, Zucca F, Fossati D, Ceriani M, Allievi J (2006) Ground deformation monitoring by using the permanent scatterers technique: the example of the Oltrepo Pavese (Lombardia Italy). Eng Geol 87:240–259

Meric O, Jongmans D, Garambois S, Giraud A, Vengeon J-M (2004) Investigation of the gravitational movement of Séchilienne by geophysical methods. In: Lacerda W, Ehrlich M, Fontoura SAB, Sayao AS (eds) Landslides: evaluation and stabilization. Ninth international symposium on landslides. A.A. Balkema Publishers, Leiden, pp 629–634

Meric O, Garambois S, Jongmans D, Wathelet M, Chatelain JL, Vengeon JM (2005) Application of geophysical methods for the investigation of the large gravitational mass movement of Séchilienne, France. Canad Geotech J 42(4):1105–1115. Accessed 15 Oct 2010

Meric O, Garambois S, Malet J-P, Cadet H, Gueguen P, Jongmans D (2007) Seismic noise-based methods for soft-rock landslide characterization. Bulletin de la Societe Geologique de France 178(2):137–148. Accessed 15 Oct 2010

Merrien-Soukatchoff V, Clément C, Senfaute G, Gunzburger Y (2005) Monitoring of a potential rockfall zone: The case of "Rochers de Valabres" site. In: Hungr O, Fell R, Couture R, Eberhardt E (eds) International conference on landslide risk management. Taylor & Francis Ltd., Vancouver, pp 416–422

Mihalinec Z, Ortolan Ž (2008) Landslide "Granice"in Zagreb (Croatia). In: Chen Z, Zhang J-M, Ho K, Wu F-Q, Li Z-K (eds) Landslides and engineered slopes: From the past to the future. Proceedings of the tenth international symposium on landslides and engineered slopes. Taylor & Francis, Xi'an, pp 1587–1593

Mikkelsen PE (1996) Field instrumentation. In: Turner AK, Schuster RL (eds) Landslides: investigation and mitigation (Special Report). National Research Council, Transportation and Research Board Special Report 247, Washington DC, USA, pp 278–316

Mikoš M, Vidmar A, Brilly M (2005) Using a laser measurement system for monitoring morphological changes on the Strug rock fall, Slovenia. Nat Hazards Earth Syst Sci 5:143–153

Mileti DS (1999) Disasters by design: A reassessment of natural hazards in the United States. Joseph Henry Press, Washington

Mills JP, Buckley SJ, Mitchell HL, Clarke PJ, Edwards SJ (2005) A geomatics data integration technique for coastal change monitoring. Earth Surf Proc Land 30(6):651–664

Milsom J (2003) Field geophysics. Wiley, New York

Ming-Gao T, Qiang XU, Huang RQ, Ming YAN (2006) 3DEC analysis on 6# high rock slope with joints in Xiaowan Hydropower Project. Hydrogeol Eng Geol (3)

Mondini A, Carlà R, Reichenbach P, Cardinali M, Guzzetti F (2009) Use of remote sensing approach to detect landslide thermal behaviour. Geophys Res Abstracts (11)

Montety V, de Marc V, Emblanch C, Malet J-P, Bertrand C, Maquaire O, Bogaard TA (2007) Identifying the origin of groundwater and flow processes in complex landslides affecting black marls: insights from a hydrochemical survey. Earth Surf Proc Land 32(1):32–48

Montgomery DR, Dietrich WE (1994) A physically based model for the Topographic control on shallow landsliding. Water Resour Res 30(4):1153–1171

Montgomery DR, Schmidt KM, Dietrich WE, McKean J (2009) Instrumental record of debris flow initiation during natural rainfall: implications for modeling slope stability. J Geophys Res 114:1–16. Accessed 28 Oct 2010

Montrasio L, Valentino R (2007) Experimental analysis and modelling of shallow landslides. Landslides 4(3):291–296

Moore JR, Gischig V, Button E, Loew S (2010) Rockslide deformation monitoring with fiber optic strain sensors. Nat Hazards Earth Syst Sci 10:191–201

Moreiras SM (2005) Landslide susceptibility zonation in the Rio Mendoza Valley, Argentina. Geomorphology 66(1–4):345–357. Accessed 25 Oct 2010

Morgenstern NR, Martin CD (2008) Landslides: seeing the ground. In: Chen Z, Zhang J-M, Ho K, Wu F-Q, Li Z-K (eds) Landslides and engineered slopes: From the past to the future. Proceedings of the tenth international symposium on landslides and engineered slopes. Taylor & Francis, Xi'an, pp 3–24

Morrissey MM, Wieczorek GF, Morgan BA (2001) A comparative analysis of hazard models for predicting debris flows in Madison County, Virginia. USGS (ed) U.S. Department of the Interior, U.S. Geological Survey, Washington

Murmelter G (2010) Erdrutsch löste Zugunglück im Vinschgau aus. Der Standard, 13.04.2010, p 6

Nagarajan R, Roy A, Vinod Kumar R, Mukherjee A, Khire MV (2000) Landslide hazard susceptibility mapping based on terrain and climatic factors for tropical monsoon regions. Bull Eng Geol Environ 58(4):275–287. Accessed 25 Oct 2010

Nakamura H (2004) Field instrumentation and laboratory investigation. In: Lacerda W, Ehrlich M, Fontoura SAB, Sayao AS (eds) Landslides: evaluation and stabilization. Ninth international symposium on landslides. A.A. Balkema Publishers, Leiden, pp 541–548

Nash DFT (1987) A comparative review of limit equilibrium methods of stability analysis. In: Anderson MG (ed) Slope stability: geotechnical engineering and geomorphology. Wiley, New York, pp 11–75

National Research Council (2004) Partnerships for reducing landslide risk: assessment of the national landslide hazards mitigation strategy. The National Academies Press, Washington

Navarro V, Yustres A, Candel M, López J, Castillo E (2010) Sensitivity analysis applied to slope stabilization at failure. Comput Geotech 37(7–8):837–845

Neuhäuser B (2005) Probabilistische Beurteilung der Rutschanfälligkeit zur Einschätzung der Gefährdung durch Hangrutschungen am Beispiel Schwäbische Alb. In: Angewandte Geoinformatik. Beiträge zum 17. AGIT-Symposium. Salzburg, Austria, pp 129–137

NOAA-USGS Debris Flow Task Force (2005) NOAA-USGS Debris-Flow Warning System—Final Report. US Geological Survey Open File Report 2006-1064

O'Callaghan JF, Mark DM (1984) The extraction of drainage networks from digital elevation data. Comput Vis Graph Image Process 28(3):323–344

Oboni F (2005) Velocity-rain relationship at the Cassas Landslide. In: Hungr O, Fell R, Couture R, Eberhardt E (eds) International conference on landslide risk management. Taylor & Francis Ltd., Vancouver, pp 280–284

Ohlmacher GC, Davis JC (2003) Using multiple logistic regression and GIS technology to predict landslide hazard in northeast Kansas, USA. Eng Geol 69(3–4):331–343

Okamoto T, Larsen JO, Matsuura S, Asano S, Takeuchi Y, Grande L (2004) Displacement properties of landslide masses at the initiation of failure in quick clay deposits and the effects of meteorological and hydrological factors. Eng Geol 72(3–4):233–251

Olalla C (2004) Recent developments in landslide monitoring. In: Lacerda W, Ehrlich M, Fontoura SAB, Sayao AS (eds) Landslides: evaluation and stabilization. Ninth international symposium on landslides. A.A. Balkema Publishers, Leiden, pp 549–555

Oppikofer T, Jaboyedoff M, Blikra L, Derron MH, Metzger R (2009) Characterization and monitoring of the Aknes rockslide using terrestrial laser scanning. Nat Hazards Earth Syst Sci 9:1003–1019

Oregon Department of Geology and Mineral Industry (2010) Debris flow warnings. http://www.oregongeology.com/sub/Landslide/debrisflow.htm. Accessed 3 Dec 2010

Ortigao B, Justi MG (2004) Geotechnical instrumentation news. Geotech News 22(3):28–31

Ortigão JAR, Sayao ASFJ (2004) Handbook of slope stabilisation. Birkhäuser, London

Ortigao JAR, Justi MG, D'Orsi R, Brito H (2002) Rio-Watch 2001: the Rio de Janeiro landslide alarm system. In: Ho KKS, Li KS (eds) Proceedings, 14th Southeast Asian geotechnics conference—Geotechnical engineering: Meeting Society's Needs. pp 237–241

Pachauri AK, Gupta PV, Chander R (1998) Landslide zoning in a part of the Garhwal Himalayas. Environ Geol 36(3–4):325–334. Accessed 25 Oct 2010

Pack R, Tarboton D (2004) Stability index mapping (SINMAP) applied to the prediction of shallow translational landsliding. Geophys Res Abstracts (6)

Pack RT, Tarboton DG, Goodwin CN (1998) SINMAP—A stability index approach to terrain stability hazard mapping. http://www.neng.usu.edu/cee/faculty/dtarb/sinmap.pdf. Accessed 26 Oct 2010

Pack RT, Tarboton DG, Goodwin CN (2001) Assessing terrain stability in a GIS using SINMAP. In: GIS 2001. 15th annual GIS conference. British Columbia, Vancouver, pp 1–9

Pack RT, Tarboton DG, Goodwin CN, Prasad A (2005) SINMAP 2—A stability index approach to terrain stability hazard mapping. http://www.hydrology.neng.usu.edu/sinmap2/sinmap2.pdf. Accessed 26 Oct 2010

Pagano L, Rianna G, Zingariello MC, Urciuoli G, Vinale F (2008) An early warning system to predict flowslides in pyroclastic deposits. In: Chen Z, Zhang J-M, Ho K, Wu F-Q, Li Z-K (eds) Landslides and engineered slopes: from the past to the future. Proceedings of the tenth

international symposium on landslides and engineered slopes. Taylor & Francis, Xi'an, pp 1259–1264
Palm H, Staab S, Schmitz R (2003) Verkehrsicherheiten an klassifizierten Straßen im Hinblick auf Steinschlag- und Felssturzgefahr. In: Rutschungen in Rheinland-Pfalz. Erkennen, Erkunden und Sanieren. Felssicherung und Sanierung von Stützmauern. Weiterbildungsseminar III. Mainz, Germany, pp 16–22
Parasnis DS (1997) Principles of applied geophysics. Springer, Berlin
Pasculli A, Sciarra N (2006) A 3D landslide analyses with constant mechanical parameters compared with the results of a probabilistic approach assuming selected heterogeneities at different spatial scales. Giornale di Geologia Applicata 3:269–280
Pasuto A, Silvano S (1998) Rainfall as a trigger of shallow mass movements. A case study in the Dolomites, Italy. Env Geol 35(2):184–189
Pasuto A, Silvano S, Berlasso G (2000) Application of time domain reflectometry (TDR) technique in monitoring the Pramollo Pass Landslide (Province of Udine, Italy). In: Bromhead E, Dixon N, Ibsen M-L (eds) Landslides in research, theory and practice. Eighth international symposium on landslides. T. Telford, London, pp 1189–1194
Persson H, Alén C, Lind BB (2007) Development of a pore pressure prediction model. In: McInnes R, Jakeways J, Fairbanks J, Mathie E (eds) Landslides and climate change. Challenges and solutions. Proceedings of the international conference on landslides and climate change. Taylor & Francis, Isle of Wight, UK, pp 21–24
Petley DN, Allison RJ (1997) The mechanics of deep-seated landslides. Earth Surf Proc Land 22(8):747–758
Petley DN, Petley DJ (2006) On the initiation of large rockslides: perspectives from a new analysis of the Vaiont movement record. Earth Environ Sci 49(2):77–84
Petley DN, Bulmer MH, Murphy W (2002) Patterns of movement in rotational and translational landslides. Geology 30(8):719
Petley DN, Hearn GJ, Hart A (2005a) Towards the development of a landslide risk assessment for rural roads in Nepal. In: Glade T, Anderson M, Crozier MJ (eds) Landslide hazard and risk. Wiley, New York, pp 597–619
Petley DN, Higuchi T, Dunning S, Rosser NJ, Petley DJ, Bulmer MH, Carey J (2005b) A new model for the development of movement in progressive landslides. In: Hungr O, Fell R, Couture R, Eberhardt E (eds) International conference on landslide risk management. Taylor & Francis Ltd., Vancouver, pp 350–358
Petley DN, Higuchi T, Petley DJ, Bulmer MH, Carey J (2005c) Development of progressive landslide failure in cohesive materials. Geology 33(3):201–204
Petley DN, Mantovani F, Bulmer MH, Zannoni A (2005d) The use of surface monitoring data for the interpretation of landslide movement patterns. Geomorphology 66(1–4):133–147
Petley DN, Petley DJ, Allison RJ (2008) Temporal prediction in landslides—Understanding the Saito effect. In: Chen Z, Zhang J-M, Ho K, Wu F-Q, Li Z-K (eds) Landslides and engineered slopes: from the past to the future. Taylor & Francis, Xi'an, pp. 794–800
Phillips J (1992a) Nonlinear dynamical systems in geomorphology: revolution or evolution? Geomorphology 5(3–5):219–229. Accessed 16 Sep 2010
Phillips J (1992b) The end of equilibrium? Geomorphology 5(3–5):195–201. Accessed 16 Sep 2010
Phillips JD (2003) Sources of nonlinearity and complexity in geomorphic systems. Progr Phys Geog 27(1):1
Phillips JD (2006) Deterministic chaos and historical geomorphology: a review and look forward. Geomorphology 76(1–2):109–121
Phillips JD, Golden H, Cappiella K, Andrews B, Middleton T, Downer D, Kelli D, Padrick L (1999) Soil redistribution and pedologic transformations in coastal plain croplands. Earth Surf Proc Land 24(1):23–39
Picarelli L, Russo C (2004) Remarks on the mechanics of slow active landslides and the interaction with man-made works. In: Lacerda W, Ehrlich M, Fontoura SAB, Sayao AS (eds)

Landslides: evaluation and stabilization. Ninth international symposium on landslides. A.A. Balkema Publishers, Leiden, pp 1141–1176

Pirulli M (2009) The Thurwieser rock avalanche (Italian Alps): Description and dynamic analysis. Eng Geol 109(1–2):80–92

Poisel R, Angerer H, Pöllinger M, Kalcher T, Kittl H (2009) Mechanics and velocity of the Lärchberg-Galgenwald landslide (Austria). Eng Geol 109(1–2):57–66

Polemio M, Petrucci O (2000) Rainfall as a landslide triggering factor: An ovewiew of recent international research. In: Bromhead E, Dixon N, Ibsen M-L (eds) Landslides in research, theory and practice. Eighth international symposium on landslides. T. Telford, London, pp 1219–1226

Prinz H, Strauß R (2006) Abriss der Ingenieurgeologie. Spektrum Akademischer Verlag, Heidelberg

Prokop A, Panholzer H (2009) Assessing the capability of terrestrial laser scanning for monitoring slow moving landslides. Nat Hazards Earth Syst Sci 9:1921–1928

Pueyo-Anchuela Ó, Pocoví Juan A, Soriano MA, Casas-Sainz AM (2009) Characterization of karst hazards from the perspective of the doline triangle using GPR–Examples from Central Ebro Basin (Spain). Eng Geol 108(3–4):225–236

Quinn P, Beven K, Chevallier P, Planchon O (1991) The prediction of hillslope flow paths for distributed hydrological modelling using digital terrain models. Hydrol Process 5(1):59–79

Rahardjo H, Ong TH, Rezaur RB, Leong EC (2007) Factors controlling instability of homogeneous soil slopes under rainfall. J Geotech Geoenviron Eng 133(12):1532–1543. Accessed 28 Oct 2010

Rahimi A, Rahardjo H, Leong E-C (2010) Effect of hydraulic properties of soil on rainfall-induced slope failure. Eng Geol 114(3–4):135–143. Accessed 28 Oct 2010

Read RS, Langenberg W, Cruden D, Field M, Stewart R, Bland H, Chen Z, Froese CR, Cavers DS, Bidwell AK, Murray C, Anderson WS, Jones A, Chen J, McIntyre D, Kenway D, Bingham DK, Weir-Jones I, Seraphim J, Freeman J, Spratt D, Lamb M, Herd E, Martin D, McLellan P, Pana D (2005) Frank slide a century later: The Turtle mountain monitoring project. In: Hungr O, Fell R, Couture R, Eberhardt E (eds) International conference on landslide risk management. Balkema Publishers, Rotterdam, pp 713–723

Reches Z, Lockner DA (1994) Nucleation and growth of faults in brittle rocks. J Geophys Res 99(B9):18159–18173. Accessed 6 Oct 2010

Reichenbach P, Cardinali M, De Vita P, Guzzetti F (1998) Regional hydrological thresholds for landslides and floods in the Tiber River Basin (central Italy). Env Geol 35(2):146–159

Reichenbach P, Galli MJ, Cardinali M, Guzzetti F, Ardizzone F (2005) Geomorphological mapping to assess landslide risk: concepts, methods and applications in the Umbria Region of Central Italy. In: Glade T, Anderson M, Crozier MJ (eds) Landslide hazard and risk. Wiley, New York, pp 429–468

Reid ME (1994) A pore-pressure diffusion model for estimating landslide-inducing rainfall. J Geol 102(6):709–717. Accessed 20 Oct 2010

Reyes CA, Fernandez LC (1996) Monitoring of surface movements in excavated slopes. In: Senneset K (ed) Landslides. Seventh international symposium on landslides. Balkema, Rotterdam, pp 1579–1584

Reynolds JM (1997) An introduction to applied and environmental geophysics. Wiley, New York

Richards A (2002) Complexity in physical geography. Geography 87(2):99–107

Rinaldi M, Casagli N, Dapporto S, Gargini A (2004) Monitoring and modelling of pore water pressure changes and riverbank stability during flow events. Earth Surf Proc Land 29(2):237–254

Roch K-H, Chwatal W, Brückl E (2006) Potentials of monitoring rock fall hazards by GPR: considering as example the results of Salzburg. Landslides 3(2):87–94

Romang H, Zappa M, Hilker N, Gerber M, Dufour F, Frede V, Bérod D, Oplatka M, Hegg C, Rhyner J (2010) IFKIS-Hydro: an early warning and information system for floods and debris flows. Nat Hazards 2(56):509–527

Rosen PA, Hensley S, Joughin IR, Li FK, Madsen SN, Rodriguez E, Goldstein RM (2002) Synthetic aperture radar interferometry. Proc IEEE 88(3):333–382

Rosser NJ, Petley DN (2008) Monitoring and modeling of slope movement on rock cliffs prior to failure. In: Chen Z, Zhang J-M, Ho K, Wu F-Q, Li Z-K (eds) Landslides and engineered slopes: from the past to the future. Proceedings of the tenth international symposium on landslides and engineered slopes. Taylor & Francis, Xi'an, pp 1265–1271

Rosser NJ, Dunning SA, Lim M, Petley DN (2005) Terrestrial laser scanning for quantitative rockfall hazard assessment. In: Hungr O, Fell R, Couture R, Eberhardt E (eds) International conference on landslide risk management. Taylor & Francis Ltd., Vancouver, pp 359–368

Ruch C (2009) Georisiken. Aktive Massenbewegungen am Albtrauf. LGRB-Nachrichten 8(2):1–2

Saito M (1965) Forecasting the time of occurence of a slope failure. In: Proceedings of the sixth international conference on soil mechanics and foundation engineering. Montreal, Canada, pp 537–541

Saito M (1969) Forecasting time of slope failure by tertiary creep. In: Seventh international conference on soil mechanics and foundation engineering. pp 677–683

Saito H, Nakayama D, Matsuyama H (2010) Relationship between the initiation of a shallow landslide and rainfall intensity–duration thresholds in Japan. Geomorphology 118(1–2):167–175. Accessed 18 Oct 2010

Sakai H (2008) A warning system using chemical sensors and telecommunicationtechnologies to protect railroad operation from landslide disaster. In: Chen Z, Zhang J-M, Ho K, Wu F-Q, Li Z-K (eds) Landslides and engineered slopes: from the past to the future. Proceedings of the tenth international symposium on landslides and engineered slopes. Taylor & Francis, Xi'an, pp 1277–1281

Sakai H, Tarumi H (2000) Estimation of the next happening of a landslide by observing the change in groundwater composition. In: Bromhead E, Dixon N, Ibsen M-L (eds) Landslides in research, theory and practice. Eighth international symposium on landslides. T. Telford, London, pp 1289–1294

Sakellariou M, Ferentinou M, Charalambous S (2006) An integrated tool for seismic induced landslide hazards mapping. In: Agioutantis Z, Komnitsas K (eds) First European conference on earthquake engineering and seismology. Proceedings of the joint event of 13th ECEE & 30th general Assembly of the ESC. Geneva, Switzerland, pp 1365–1375

Santurri L, Carlà R, Fiorucci F, Aiazzi B, Baronti S (2010) Assessment of very high resolution satellite data fusion techniques for landslide recognition. In: Wagner W, Székely B (eds) ISPRS TC VII Symposium—100 years if ISPRS. Vienna, Austria, pp 493–497

Sass O, Krautblatter M (2007) Debris flow-dominated and rockfall-dominated talus slopes: Genetic models derived from GPR measurements. Geomorphology 86(1–2):176–192

Sass O, Bell R, Glade T (2008) Comparison of GPR, 2D-resistivity and traditional techniques for the subsurface exploration of the Öschingen landslide, Swabian Alb (Germany). Geomorphology 93(1–2):89–103

Sato HP, Harp EL (2009) Interpretation of earthquake-induced landslides triggered by the 12 May 2008, M7.9 Wenchuan earthquake in the Beichuan area, Sichuan Province, China using satellite imagery and Google Earth. Landslides 6(2):153–159

Schaefer M, Inkpen R (2010) Towards a protocol for laser scanning of rock surfaces. Earth Surf Process Landforms 35:417–423

Schmidt J, Turek G, Clark MP, Uddstrom M, Dymond JR (2008) Probabilistic forecasting of shallow, rainfall-triggered landslides using real-time numerical weather predictions. Nat Hazards Earth Syst Sci 8:349–357

Schmutz M, Guerin R, Schott JJ, Maquaire O, Descloitres M, Albouy Y (2000) Geophysical method contribution to the Super Sauze (South France) flowslide knowledge. In: Bromhead E, Dixon N, Ibsen M-L (eds) Landslides in research, theory and oractice. Eighth international symposium on landslides. T. Telford, London, pp 1321–1326

Schneider-Muntau B, Zangerl C (2005) Numerical modelling of a slowly creeping landslide in crystalline rock—a case study. In: Impact of the human activity on the geological

environment. Proceedings of the fifth ISRM regional symposium Eurock. Brno, International Society for Rock Mechanics, Czech Republic, pp 535–540
Schrott L, Sass O (2008) Application of field geophysics in geomorphology: advances and limitations exemplified by case studies. Geomorphology 93(1–2):55–73
Schrott L, Hördt A, Dikau R (2003) Geophysical applications in geomorphology. Borntraeger, Berlin
Schulz WH (2004) Landslides mapped using LIDAR imagery, Seattle, Washington. U.S. Department of the Interior, U.S. Geological Survey
Schumm SA (1979) Geomorphic thresholds: The concept and its applications. Trans Inst Brit Geogr NS4:485–515
Schuster RL, Highland LM (2007) The third Hans Cloos Lecture. Urban landslides: socioeconomic impacts and overview of mitigative strategies. Bull Eng Geol Environ 66(1):1–27
Schuster RL, Wieczorek GF (2002) Landslide triggers and types. In: Rybár J, Stemberk J, Wagner P (eds) Landslides: proceedings of the first European conference on landslides, Taylor & Francis, Prague, June 24–26, 2002, pp 59–78
Sekiguchi T, Sato HP (2004) Mapping of micro topography using airborne laser scanning. Landslides 1(3):195–202
Sengupta A, Gupta S, Anbarasu K (2009) Rainfall thresholds for the initiation of landslide at Lanta Khola in north Sikkim, India. Nat Hazards 52(1):31–42
Shi B, Wang B, Li K, Haibo H, Wei G, Piao C (2008a) Distributive monitoring of the slope engineering. In: Chen Z, Zhang J-M, Ho K, Wu F-Q, Li Z-K (eds) Landslides and engineered slopes: from the past to the future. Proceedings of the tenth international symposium on landslides and engineered slopes. Taylor & Francis, Xi'an, pp 61–68
Shi YX, Zhang Q, Meng XW (2008b) Optical fiber sensing technology used in landslide monitoring. In: Chen Z, Zhang J-M, Ho K, Wu F-Q, Li Z-K (eds) Landslides and engineered slopes: from the past to the future. Proceedings of the tenth international symposium on landslides and engineered slopes. Taylor & Francis, Xi'an, pp 921–925
Sidle RC, Wu W (1999) Simulating effects of timber harvesting on the temporal and spatial distribution of shallow landslides. Zeitschrift für Geomorphologie 43:15–201
Singer J, Schuhbäck S, Wasmeier P, Thuro K, Heunecke O, Wunderlich T, Glabsch J, Festl J (2009) Monitoring the Aggenalm landslide using economic de-formation measurement techniques. Austrian J Earth Sci 102(2):20–34
Sirangelo B, Braca G (2004) Identification of hazard conditions for mudflow occurrence by hydrological model: application of FLaIR model to Sarno warning system. Eng Geol 73(3–4):267–276
Sitharam TG, Maji VB, Verma AK (2007) Practical equivalent continuum model for simulation of jointed rock mass using FLAC3D. Int J Geomech 7:389
Slaymaker O (1991) Mountain geomorphology: A theoretical framework for measurement programmes. Catena 18(5):427–437. Accessed 2 Nov 2010
Smith R (1991) The application of cellular automata to the erosion of landforms. Earth Surf Proc Land 16(3):273–281
Smith MJ, Chandler J, Rose J (2009) High spatial resolution data acquisition for the geosciences: kite aerial photography. Earth Surf Proc Land 34(1):155–161
Soeters R, Van Westen CJ (1996) Slope instability recognition, analysis, and zonation. In: Turner AK, Schuster RL (eds) Landslides: investigation and mitigation (Special Report). National Research Council, Transportation and Research Board Special Report 247, Washington, DC, USA, pp 129–177
Sorensen JH (2000) Hazard warning systems: review of 20 years of progress. Nat Hazards Rev 1(2):119–125
Sosio R, Crosta GB, Hungr O (2008) Complete dynamic modeling calibration for the Thurwieser rock avalanche (Italian Central Alps). Eng Geol 100(1–2):11–26. Accessed 28 Oct 2010

Spickermann A, Schanz T, Datcheva M (2003) Numerical study of a potential landslide in the Swiss Alps. In: Aifantis EC (ed) Fifth euromech solid mechanics conference. Thessaloniki, Greece, pp 17–22

Stähli M, Bartelt P (2007) Von der Auslösung zur Massenbewegung. In: Hegg C, Rhyner J (eds) Warnung bei aussergewöhnlichen Naturereignissen. Forum für Wissen. pp 33–38

Stark TD, Choi H (2008) Slope inclinometers for landslides. Landslides 5(3):339–350

Stead D, Eberhardt E, Coggan JS (2006) Developments in the characterization of complex rock slope deformation and failure using numerical modelling techniques. Eng Geol 83(1–3):217–235. Accessed 28 Oct 2010

Strenger MP (2009) Niederschlagsschwellenwerte bei der Auslösung von Muren. University Vienna, Austria

Supper R, Römer A (2003) New achievments in development of a high-speed geoelectrical monitoring system for landslide monitoring. In: Proceedings of the environmental and engineering geophysical society. Prague, Czech Republic, pp 1–6

Süzen ML, Doyuran V (2004) A comparison of the GIS based landslide susceptibility assessment methods: multivariate versus bivariate. Env Geol 45(5):665–679

Tangestani MH (2003) Landslide susceptibility mapping using the fuzzy gamma operation in a GIS, Kakan catchment area, Iran. In: Disaster Management. Proceeding of the Map India 2003 conference. New Delhi, India, pp 107–134

Tarantino C, Blonda P, Pasquariello G (2004) Application of change detection techniques for monitoring man-induced landslide causal factors. In: Geoscience and remote sensing. Proceedings of the IGARSS symposium. pp 1103–1106

Tarboton D (1997) A new method for the determination of flow directions and upslope areas in grid digital elevation models. Water Resour Res 33(2):11

Telford WM, Geldart LP, Sheriff RE (1990) Applied geophysics. Cambridge University Press, Cambridge

Teoman MB, Topal T, Isik NS (2004) Assessment of slope stability in Ankara clay: a case study along E90 highway. Env Geol 45(7):963–977

Terlien MT (1998) The determination of statistical and deterministic hydrological landslide-triggering thresholds. Env Geol 35(2):124–130

Terlien MTJ, Van Westen CJ, Van Asch T (1995) Deterministic modelling in GIS-based landslide hazard assessment. In: Carrara A, Guzzetti F (eds) Geographical information systems in assessing natural hazards. Kluwer, Dordrecht, pp 57–77

Terranova O, Antronico L, Gulla G (2007) Landslide triggering scenarios in homogeneous geological contexts: The area surrounding Acri (Calabria, Italy). Geomorphology 87(4):250–267

Terzaghi K (1925) Erdbaumechanik auf bodenphysikalischer Grundlage. F. Deuticke, Vienna

Terzaghi K (1950) Mechanisms of landslides. In: Paige S (ed) Application of geology to engineering practice. Geological Society of America, Berkley, pp 83–123

Terzaghi K (1961) Die Bodenmechanik in der Baupraxis. Springer, Berlin

Terzaghi K, Peck RB, Mesri G (1996) Soil mechanics in engineering practice. Wiley, New York

Thiebes B (2006) Räumliche Gefährdungsmodellierung flachgründiger Hangrutschungen—GIS gestützte Analyse an der Schwäbischen Alb. University of Bonn, Germany

Thiebes B, Bell R, Glade T (2010) Bewegungsanalyse-Frühwarnmodell. In: Bell R, Pohl J, Glade T, Mayer J, Greiving S (eds) Integrative Frühwarnsysteme für gravitative Massenbewegungen (ILEWS) Monitoring, Modellierung, Implementierung. Klartext, Essen, pp 150–151

Thuro K, Wunderlich T, Heunecke O, Singer J, Schuhbäck S, Wasmeier P, Glabsch J, Festl J (2009) Low cost 3D early warning system for unstable alpine slopes—the Aggenalm Landslide monitoring system. Geomech Tunn 2(3):221–237

Tianchi L (1994) Landslide disasters and human responses in China. Mountain Res Develop 4(14):341–346. Accessed 16 Sep 2010

Tiranti D, Rabuffetti D (2010) Estimation of rainfall thresholds triggering shallow landslides for an operational warning system implementation. Landslides 4(7):471–481

Tohari A, Nishigaki M, Komatsu M, Kankam-Yeboah K, Daimuru S (2004) Field monitoring of hydrological response of a residual soil slope to rainfall. In: Lacerda W, Ehrlich M, Fontoura SAB, Sayao AS (eds) Landslides: evaluation and stabilization. Ninth international symposium on landslides. A.A. Balkema Publishers, Leiden, pp 749–754

Topal T, Akin M (2008) Investigation of a landslide along a natural gas pipeline (Karacabey-Turkey). In: Chen Z, Zhang J-M, Ho K, Wu F-Q, Li Z-K (eds) Landslides and engineered slopes: from the past to the future. Proceedings of the tenth international symposium on landslides and engineered slopes. Taylor & Francis, Xi'an, pp 1647–1652

Tropeano D, Turconi L (2004) Using historical documents for landslide, debris flow and stream flood prevention. Applications in Northern Italy. Nat Hazards 31(3):663–679

Turcotte DL, Malamud BD (2004) Landslides, forest fires, and earthquakes: examples of self-organized critical behavior. Phys A Statist Mech Appl 340(4):580–589

Turner AK, McGuffey VC (1996) Organization of investigation process. In: Turner AK, Schuster RL (eds) Landslides: investigation and mitigation (Special Report). National Research Council, Transportation and Research Board Special Report 247, Washington, pp 121–128

Twigg J (2003) The human factor in early warning: risk perception and appropriate communications. In: Zschau J, Küppers AN (eds) Early warning systems for natural disaster reduction. Springer, Berlin, pp 19–27

Uchida T, Kosugi K, Mizuyama T (2001) Effects of pipeflow on hydrological process and its relation to landslide: a review of pipeflow studies in forested headwater catchments. Hydrol Process 15(11):2151–2174

UNISDR (2004a) Early Warning Systems. In: Living with Risk. UN/ISDR, Geneva, Switzerland, pp 358–383

UNISDR (2004b) ISDR: Platform for the Promotion of Early Warning. http://www.unisdr.org/ppew/whats-ew/ew-made.htm. Accessed 19 Nov 2010

UNISDR (2006a) Compendium of early warning systems. UN/ISDR, Bonn, Germany

UNISDR (2006b) Global survey of early warning systems. UN/ISDR

UNISDR (2009) ISDR?: Terminology. http://www.unisdr.org/eng/library/lib-terminology-eng%20home.htm. Accessed 15 Sep 2010

US Army Corps of Engineers (2003) Slope stabiliy. Washington, D.C., USA

USGS (2006) Landslide Hazards in the Seattle, Washington, Area. Department of the Interior and U.S. Geological Survey

Vallone P, Giammarinaro MS, Crosetto M, Agudo M, Biescas E (2008) Ground motion phenomena in Caltanissetta (Italy) investigated by InSAR and geological data integration. Eng Geol 98(3–4):144–155

Van Westen CJ (2007) Mapping landslides: recent developments in the use of digital information. In: Turner A, Schuster RL (eds) Landslides and society? Proceedings of the first North American conference on landslides, Vail, Colorado, USA, June 3–8, 2007. Association of Environmental and Engineering Geologists, Vail Colorado, USA, pp 221–238

Van Westen CJ, Rengers N, Terlien MTJ, Soeters R (1997) Prediction of the occurrence of slope instability phenomenal through GIS-based hazard zonation. Geologische Rundschau 86(2):404–414

Varnes DJ (1984) Landslide hazard zonation: A review of principles and practice. UNESCP Press, Paris

Vlcko J (2004) Extremely slow slope movements influencing the stability of Spis Castle, UNESCO site. Landslides 1(1):67–71

Voight B (1988) A method for prediction of volcanic eruptions. Nature 332(6160):125–130. Accessed 6 Oct 2010

Voight B (1989) A relation to describe rate-dependent material failure. Science 243(4888):200

Volkmann G, Schubert W (2005) The use of horizontal inclinometers for the optimization of the rock mass-support interaction. In: Erdem Y, Solak T (eds) Underground space use-analysis of the past and lessons for the future. Taylor & Francis, Routledge, pp 967–972

Von Elverfeldt K (2010) Systemtheorie in der Geomorphologie. Problemfelder, erkenntnistheoretische Konsequenzen und praktische Implikationen. University of Vienna, Austria

Walstra J, Chandler JH, Dixon N, Dijkstra TA (2004) Extracting landslide movements from historical aerial photographs. In: Lacerda W, Ehrlich M, Fontoura SAB, Sayao AS (eds) Landslides: Evaluation and stabilization. Ninth international symposium on landslides. A.A. Balkema Publishers, Leiden, pp 843–850

Walter M, Joswig M (2009) Seismic characterization of slope dynamics caused by soft rock-landslides: The Super-Sauze case study. In: Malet J-P, Remaître A, Bogaard T (eds) Landslide processes: from geomorphic mapping to dynamic modelling. Proceedings of the landslide processes conference. CERG Editions, Strasbourg, France, pp 215–220

Wang B-J, Li K, Shi B, Wei G-Q (2008a) Test on application of distributed fiber optic sensing technique into soil slope monitoring. Landslides 6(1):61–68

Wang FW, Wang G, Zhang YM, Huo ZT, Peng XM, Araiba K, Tekeuchi A (2008b) Displacement monitoring on Shuping landslide in the three Gorges Dam Reservoir area, China from August 2004 to July 2007. In: Chen Z, Zhang J-M, Ho K, Wu F-Q, Li Z-K (eds) Landslides and engineered slopes: from the past to the future. Proceedings of the tenth international symposium on landslides and engineered slopes. Taylor & Francis, Xi'an, pp 1321–1327

Wang H, Harvey AM, Xie S, Kuang M, Chen Z (2008c) Tributary-junction fans of China's Yangtze Three-Gorges valley: Morphological implications. Geomorphology 100(1–2):131–139

Wang F, Zhang Y, Huo Z, Peng X (2009) Monitoring on shuping landslide in the three Gorges Dam Reservoir, China. In: Wang F, Li T (eds) Landslide disaster mitigation in three gorges reservoir, China. Springer, Berlin, pp 257–273

Wasowski J, Lollino P, Limoni PP, Del Gaudio V, Lollino G, Gostelow P (2004) Towards an integrated field and EO-based approach for monitoring peri-urban slope instability. In: Lacerda W, Ehrlich M, Fontoura SAB, Sayao AS (eds) Landslides: evaluation and stabilization. Ninth international symposium on landslides. A.A. Balkema Publishers, Leiden, pp 809–816

Watson AD, Moore DP, Stewart TW (2004) Temperature influence on rock slope movements at Checkerboard Creek. In: Lacerda W, Ehrlich M, Fontoura SAB, Sayao AS (eds) Landslides: evaluation and stabilization. Ninth international symposium on landslides. A.A. Balkema Publishers, Leiden, pp 1293–1298

Webster TL, Dias G (2006) An automated GIS procedure for comparing GPS and proximal LiDAR elevations. Comput Geosci 32(6):713–726

White G, Haas JE (1975) Assessment of research on natural hazards. MIT Press, Cambridge

Wieczorek GF (1987) Effect of rainfall intensity and duration on debris flows on the central Santa Cruz mountains, California. In: Costa JE, Wieczorek GF (eds) Debris flows/avalanches: process, recognition, and mitigation. Reviews in Engineering Geology 7. Geological Society of America, Boulder, pp 93–104

Wieczorek GF (1996) Landslide triggering mechanisms. In: Turner AK, Schuster RL (eds) Landslides: investigation and mitigation (Special Report). National Research Council, Transportation and Research Board Special Report 247, Washington, D.C., USA, pp 76–90

Wieczorek GF, Glade T (2005) Climatic factors influencing occurrence of debris flows. In: Jakob M, Hungr O (eds) Debris-flow hazards and related phenomena. Springer, Berlin, pp 325–362

Wieczorek GF, Guzzetti F (1999) A review of rainfall thresholds for triggering landslides. In: Claps P, Siccardi F (eds) Mediterranean storms. Proceedings Plinius conference '99. Maratea, Italy, pp 407–414

Wieczorek GF, Gori PL, Highland LM (2005) Reducing landslide hazards and risk in the United States: The role of the US geological survey. In: Glade T, Anderson M, Crozier MJ (eds) Landslide hazard and risk. Wiley, New York, pp 351–375

Wienhöfer J, Lindenmaier (2009) Temporal variability of a slow-moving landslide: the Heumöser case study in Vorarlberg, Austria. In: Malet JP, Remaître A, Bogaard T (eds) Landslide processes: from geomorphological mapping to dynamic modelling. Proceedings of the international conference on landslide processes. CERG Editions, Strasbourg, pp 221–226

Wilkinson PL, Brooks SM, Anderson MG (2000) Design and application of an automated non-circular slip surface search within a combined hydrology and stability model (CHASM). Hydrol Process 14(11–12):2003–2017

Wilkinson PL, Anderson MG, Lloyd DM (2002a) An integrated hydrological model for rain-induced landslide prediction. Earth Surf Proc Land 27(12):1285–1297

Wilkinson PL, Anderson MG, Lloyd DM, Renaud JP (2002b) Landslide hazard and bioengineering: towards providing improved decision support through integrated numerical model development. Environ Model Softw 17(4):333–344

Willenberg H, Spillmann T, Eberhardt E, Evans KF, Loew H, Maurer H (2002) Multidisciplinary monitoring of progressive failure process in brittle rock slopes—concepts and system design. In: Rybár J, Stemberk J, Wagner P (eds) First European conference on landslides. Balkema Publishers, Prague, pp 477–483

Willenberg H, Evans KF, Eberhardt E, Loew S, Spillmann T, Maurer HR (2004) Geological, geophysical and geotechnical investigations into the internal structure and kinematics of an unstable, complex sliding mass in crystalline rock. In: Lacerda W, Ehrlich M, Fontoura SAB, Sayao AS (eds) Landslides: evaluation and stabilization. Ninth international symposium on landslides. A.A. Balkema Publishers, Leiden, pp 489–494

Willenberg H, Loew S, Eberhardt E, Evans K, Spillmann T, Heincke B, Maurer H, Green A (2008) Internal structure and deformation of an unstable crystalline rock mass above Randa (Switzerland): Part I—Internal structure from integrated geological and geophysical investigations. Eng Geol 101(1–2):1–14

Wilson RC (1989) Rainstorms, pore pressures, and debris flows: A theoretical framework. In: Sadler PM, Morton DM (eds) Landslides in semi-arid environment. Inland Geological Society, Riverside, pp 101–117

Wilson RC (2005) The rise and fall of a Debris-Flow warning system for the San Francisco Bay Region, California. In: Glade T, Anderson M, Crozier MJ (eds) Landslide hazard and risk. Wiley, New York, pp 493–516

Wilson RC, Wieczorek GF (1995) Rainfall thresholds for the initiation of debris flows at La Honda, California. Environ Eng Geosci 1(1):11–27. Accessed 18 Oct 2010

Wilson RC, Mark RK, Barbato G (1993) Operation of a real-time warning system for debris flows in the San Francisco Bay area, California. In: Shen HW, Su ST, Wen F (eds) Proceedings of the 1993 conference on hydraulic engineering, pp 1908–1913

Wong HN, Ho KKS (2000) Learning from slope failures in Hong Kong. In: Bromhead E, Dixon N, Ibsen M-L (eds) Landslides in research, theory and practice. Proceedings of the eighth international symposium on landslides. Thomas Telford, London

Wu TH (1996) Soil strength properties and their measurement. In: Turner AK, Schuster RL (eds) Landslides: investigation and mitigation (Special Report). National Research Council, Transportation and Research Board Special Report 247, Washington, D.C., USA, pp 319–336

Wu W, Sidle RC (1995) A distributed slope stability model for steep forested basins. Water Resour Res 31(8):2097–2110. Accessed 26 Oct 2010

Wu W, Sidle RC (1997) Application of a distributed shallow landslide analysis model (dSLAM) to managed forested catchments in Oregon, USA. In: Human impact on erosion and sedimentation. Proceedings of the Rabat Symposium. IAHS Publication 245, pp 213–222

Wu MJ, Li ZC, Yuan PJ, Jiang YH (2008) Twenty years of safety monitoring for the landslide of Hancheng PowerStation. In: Chen Z, Zhang J-M, Ho K, Wu F-Q, Li Z-K (eds) Landslides and engineered slopes: from the past to the future. Proceedings of the tenth international symposium on landslides and engineered slopes. Taylor & Francis, Xi'an, pp 1335–1341

Wu YP, Yin KL, Jiang W (2009) Early warning of landslide risk in Yongjia County, Zhejiang Province. J Nat Disast 18(2):124–130

Xie M, Esaki T, Zhou G (2004) GIS-based probabilistic mapping of landslide hazard using a three-dimensional deterministic model. Nat Hazards 33(2):265–282. Accessed 26 Oct 2010

Xu Q, Zeng Y (2009) Research on acceleration variation characteristics of creep landslide and early-warning prediction indicator of critical sliding. Yanshilixue Yu Gongcheng Xuebao/ Chinese J Rock Mech Eng 28(6):1099–1106

Yagoda-Biran G, Hatzor YH, Amit R, Katz O (2010) Constraining regional paleo peak ground acceleration from back analysis of prehistoric landslides: example from Sea of Galilee, Dead Sea transform. Tectonophysics 490(1–2):81–92. Accessed 28 Oct 2010

Yang X, Chen L (2010) Using multi-temporal remote sensor imagery to detect earthquake-triggered landslides. Int J Appl Earth Observ Geoinform 6(12):487–495. Accessed 16 Sep 2010

Ye Y, Mu Q, Zhang C (2009) Tunnel construction multivariate information forewarning and safety management system research. Yanshilixue Yu Gongcheng Xuebao/Chinese J Rock Mech Eng 28(5):900–907

Yin Y (2009) Landslide mitigation strategy and implementation in China. In: Sassa K, Canuti P (eds) Landslides-disaster risk reduction. Springer, Berlin, pp 482–484

Yin JH, Zhu HH, Jin W (2008) Monitoring of soil nailed slopes and dams using innovative technologies. In: Chen Z, Zhang J-M, Ho K, Wu F-Q, Li Z-K (eds) Landslides and engineered slopes: from the past to the future. Proceedings of the tenth international symposium on landslides and engineered slopes. Taylor & Francis, Xi'an, pp 1361–1366

Yin Y, Wang H, Gao Y, Li X (2010a) Real-time monitoring and early warning of landslides at relocated Wushan Town, the Three Gorges Reservoir, China. Landslides 7(3):339–349

Yin Y, Zheng W, Liu Y, Zhang J, Li X (2010b) Integration of GPS with InSAR to monitoring of the Jiaju landslide in Sichuan, China. Landslides 7(3):359–365

Yu YF, Lam J, Siu CK, Pun WK (2004) Recent advance in landslip warning system. In: Recent advances in geotechnical engineering. Proceedings of the twenty-fourth geotechnical division Annual Seminar. Institution of Engineers, Hong Kong, pp 139–147

Zaitchik BF, van Es HM (2003) Applying a GIS slope-stability model to site-specific landslide prevention in Honduras. J Soil Water Conserv 58(1):45–53

Zhang Q, Wang L, Zhang XY, Huang GW, Ding XL, Dai WJ, Yang WT (2008) Application of multi-antenna GPS technique in the stability monitoring of roadside slopes. In: Chen Z, Zhang J-M, Ho K, Wu F-Q, Li Z-K (eds) Landslides and engineered slopes: from the past to the future. Proceedings of the tenth international symposium on landslides and engineered slopes. Taylor & Francis, Xi'an, pp 1367–1372

Zhao XB, Zhao J, Cai JG, Hefny AM (2008) UDEC modelling on wave propagation across fractured rock masses. Comput Geotech 35(1):97–104

Zhong L, Xiao S, Zhou Y (2009) Research on the early warning and forecast system of geologic hazards in Hubei Province based on WEBGIS. In: First international workshop on education technology and computer science. Wuhan, Hubei, China, pp 602–606

Zhou PG, Chen HQ (2005) Research on geologic hazard risk management in china based on geologic hazard survey and zoning. In: Hungr O, Fell R, Couture R, Eberhardt E (eds) International conference on landslide risk management. Taylor & Francis, Vancouver, pp 54–60

Zschau J, Küppers AN (2003) Early warning systems for natural disaster reduction. Springer, Berlin

Zschau J, Merz B, Plate EJ, Goldammer JG (2001) Vorhersage und Frühwarnung. In: Plate EJ, Merz B (eds) Naturkatastrophen. Schweizerbart'Sche Verlagsbuchhandlung, pp 273–350

Chapter 3
Study Area

3.1 Regional Setting

In the following, an introduction to the study area Lichtenstein-Unterhausen at the Swabian Alb, South-West Germany is presented. Therein, geological, climatic and geomorphic properties are described, and an emphasis is put on landslide processes. The location of the study area is illustrated in Fig. 3.1.

The Swabian Alb is part of the South German cuesta landscape and extends from south west (High Rhine at Schaffhausen) to the north east (Nördlinger Ries) over a distance of 220 km with a mean width of 40 km. Elevations above 1000 m are present in the West Alb, while Central and East Alb exhibit maximum elevations of 700–800 m (Geyer and Gwinner 1986).

The Swabian Alb is a rural area with a low population density (148 inhabitants/km^2 in 1990) (Grees 1993). Grassland and forest occupy the largest proportion of land area (>60%). Settlement areas (8%) are often located in the valley bottoms and fields (29%) are primarily cultivated on the plateau.

3.1.1 Geology

The present landscape of the Swabian Alb is strongly influenced by Jurassic sediments, but also tertiary and quaternary processes influenced landscape development. Leser (1982) emphasises the relationships of current and past climatic factors for landscape evolution, such as rainfall and temperature, and weathering, pedogenesis and erosion processes, including landslides.

Lower Jurassic deposits are found in the foreland of the Swabian Alb, while Middle Jurassic sediments are located more towards the cuesta ridge (Albtrauf) and the plateau. The latter mainly consists of Upper Jurassic sediments (Geyer and Gwinner 1997). In addition, some 350 tuff diatremes of tertiary age illustrate volcanic activity in the area around Urach (Rothe 2005). Other features include

B. Thiebes, *Landslide Analysis and Early Warning Systems*, Springer Theses,
DOI: 10.1007/978-3-642-27526-5_3,

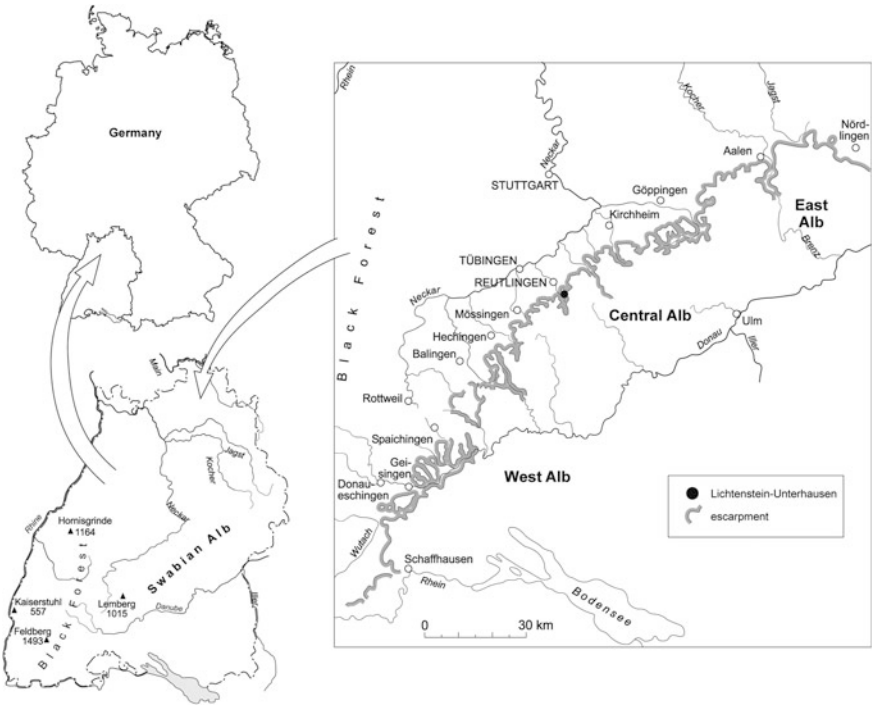

Fig. 3.1 Location of Swabian Alb and the local study area Lichtenstein-Unterhausen

tertiary weathering products and quaternary deposits from limestone solution, as well as slope debris and deposits from landslides and fluvial processes. Tertiary deposits in the southern Alb area are primarily molasse (Walter 1995). Figure 3.2 illustrates the Geology of the Swabian Alb. More detailed information on Jurassic strata is presented in Table 3.1. Therein, strata are described by their German names instead of the English translation, to prevent confusion. Petrographic descriptions however, were translated to improve understanding of strata properties.

In the Lower Jurassic strata, clays and marls are dominating, which also can be bituminous, and are interstratified with lime and sandy materials. Middle Jurassic sediments are predominantly clays with fine sands and ferriferous lime sandstones horizons, while Upper Jurassic strata comprise bedded layers of limestone and marls (Geyer and Gwinner 1997). Strata are generally dipped towards south-east by 2.5–3°; however, inclination may vary due to local folding features (Roth 2004). Figure 3.3 illustrates the geological properties of South Germany's cuesta landscape as a cross section, including the foreland, escarpment and plateau of the Swabian Alb.

Several tectonic fault lines are located in the Swabian Alb (Fig. 3.2), occasionally causing earthquakes. The strongest seismic events of the recent past include earthquakes in 1911, 1943 and 1978 in the area of Albstadt which also

Table 3.1 Jurassic strata in the Swabian Alb (after Ohmert et al. 1988; Geyer and Gwinner 1997; Wagenplast 2005; Bell 2007)

	Stage	Code	Stratum	Petrography	Thickness (m)
Upper Jurassic	Tithonian	ti1	Hangende Bankkalke	Yellowish grey to greyish brown, well bedded limestones (10–35 cm thick) with marly lime and marl interstices	80–300
	Kimmeridgian	ki5	Zementmergel	Blueish grey, yellowish grey and light grey marls, lime marls, marl lime and lime, partly massive	0–120
		Ki4	Liegende Bankkalke	Light yellowish to grey alternating sequences of lime- and marl lime beds (10-40 cm thick) separated by marl beds	30–80
		ki3	Obere Felsenkalke	Dominantly massive lime; dense and crystalline limestone beds (10–40 cm thick), increasing marl interstices to top	25–35, up to 60 (massive)
		ki2	Untere Felsenkalke	Dominantly massive lime; alongside well layered, dense, slightly crystalline limestone beds (10–150 cm thick); lower and middle sections increasingly interstratified by marl interstices and beds, upper section very thin marl layers partly missing	30–50, >100 (massive)
		ki1	Lacunosamergel (Kimmeridge-Mergel)	Grey marl and marl limestones (5–50 cm thick) with varying clay content	20–60
	Oxfordian	ox2	Wohlgeschichtete Kalke (Oxford-Kalk)	Light grey to yellowish grey, uniformly stratified limestone beds (10–60 cm thick) with thin marl beds, partly massive	15–80
		ox1	Impressamergel (Oxford-Mergel)	Alternation of marl and marl lime beds; also clay marls at basis; lime stone beds to the top; partly massive in West Alb	50–125

(continued)

Table 3.1 (continued)

	Stage	Code	Stratum	Petrography	Thickness (m)
Middle Jurassic	Callovian	cl	Ornatenton	Dark grey claystones (5-15% calcium carbonate) with oolitic iron horizons; Phosphorite and marl lime concretions	3.3–37
	Bathonian	bt	Parkinsorien-Oxycerieten	Dark clay stones with interstratified marl lime beds	0.7–70
	Bajocian	bj2	Oolithische Laibsteinschichten	Dark grey to bluish grey, partly sandy foliated, partly plastic clays and clay marls, pyrite and limonite concretions, interstratified marl lime beds	5–42
		bj1	Kalksandige Braunjuratone	Dark grey to yellowish, sandy clays, clay marls and marls with scattered lime sandstone; frequent limonite concretions	3–39
	Aalenian	al2	Eisensandstein- or Eichberg-Formation (Sandfaserige Braunjuratone)	Alternating of sandy clays and clay marls (60-80% of entire stratum thickness), ferriferous sandstones, oolitic iron and sandy marl lime	24–75
		al1	Opalinuston	Bluish black to dark grey, brittle, often shale clays and clay marls, partly pyrite; scattered marl lime beds and sand marl beds	80–131
Lower Jurassic	Toarcian	tc2	Jurensis-Mergel	Shale, yellowish grey to light grey marl and lime marl alternating with cloddy, grey blue to yellowish grey marl lime beds; at basis partly bituminous	0.6–13
		tc1	Posidonienschiefer	Alternating blackish grey, bituminous clay marl shale, scattered bituminous marl lime beds; also called oil shale	4–16
	Pliensbachian	pb2	Amaltheen-Tone	Dark grey to dark blue, partly clay shale with alternating lime marls and marl lime beds; clays contain many pyrite concretions	9–28
		pb1	Numismalis-Mergel	Grey marls and lime marls; partly light grey marl lime beds	2–13
	Sinemurian	si2	Turneri-Tone	Dark grey, partly clay and clay marl shale; numerous pyrite and limonite concretions; marl lime beds	0–43
		si1	Gryphaeenkalke oder Arietenkalke	Rich in fossils, often dark blue grey lime beds alternating with clay shale and dendritic marls	2–6
	Hettanganian	he2	Angulatensandsteine bzw. -tone	Dark, often sandy clay and clay marl shale interstratified with marl lime and lime sandstone beds	1.7–16
		he1	Psilonentone	Clay and clay marls, at basis dark grey, hard lime beds	3.5–11

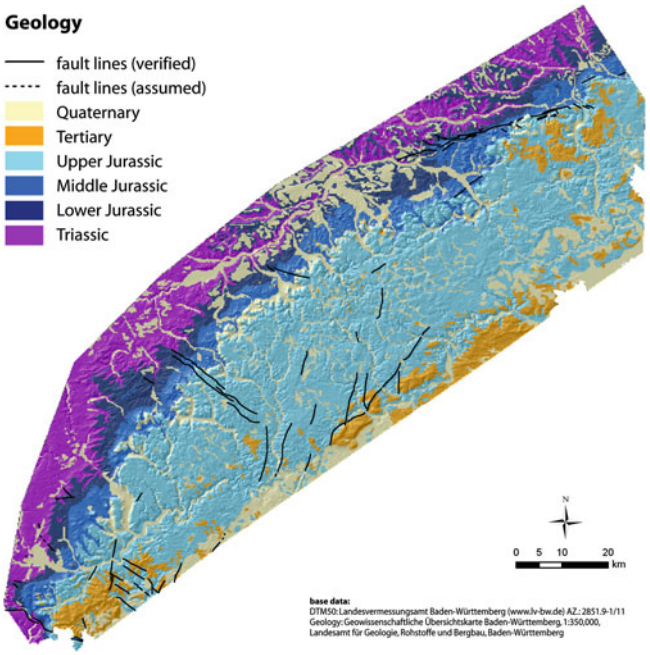

Fig. 3.2 Geological features and fault lines in the Swabian Alb (after Bell 2007)

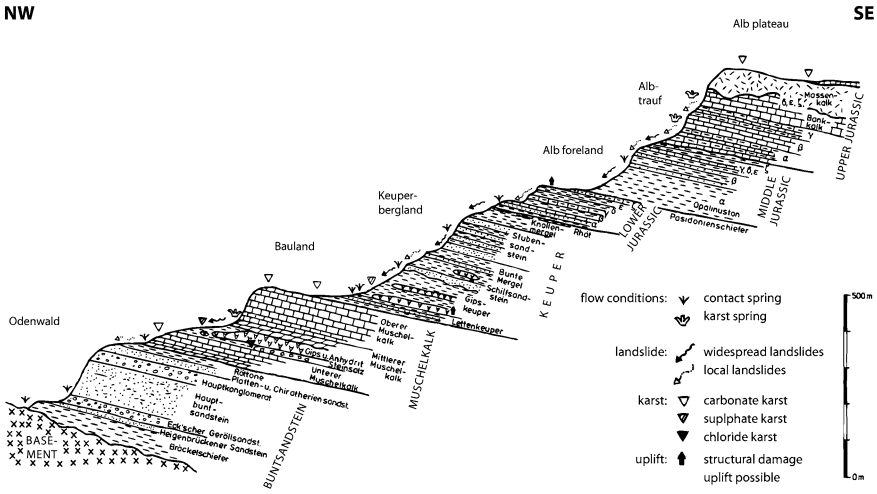

Fig. 3.3 Schematic profile across the South German cuesta landscape with indication of landslide susceptible areas and karst features (after Wagenplast 2004)

triggered landslides (Rothe 2005). A recent study by Meyenfeld (2009) analysed the effects of earthquakes on landslide triggering at the Swabian Alb and emphasized the importance of seismic shaking for landslide initiation.

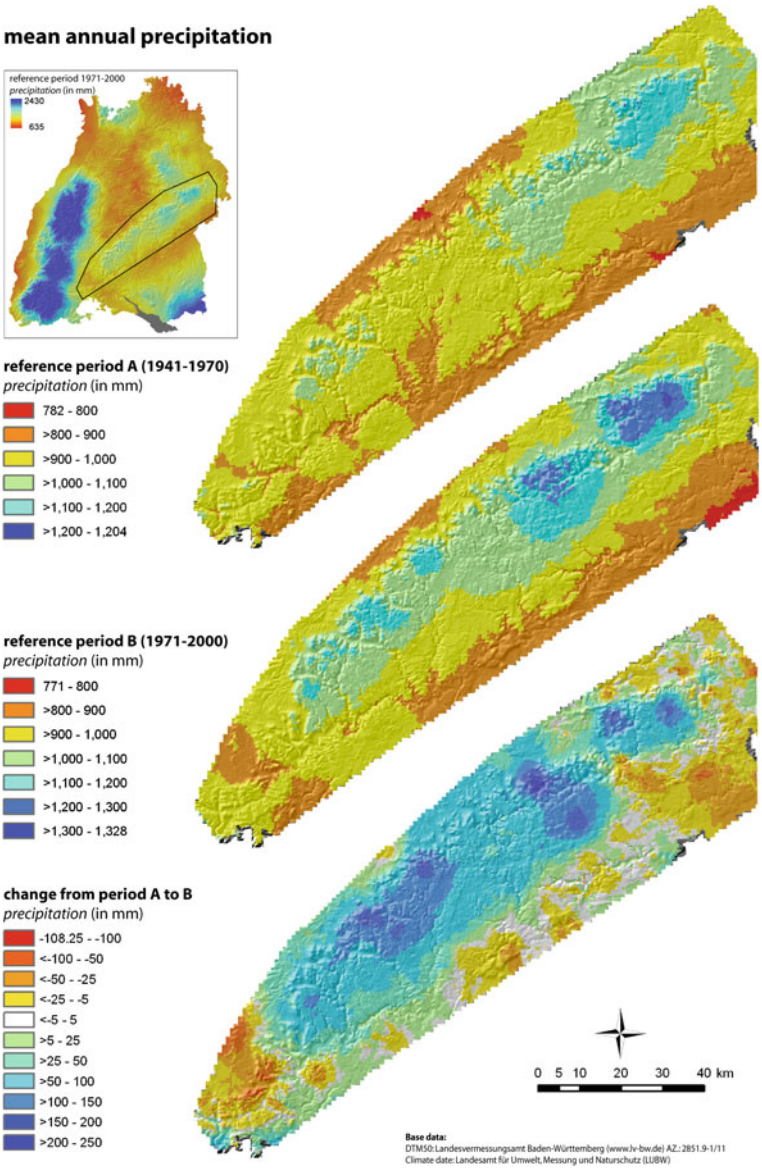

Fig. 3.4 Mean annual precipitation in the Swabian Alb region for period A (1941–1970) and period B (1971–2000) (after Bell 2007)

The potential earthquake threat is accounted for in spatial planning and adaptation of building codes according to earthquake zones (Wirtschaftsministerium Baden-Württemberg 2001).

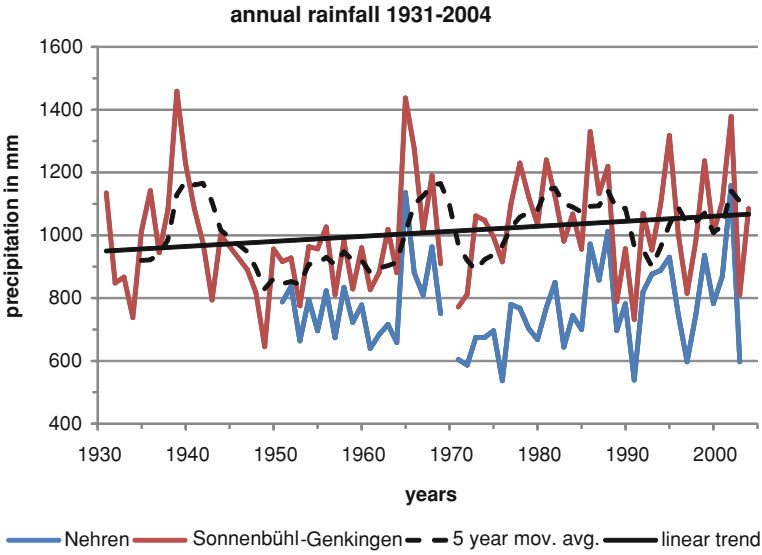

Fig. 3.5 Annual rainfall for two selected weather stations from 1931 to 2004. Five year moving average and linear trend refer to Sonnenbühl-Genkingen

3.1.2 Climate

The climate at the Swabian Alb is typical for Central European regions in the transition zone between oceanic and continental climate conditions (Leser 1982). Local relief and the orientation of the Albtrauf escarpment, however, have strong effects on meso-scale climate. Figure 3.4 illustrates mean annual precipitation for the Swabian Alb for two reference periods and the changes between them. Orographic effects on distribution of rainfall amounts can be observed by, for example, drier conditions one the lee side of the Black Forest, and higher rainfall along the escarpment and on the plateau.

The variability of local climatic conditions can be illustrated by the comparison of two weather stations, Sonnenbühl-Genkingen and Nehren, of which the former is located on the plateau close to the escarpment, and the latter in the foreland (Fig. 3.5). The distance between the stations is roughly 10 km. Precipitation trends are fairly similar; however, Sonnenbühl-Genkingen receives significantly more rainfall. In addition, annual rainfall maxima strongly vary for Sonnenbühl-Genkingen between a maximum of approximately 650 mm and more than 1450 mm with extremely wet years in 1941, 1965 and 2002. An overall trend of increased annual precipitation can be observed.

Distribution of monthly precipitation is illustrated in Fig. 3.6 and demonstrates a high variability. Most precipitation generally occurs in spring and early summer. However, comparison of two reference periods indicates a shift from two rainfall maxima in June and August to one maximum in July.

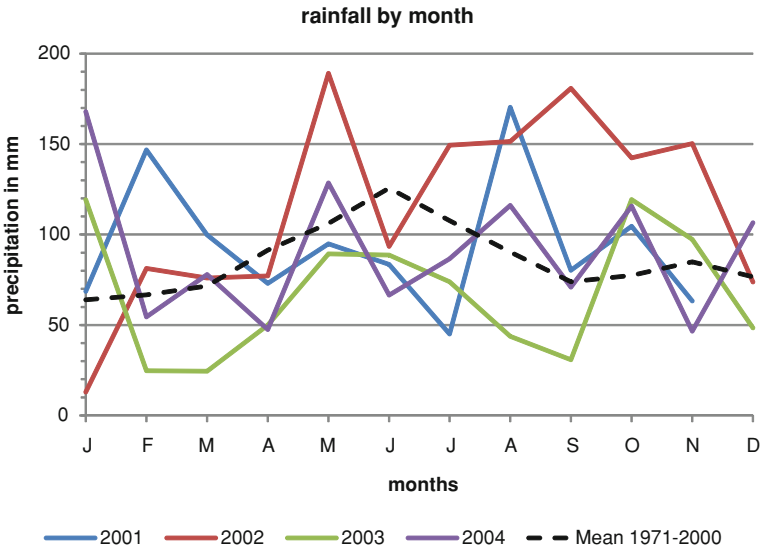

Fig. 3.6 Rainfall by month for selected years for Sonnenbühl-Genkingen station

Mean temperatures in the Swabian Alb vary between 6 and 9°C, with lower temperatures associated with higher elevations on the plateau. Precipitation in winter often occurs as snow, especially in higher elevation areas. Therefore, runoff is often delayed until spring snow melt.

3.1.3 Hydrology

The Swabian Alb is located at the divide between the watersheds draining into the rivers Rhine and Danube. Limestones of the Upper Jurassic, however, are strongly affected by karst processes, thus phreatic watersheds vary from surficial ones. Terhorst (1997) distinguishes between shallow and deep karst. Shallow karst is found in the vicinity of the Albtrauf escarpment and exhibits karst drainage above the elevation of the receiving river causing springs, whereas deep karst drainage occurs below. Only few rivers can be found on the Swabian Alb plateau due to underground karst drainage (Geyer and Gwinner 1997), thus, dry valleys are a common feature on the plateau. Drainage density in the foreland of the Swabian Alb is higher due to less permeable geological strata.

3.1.4 Geomorphology

The landscape of the Swabian Alb was essentially formed under climatic conditions differing from the present (Blume 1971; Dongus 1977; Leser 1982; Brunotte et al. 2007). 18 million years ago, at the time of volcanic activity in the Urach-Kirchheim

Table 3.2 Lithology and typical landslide processes at the Swabian Alb (after on Terhorst 1997)

Lithology	Code	Landslide type
Mittel-Kimmeridge-Kalk	ki2,3,4	Rotational slides, rock and debris falls, rock topples, translational debris slides
Unter-Kimmeridge Mergel	ki1	Flows
Oxford-Kalke	ox2	Combined rotational slides, debris falls, translational debris slides
Oxford-Mergel	ox1	Flows
Braunjuratone, especially Ornaten- and Opalinustone	cl, bt, bj2, al1	Flows, translational slides
Braunjurakalke and –sandsteine	bj1, al2	Rotational slides, flows

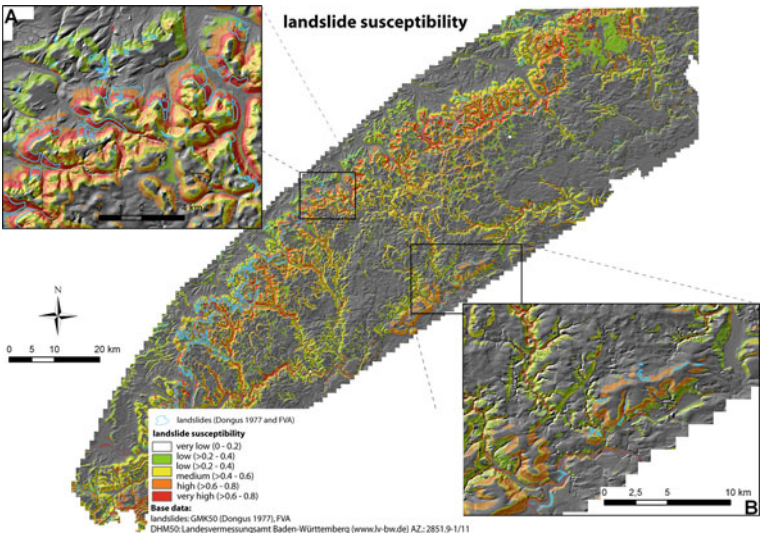

Fig. 3.7 Landslide susceptibility in the Swabian Alb (after Bell 2007). Magnified areas show Irrenberg (**A**) and Fils valley (**B**)

area. The escarpment of the Swabian Alb was about 20 km further north than it is today (Geyer and Gwinner 1986, 1997) which relates to an overall relocation of 1 m/1,000 years (Kallinich 1999). Pleistocene relocation has been assessed to be 2–3 km/1,000 years (Dongus 1977), although the involved processes are not entirely clarified (Terhorst 1997). Detailed discussion of the relocation of the Albtrauf escarpment is provided by Kallinich (1999). Blume (1971) regards solifluction and fluvial erosion as the dominant processes, and rates landslide processes only of local importance for relocation of the Albtrauf escarpment. In contrast, Dongus (1977) emphasizes landslides as one important erosion factor. For Holocene times, most authors assume low geomorphological activity (Büdel 1944; Bleich 1960; Weippert 1960) apart from fluvial erosion and sedimentation, soil erosion, karst processes and local landslides. A geomorphological map (1:100,000) for the Swabian Alb was

Fig. 3.8 Photo of study area taken facing north east. Lines indicate the boundaries of the landslide bodies

established by Dongus (1977), and a 1:25,000 map is available for the map sheet of Mössingen (Leser 1982).

3.1.5 Landslides

Several studies have focussed on landslide processes within the Swabian Alb. Early extensive research include the works of Hölder (1953), Bleich (1960) and Reiff (1968). Within the MABIS project carried out by the University Tübingen, a wide range of methodological approaches were applied (e.g., Bibus 1985, 1986; Kraut 1995; Wiegand 1996; Terhorst 1997; Kallinich 1999; Knipping 1999; Riedinger and Terhorst 1999; Kreja 2000; Thein 2000; Kreja and Terhorst 2005; Neuhäuser and Terhorst 2007). Within the InterRISK project the focus was put onto local and regional landslide hazard and risk analysis, with methodological approaches including analysis of historic sources, geomorphological mapping, geophysical measurements and landslide modelling (Bell 2007; Bell et al. 2006; Brennecke 2006; Kohn 2006; Kruse 2006; Thiebes 2006; Holland 2007). A general relationship between lithology and landslide activity was presented by Terhorst (1997) illustrated in Table 3.2.

Landslide inventories for subareas of the Swabian Alb were established e.g., by Kraut (1995, 1999), Brennecke (2006) and Kohn (2006). Large scale geomorphological maps (1:5,000 to 1:10,000) including landslide processes were

Fig. 3.9 Crack in a house due to slope movements

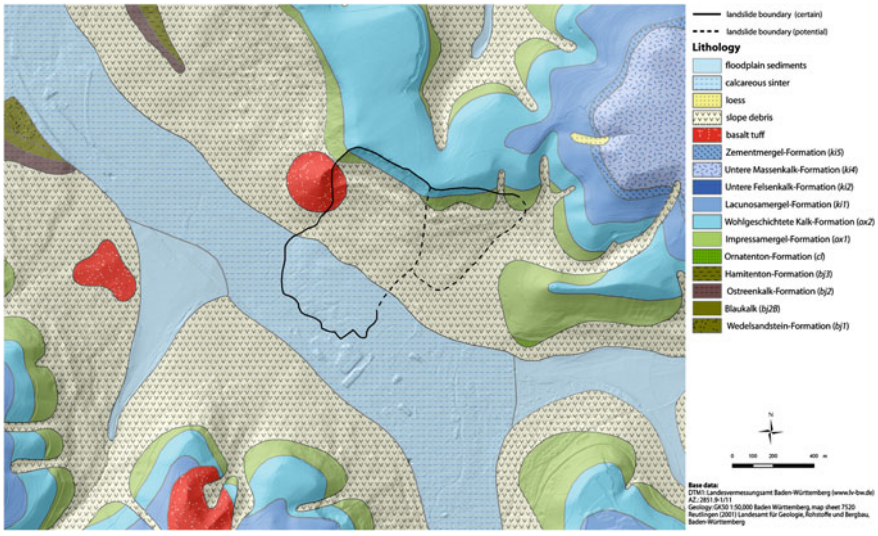

Fig. 3.10 Geological map (1:50,000) and landslide boundaries for the local study area Lichtenstein-Unterhausen (after Bell 2007)

established by Kößler (1997), Terhorst (1997), Kallinich (1999), Kreja (2000) and Bell (2007). A more general map (1:50,000) was developed by Kallinich (1999) for several study areas along the Albtrauf escarpment.

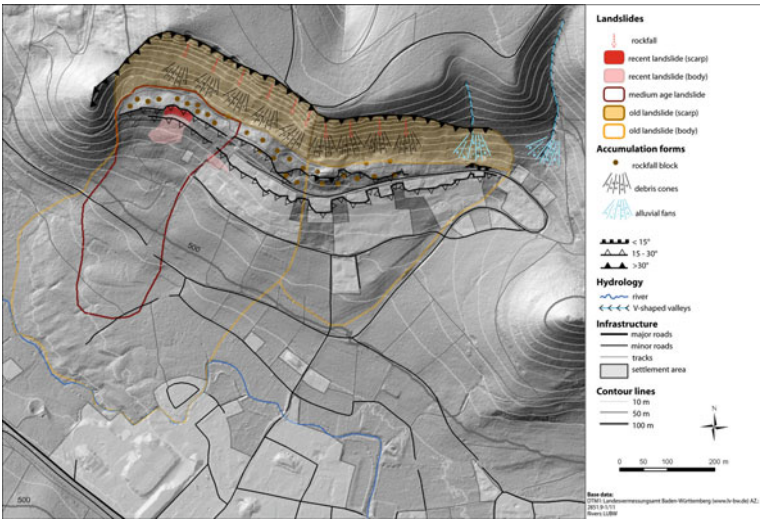

Fig. 3.11 Geomorphological map for the local study area Lichtenstein-Unterhausen (after Bell 2007)

A dendro-geomorphological investigation was carried out by Holland (2007) in which phases of landslide activity were analysed for the Urselberg landslides in Pfullingen.

Several geophysical methods have been applied in local study areas, e.g. seismic (Hecht 2001), geoelectric (Bell et al. 2006; Kruse 2006; Sass et al. 2008), radio-magnetotellurics (Kruse 2006) and georadar (Sass et al. 2008). Kruse and Bell worked on the same landslide, which is also investigated in this work.

Statistical models for delineation of landslide prone areas were established for several areas of the Swabian Alb (Wiegand 1996; Thein 1999, 2000; Bell 2007; Neuhäuser et al. 2005; Neuhäuser and Terhorst 2007). Figure 3.7 illustrates landslide susceptibility for the Swabian Alb developed by Bell (2007), which later has been integrated into regional planning.

Deterministic models for landslide susceptibility modelling have been applied by Kreja (2000), Kreja and Terhorst (2005) and Thiebes (2006). Based on a susceptibility map established by Neuhäuser et al. (2005), Papathoma-Köhle et al. (2007) carried out an analysis of landslide vulnerability for Lichtenstein-Unterhausen to develop a framework to be used in holistic risk assessment.

Research carried out within the InterRISK and ILEWS projects (Röhrs and Dix 2010) was able to extract 216 landslide events from historic data sources, of which most were unknown before. Events date back almost 600 years; however, the majority of detected landslides occurred within the last 300 years. Large landslide events in historic times include the events in Greut (1805) and in Ratshausen (1787 and 1789), in which landslide masses moved far down to the valley floor and blocked the rivers, so that landslide damned lakes were

formed (Groschkopf 1957; Riede 1990; Borngraeber and Geyer 2002). The Plettenberg landslide (1851) and the landslide at the Bronner Mühle (1960) were deep-seated first-time slope failures involving bedrock material. The Irrenberg landslide (1972) was triggered by strong rainfall which occurred after a long dry period, which caused shrinkage cracks to open up, thus, increasing infiltration rates (Fundinger 1985). The most recent large landslide was triggered on 12.04.1983 at the Hirschkopf in Mössingen which involved 6 million m^3 of material (Schädel and Stober 1988). The Mössingen landslides was a reactivation of an old landslide body and has been investigated in detail by several researchers (Bibus 1985, 1986; Fundinger 1985; Schädel and Stober 1988). Final slope failure was preceded by crack openings at the Albtrauf escarpment (Bibus 1985; Schädel and Stober 1988) and caused 1.5 million € damage to forest paths and woods (Fundinger 1985). Another recent example of landslide activity in the Swabian Alb took place in January 2011 close to the community of Lichtenstein, when a 30 m segment of a street collapsed and temporarily interrupted traffic (Müller 2011, personal communication). The landslide cause was reported to be heavy rainfall combined with significant snow melt.

3.2 Local Study Area

In the following, an introduction to the local study area Lichtenstein-Unterhausen in the Echaz valley south of the city of Reutlingen (Fig. 3.1) is presented. Several general aspects regarding the Swabian Alb described previously also apply for the local study area and require no repetition. Therefore, following paragraphs primarily focus on local characteristics, such as geology geomorphology and research of previous investigations.

The slope under investigation faces south-west and occupies an area of approximately 0.5 km^2 (Fig. 3.8). The highest altitude is approximately 780 m AMSL, while the river in the valley is at an elevation of approximately 465 m AMSL. The local study area comprises two large landslide bodies with head scarps at approximately 660 m AMSL. Today, steep slopes and higher elevations areas are dominantly occupied by forest, while lower slopes feature pasture. Settlement activity on the slope under investigation started in the 1960 s and continues today. The local development plan obligates all construction works to be preceded by a geological survey by experts (Heyd 2005 in Bell 2007). However, at least one building suffers frequent cracking due to slope movement in summer and autumn (Fig. 3.9) (Siegler 2005 in Bell 2007). An interesting feature of the local study area is a steep and almost bare limestone scree slope located below the landslide head scarps. The limestone was mined in earlier times and an overall volume of approximately 30,000 m^3 had been extracted (Schönwälder 2006 in Bell 2007).

3.2.1 Geology

The lithology of the study area primarily consists of Upper and Middle Jurassic sediments dipping south west by 1–2° (Fig. 3.10). Slopes are mostly covered by slope debris from Pleistocene solifluction and landslide activity. In addition, fluvial deposits and tufa of late glacial and Holocene age cover the valley bottom. At the highest elevations in the study area Untere Massenkalk Formation (*joMu*) of the Upper Jurassic are present, which consist of series of massive limestone layers intersected by thin marl interstices. Below approximately 730 m AMSL Zementmergel (*ki5*) with an average thickness of 20 m overlies Lacunosamergel (*ki1*) located above approximately. 670 m AMSL. The Upper Jurassic Wohlgeschichtete Kalk Formation (*ox2*) forms a plateau with an elevation of approximately 660 m AMSL. This stratum comprises a series of stratified limestone beds intersected by thin layers of lime marl beds. The underlying Impressamergel (*ox1*) forms steep slopes and can be found up to approximately 610 m AMSL. However, the material is often locally relocated further downslope due to rotational landslide processes. The *ox1*-stratum is characterised by an alternation of marl and marl lime beds. Upper sections mainly consist of massive limestone beds while lower sections also comprise clay marls. Below the *ox1* stratum Medium Jurassic Ornatenton is present which consists of dark claystones with 5–15% of calcium carbonate. The material is often deeply weathered and prone to landslide processes (Ohmert et al. 1988). A thin stratum of Bathonian clays (*bt*), sometimes termed Dentalienton, can be assumed for the study area (Ohmert et al. 1988), however, no outcrops are present. Bajoicum strata *bj3*, *bj2* and *bj1* were mapped in the northwestern part of the study area and comprise clays marl-stones and sandy limestones with clay sections. At several locations volcanic tuff is displayed in the map, originating from tertiary volcanic activity.

3.2.2 Geomorphology

A comprehensive geomorphological map based on field mapping and analysis of a 1 m DTM was established by Bell (2007) (Fig. 3.11). The slope is dominated by two large landslides bodies of which the western is significantly larger. Landslide deposits of the larger mass reach down to the valley floor and altered the course of the river Echaz. Both landslide bodies feature a steplike morphology with flat areas in the head area below the head scarp. Two younger landslides are located on the western landslide body. These movements comprise reactivation of material affected by the older phase of landslide activity. A recent landslide event took place in 1984 on the western end of the settlement area, when a small rotational landslide was triggered by construction works not adapted to local conditions. Superficial and shallow landslide activity can be observed on all slope areas without settlement. A highly active scree slope formed of loose limestone is

located above the head of the oldest landslide deposit. Limestone rocks originating from the *ox2* limestone stratum in the landslide head scarp areas spread at the foot of the scree slope indicate high rockfall activity.

3.2.3 Previous Investigations

The local study area investigated in this thesis has already been studied by the preceding research project InterRISK. Therein, an initial landslide monitoring system was installed comprising inclinometers, geodetic levelling and temporary tiltmeter measurements (Bell 2007). In addition, Kruse (2006) performed a series of geoelectrical measurements to investigate hydrological processes within the landslide bodies.

Based on monitoring results, Bell (2007) concluded that at least parts of the landslide are seasonally reactivating leading to extremely slow displacement rates. Two distinct patterns of movement were distinguished: a deep-seated sliding process down to the bedrock in approximately −15.5 m depth, occurring in spring; and a flow or creep movement of the upper 8.5 m in summer and autumn. Comparison of landslide movement with rainfall data showed no clear relationship. However, a correlation between snow melting and deep-seated sliding could be established. More extensive interpretations of landslide behaviour were limited by the lack of detailed climatic data, the small extent and short period of the slope monitoring, and extremely slow movement rates close to the instruments' noise levels.

Four monthly geoelectrical surveys were performed by Kruse (2006). One of the main results of the investigation was that the limestone scree allows for quick infiltration of rainfall and melting snow, possibly an important factor for initiation of landslide movement. It was, however, neither possible to establish a relationship between geoelectrical monitoring data and landslide displacement, nor to fully describe subsurface hydrological processes.

A recently carried out study of potential damage related to a full reactivation of the landslide bodies in Lichtenstein-Unterhausen (Greiving 2010) resulted in a maximum loss of private property equal to 18.5 million EUR in addition to 1.7 million EUR damage communal infrastructure.

References

Bell R (2007) Lokale und regionale Gefahren- und Risikoanalyse gravitativer Massenbewegungen an der Schwäbischen Alb. University of Bonn, Germany

Bell R, Kruse J-E, Garcia A, Glade T, Hördt A (2006) Subsurface investigations of landslides using geophysical methods-geoelectrical applications in the Swabian Alb (Germany). Geographica Helvetica 3:201–208

Bibus E (1985) Massenverlagerung im Wald und ihre Folgeschäden am Beispiel des Hirschkopfes beiMössingen. Allgemeine Forstzeitschrift 35:901–910
Bibus E (1986) Die Rutschung am Hirschkopf bei Mössingen (Schwäbische Alb). Geowissenschaftliche Rahmenbedingungen-Geoökologische Folgen. Geoökodynamik 7:333–360
Bleich KE (1960) Das Alter des Albtraufs. Jahreshefte des Vereins für Vaterländische Naturkunde in Württemberg 115:39–92
Blume H (1971) Probleme der Schichtstufenlandschaft. Wissenschaftliche Buchgesellschaft, Darmstadt
Borngraeber O, Geyer M (2002) Geologische Karte von Baden-Württemberg, Blatt 7324 Geislingen a.d. Steige-West. Landesamt für Geologie. Rohstoffe und Bergbau, Germany
Brennecke M (2006) Erstellung einer Inventarkarte gravitativer Massenbewegungen an der Schwäbischen Alb—Kartierung aus Luftbildern und einem digitalen Höhenmodell. University of Bonn, Germany
Brunotte E, Glaser R, Radtke U, Reuber P (2007) Schichtstufen und Schichtkämme. In: Gebhardt H (ed) Geographie. Elsevier, Physische Geographie und Humangeographie. Munich, Germany, pp 323–325
Büdel J (1944) Die morphologischen Wirkungen des Eiszeitklimas im gletscherfreien Gebiet. Beiträge zur Geomorphologie der Klimazonen und Vorzeitklimate I. Geologische Rundschau (34):482–519
Dongus H (1977) Die Oberflächenformen der Schwäbischen Alb und ihres Vorlandes. Marburger Geographische Schriften, Marburg
Fundinger A (1985) Ingenieurgeologische Untersuchung und geologische Kartierung (Dogger/Malm) der näheren Umgebung der Rutschungen am Hirschkopf bei Mössingen und am Irrenberg bei Thanheim (Baden-Würrtemberg). Geowissenschaftliche Fakultät University Tübingen, Germany
Geyer O, Gwinner MP (1986) Geologie von Baden-Württemberg. E. Schweizerbart, Stuttgart
Geyer OF, Gwinner MP (1997) Sammlung geologischer Führer, Bd.67, Die Schwäbische Alb und ihr Vorland, 3rd edn. Borntraeger, Stuttgart
Grees H (1993) Die Schwäbische Alb. In: Borcherdt C (ed) Geographische Landeskunde von Baden-Württemberg. Schriften zur politischen Landeskunde Baden-Württembergs, Band 8. Stuttgart, Germany: W. Kohlhammer GmbH, pp 332–362
Greiving S (2010) Risikomanagement. In: Bell R, Pohl J, Glade T, Mayer J, Greiving S (eds) Integrative Frühwarnsysteme für gravitative Massenbewegungen (ILEWS) Monitoring, Modellierung, Implementierung. Klartext, Essen, pp 203–230
Groschkopf P (1957) Der große Bergsturz von 1805 bei Hausen-Fils. Geschichtliche Mitteilungen von Geislingen und Umgebung 15:81–83
Hecht S (2001) Anwendung refraktionsseismischer Methoden zur Erkundung des oberflächennahen Untergrundes: Mit acht Fallbeispielen aus Südwestdeutschland. University of Stuttgart, Germany
Hölder H (1953) Erosionsformen am Trauf der Schwäbischen Alb. Neues Jahrbuch fürGeologie und Paläontologie 97:345–378
Holland R (2007) Dendrogeomorphologische Untersuchungen an einem Rutschhang am Ursulaberg, Pfullingen, Schwäbische Alb. University of Bonn, Germany
Kallinich J (1999) Verbreitung, Alter und Ursachen von Massenverlagerungen an der Schwäbischen Alb auf der Grundlage von geomorphologischen Kartierungen. In: Bibus E, Terhorst B (eds) Angewandte Studien zu Massenbewegungen. Tübinger Geowissenschaftliche Arbeiten, pp 59–82
Knipping M (1999) Pollenanalytische Datierungen an Feuchtsedimenten auf Hangrutschungen in Südwestdeutschland. In: Bibus E, Terhorst B (eds) Angewandte Studien zu Massenbewegungen, Tübinger Geowissenschaftliche Arbeiten, pp 117–128
Kohn J-C (2006) Potenzial der Auswertung des Archivs der Straßenbauverwaltung für die Risikoforschung—Nutzung des Archivs der Baustoff und Bodenprüfstelle Ludwigsburg als historische Quelle. University of Bonn, Germany

Kößler U (1997) Relief, Böden und Deckschichten in ausgewählten Gebieten der Jurastufe bei Göppingen. University Tübingen, Germany

Kraut C (1995) Der Einfluß verschiedener Geofaktoren auf die Rutschempfindlichkeit an der Schichtstufe der Schwäbischen Alb. University Tübingen, Germany

Kraut C (1999) Der Einfluss verschiedener Geofaktoren auf die Rutschempfindlichkeit an der Schichtstufe der Schwäbischen Alb. In: Bibus E, Terhorst B (eds) Angewandte Studien zu Massenbewegungen. Tübinger geowissenschaftliche Arbeiten, pp 129–148

Kreja R (2000) Die Entwicklung einer Gefährdungskarte für Rutschungen am Schönberger Kapf bei Öschingen unter Anwendung eines Geographischen Informationssystems. University Tübingen, Germany

Kreja R, Terhorst B (2005) GIS-gestützte Ermittlung rutschungsgefährdeter Gebiete am Schönberger Kapf bei Öschingen (Schwäbische Alb). Die Erde 136(4):395–412

Kruse JE (2006) Untergrunderkundung und Monitoring von gravitativen Massenbewegungen mit Gleichstromgeoelektrik und Radiomagnetotellurik. University of Bonn, Germany

Leser H (1982) Erläuterungen zur Geomorphologischen Karte 1:25,000 der Bundesrepublik Deutschland. GMK 25 Blatt 9 7520 Mössingen Geomorphologische Detailkartierung in der Bundesrepublik Deutschland, Stuttgart

Meyenfeld H (2009) Modellierungen seismisch ausgelöster gravitativer Massenbewegungen für die Schwäbische Alb und den Raum Bonn und Erstellen von Gefahrenhinweiskarten. University of Bonn, Germany

Neuhäuser B, Terhorst B (2007) Landslide susceptibility assessment using. Geomorphology 86(1–2):12–24

Neuhäuser B, Strobl J, Blaschke T, Griesebner G (2005) Probabilistische Beurteilung der Rutschanfälligkeit zur Einschätzung der Gefährdung durch Hangrutschungen am Beispiel Schwäbische Alb (Probabilistic Assessment of Landslide Susceptibility for Landlside Hazard Estimation in the Swabian Alb). In: Angewandte Geoinformatik 2005–Beiträge zum 17. AGIT-Symposium Salzburg. Wichmann Verlag, Heidelberg, Germany, pp 129–137

Ohmert W, Von Koenigswald W, Münzing K, Villinger E (1988) Erläuterungen zu Blatt 7521 Reutlingen (Geologische Karte 1:25.000 von Baden Württemberg). Geologisches Landesamt Baden-Württemberg

Papathoma-Köhle M, Neuhäuser B, Ratzinger K, Wenzel H, Dominey-Howes D (2007) Elements at risk as a framework for assessing the vulnerability of communities to landslides. Nat Hazards Earth Syst Sci 7(6):765–779 Accessed 1 Oct 2010

Reiff H-J (1968) Die Bergrutsche und Bergschlipfe am Trauf der Schwäbischen Alb. University Tübingen, Germany

Riede G (1990) Heimat-Chronik Ratshausen. Eigenverlag, Germany

Riedinger R, Terhorst B (1999) Vegetationsökologische Befunde in Rutschgebieten der Mittleren Schwäbischen Alb. In: Bibus E, Terhorst B (eds) Angewandte Studien zu Massenbewegungen. Tübinger Geowissenschaftliche Arbeiten, pp 97–116

Röhrs M, Dix H (2010) Rekonstruktion historischer Ereignisse. In: Bell R, Pohl J, Glade T, Mayer J, Greiving S (eds) Integrative Frühwarnsysteme für gravitative Massenbewegungen (ILEWS) Monitoring, Modellierung, Implementierung. Klartext, Essen, pp 46–61

Roth R (2004) Das Ermstal zwischen Neckartenzlingen und Bad Urach: eine Studie zur Erd- und Landschaftsgeschichte eines schwäbischen Flusstals. Theiss Verlag, Stuttgart

Rothe P (2005) Die Geologie Deutschlands. 48 Landschaften im Portrait, 2nd edn. Primus Verlag, Darmstadt

Sass O, Bell R, Glade T (2008) Comparison of GPR, 2D-resistivity and traditional techniques for the subsurface exploration of the Öschingen landslide, Swabian Alb (Germany). Geomorphology 93(1–2):89–103

Schädel K, Stober I (1988) Rezente Großrutschungen an der Schwäbischen Alb. Jahreshefte des Geologischen Landesamtes Baden-Württemberg (30):431–439

Terhorst B (1997) Formenschatz, Alter und Ursachenkomplexe von Massenverlagerungen an der schwäbischen Juraschichtstufe unter besonderer Berücksichtigung von Boden- und Deckschichtenentwicklung. Tübingen, Germany

Thein S (1999) Massenverlagerungen an der Schwäbischen Juraschichtstufe-statistische Bewertungsmodelle und Entwicklung von Gefährdungskarten unter Anwendung eines Geographischen Informationssystems. In: Bibus E, Terhorst B (eds) Angewandte Studien zu Massenbewegungen. Tübinger Geowissenschaftliche Arbeiten. pp 59–82

Thein S (2000) Massenverlagerungen an der Schwäbischen Alb-Statistische Vorhersagemodelle und regionale Gefährdungskarten unter Anwendung eines Geographischen Informationssystems. Tübingen, Germany

Thiebes B (2006) Räumliche Gefährdungsmodellierung flachgründiger Hangrutschungen-GIS gestützte Analyse an der Schwäbischen Alb. University of Bonn, Germany

Wagenplast P (2005) Ingenieurgeologische Gefahren in Baden-Württemberg. Landesamt für Geologie, Rohstoffe und Bergbau, Freiburg

Walter R (1995) Geologie von Mitteleuropa. 6th ed Schweizerbart'Sche Verlagsbuchhandlung

Weippert D (1960) Zur Gliederung, Bildung und Altersstellung des Kalksteinschutts am Trauf derwestlichen Schwäbischen Alb. Eiszeitalter und Gegenwart 11:24–30

Wiegand T (1996) Modellierung von Massenverlagerungen und ihre Darstellung in Gefährdungskarten auf Blatt 7719 Balingen mit Hilfe von Geographischen Informations systemen. University of Tübingen, Germany

Wirtschaftsministerium Baden-Württemberg (2001) Erdbebensicheres Bauen. Planunshilfe für Bauherren, Architekten und Ingenieure., Stuttgart

Chapter 4
Data

Various data sources were used within this study. A compilation of all data and their characteristics and sources is illustrated in Table 4.1. Additional information is presented in the following.

The Digital Terrain Model (DTM) provides detailed information on topography and was acquired between 2002 and 2004 by airborne laserscanning during periods with low vegetation cover (December to April) (Landesvermessungsamt Baden-Württemberg 2010). Vegetation and infrastructure, such as houses and bridges were removed by post-processing to produce a hydrological correct DTM with a spatial resolution of 1 × 1 m.

Geological maps for the local study area are available in 1:25,000 and 1:50,000 scales, however, only the latter exists as a digital version. Additional information on geological characteristics of the local study area, including detailed description of several drillings, is available from Ohmert et al. (1988).

Several sources of information on landslides in the Swabian Alb were available for this study.

Kallinich (1999) mapped plateau areas of large rotational landslides and recent, mostly small landslides located nearby. Field mapping was carried out at 1:25,000 scale, the final was presented in 1:50,000 scale.

A landslide inventory and database was established by Tübingen University and is essentially based on the work of Kraut (1995). Data was acquired by an analysis of literature sources, and geological and forestry site maps. The latter distinguish between active landslide susceptibility, inactive landslide and potentially susceptible to landslides, and were produced for all state-owned forests in Baden-Württemberg.

Landslide locations are illustrated as point information, and timing is acknowledged.

Within the InterRISK and ILEWS projects, investigations using historical archives have been carried out to extract information related to landslide occurrences in the Swabian Alb. Data sources included several national and communal archives and forestry records. Additional information is provided by Röhrs and Dix (2010).

B. Thiebes, *Landslide Analysis and Early Warning Systems*, Springer Theses,
DOI: 10.1007/978-3-642-27526-5_4, © Springer-Verlag Berlin Heidelberg 2012

Tab. 4.1 Overview of data used within this study

Data type	Info	Format	Resolution	Source
Topography				
DTM1 (Digital Terrain Model)	Airborne laser scans acquired between 2002 and 2004, available for the entire Swabian Alb	ESRI grid	1 × 1 m	Umweltministerium Baden-Württemberg (UM BW), Landesanstalt für Messung, Umwelt und Naturschutz (LUBW), Landesvermessungsamt Baden-Württemberg (LV BW)
Geology				
GK25 (Geological map)	Map sheet 7521 (Reutlingen)	Printed map	1:25,000	Landesamt für Geologie, Rohstoffe und Bergbau Baden-Württemberg (LGRB BW)
GK50 (Geological map)	Map sheet 7520 (Reutlingen)	ESRI shape files (polygons)	1:50,000	LGRB BW
Landslides				
General landslide map	For parts of Swabian Alb	Printed map	1:25,000, 1:50,000	Kallinich (1999)
Inventory University of Tübingen	For parts of Swabian Alb	EXCEL table with point coordinates		Working group Bibus and Terhorst, Institute of Geography, University of Tübingen; Forstliche Versuchs- und Forschungsanstalt Baden-Württemberg (FVA)
Inventory InterRSIK/ ILEWS	Historical research in archives and forestry records	Text and EXCEL files		InterRISK project (Röhrs and Dix 2010)
Inventory Filstal April 1994	Event inventory	ESRI shape files (polygons)		Bell et al. (2010, personal communication)

(continued)

Tab. 4.1 (continued)

Data type	Info	Format	Resolution	Source
Inventory Upper Filstal	Interpretation of aerial photos and DTM	ESRI shape files (polygons)		Brennecke (2006)
Inventory Department of Transportation Stuttgart	Archive analysis and DTM mapping	ESRI shape files (points and polygons)		Kohn (2006)
Climate				
Station data	Temperature, precipitation	EXCEL and text files	30 min to daily	DWD, LUBW
Regionalised rainfall data	Interpolated rainfall and temperature, modelled evaporation and snow water equivalent	ESRI grid	500 × 500 m	LUBW
ILEWS weather station	Precipitation, humidity, temperature, air pressure, wind, radiation, snow height	Raw data	Hourly measurement	Camek et al. (2010) (ILEWS)
COSMO-DE (rainfall forecasts)	2 cumulative model runs per day with 13 predictions each	GRIB files	Hourly measurement	DWD
KOSTRA-DWD (rainfall intensity probabilities)	Available for Baden-Württemberg	Software program	8.45 × 8.45 km	LUBW
Geophysical data				
Geoelectric	1 profile	Analysed data	Monthly measurement	Kruse (2006) and Bell (2007)
Geoelectric	2 profiles	Analysed data	Single measurement	Wiebe and Krummel (2010) (ILEWS)
Geoseismic	4 profiles	Analysed data	Single measurement	Bell et al. (2010) (ILEWS)

(continued)

Tab. 4.1 (continued)

Data type	Info	Format	Resolution	Source
Movement monitoring				
Geodetic monitoring	Geodetic network and geodetic height	Analysed data	Measurements every 3 months	Aslan et al. (2010) (ILEWS)
Inclinometers	3 inclinometers	Raw data	Measurements every 3 months	InterRISK project, Bell (2007), Bell and Thiebes (2010) (ILEWS)
Inclinometer chain	5 inclinometer between 3 and 15 meter depth	Raw data	Measurements every 30 min	Bell and Thiebes (2010) (ILEWS)
Hydrological monitoring				
Tensiometers and TDR sensors	27 sensors each at 9 locations	Raw data	Hourly measurements	Camek and Becker (2010) (ILEWS)
Geoelectrical monitoring	2 profiles	Raw and analysed data	Measurements every 2 h	GeoFact (ILEWS)
Drill cores				
InterRISK	3 drill cores	Drill cores and laboratory results		Bell (2007)
ILEWS project	2 drill cores	Drill cores and laboratory results		University of Vienna (ILEWS)
Geotechnical data				
Laboratory analyses	Soil particle distribution, water content, CaCO3, soil water retention curves	EXCEL file		Christa Herrmann, University of Vienna
Substrate database	Collection of values from literature	ACCESS data base		Meyenfeld (2010, personal communication)
SPAW model	Geotechnical parameter values	Software program		Saxton and Rawles (2006)

Another landslide inventory was provided by Bell et al. (2010, personal communication), and contains information on a multiple landslide event in the Fils Valley in April 1994.

Brennecke (2006) created a landslide inventory based on interpretation of aerial photographs and hillshade analysis. Four landslide process types were distinguished, i.e. rotational and translational slides, flows and complex landslides.

Kohn (2006) compiled a landslide inventory based on archive data from the Department of Transportation of the administrative district Stuttgart. Parts of the archived landslide were later mapped on a DTM. However, only a small part of its study area covers the Swabian Alb and could be employed within this study.

Climatic data available for this study derives from three sources: National Meteorological Service Deutscher Wetterdienst (DWD), Landesanstalt für Messung, Umwelt und Naturschutz Baden-Württemberg (LUBW), and data from a local weather station installed and operated by the ILEWS project. Additional information on rainfall forecasts (COSMO-DE) and rainfall intensities for scenarios of various annual probabilities (KOSTRA) was also utilised within this study.

Data on precipitation and temperature for 14 DWD and 16 LUBW stations within the Swabian Alb covers the period until 2006 and provides a temporal resolution of 30 min–1h. For two stations located close to the local study area Lichtenstein-Unterhausen data extends to 2011. Additional rainfall data from all DWD weather stations was provided by DWD for the period from 2006 to 2009.

For the period 1983–2003 regionalised climate data were provided by LUBW. Data on precipitation, temperature, and modelled evaporation and snow height as water equivalent are available as 500 × 500 m grid data with a daily resolution. Interpolated precipitation and temperature data are considered to be very reliable by LUBW. Modelling results, however, exhibit larger uncertainties as local characteristics such as wind drift are not represented. For a 10 day period however, data is assumed to be reliable (Gudera in Bell 2007). Additional information on regionalised climate data is available in Ministerium für Umwelt und Verkehr (UVM) and Landesanstalt für Umweltschutz (LfU) (2004).

A weather station was installed in the local study area by the ILEWS project in August 2008. Measured parameters include:

- precipitation (two tipping bucket rain gauges of which one is heated)
- relative humidity (capacitative humidity sensor by polymer)
- air temperature (resistance temperature)
- air pressure (capacitative absolute pressure sensor)
- wind direction (potentiometer) and wind velocity (Reed switch)
- global radiation (thermopile)
- reflected radiation (thermopile)
- snow height (ultrasound)
- volumetric soil water content (TDR sensors)
- soil suction in 30 and 50 cm depth (tensiometer)
- soil temperature (semiconductor sensor in TDR probe).

All parameters are measured at intervals of 60 min and subsequently transferred to a data server and parsed into the ILEWS project server available by ODBC. However, no data from the weather station is available from mid-September to mid-November 2009 due to damage caused by animals, and for two weeks in July 2010 due to power failure. Additional information on climatic monitoring is provided by Camek and Becker (2010).

COSMO-DE is the most complex weather forecasting model employed by DWD for short-term prediction of weather conditions (Deutscher Wetterdienst (DWD) 2010a, b). COSMO-DE is the German contribution to the Consortium for Small-scale Modeling (COSMO) founded in 1998. The goal of COSMO-DE is modelling of meteorological processes and prediction of parameters such as air pressure, temperature, wind, water vapour, clouds and precipitation with the aim to provide timely warning for severe weather conditions. Further information on COSMO can be found on the consortium's website (Consortium for Small Scale Modeling 2007). Within COSMO-DE meteorological processes are simulated in eight daily model runs, each with prediction time of 18 h. COSMO-DE predictions have a very high spatial resolution of 0.025 degrees (2.8 × 2.8 km grid cells) and 50 vertical levels, and cover Germany and parts of the surrounding countries. Rainfall forecast from COSMO-DE model were provided by the DWD for the period from September 2006 to December 2009 as cumulative simulation runs. For every day, two simulations, each with a simulated length of 12 h, are available in GRIB format.

Information on the probability of rainfall events was available from the KOSTRA atlas distributed by the DWD. KOSTRA (Koordinierte Starkniederschlags-Regionalisierungs-Auswertungen) represents a collection of maps implemented as an interactive computer program. KOSTRA provides rainfall intensities for events of a certain annual probability and was primarily developed for the design of technical water management systems, e.g., urban drainage infrastructure. KOSTRA is based on complex statistical regionalisation of precipitation data between 1951 and 2000 of 4500 climate stations in Germany. Annual rainfall probabilities vary between 0.5 and 100 years; storm duration between 5 min and 72 h. Information on storm characteristics can be retrieved for single grid cells of 8.45 × 8.45 km and exported as scenarios with varying rain intensities over the course of the storm events. Additional information on KOSTRA is available in Bartels et al. (2005) and Malitz (2005).

Kruse (2006) carried out monthly geoelectrical surveys on the test slope in Lichtenstein-Unterhausen from January to March 2006, which were later continued by Bell (2007). Investigations utilised an ABEM Terrameter SAS 300 apparatus, and results are available as inverted plots. Further information is available in Bell et al. (2006), Kruse (2006), and Bell (2007).

In the initial phase of the ILEWS project, geophysical investigtations were carried out featuring geoelectrical and geoseismic surveys (Bell et al. 2010). Two geoelectrical profiles were acquired with an AGI STING/SWIFT R1 IP apparatus with Wenner and Schlumberger plot configuration. Within a 24 h period 2 profiles were measured, each 126 m long (3 m electrode spacing and 42 electrodes with

3 m spacing) with an average penetration depth of approximately 20 m. Seismic prospection was carried out in cooperation with partners from the ILEWS project applying a Bison 9048DIFP apparatus with 49 geophones with 4 metres spacing to measure 4 profiles. All geophysical prospection data was analysed and processed by Heinrich Krummel from the company geoFact and is available as data inversion plots.

A geodetic network in the local study area, consisting of 15 installed points, was measured every three months between November 2007 and December 2009 by a working group within the ILEWS project (Aslan et al. 2010). Measurements were taken by a Leica TCRP 1201 + (SN 238310). In addition, geodetic heights were assessed with a Trimble DiNi 12 (SN 700118). A total number of seven measurements are available as maps displaying deformation. Unfortunately, most epochs do not include measurement of stable points outside of the potential landslide area. Therefore, data only provides information on relative deformation within the geodetic network.

Additional information on slope movement existed from five inclinometers positioned in the local study area, of which three have been installed within the InterRISK project, and two during the ILEWS project. Manual measurements of inclinometers began in 2004 (Bell 2007) and were continued periodically with a mobile NMG probe by Glötzl with an accuracy of 0.01–0.1 mm per step. This relates to an error margin of 0.2–0.3 mm for 10 and 15 m depths, respectively. In addition, an automated inclinometer chain by Glötzl (NMGD VP/2/10) with five sensors in depths from 3 to 15 m in one borehole has been in operation since May 2009. Linearity of the automated system is ±0.2%, and hysteresis ±0.02% of the final value. The error margin is approximately 1.5–3 mm at the surface (Glötzl 2010, personal communication). Measurements are taken every hour and are processed by GLA software by Glötz, and consequently retrieved by ILEWS data server. However, for some periods no measurements were possible due to damage by construction works and electrical power failure. Additional information is also provided by Bell and Thiebes (2010).

The local monitoring system installed and operated by the ILEWS project included tensiometers, TDR probes and two geoelectrical profiles to asses slope hydrology. Management and maintenance of the technical slope hydrology monitoring system were carried out by ILEWS project partners (Camek et al. 2010).

Tensiometers and TDR probes were in most cases connected to computers in the field by cable; however, for one location wireless radio transmission was applied. T8 tensiometers from UMS were applied within the ILEWS project, measuring soil suction if installed above the local groundwater table. In addition, tensiometers can also be utilised as piezometers if they are located within the phreatic zone. Measurement of volumetric water content was achieved by TDR sensors (TRIME PICO probes by IMKO). Tensiometers and TDR probes provide detailed data on soil hydrology with hourly measurements available from August 2008 to July 2010. However, for certain periods no data is available due to power failures. Moreover, tensiometers require frequent refills with water to ensure

correct measurements of soil suction. Unfortunately, ongoing maintenance of tensiometers could not always be ensured which caused some sensors to run dry.

Geoelectrical monitoring in the local study area Lichtenstein-Unterhausen is maintained by the ILEWS project partner geoFact (Wiebe and Krummel 2010) and started in June 2008 with a vertical slope profile followed by a horizontal profile in August 2009. A LGM 4-Punkt light 10 W apparatus by Lippmann Geophysikalische Messinstrumente was applied for geoelectrical monitoring and took measurements every two hours. Altogether, 48 electrodes were installed on the vertical profile, and 36 on the horizontal profile. Measurement data is stored on the in-field computer and consequently retrieved by the ILEWS data server. Data is available on the web-based ILEWS data platform allowing for simple data analyses, such as visualisation of single data points and resistivity pseudo-sections. More advanced data analyses including time-lapse inversion of data were performed manually by geoFact.

From the InterRISK project, three bore logs originating from inclinometer installations were available, including laboratory results reflecting water, $CaCo_3$ content and soil particle size distributions. Two additional bore logs were acquired during the ILEWS project and subsequently analysed in the laboratory by Christa Herrmann, Institute for Geography and Regional Research, University of Vienna. Soil particle size distribution was carried out according to Austrian Norm (ÖNORM) by Köhn pipette analysis. In addition, contents of water and $CaCO_3$ were assessed. For a small number of samples water retention curves were elaborated.

A collection of geotechnical parameter values (cohesion, angle of internal friction, density etc.) based on experimental analysis in the literature was provided by Meyenfeld (2010, personal communication). The database contains 1,288 entries for a large variety of rock and soil materials, often including minimum and maximum values.

Another source of information for geotechnical and hydrological parameterisation was the soil database integrated into the SPAW (Soil-Plant-Air-Water) model that was developed by Saxton and Rawls (2006). The database was developed as a computer program, in which soil hydrological parameters can be selected based on soil particle size distributions as input parameters.

References

Aslan AM, Burghaus S, Li L, Schauerte W, Kuhlmann H (2010) Bewegungen an der Oberfläche. In: Bell R, Pohl J, Glade T, Mayer J, Greiving S (eds) Integrative Frühwarnsysteme für gravitative Massenbewegungen (ILEWS) Monitoring, Modellierung, Implementierung. Klartext, Essen, pp 74–84

Bartels H, Dietzer B, Malitz G, Albrecht FM, Guttenberg J (2005) KOSTRA-DWD-2000. Starkniederschlagshöhen für Deutschland (1951–2000). Fortschreibungsbericht. Deutscher Wetterdienst (DWD) Abteilung Hydrometeorologie, Offenbach

Bell R (2007) Lokale und regionale Gefahren-und Risikoanalyse gravitativer Massenbewegungen an der Schwäbischen Alb. University of Bonn, Germany

Bell R, Thiebes B (2010) Untergrundbewegungen. In: Bell R, Pohl J, Glade T, Mayer J, Greiving S (eds) Integrative Frühwarnsysteme für gravitative Massenbewegungen (ILEWS) Monitoring, Modellierung, Implementierung. Klartext, Essen, pp 84–92

Bell R, Kruse J-E, Garcia A, Glade T, Hördt A (2006) Subsurface investigations of landslides using geophysical methods—geoelectrical applications in the Swabian Alb (Germany). Geographica Helvetica (3), pp 201–208

Bell R, Wiebe H, Krummel H (2010) Vorerkundung. In: Bell R, Pohl J, Glade T, Mayer J, and Greiving S (eds) Integrative Frühwarnsysteme für gravitative Massenbewegungen (ILEWS) Monitoring, Modellierung, Implementierung. Klartext, Essen, pp 62–69

Brennecke M (2006) Erstellung einer Inventarkarte gravitativer Massenbewegungen an der Schwäbischen Alb—Kartierung aus Luftbildern und einem digitalen Höhenmodell unpublished Dimplomarbeit. University of Bonn, Germany

Camek T, Becker R (2010) Klima. In: Bell R, Pohl J, Glade T, Mayer J, and Greiving S (eds) Integrative Frühwarnsysteme für gravitative Massenbewegungen (ILEWS) Monitoring, Modellierung, Implementierung. Klartext, Essen, pp 69–74

Camek T, Becker R, Öhl S (2010) Bodenfeuchte (TDR, Tensiometer). In: Bell R, Pohl J, Glade T, Mayer J, Greiving S (eds) Integrative Frühwarnsysteme für gravitative Massenbewegungen (ILEWS) Monitoring, Modellierung, Implementierung. Klartext, Essen, pp 92–100

Consortium for Small Scale Modeling (2007) Operations at DWD—COSMO-DE [Online]. Available at: http://www.cosmo-model.org/content/tasks/operational/dwd/default_de.htm. Accessed 24 Jan 2011

Deutscher Wetterdienst (DWD) (2010a) COSMO [Online]. Available at: http://www.dwd.de/sid_T1MhMx2KB2L6TQDG8c2s8CgyWLG6vd2H4M46N37j5N8wb2tMxzHr!626907054!791452674!1290927658132/bvbw/appmanager/bvbw/dwdwwwDesktop?_nfpb=true&_pageLabel=_dwdwww_spezielle_nutzer_forschung_analyse&T2040905640115467453372 6gsbDocumentPath=Navigation%2FForschung%2FAnalyse__Modellierung%2FFU__koop__proj__COSMO__node.html%3F__nnn%3Dtrue&_state=maximized&_windowLabel=T2040905640115467453372 6. Accessed 24 Jan 2011

Deutscher Wetterdienst (DWD) (2010b) Wettervorhersagemodelle [Online]. Available at: http://www.dwd.de/sid_D31WN9NSVwLdMVZnCBnG6ppbNKJTvH6pMsg3sSWmRmVHMvscH7T1!-183911575!-240204644!1295863186793/bvbw/appmanager/bvbw/dwdwwwDesktop?_nfpb=true&_pageLabel=_dwdwww_spezielle_nutzer_forschung_analyse&T1220383709113 9841917821gsbDocumentPath=Content%2FForschung%2FFE1%2FNumerische__Vorhersagemodelle%2FFU__Numerische__Vorhersagemodelle__teaser html&_state=maximized&_windowLabel=T1220383709113984191782 1&lastPageLabel=_dwdwww_spezielle_nutzer_forschung_analyse. Accessed 24 Jan 2011

Kallinich J (1999) Verbreitung, Alter und Ursachen von Massenverlagerungen an der Schwäbischen Alb auf der Grundlage von geomorphologischen Kartierungen. In: Bibus E, Terhorst B (eds) Angewandte Studien zu Massenbewegungen. Tübinger Geowissenschaftliche Arbeiten, pp 59–82

Kohn J-C (2006) Potenzial der Auswertung des Archivs der Straßenbauverwaltung für die Risikoforschung—Nutzung des Archivs der Baustoff und Bodenprüfstelle Ludwigsburg als historische Quelle. University of Bonn, Germany

Kraut C (1995) Der Einfluß verschiedener Geofaktoren auf die Rutschempfindlichkeit an der Schichtstufe der Schwäbischen Alb. University Tübingen, Germany

Kruse JE (2006) Untergrunderkundung und Monitoring von gravitativen Massenbewegungen mit Gleichstromgeoelektrik und Radiomagnetotellurik. University of Bonn, Germany

Landesvermessungsamt Baden-Württemberg (2010) Geodaten [Online]. Available at: http://www.lv-bw.de/lvshop2/index.htm. Accessed 22 March 2011

Malitz G (2005) KOSTRA-DWD-2000. Starkniederschlagshöhen für Deutschland (1951–2000). Grundlagenbericht. Deutscher Wetterdienst (DWD), Hydrometeorologie, Offenbach

Ministerium für Umwelt und Verkehr (UVM) and Landesanstalt für Umweltschutz (LfU) (eds) (2004) Wasser- und Bodenatlas Baden-Württemberg. Stuttgart, Karlsruhe

Ohmert W, Von Koenigswald W, Münzing K, Villinger E (1988) Erläuterungen zu Blatt 7521 Reutlingen (Geologische Karte 1:25.000 von Baden Württemberg). Geologisches Landesamt Baden-Württemberg

Röhrs M, Dix H (2010) Rekonstruktion historischer Ereignisse. In: Bell R, Pohl J, Glade T, Mayer J, Greiving S (eds) Integrative Frühwarnsysteme für gravitative Massenbewegungen (ILEWS) Monitoring, Modellierung, Implementierung. Klartext, Essen, pp 46–61

Saxton KE, Rawls WJ (2006) Soil water characteristic estimates by texture and organic matter for hydrologic solutions. Soil Sci Soc Am J 5(70):1569–1578

Wiebe H, Krummel H (2010) Bodenfeuchte (Geoelektrik). In: Bell R, Pohl J, Glade T, Mayer J, Greiving S (eds) Integrative Frühwarnsysteme für gravitative Massenbewegungen (ILEWS) Monitoring, Modellierung, Implementierung. Klartext, Essen, pp 100–116

Chapter 5
Methodology

A wide range of methods was applied within this study to investigate and model a landslide in Lichtenstein-Unterhausen, and to develop and implement local and regional scale technical landslide early warning systems as part of an integrated early warning chain. In the following, the methodological approaches of this study are presented.

5.1 Local Scale

The methodological approach of this work includes planning and installation of a monitoring system to assess slope movement and hydrological processes, data analysis to investigate processes leading to landslide reactivation, simulation of slope behaviour by a coupled hydrology and slope stability model, and the design and implementation of the model as a technical early warning and decision-support system.

5.1.1 Field Work

Planning of a monitoring system for slope movement and hydrology was carried out cooperatively with the other ILEWS project members during a field inspection. The goal of an extended monitoring system was to gain more information on slope movement and hydrological processes especially in the area where slope movement had been causing cracking to a house, but also for the entire landslide mass. Additional criteria to be considered in the design of the monitoring systems were geomorphological features and the results of geophysical prospection of previous studies (Bell 2007; Kruse 2006) and additional surveys carried out within the

B. Thiebes, *Landslide Analysis and Early Warning Systems*, Springer Theses,
DOI: 10.1007/978-3-642-27526-5_5, © Springer-Verlag Berlin Heidelberg 2012

ILEWS project (Bell et al. 2010), as well as technical issues, such as accessibility of the locations with drilling equipment.

Most drillings were carried out with a percussion drilling machine (GTR 780 V by Geotool) mounted on a rubber chain crawler. The drilling rig uses a drop weight of 63.5 kg and a drop height of 75 cm. For locations impossible to access by the large drilling machine, a pneumatic percussion cone penetrometer from Stitz GmbH with a drop weight of 50 kg and a drop height of 50 cm was employed.

To increase the speed of drilling windowed 80 mm sampling tubes were utilised for installation of hydrological sensors. However, no undisturbed samples could be extracted with these sampling tubes. Drillings for inclinometer installations were carried out with closed 100 mm sampling tubes with plastic tubes that allowed extraction of subsurface materials in a relatively undisturbed condition and the subsequent use for later core interpretation and laboratory analyses.

In addition to the already existing three inclinometers, two more inclinometers and one inclinometer chain were installed. Since improved drilling equipment was available to the ILEWS project in comparison to the preceding InterRISK project, additional inclinometers were placed close to the already existing ones and to an increased depth. After borehole drilling, 55 mm inclinometer pipes were inserted into the boreholes and fixed with a mixture of concrete and bentonite.

Periodic measurements of all inclinometers were carried out approximately every three months with a mobile NMG probe by Glötzl. Each inclinometer was measured in 50 cm steps in A and B directions to assess downslope and sideways displacements. All inclinometer measurements were carried out twice to minimise errors.

An inclinometer chain was installed in the already existing borehole Lic02 with a depth of approximately 15.50 m with the aim to increase the temporal resolution of slope movement measurements. The inclinometer chain consisted of five inclinometer probes located every three metres between 3 and 15 m depth. The inclinometer chain was connected to the controlling computer located in field by cable, allowing remote control by a VPN tunnel.

Even though hydrological monitoring within the ILEWS project was managed by project partners, drilling and installation of all tensiometers and TDR sensors were carried out by the author with the help of field workers. Cooperatively, nine locations were determined for installation of hydrological sensors. At each location boreholes were brought down to depths of approximately 2, 5 and 10 m for installation of tensiometers and TDR probes. In each borehole one TDR probe and one tensiometer located above were installed. After drilling to a desired depth, a 30 cm thick fill of sieved soil material from the same depth was inserted to provide sufficient space for the forks of the TDR probe. On top of this, 30 cm of sieved material was filled in before a tensiometer was installed into the borehole.

A low-cost infrared borehole camera provided by the ILEWS project partner IMKO was used in the field to check subsurface conditions and to control correct sensor installation.

5.1.2 Data Analysis

Core samples and data from laboratory investigations were analysed to improve understanding of subsurface conditions, which form an important element of slope stability modelling and subsequent landslide early warning. The variety of data on slope movement and hydrological processes were analysed to investigate the processes leading to landslide reactivation.

5.1.2.1 Core Samples

Two core samples from inclinometer installations were available for further analyses. Initially, cores were visually interpreted to differentiate layers based on material characteristics, colour and water content. Samples of each layer were taken for laboratory analyses of soil water content, $CaCO_3$ content and grain size distribution analysis carried out by a laboratory technician. In addition, four samples were prepared for elaboration of soil water retention curves. Soil skeleton was assessed by visual judgment.

5.1.2.2 Slope Movement Data

Data from manual inclinometer measurements was compiled and plotted with software by Glötzl (GLNP v4) to visualise displacements between single monitoring campaigns.

Data from inclinometer chain was analysed on the ILEWS project online platform where displacements between selectable points in time can be visualised. A more detailed analysis of inclinometer chain data was carried out plotting the displacements of each probe over time.

Data from geodetic measurements carried out by an ILEWS project partner were available as maps displaying displacements and change of geodetic height between single measurements, and were compared to inclinometer data. In addition, geodetic information were utilised as a basis for interpretation of slope movements for a larger area of the local study area.

5.1.2.3 Hydrological Data

Data from local weather station and slope hydrology monitoring system was exported from the ILEWS database and plotted for further analysis of hydrological conditions. Data were carefully checked for plausibility and possible errors or biases. Investigation concentrated on the assessment of seasonal changes of groundwater conditions for subsequent modelling of slope stability. A more detailed analysis of the effects of rainfall and snow melting on soil water content

and soil suction was carried out for single events. For this, geoelectrical data in the form of time lapse inversions from the ILEWS project partner geoFact and inclinometer chain data were also integrated.

5.1.3 Landslide Early Warning Modelling

Two approaches for the integration of the physical-based landslide simulation model CHASM into a prototypic early warning system were developed in this work. The first application was designed to continuously simulate slope stability for a pre-defined slope profile integrating antecedent rainfall conditions, groundwater table data based on monitoring results, and rainfall forecasts. A second application was developed to aid decision-support and to allow quick assessment of slope stability for freely selectable slope profiles using various rainfall and groundwater scenarios. As noted before, technical solutions were implemented by the ILEWS project partners (Jäger et al. 2010). However, design of the technical early warning system, and configuration of CHASM, were part of the work achieved by the author of this study.

In this study, the physically-based landslide simulation model CHASM (Combined Hydrology and Stability Model) was used to simulate the behaviour of the landslide under investigation. This model was chosen because it combines slope hydrological process simulation with slope stability calculation. Moreover, developers of CHASM agreed on cooperation and a joint development. A brief description has already been presented in Sect. 2.3.2. More detailed information on CHASM is provided in the following. Additional information, including derivation of equations applied in CHASM is available elsewhere (Anderson and Richards 1987; Anderson et al. 1996; Anderson and Thallapally 1996; Collison and Anderson 1996; Wilkinson et al. 2000; Wilkinson et al. 2002a).

Within CHASM pore water pressures in response to individual rainfall events and the effects on slope stability can be simulated. The model comprises two main elements: hydrological and slope stability modelling. The first version of CHASM was developed in an UNIX environment using Fortran '77, but has later been implemented within a Microsoft Windows environment using C ++ with the addition of a graphical user-interface (GUI). The procedure for hydrological modelling adopted in CHASM is a forward explicit finite difference scheme (Wilkinson et al. 2002a). The slope is divided into a series of columns of which each is subdivided into regular cells. Detention storage, infiltration, evapotranspiration, and unsaturated and saturated flow regimes are modelled within CHASM. Rainfall can infiltrate into the top cells and is controlled by the infiltration capacity. Infiltration is calculated using Darcy's Law (Darcy 1856) with the conductivity being equal to the average of the saturated conductivity and the hydraulic conductivity of the top two cells. Unsaturated vertical flow within each column is computed using Richards's equation (Richards 1931). Unsaturated conductivity is defined by the Millington–Quirk (1959) procedure. Flow between

columns is simulated by Darcy's equation for saturated flow, adopting the Dupuit–Forcheimer (Forchheimer 1930) assumption. Numerical stability of the solution to the Richards equation depends on time step and iteration period and applies a methodology proposed by Beven (1985) in which the required time step (iteration period) is based on the distance between the computational nodes, the gradient of the suction–moisture curve at a given suction value and the flow velocity. For most applications the commonly recommended spatial and temporal resolutions are an individual element size of 1 × 1 m area, and 60 s iteration period (Wilkinson et al. 2002a; Wilkinson et al. 2002b). Slope curvature (convexity and concavity) can be integrated by adjusting the column breadth to investigate the effects of three-dimensional topography on pore pressure. Simulated hydrological conditions are then integrated into standard two-dimensional stability analysis.

The stability assessment techniques used in CHASM are Bishop's simplified circular method (Bishop 1955) and Janbu's non-circular method (Janbu 1954). These limit equilibrium methods determine the shear strength along the failure surface, the mobilised shear strength, and the ratio between these two [Factor of Safety]; thus providing a measure of the relative slope stability. On each hour of a CHASM simulation, predicted hydrological conditions are coupled to a limit equilibrium equation determining slope stability. Both negative and positive pore water pressures are incorporated into the effective stress determination by the Mohr–Coulomb equation for soil shear strength. A minimum FoS is computed of which temporal variations arise from hydrodynamic responses and changes in the position of the critical slip surface. An overview of the structure of the CHASM model (Fig. 5.1) and CHASM key input parameters (Table 5.1) are presented below.

The main output of a CHASM run is the calculated minimum FoS for each hour of simulation, along with the respective shear surface parameters. Additional output files contain data on pore water pressure and soil moisture for each cell. For simulation in which a FoS below 1.0 is calculated, an empirical relation (Finlay et al. 1999) of slope height and slope angle is applied to simulate landslide run-out onto a horizontal plain (CHASM 2008).

CHASM is continuously being developed and enhanced. One recent extension includes the integration of vegetation into hydrological simulations and computation of slope stability (Collison and Anderson 1996). Effects of vegetation on hydrology and slope stability, such as interception, evapotranspiration, root reinforcement and changes to hydraulic conductivity and surcharge are incorporated into CHASM by several routines. Test applications of the CHASM vegetation extension are provided in for example Collison and Anderson (1996) and Wilkinson et al. (2002a).

Other features of CHASM include the integration of stabilising measures, such as geo-textiles, geo-grids and earth nails. In addition, effects of seismicity on slope stability can be assessed based on an empirical guideline (Charalambus 2003) to estimate the horizontal seismic acceleration to induce instability.

Inherent in the structure and methodology of CHASM are limitations deriving from the hydrology scheme and the method of stability analysis. Hydrological

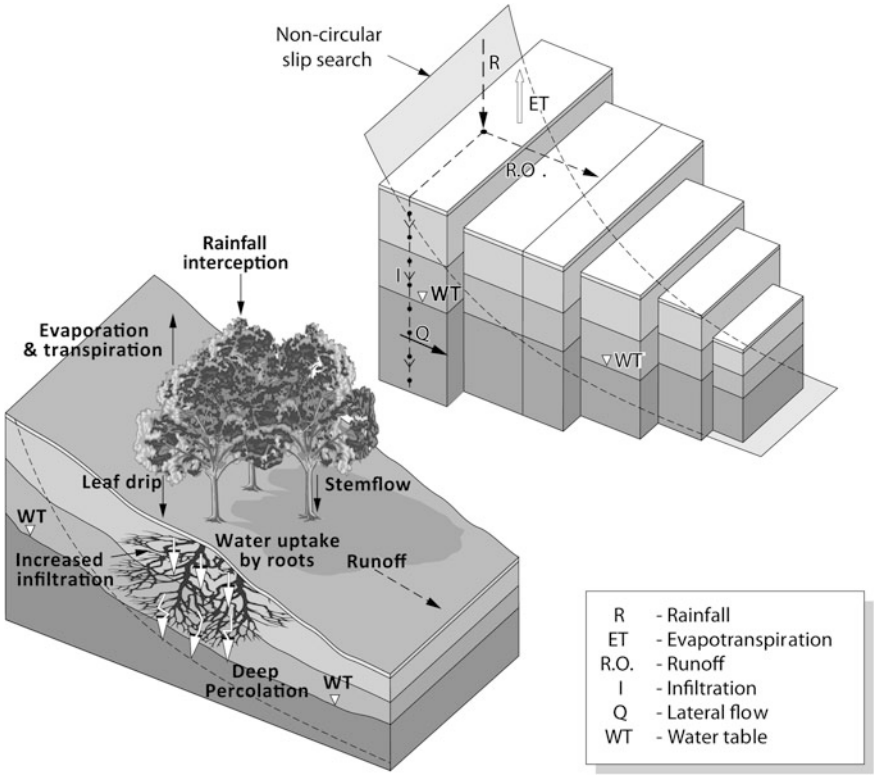

Fig. 5.1 CHASM structure (based on Wilkinson et al. 2002b)

Table 5.1 Key input parameters required by CHASM (based on Wilkinson et al. 2002a)

Theme	Parameter	Symbol	Units
Geometry	Slope height	H	m
	Slope angle	α	Degrees
	Slope convergence/divergence	C	m
Numerical	Mesh resolution	w, d, b	m
	Iteration period	t	s
	Shear surface search	x/y	Coordinates
Hydrological	Rainfall	p	ms^{-1}
	Hydraulic conductivity	K_{sat}	ms^{-1}
	Initial surface suction	Ψ	m
	Initial water table height	wt	m
	Saturated moisture content	θ_{sat}	m^3m^{-3}
	Suction-moisture curve	$\Psi - \theta$	$m-m^3m^{-3}$
Geotechnical	Effective angle of internal friction	φ'	degrees
	Unsaturated/saturated bulk density	γ_{unsat}, γ_{sat}	kNm^{-3}
	Effective cohesion	c'	kNm^{-3}

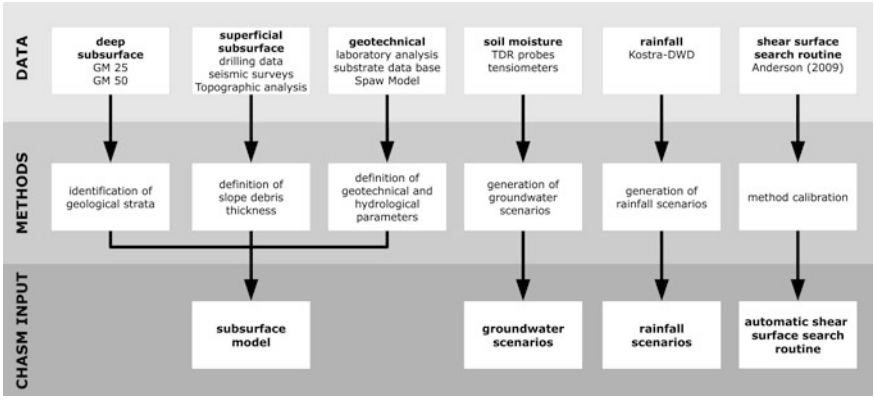

Fig. 5.2 Overview on CHASM input data generation

simulations are based on simplifying assumptions of flow representation and can not integrate soils exhibiting strong anisotropy in hydraulic conductivity or preferential flows for example through macropores. Limit equilibrium methods, as implemented within CHASM, simplify the process of slope failure and can not accommodate progressive failure mechanisms or the complex kinematics of three-dimensional slope failures.

More detailed information on how CHASM was used within this study is presented in Sect. 5.1.3.2.

5.1.3.1 Generation of Input Data

The methodological approach to create input data for CHASM modelling is illustrated in Fig. 5.2 and additional information is provided below.

Subsurface model

A general model combining surface and subsurface information, as well as geotechnical parameters was developed to facilitate slope modelling in the local study area. The subsurface model also formed the basis for the developed decision-support CHASM application allowing free slope profile selection (Sect. 1.1.3.4).

Information on geological conditions was extracted from available geological maps (1:25,000 and 1:50,000). These maps show that large areas are covered by a layer of slope debris ("Hangschutt") deriving primarily from solifluction (Ohmert et al. 1988 p.128), weathering, soil development, erosion and accumulation, as well as fluvial and landslide processes. However, several outcrops of geologic strata allowed interpolation of upper and lower limits of strata throughout the entire local study area under the assumption that no strong features such as folding are present. In this study it was assumed that boundaries of geological strata are parallel to contour lines, neglecting the general dipping of geological strata quantified by Leser (1982) as 1–2°. Based on altitude information Digital Terrain

Models (DTM) for each stratum were computed in GIS by a series of RASTERCALCULATOR commands (Appendix VI) using the DTM1 (1 × 1 m resolution).

For estimation of slope debris thickness information available from drillings and data from geophysical surveys were utilised. In general, a stepwise GIS approach was applied to create a realistic representation of slope debris cover for the local study. For subareas assumed to exhibit similar geomorphological conditions, the depth of debris cover was assessed using the available data, and stored as point data within GIS. Subsequently, a smooth debris cover layer was computed by spatial interpolation techniques.

Determination of slope debris thickness for the local study area utilised available drilling data presented by Ohmert et al. (1988). However, most of the described drillings were not carried out within the boundaries of the study area. Debris thickness was therefore estimated, assuming that a similar debris cover is present in corresponding relative slope positions.

Landslide deposits required a more elaborate approach to be realistically determined. Five drillings were available from the InterRISK and ILEWS projects, however; only one drilling (Lic02) penetrated the bedrock and gives an exact depth. As an additional source of information, data from geoseismic prospection were utilised, which had been carried out within the ILEWS project (Bell et al. 2010) on the upper section of the western landslide body. Inverted data plots from four surveyed profiles on the upper western landslide deposits were interpreted and respective bedrock depths were assessed. Therein, known depth at Lic02 was used for calibration. Derived thickness of slope debris was stored as point data in GIS.

Neither drillings nor geophysical data were available for the eastern landslide body and the lower part of the western landslide depositions. For these areas, landslide deposits were assessed using an iterative GIS approach. A Triangulated Irregular Network (TIN) was computed connecting points of the same height along landslide boundaries to create a DTM without landslide deposits. In addition, topographical analysis of landslide deposit height were integrated.

Another DTM was created for the limestone scree slope in the landslide head scarp area. Determination of thickness was based on geoelectric measurements by Kruse (2006) in which the monitored profile extended far upslope. Maximum depth and bedrock boundary were assessed using inverted data plots, and measured depths were stored as point data in GIS. Since geoelectric data for the limestone scree was only available for one profile, thickness of loose material for the remaining areas had to be assumed before spatial interpolation.

The final subsurface model was simplified for subsequent modelling in CHASM in which only four material layers can be used. The selected layers include: Upper Jurassic, Middle Jurassic, slope debris, limestone scree slope.

Modelling slope stability with CHASM required determination of material parameters, including effective angle of internal friction, effective cohesion, hydraulic conductivity saturated and unsaturated bulk density, saturated moisture content, suction moisture curve. Since no shear tests were available to this study, parameter values were estimated from literature sources and software models.

Friction angle, cohesion and bulk density values were determined using a substrate database created by Meyenfeld (2010, personal communication) containing a wide selection of parameter values from literature sources. However, parameters in the database exhibit large variations and value definition therefore required interpretation and subjective judgement. Still, during sensitivity analysis of CHASM, all values were manipulated and adjusted to increase the predictive abilities of the model.

In addition to laboratory results, the SPAW model (Saxton and Willey 2006; Saxton and Rawls 2006; Sung and Iba 2010) was utilised to define values for soil suction characteristics, saturated moisture content and hydraulic conductivity for the materials in the local study area. Essential input data for the SPAW model were soil particle distributions available from laboratory analyses.

As an additional source of information, primarily for determination of hydraulic conductivity (K_{sat}) values, standard parameter values available in for example Bear (1972) and DIN standard (DIN 18130) were used for orientation.

Groundwater scenarios

Hydrological monitoring data was utilised to create scenarios of groundwater table positions for subsequent modelling of slope stability in CHASM. Available ground water data from each sensor location was analysed and annual variability was assessed. For this, monitoring data until December 2009 was used. However, results were verified against later monitoring data. Determination of groundwater table positions primarily exploited tensiometer data, which provide relative water table height by measured excess pressure. Excess pore pressure was related to relative water table height by

$$100\,\text{hPa} = 102.15\,\text{cm}$$

as proposed by the sensor manufacturer (UMS 2007).

Two groundwater table positions were generated to describe maximum and minimum groundwater table position. Data was stored as point data in GIS and interpolated to the entire study area by Inverse Distance Weighting, as this method provided the results judged as the most realistic.

Rainfall scenarios

Rainfall scenarios for CHASM simulations were derived from the KOSTRA software for the local study area Lichtenstein-Unterhausen. In addition, it was investigated how KOSTRA rainfall intensities vary for neighbouring areas and for different time spans, i.e. summer, winter, and entire year. KOSTRA was used to generate rainfall scenarios of various storm durations, annual occurrence probabilities and rainfall intensity distributions. Three types of scenarios, i.e. normal, maximum intensity and worst case, were generated for subsequent CHASM modelling. Normal scenarios were based on KOSTRA default settings for determination of rainfall intensities. In maximum intensity scenarios KOSTRA default settings were increased to the maximum of the permitted range of approximately 4–12%, depending on annual occurrence probability and storm duration.

A tolerance range for KOSTRA scenarios is advised within the model's outputs if scenarios are to be used for planning purposes. For annual probabilities of less than 5 years the advised tolerance range is ±10, ±15% for annual probabilities between 5 and 50 years, and ±20% for events of 50–100 year reoccurrence intervals. These uncertainties were integrated as additional rainfall to create worst-case scenarios. All rainfall scenarios created were transformed into text-files in the format required for CHASM modelling.

Shear surface search
Calculation of slope stability within CHASM requires definition of shear surface parameters, which for single slope analysis can be ascertained by calibration. However, development of the decision-support application of CHASM allowing free slope profile selection required to establish rules for automatic slip surface search. Therefore, the aim was to concentrate shear surface search into areas most prone to slope failure, whilst still allowing for various possible shear surface positions in a reasonable amount of time. In addition, time needed for calculation of stability conditions should be acceptable for the usage within a web-based decision-support system. The basis for the developed shear surface search was a procedure provided by Anderson (2009, personal communication), which was modified to better fit slope conditions in the local study area. The modified slip surface search procedure was tested on various slope profiles and subsequently integrated into the web-based application (Sect. 5.1.3.4).

5.1.3.2 Model Application

In this study, the physically-based model CHASM was used to assess slope stability for the local study area, with a focus on partial reactivation of an existing landslide body. For subsequent integration of CHASM into an early warning system slope behaviour was simulated to attempt to predict landslide failure timing. For this study a CHASM version including a GUI was available but was only used initially due to the difficulties entering complex slope morphologies. Instead, the command-line based version of CHASM (v4.12.5) was utilised for the majority of CHASM model runs.

CHASM simulations applied Bishop's methodology for circular shear surfaces, as the available CHASM version did not include Janbu's procedure for non-circular shear surface morphology. The effects of vegetation on slope stability were neglected in this study and the respective CHASM extension was not used. The majority of CHASM simulation computed slope stability for two dimensional slope profiles; however three dimensional topography was integrated into some test simulation to investigate possible improvements of the model results.

A sensitivity analysis for CHASM input parameters was carried out to assess their influence on slope stability calculation, as well as to find the best suited parameter combination to reflect real slope behaviour. Sensitivity analysis included geotechnical parameters, rainfall conditions and groundwater table positions.

CHASM simulations were initially carried out to assess the areas and slope positions most susceptible to future slope failures. Based on the results it was decided to focus further simulations on a profile containing the damaged house in which slope movements had been detected, and where monitoring data on slope movement and hydrological processes were available. For this profile, slope stability was assessed for various slip surface positions and subsequently integrated into an automated early warning system.

Analysis of CHASM results concentrated on the FoS as the prime output of CHASM. Herein, the temporal development of the FoS as a response to rainfall and hydrological processes was assessed. For a limited number of simulations hydrological outputs of CHASM were analysed.

5.1.3.3 CHASM Early Warning Model

Integration of CHASM into a prototypic landslide early warning system was based on the experience of extensive model applications for the slope under investigation. For early warning, the slope profile containing the damaged house was selected together with the CHASM control parameters previously analysed to be the most appropriate. An early warning procedure was designed which includes specifications on the integration of antecedent rainfall, hydrological monitoring data and rainfall forecasts. However, since only historic rainfall forecasts were available to this study, all simulated warnings are of hypothetical character. For integration of antecedent rainfall conditions, data from the ILEWS weather station was used. Hydrological field conditions were integrated in the form of groundwater scenarios developed beforehand, which are chosen according to in-field measurements of the monitoring system. Available rainfall forecast from the COSMO-DE were utilised for early warning and integrated into the CHASM simulation as rainfall scenarios.

5.1.3.4 CHASM Decision-Support Tool

The second application of CHASM as a decision-support tool also to be used in early warning context was essentially based on all previously generated input data on rainfall, subsurface and hydrological conditions. In addition, the modified automated shear surface procedure was integrated to ensure appropriate calculation of slope stability. The cooperatively developed web-application was tested for several slope profiles with the aim to detect bugs and optimise its performance. In addition, a step by step guide explaining the usage of the developed application to end users was prepared (see Appendix VIII).

5.2 Regional Scale

On a regional scale, the methodological approach of this work includes analysis of available landslide inventory data, verification and testing of existing rainfall thresholds for landslide initiation for the Swabian Alb, development and implementation of a regional landslide early warning system.

Similar to other works, rainfall thresholds form the basis for regional early warning in this study. However, in this study it was not the aim to establish a new rainfall threshold for the Swabian Alb, as the data was judged inappropriate to derive reliable threshold values. Instead, rainfall thresholds established for other regions that were available were tested for their applicability in the Swabian Alb and implemented within a technical warning system.

5.2.1 Inventory Analysis

Data on landslide occurrences in the Swabian Alb was evaluated for its use for validation of rainfall thresholds. The most important criterion therefore was the availability of information regarding the timing of slope failure, which had to be as exact as possible. In addition, events including multiple landslides are preferred for analysis, to ensure that the landslides are not local phenomena such as results of inadequate construction works but are the consequence of rainfall thresholds exceedance. Another criterion for the selection of landslide events for threshold validation was the availability of rainfall data for the place and time of slope failure.

5.2.2 Threshold Verification

The applicability of existing rainfall thresholds to the Swabian Alb was evaluated for the selected landslide events with known date of failure with rainfall records available as interpolated climate data with a daily resolution. Table 5.2 provides an overview on the thresholds tested in this study.

Four thresholds were tested for their performance in the Swabian Alb. Caine's (1980) intensity-duration threshold was the first threshold established for landslide initiation, and forms a benchmark for other, more recent intensity-duration relationships. However, Caine (1980) could only use a limited data source of 73 landslide events for rainfall threshold derivation. A more recently established global intensity-duration rainfall threshold by Guzzetti et al. (2008) was based on a significantly larger database of 2,626 rainstorm events that caused landslides. The third intensity-duration threshold is the one applied in the landslide early warning system operating in Seattle (Chleborad 2000, 2003; Chleborad et al. 2006). This system also utilises a threshold based on cumulative rainfall of 3 and 15 days, and was also tested in this study.

Table 5.2 Rainfall thresholds tested within this study

Type	Scale	Value	Landslide types	Duration in hours	Source
Intensity-duration	Global	$I = 14.82 \times D^{-0.39}$	All types	$0.167 < D < 500$	Caine (1980)
Intensity-duration	Global	$I = 2.2 \times D^{-0.44}$	Shallow landslides, debris flows	$0.1 < D < 1000$	Guzzetti et al.(2008)
Intensity-duration	Seattle area	$I = 3.257D^{-1.13}$	Soil slides	$20 < D < 55$	Chleborad et al. (2006)
Cumulative rainfall	Seattle area	$P_3 = 3.5–0.67P_{15}$	Soil slides	$72 < D < 360$	Chleborad et al. (2006)

Analysis of intensity-duration relationship of landslide initiation required definition of the rainfall event that triggered slope failure. Even if the date of landslide occurrence is known, triggering rainfall events may not easily be identified, for example in cases where a strong storm event is preceded by only very low precipitation rates. In this study, intensity and duration of triggering rainfall events were determined in three ways: (1) only accounting for the precipitation on the day of landslide triggering, (2) for the days previous to landslide triggering on which a minimum rainfall amount was recorded (amount determined by data analysis), and (3) for the time span preceding landslide triggering up until the day where no rainfall was measured. In addition to rainfall, snow melt was integrated in the threshold verification. Threshold verification utilised regionalised weather data as the data source.

5.2.3 Early Warning

The goal of the regional landslide early warning was to design and implement a prototypic system for the Lichtenstein-Unterhausen region based on rainfall thresholds, in which rainfall forecasts and actual measurements are integrated. Development of a regional early warning system constituted a cooperative work of the author of this thesis and of several individuals of the company of Geomer, who were partners in the ILEWS project. It is important to mention, that all technical solutions were entirely implemented by Geomer described in detail elsewhere (Jäger et al. 2010).

Design of a regional technical landslide early warning system included two main elements: determination of rainfall thresholds, and implementation of a technical information and warning system integrating rainfall measurements and forecasts. Since no reliable rainfall thresholds were available for the Swabian Alb,

only preliminary thresholds were implemented. Within this study, thresholds reflect measured precipitation and forecasted rainfall. It was judged for the regional landslide early warning system to be easily adjustable and extendable in case additional data becomes available, or other regions are to be integrated.

The technical regional landslide early warning system utilised rainfall measurements from the ILEWS weather station and rainfall forecast by the DWD (COSMO-DE). An information and warning platform implemented by Geomer (Jäger et al. 2010) was developed to be able to assess current rainfall conditions and provide warnings in case thresholds are exceeded.

References

Anderson MG, Richards K (1987) Modelling slope stability: the complementary nature of geotechnical and geomorphological approaches. In: Anderson MG (ed) Slope stability: geotechnical engineering and geomorphology. Wiley Ltd, Chichester, pp 1–9

Anderson MG, Lloyd DM, Park A, Hartshorne J, Hargraves S Othman A (1996) Establishing new design dynamic modelling criteria for tropical cut slopes. In: Senneset K (ed) Landslides. 7th international symposium on landslides, Trondheim, Norway: Balkema, Rotterdam, pp 1067–1072

Anderson SA, Thallapally LK (1996) Hydrologic response of a steep tropical slope to heavy rainfall. In: Senneset K (ed) Landslides. 7th international symposium on landslides. Balkema, Trondheim–Rotterdam, Norway, pp 1489–1495

Bell R (2007) Lokale Und Regionale Gefahren-Und Risikoanalyse Gravitativer Massenbewegungen an Der Schwäbischen Alb. Dissertation. University of Bonn, Germany

Bear J (1972) Dynamics of fluids in porous media. Dover, New York

Bell R, Wiebe H, Krummel H (2010) Vorerkundung. In: Bell R, Pohl J, Glade T, Mayer J, Greiving S (eds) Integrative Frühwarnsysteme für gravitative Massenbewegungen (ILEWS) monitoring, modellierung, implementierung. Klartext, Essen, Germany, pp 62–69

Beven KJ (1985) Distributed models. In: Anderson MG, Burt TB (eds) Hydrological forecasting. Wiley, New York, pp 405–435

Bishop AW (1955) The use of the slip circle in the stability analysis of slopes. Geotech 5(1):7–17

Caine N (1980) The rainfall intensity: duration control of shallow landslides and debris flows. Geografiska Annaler. Series A Phys Geogr 62(1/2):23–27 Available at Accessed 18 Oct 2010

Charalambus S (2003) Methodology development for the stability evaluation of natural and man-made slopes against static and seismic loads in a GIS environment. Technical University of Athens, Greece

CHASM (2008) CHASM Software—Combined hydrology & slope stability model [Online]. Available at http://chasm.info/ Accessed 14 Feb 2011

Chleborad AF (2000) Preliminary method for anticipating the occurrence of precipitation-induced landslides in Seattle, Washington. U.S. Geological Survey Open-File Report 03–463

Chleborad AF (2003) Preliminary evaluation of a precipitation threshold for anticipating the occurrence of landslides in the Seattle, Washington, area. Denver, Colorado, US U.S. Deptartment of the Interior, U.S. Geological Survey, Denver, Colorado

Chleborad AF, Baum RL, Godt JW (2006) Rainfall thresholds for forecasting landslide in the Seattle. Washington, Area—exceedance and probability. U.S. Geological Survey Open File Report 2006–1064

Collison AJC, Anderson MG (1996) Using a combined slope hydrology/stability model to identify suitable conditions for landslide prevention by vegetation in the humid tropics. Earth Surf Proc Land 21(8):737–747

Darcy H (1856) Les fontaines publiques de la ville de Dijon. Victor Dalmont, Paris, France
Finlay PJ, Mostyn GR, Fell R (1999) Landslide risk assessment: prediction of travel distance. Can Geotech J 36(3):556–562
Forchheimer P (1930) Hydraulik. Leipzig and Berlin, Teubner
Guzzetti F, Peruccacci S, Rossi M, Stark CP (2008) The rainfall intensity–duration control of shallow landslides and debris flows: an update. Landslides 5(1):3–17
Jäger S, Paulsen H, Mayer C, Huber B, Dietz R, Greve K, Camek T (2010) Informationstechnik in der Frühwarnmodellierung. In: Bell R, Pohl J, Glade T, Mayer J, Greiving S (eds) Integrative Frühwarnsysteme für gravitative Massenbewegungen (ILEWS) monitoring, modellierung, implementierung. Klartext, Essen, Germany, pp 155–179
Janbu N (1954) Application of composite slip surface for stability analysis. In: Proceedings of the European conference on the stability of earth slopes. pp 43–49
Kruse JE (2006) Untergrunderkundung und monitoring von gravitativen Massenbewegungen mit Gleichstromgeoelektrik und Radiomagnetotellurik. University of Bonn, Germany
Leser H (1982) Erläuterungen zur Geomorphologischen Karte 1:25, 000 der Bundesrepublik Deutschland. GMK 25 Blatt 9 7520 Mössingen Geomorphologische Detailkartierung in der Bundesrepublik Deutschland. Geo Center, Stuttgart, Germany
Millington RJ, Quirk JP (1959) Permeability of porous media. Nature 183:387–388
Ohmert W, Von Koenigswald W, Münzing K, Villinger E (1988) Erläuterungen zu Blatt 7521 Reutlingen (Geologische Karte 1:25.000 von Baden Württemberg). Geologisches Landesamt Baden-Württemberg
Richards LA (1931) Capillary conduction of liquids through porous mediums. Physics 1:318–333
Saxton KE, Rawls WJ (2006) Soil water characteristic estimates by texture and organic matter for hydrologic solutions. Soil Sci Soc Am J 5(70):1569–1578
Saxton KE, Willey MP (2006) The SPAW model for agricultural field and pond hydrologic simulation. In: Singh VP, Frevert D (eds) Mathematical modeling of watershed hydrology. CRC Press, Boca Raton, pp 401–435
Sung CT, Iba J (2010) Accuracy of the Saxton-Rawls method for estimating the soil water characteristics for mineral soils of Malaysia. Pertanika J Trop Agric Sci 33(2):297–302
MS U (2007) Bedienungsanleitung T8 Langzeitmonitoring-Tensiometer. UMS GmbH, München
Wilkinson PL, Anderson MG, Lloyd DM (2002a) An integrated hydrological model for rain-induced landslide prediction. Earth Surf Proc Land 27(12):1285–1297
Wilkinson PL, Anderson MG, Lloyd DM, Renaud JP (2002b) Landslide hazard and bioengineering: towards providing improved decision support through integrated numerical model development. Environ Model Softw 17(4):333–344
Wilkinson PL, Brooks SM, Anderson MG (2000) Design and application of an automated non-circular slip surface search within a combined hydrology and stability model (CHASM). Hydrol Process 14(11–12):2003–2017

Chapter 6
Results

6.1 Local Scale

6.1.1 Field Work

The work in field constituted an important element of this study and required a considerable amount of time. Altogether, over 9 weeks were spent in field during several field campaigns between 2007 and 2008, primarily for drilling and subsequent sensor installation. Additional field work included periodic manual inclinometers measurements between 2007 and 2011.

Drillings had to negotiate difficult subsurface conditions, which hindered quick installation of sensors. In many cases, parts of the boreholes collapsed and had to be drilled several times. Investigations of borehole properties with an infrared borehole camera showed very heterogeneous subsurface material characteristics. Figure 6.1 illustrates subsurface conditions in the Lic05 drilling down a depth of approximately 3.7 m. The uppermost material consists of loose material rich in limestone fragments, which tended to collapse during drilling procedure (pictures 1–5). Pictures 6–12 show very smooth borehole walls consisting of compact clay. In contrast, the last three pictures display the sudden change of material with large limestone blocks and collapsed borehole walls opening to a cavity.

Altogether, nine locations were selected for the installation of hydrological sensors, i.e. TDR sensors and tensiometers (Fig. 6.2). Sensors were primarily placed along a cross and a longitudinal profile for which also geoelectrical monitoring surveys and a seismic survey during initial prospection were carried out. Additional sensors were placed on the meadow where inclinometer Lic04 was installed during the InterRISK project and at a location in the forest (p41) above the road. Aspired depths of sensors of 2, 5 and 10 m could not be achieved at all locations due to the difficult subsurface conditions and the used drilling equipment. Installation depths of hydrological sensors are summarised in Table 6.1.

B. Thiebes, *Landslide Analysis and Early Warning Systems*, Springer Theses,
DOI: 10.1007/978-3-642-27526-5_6, © Springer-Verlag Berlin Heidelberg 2012

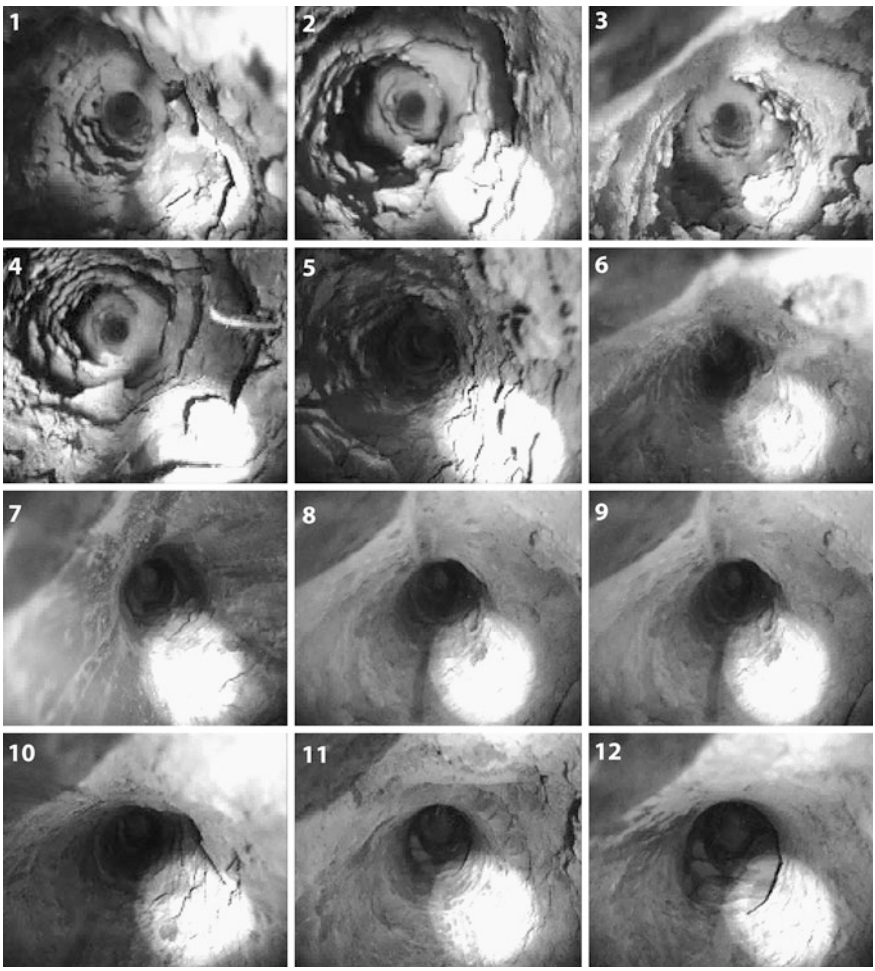

Fig. 6.1 Pictures taken with borehole camera in boreholelic05 drilling (from surface and depth of approximately 3.7 m depth)

Additional sensors were installed at the ILEWS weather station with TDR sensors in depths of 35 and 55 cm, tensiometers in 65 and 45 cm, and pf metres in 65 and 45 cm. A more detailed description of hydrological monitoring results is presented in Sect. 6.1.2.1.

Periodic manual inclinometer measurements commenced during the InterRISK project were continued approximately every 3 months. However, after the project ended in May 2010, measurements could only be carried out less frequently. Detailed information on the results of inclinometer measurements are presented in Sect. 6.1.2.2.

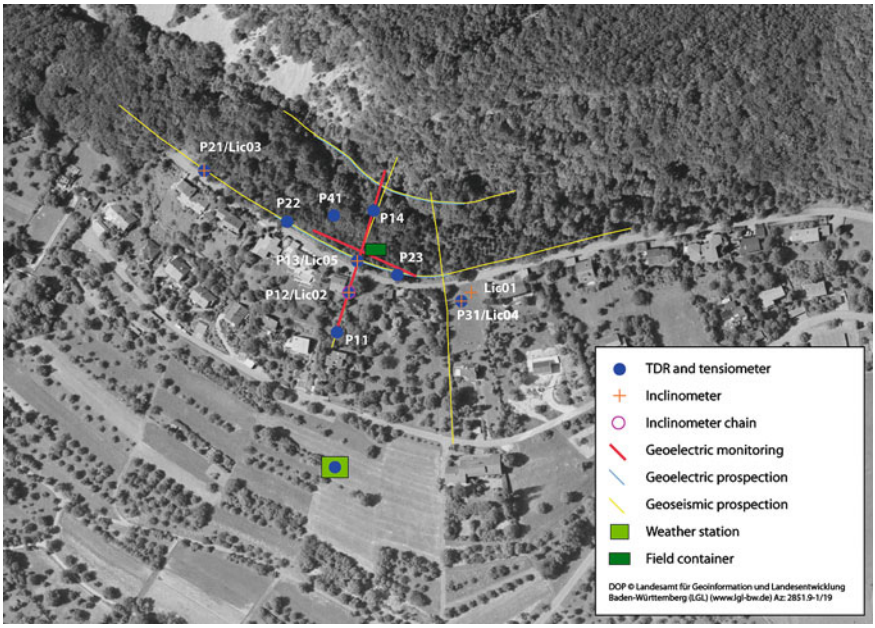

Fig. 6.2 Local monitoring system

Table 6.1 Installation depths (in cm) for hydrological sensors in relation to aspired depths

	2 m		5 m		10 m	
Location ID	TDR	Tensiometer	TDR	Tensiometer	TDR	Tensiometer
P11	195	175	470	450	880	860
P12	235	200	420	385	950	920
P13	165	135	355	330	840	775
P14	200	170	475	420	915	885
P21	160	130	450	440	730	715
P22	210	190	360	340	710	700
P24	210	185	480	450	950	935
P31	175	160	460	420	960	930
P41	190	170	390	370	710	695

6.1.2 Data Analysis

6.1.2.1 Core Samples

In this study, two core samples from drillings Lic04 and Lic05 were investigated in detail. Both cores provide a continuous overview on subsurface conditions down to a depth of approximately 11 m; however, for some sections material was lost during core extraction.

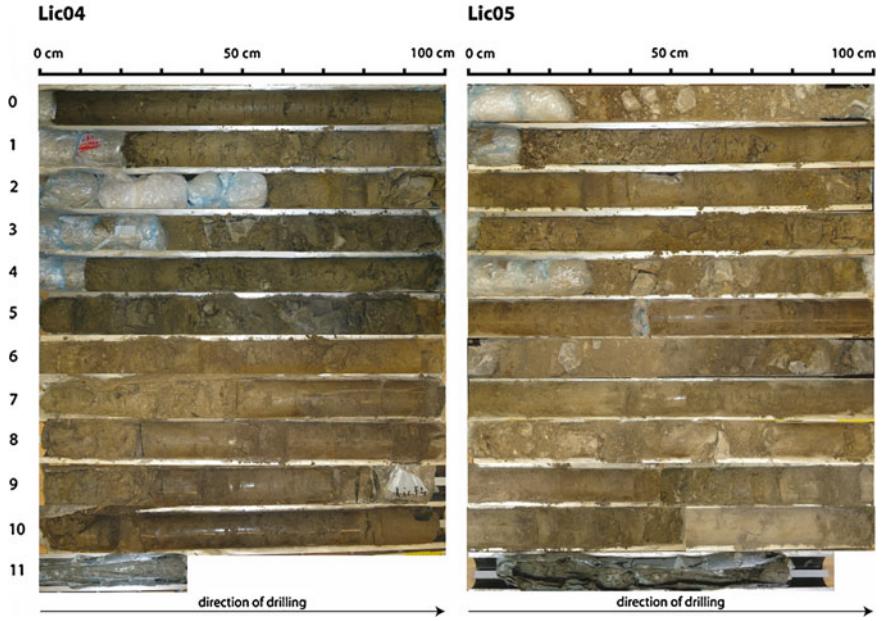

Fig. 6.3 Photos of core samples from Lic04 to Lic05 boreholes

A total number of 81 samples were prepared from cores for subsequent laboratory analysis of grain size distribution, water content, $CaCO_3$ content. Three additional samples were extracted for laboratory analysis of soil suction behaviour. Core samples are presented in Fig. 6.3, and some results will be highlighted in the following. A graphical representation including laboratory results can be found in the Appendix I.

The first metre of the Lic04 contains plastic loamy material with a dark brown colour indicating soil development processes. Between 1 and 7 m depth layers of light brown relatively plastic loam and dark fine-bedded marls, both with varying content of limestone fragments, alternate. In addition several large limestone blocks can be found in e.g. 3, 5.2 and 5.7 m depth. In 7 m depth very soft and moist material overlays compact clay. Drilling at Lic04 ended in a depth of 11.3 m when a hard layer was reached, which could not be bored with the available drilling machine. The last plastic bore log tube was broken due to high impact force and contains very soft and slurry material.

A total number of 31 samples were prepared from Lic04 core sample for laboratory analyses. Samples were classified according to Austrian OENORM standard as lehmiger Ton, schluffiger Lehm, Lehm, and scattered Ton (Fig. 6.4). This relates to silty clay and silty clay loam in the US texture definition. Clay content varies between 34.6 and 49.6% with an average of approximately 43%. Sand content is generally low with less than 1 and a maximum of 11% (average 3.7%). Visually assessed soil skeleton content varies between 10 and approximately 40%;

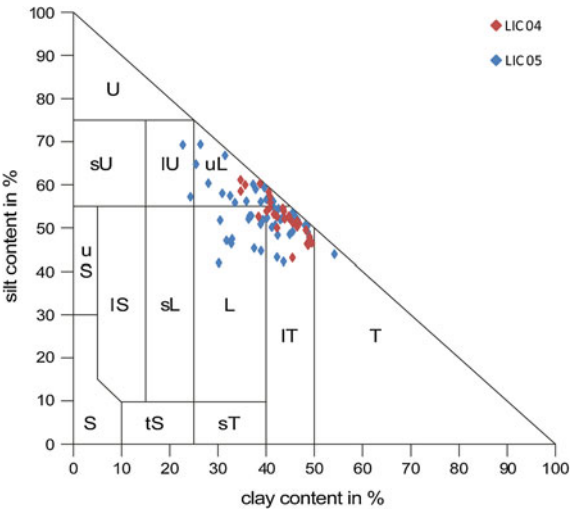

Fig. 6.4 Soil textures according to OENORM

however, for sections with large limestone blocks content rises to 90%. Content of $CaCO_3$ in the analysed fine material samples varies between 41.1 and a maximum of 77.18% (average 58%). For water content, values between 6.7 and 38.2% were assessed, with the highest values measured close to the surface, in a depth of approximately 9 m.

The first approximately 1.5 m of Lic05 core sample contains very light material with a high content of limestone fragments. Deeper layers comprise more plastic materials, and sections with very high content of soil skeleton including complete limestone blocks, for example around 4.5 m depth, and between 6 and 7 m. The drilling from 6 to 7 m had to be repeated three times because borehole walls had col lapsed and the borehole had been filled up with material. Similar materials characteristics as described above can be found until 11 m. The last 30 cm drilled at Lic05 contain similar material to Lic04, with very soft and moist soil. Again, the plastic bore log tube of the last metre was partly burst due to the high forces that impacted when a hard material layer was reached.

From Lic05 core sample a total number of 50 samples were prepared for laboratory analyses. In OENORM these were defined as lehmiger Ton and schluffiger Lehm (Fig. 6.4), which relates to definition silty clay, silty clay loam, silt loam and clay loam in US texture classification.

Clay content varies between 22.6 and 54.1% and averages 38%. Mean sand content is low (7%) with a maximum value of 27.5% in a depth of 10.7 m. Soil skeleton content varies strongly in the Lic05 borelog, with some sections entirely consisting of limestone blocks, while others are almost free of any larger skeleton. A high mean content $CaCO_3$ of 67% in the fine grained material can be found throughout the core sample with maximum values of over 80% closer to the surface. Water content varies between 4 and a maximum value of over 37% at the base of the borelog.

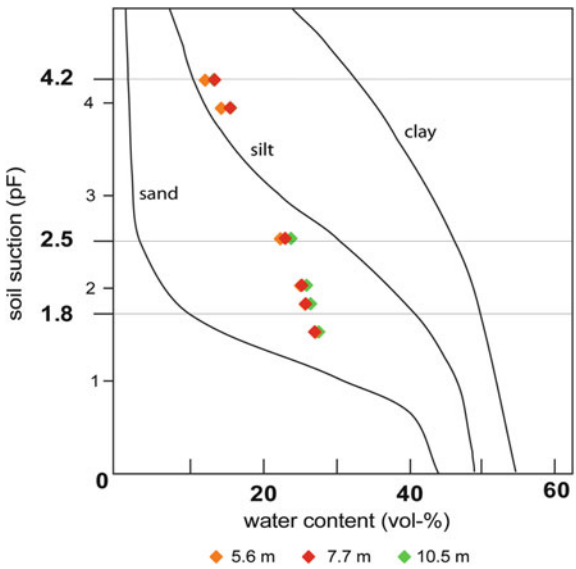

Fig. 6.5 Soil suction characteristics in comparison to sand, silt and clay soils (after Scheffer and Schachtschabel 2009)

Three soil samples from Lic05 core sample were prepared from depths of 5.6, 7.7 and 10.5 m for elaboration of soil water retention characteristics in laboratory. Results are presented in Fig. 6.5. All three samples show similar results with mean volumetric water content of approximately 13–16% for high suctions (pF 4.2–4.0, or 15,000–8,000 hPa, respectively). For lower suctions (pF 2.5–1.5, or 300–30 hPa) water content lies between 23 and 28%.

Discussion

Drilling cores and borehole camera investigations document heterogenic subsurface conditions in the local study area. In all drill cores, layers of blocky limestones can be found. However, similar conditions cannot be expected for the entire local study area since the material is disturbed due to former landslide activity.

Even though drillings carried out could not reach the bedrock, they provided some interesting information. Both inclinometer drillings, i.e. Lic04 and Lic05 had to be stopped, when a very hard layer was reached in approximately 11 m depth. In both drill cores, moist material could be found at the greatest depths, which possibly indicates the position of impermeable material layers, which could also act as shear surfaces. Still, without further drillings to greater depths using improved equipment it is difficult to verify, if displacements occur along this material interface.

Laboratory analysis of soil properties provided essential information on material characteristics in the local study area. However, since soil particle distribution analysis only uses fine material, the influence of large particles on hydrological

Fig. 6.6 Overview on periodic and permanent landslide monitoring

processes and subsequently slope stability can easily be underestimated. Additional shear tests could improve the understanding of geotechnical behaviour.

6.1.2.2 Slope Movement Data

Slope movement data from geodetic surveys carried out by Aslan et al. (2010), and inclinometers measurements including one inclinometer chain were available to analyse slope movements. An overview on the timing of displacement measurements is presented in Fig. 6.6.

Tachymetry measurements by an ILEWS project partner (Aslan et al. 2010) provided some information on surface displacement between several epochs. In Fig. 6.7, relative deformation of geodetic network of all nine epochs between November 2007 and December 2009 is displayed together with confidence ellipse indicating uncertainties of measurements, i.e. noise levels. Measured displacements are generally extremely low and are in the range of millimetres. Largest movements can be observed for point 201, located in the western part, and at points 205, 206, 207 and 306 in the East. For these points, downslope displacements cumulate to 5–8 mm. Similar directions of movement were also recorded further South at points 105 and 106. Other network points, however, exhibited upslope movements for at least some of the epochs, e.g. points 201, 202, 203, 101 and 304. The clearest movement trends can be observed for the eastern part of the network. For points 101, 102, 104, and 203 movement rates are small in relation to noise level and no clear movement trends can be found.

In Fig. 6.8, the change of geodetic height for three selected points, i.e. 201, 204 and 206 is illustrated. Measurements and subsequent calculation of height changes were elaborated by (Aslan et al. 2010), however, following description and interpretation are made by the author of this thesis. Measurements show a seasonal variation of geodetic height for all three points. A general trend of lower point positions during summer and autumn measurements can be observed. Largest changes are recorded for point 201 in the western part of the study area, which shows a total variation of geodetic height of over 1.5 cm. Increased geodetic height coincides with upslope displacements, and lower heights can be observed when also a downslope movement occurred. Manual inclinometer measurements in the local study area were carried out monthly within the InterRISK project.

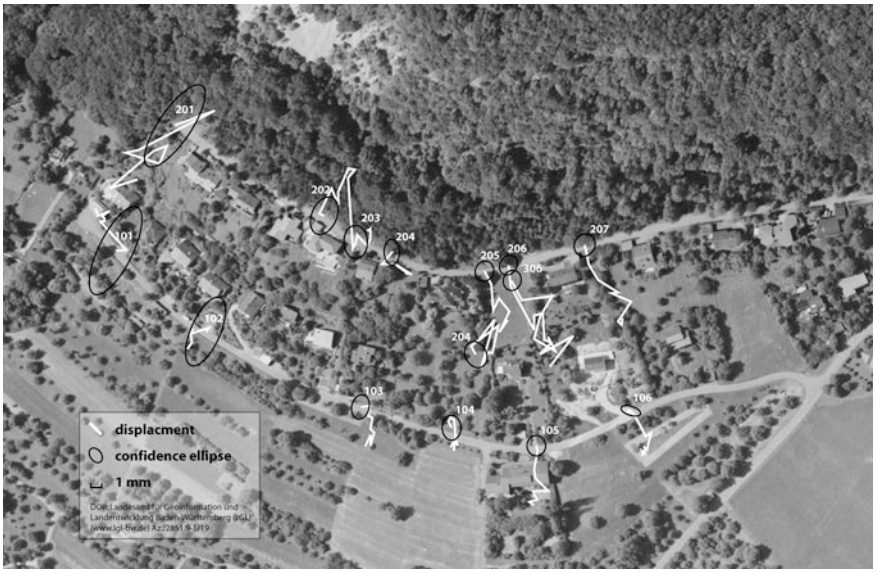

Fig. 6.7 Cumulative geodetic displacement measurement from nine epochs (after Aslan et al. 2010)

From 2007, measurements were undertaken approximately every 3 months by the author.

Inclinometer Lic01 was installed during the InterRISK project, and is located in the eastern part of the study area, approximately 10 m away from inclinometer Lic04 and the hydrological monitoring at p31. With a maximum depth of 9.5 m, the inclinometer could not be fixed into stable bedrock. Since 2004 displacements of approximately 4 mm in both upslope and downslope direction were recorded in 2 and 4 m depth, respectively. The relatively large downslope displacement documented by tachymetry measurements can not be observed. A selection of manual measurements undertaken between 2004 and 2011 are provided in Appendix II.

The closely positioned inclinometer Lic04 was installed in May 2008, and has a depth of 11 m, which is still above the stable bedrock. Inclinometer measurements (see Appendix IV) document constant but extremely slow movements occurring over entire profile. Records show a downslope and a west-directed component.

Inclinometer Lic03 is located on the western landslide body, directly neighbouring hydrological monitoring position p21. The inclinometer was installed during the InterRISK project, and has a maximum depth of 8.5 m, which is above the bedrock. Between 2005 and 2011 extremely slow movements of 2–3 mm into an upslope and eastern direction was recorded (see Appendix III). The relatively large displacements documented by geodetic measurements can not be observed in inclinometer data.

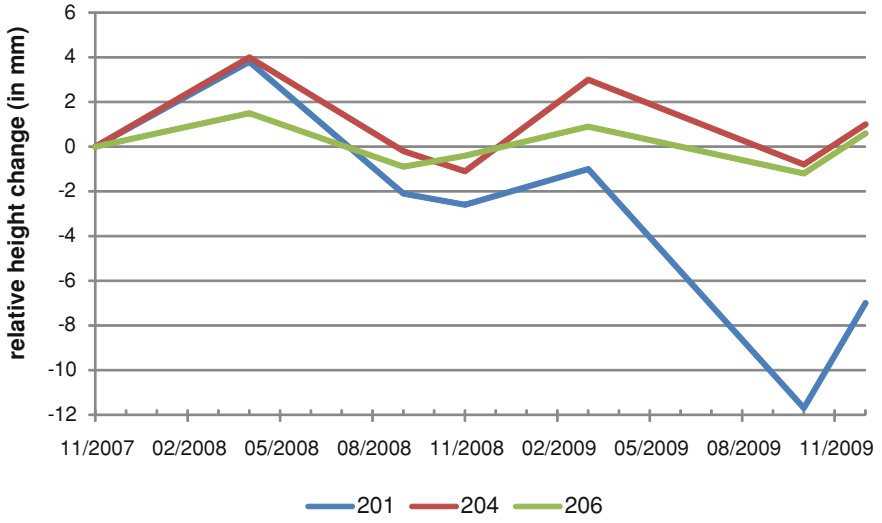

Fig. 6.8 Relative height change for points 201, 204 and 206 (after Aslan et al. 2010)

Inclinometer Lic05 is located at the crossing of geoelectrical profiles, directly neighbouring hydrological monitoring position p13. Maximum depth of the inclinometer is 10.5 m which is still above the stable bedrock. Recorded displacements are very small but above error margin of the used inclinometer probe. Movements of approximately 5 mm in an upslope direction, and approximately 3 mm into a western direction can be observed (Fig. 6.9). Results of inclinometer at Lic05 are in agreement with tachymetry measurements, which also documented an upslope directed displacement with a similar magnitude for this location (point 203).

Largest displacements were recorded at inclinometer Lic02, which is the only one that is fixed into stable bedrock at a depth of 15.5 m. It is located next to the damaged house at hydrological monitoring site p12. A selection of manual displacement records from 2004 to 2011 is displayed in Fig. 6.10. Both, the flowing movement in a maximum depth of 8.5 m in summer and autumn, and the sliding movement in spring in a depth 15 m continued. Downslope displacements add up to approximately 1.5 cm in 6.5 years relating to an annual displacement of 2–3 mm. In addition, smaller movements of about 3 mm in a western direction can be observed.

When analysing all single measurements, an upslope orientated rotational movement occurs before deep sliding commences in spring can be observed. These movements can be found in the first measurements in 2005, 2006 and 2009 when compared to the directly preceding records. In 2007, however, both, the upslope rotation and the deep sliding movement did not occur. In 2008 the sliding movement was very small, and no clear rotational component can be detected. Sliding movement is also not present in 2010 measurement, which was carried out

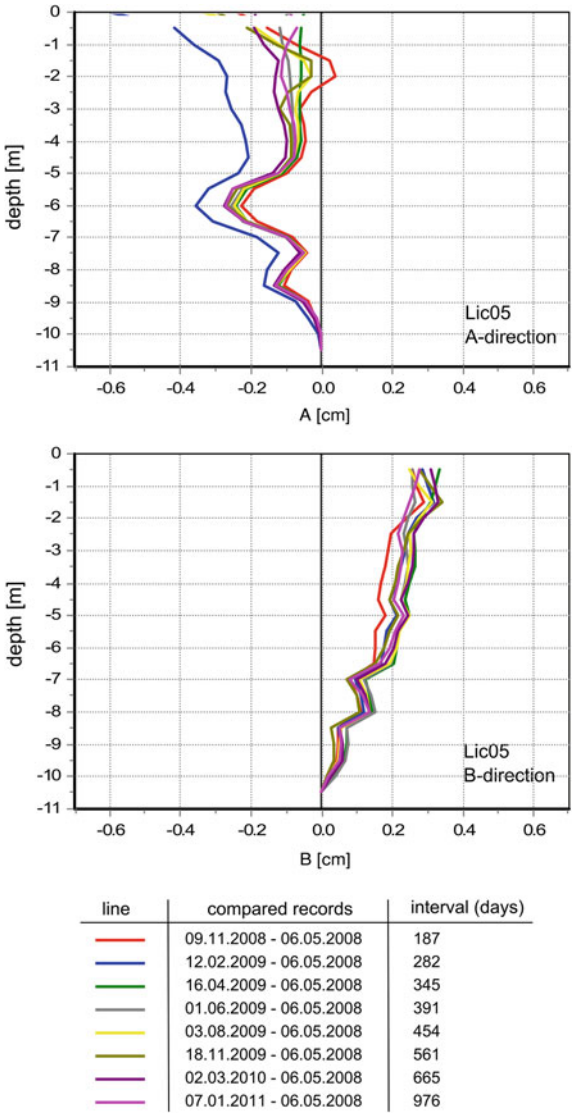

Fig. 6.9 Selected records of Lic05 inclinometer measurements

in early March. The 2011 records acquired in January, document further deep sliding but no significant rotational component.

No direct comparison to geodetic measurements can be made because the inclinometer was not linked to the network.

In comparison to manual inclinometer records to inclinometer chain measurements (see Fig. 6.11) in 3, 6, 9, 12 and 15 m depth, data from the latter has a lower accuracy and more scatter, especially if short periods are analysed. Temporal resolution, however, is significantly higher with measurement intervals of 30 min.

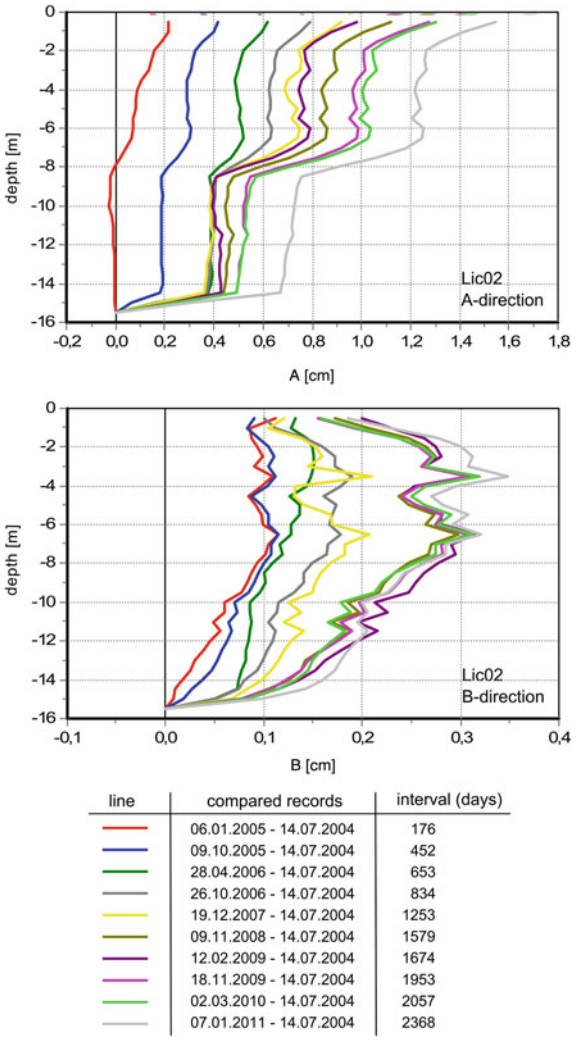

Fig. 6.10 Selected records of manual inclinometer measurements at Lic02

In a selection of inclinometer chain records for periods of 2009 and 2010 is presented. The total displacement recorded between early 2009 and late 2010 adds up to approximately 2 mm, similar to manual measurements.

Even though displacement values are extremely slow and are still in the error margin, some general movement trends can be observed. Dominantly, the shallow downslope flow movement prevails. The deep sliding movement, however, cannot be detected due to the position of the deepest inclinometer probe at 15 m depth.

To better understand the temporal dynamics of slope displacements, raw data was analysed and thoroughly checked. It was found that extraction of the inclinometer chain for manual measurements resulted in sudden jumps in displacements data lasting for some days, until records return to more stable values.

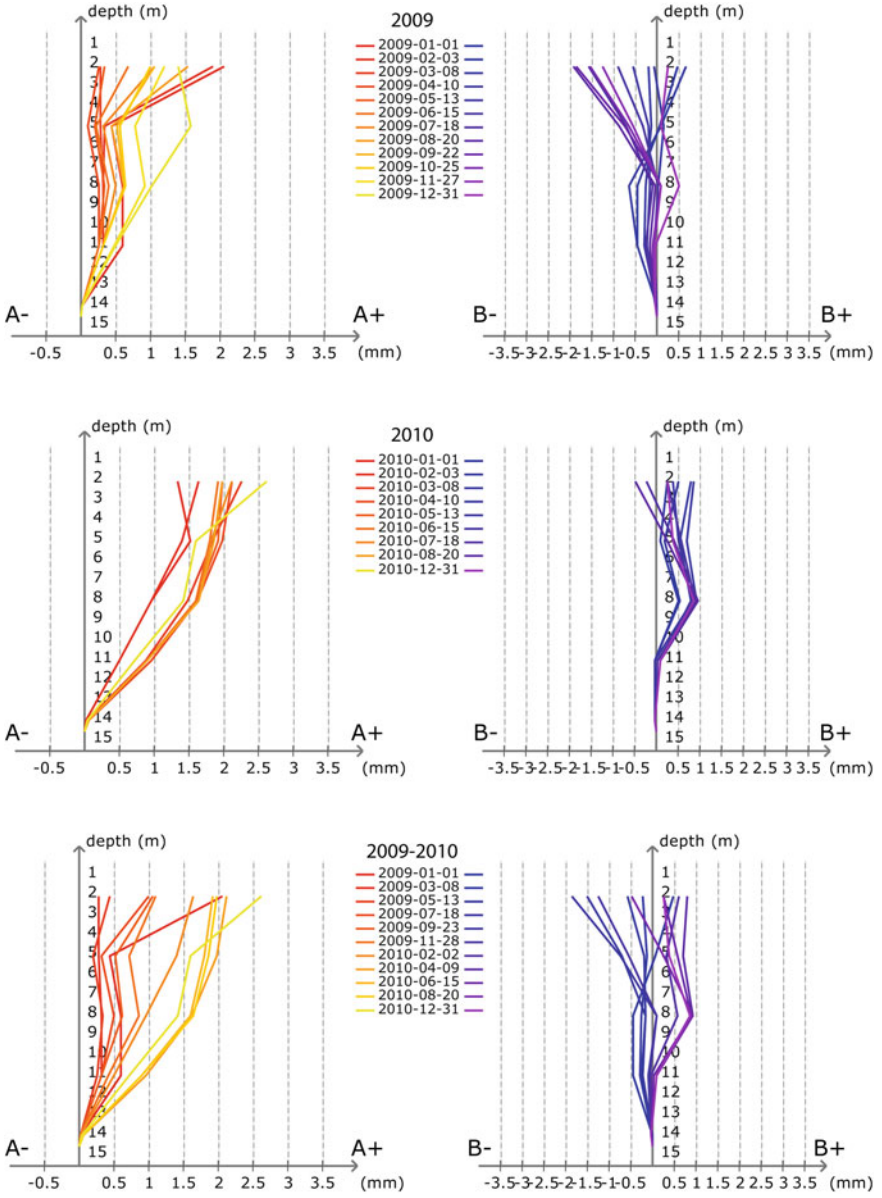

Fig. 6.11 Measured displacements of inclinometer chain for 2009, 2010 and 2009 to 2010

All records from the dates and the following 4 days, on which the inclinometer chain was extracted were deleted from the data set. In addition, reference values which previously had in some cases an offset of some days were adjusted. Results for A and B direction are presented in Figs. 6.12 and 6.13, respectively.

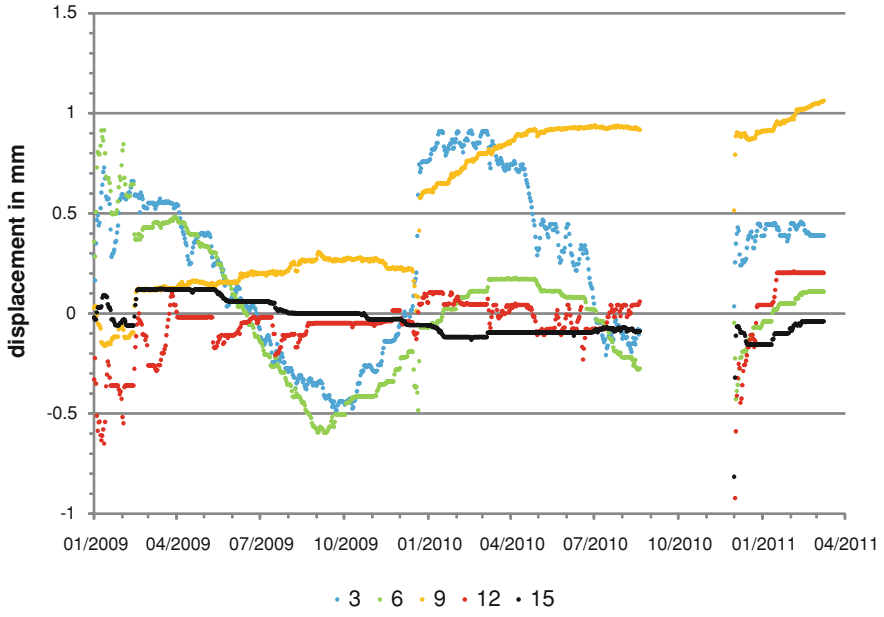

Fig. 6.12 Daily mean displacement changes measured by inclinometer chain for B direction

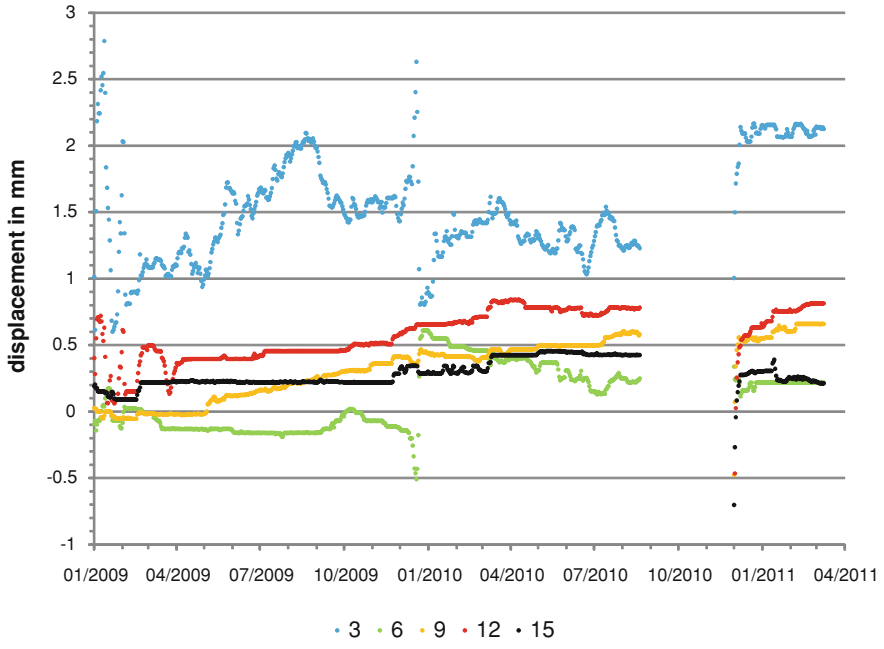

Fig. 6.13 Daily mean displacement changes measured by inclinometer chain for A direction

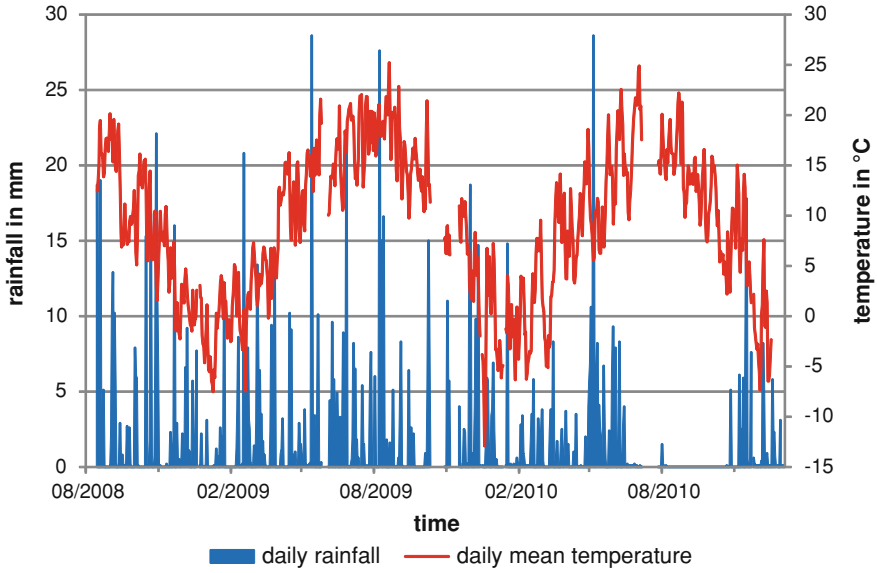

Fig. 6.14 Daily rainfall and daily mean temperature measured by ILEWS weather station

Records start with some scatter during January 2009 but quickly adjust to more stable conditions. The correction procedure described above reduced total displacements by for example, 0.3 mm for the 3 m inclinometer probe. Still, a total downslope displacement of 2 mm until September 2009 alone was recorded for this sensor. Movement, however, was not continuous, but exhibited several phases of reversed direction. Periods of upslope movement can also be observed for the 6 m probe; but timing of these does not reflect patterns similar to the 3 m sensor. Data from the probes located in deeper positions is generally steadier. The probe in 15 m depth exhibited three phases of larger movement, i.e. early 2009, between December 2009 and March 2010, and again in early 2011. However, the inclinometer chain was also removed from the borehole during these times.

Similar to the A direction, no sudden changes can be observed in the daily mean displacement changes of the inclinometer chains in B direction (Fig. 6.12). Records begin with some initial scatter. However, from February 2009, relatively smooth changes can be observed for 3 and 6 m sensors. A more step like course of displacement is documented by the inclinometer probes in 12 and 15 m depth.

For both A and B direction, greatest daily displacements variations documented by the inclinometer chain are lower than 0.5 mm. Movements in this order of magnitude are still in the margin of error and therefore have to be interpreted with great care.

Discussion

Based on geodetic measurements, three areas with similar movement trends can be determined: the eastern part showing a general downslope displacement, the

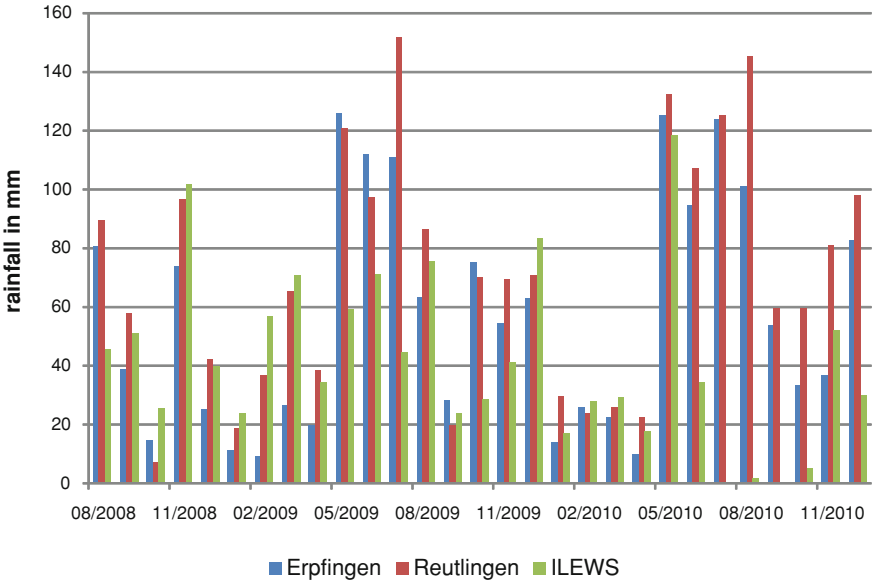

Fig. 6.15 Comparison of monthly rainfall of ILEWS weather stations with stations in Reutlingen and Erpfingen

western part moving into downslope and western direction, with certain epochs indicating upslope movements, and the middle part moving slightly upslope in the upper section downslope in the lower section. More detailed interpretation of the boundaries of observed slope deformation requires integration of subsurface data provided by inclinometers.

Geodetic monitoring of surface displacements carried out by Aslan et al. 2010 enhances the understanding of general landslide movement patterns. However, since fixed points outside the landside body were only integrated into some of the epoch measurements, only statements on relative deformation in the upper slope areas can be made. Direct comparisons to inclinometer data is hindered by different dates of measurements, and also because only three inclinometers were directly integrated into the geodetic point network. For some parts, uncertainties are relatively large in comparison to measured slope movements.

Observed variations of geodetic height of up to 1.2 cm can not only be explained by rotational slope movements. Possibly, the measured variations are attributed to swelling and drying of clay-rich subsurface materials. Lowest positions of geodetic points generally coincide with the periods where the driest subsurface conditions were recorded. Higher positions were always recorded in early spring, when the wettest conditions were measured. Continuation of geodetic measurements could aid to verify this hypothesis.

The extremely slow movements documented by the 6.5 years of inclinometer measurements also continued during this study. For most inclinometers,

displacements are still smaller than the error margin of the applied sensors. However, at inclinometer Lic02, measured displacements are clearly beyond the error margin by now. Previous investigation by Bell (2007) showed a direct relation between the 8.5 m deep flowing displacement with crack development at the house next to the inclinometer. High precision tilt measurements (Bell 2007) were also able to verify rotational components in the observed manual inclinometer measurements. Therefore, it can be assumed that rotational movements documented within this study are also real.

Similar to previous studies in Lichtenstein-Unterhausen (Bell 2007; Bell and Thiebes 2010), two depths of slope displacements can be observed in data from manual measurements in Lic02 which vary seasonally. These movements were described as a superficial flow movement reaching down to a maximum depth of 8.5 m, and a deep sliding movement occurring at approximately 15.5 m depth. In general, the same statement can be made with respect to new data acquired in this study. However, when taking into account all available manual inclinometer measurements some interesting processes can be observed from approximately 2007 on. The flow-specific gradual decrease of displacement with greater depths seems to slowly transition into a more even horizontal movement, possibly indicating the onset of a progressive development of a shear surface.

The rotational movements documented by monthly manual inclinometer measurements carried out by Bell (2007) can still be observed in some of this study's results; however, lower monitoring frequency makes detection more difficult.

A direct comparison of displacements documented by inclinometer to results of the geodetic monitoring can only be made for Lic01, Lic03 and Lic05 as these are incorporated in the geodetic network.

Lic01 and geodetic point 306 show similar displacements in B+ and B− direction. The large total downslope displacements of the geodetic points however, can not be observed in which might be attributed to the inclinometer installation above stable bedrock in 9.5 m.

Displacements documented by Lic03 are partly in agreement with geodetic measurements at point 201; however the magnitude of movement is smaller in the inclinometer data. Similar to geodetic data, also inclinometer data illustrates in B+, i.e. western direction.

For the eastern part of the geodetic network, i.e. points 205–207, 306, 105 and 106, a relatively strong downslope movement trend was observed, which is similarly observable in Lic04 inclinometer data, which is located between the respective points. Still, the magnitude of displacement is smaller in Lic04, which is possibly related to the installation above stable bedrock and a potential movement deeper than 11 m.

A comparison of data from inclinometer Lic05 and the geodetic network point 204 are in agreement regarding the lack of any significant downslope movement. Rotational movements of Lic05, however, can not be observed in geodetic data. Therefore, it has to be questioned if the consistent rotational displacement component documented by Lic05 and Lic02 are caused by the same movement process.

Unfortunately, the sliding movement documented by manual measurements of Lic02 can not be observed in the inclinometer chain data due to the positioning of the lowest sensors. Due to limited project funding, further drillings to a great depth, and subsequently deeper installations of the inclinometer chain could not be carried out. However, general trends of movement documented by manual inclinometer measurements are also visible in inclinometer chain data. Still, extremely slow movements are in the range of the error margin and have to be interpreted carefully.

The very good temporal resolution of the automated inclinometer chain is potentially of great value for the analysis of movement triggering events. However, no significant displacement occurred during the project duration and single dates of the slope movement initiation can not be determined. Instead, relatively steady displacements are documented. Particularly regarding the deep sliding movement, no period of accelerated movement can be defined.

6.1.2.3 Hydrological Data

Within this study, climate data from the ILEWS weather station posed an important data source for the analysis of hydrological processes and landslide reactivation. Climatic data is available from mid August 2008 to late March 2011, however due to technical problems (power failures, damage induced by animals) no measurements were recorded during some periods. Fig. 6.14 displays data for daily rainfall and mean daily temperature from the ILEWS weather station. While temperature data shows a plausible course, rainfall data shows some disputable characteristics during summer 2010, with almost no recorded rainfall. The reason for this was found out to be neglected maintenance of the weather station leading to false measurements from approximately spring 2010 on.

In comparison to other weather stations located nearby (Fig. 6.15), the ILEWS station generally recorded similar monthly rainfall amounts, when taking into account periods with station malfunctions. However, data strongly differs from June 2009 on where significantly less precipitation was recorded, indicating malfunction of the ILEWS station due to insufficient maintenance because of limited availability of resources. A correlation of ILEWS rainfall data with the other weather station Erpfingen and Reutlingen for the period between August 2008 and January 2009 resulted in R^2 values of 0.57 and 0.50, respectively. Since linear regression of rainfall data produced relatively low correlation values, no interpolation of precipitation values for 2010 were elaborated.

Inadequate maintenance of the ILEWS weather station also influenced measurements of snow height by ultrasound distance measurement. Raw data is illustrated in Fig. 6.16 with an inverted distance y-axis for easier interpretation. Data shows considerable scatter and even fluctuations of distance measurements even during summer which can not be related to snow accumulation. To derive reasonable snow height records, a detailed data analysis and correction was carried out for the following use within analysis of snow melting and hydrological response.

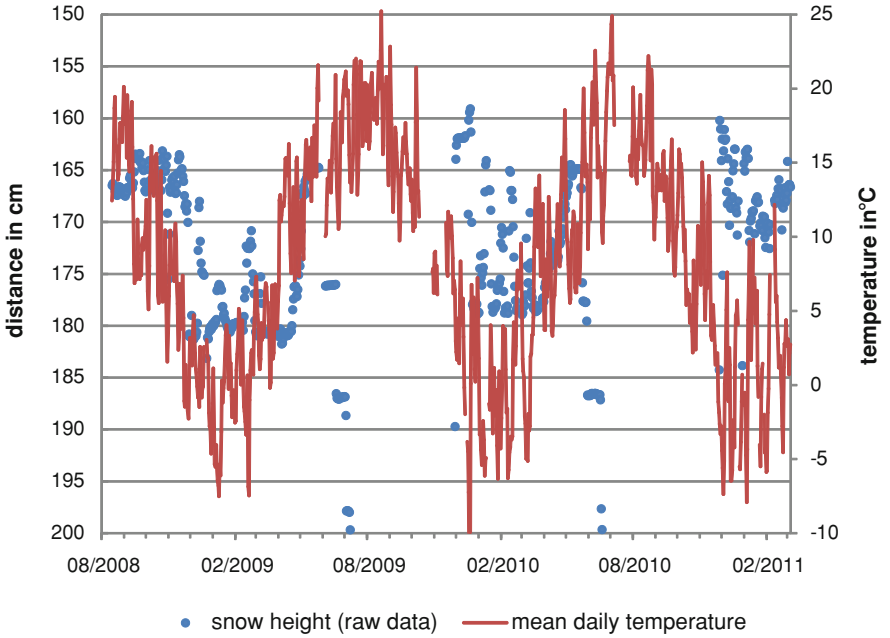

Fig. 6.16 Raw data from ultrasound distance measurement of snow height in comparison to daily mean temperature

Since the base distance at the beginning of each winter season varies in each period, no single correction factor could be applied. Detailed data analysis considering temperature and precipitation data led to determination of the three correction factors for each winter season: 1.81 for winter 2008/2009, 1.78 for winter 2009/2010 and 1.79 for winter 2010/2011.

In addition to correction factors, several records were deleted in the data set where snow was considered unlikely due to daily mean temperatures. Adjusted snow height data is presented in Fig. 6.17. Visual interpretation of plotted adjusted snow height data indicate a relationship between daily mean temperatures and the variation of snow height with a diametrically course of both factors.

In winter 2008/2009 the local study area experienced snow coverage from early December 2008 until early March with an period of snow melting due to higher temperatures in late December and early January. The winter period of 2009/2010 exhibited similar snow height conditions, with development of a snow cover in mid December which lasted until March. Absolute snow height almost reached 20 cm in early winter season. Additional snow fell during the winter season, but also melted during short periods of high air temperatures. In winter 2010/2011 snow covered the local study area between late November to early February with a maximum thickness of almost 20 cm. Warmer periods in late December and early January caused strong snow melt.

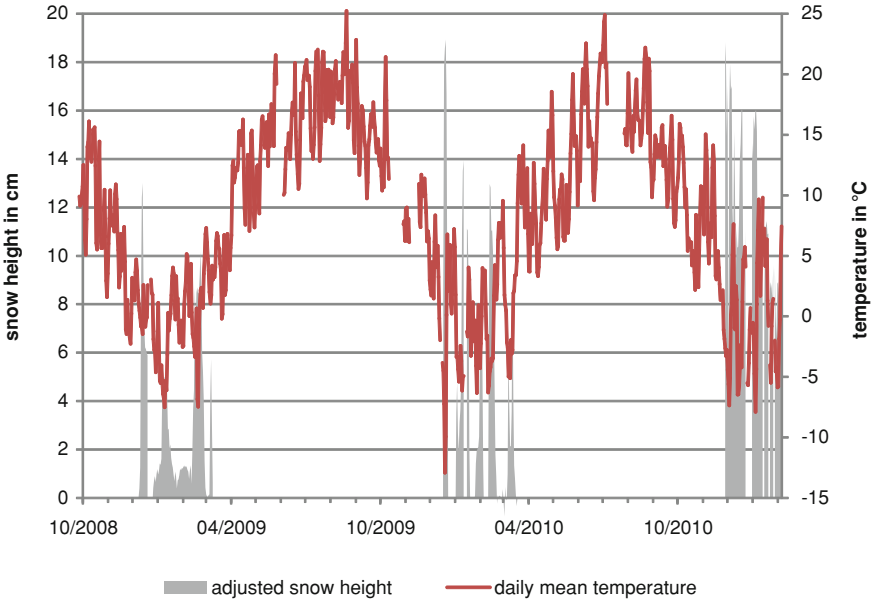

Fig. 6.17 Adjusted snow height and mean daily temperature

In Figs. 6.18, 6.19, 6.20, 6.21, 6.22, 6.23, 6.24 and 6.25, data from hydrological monitoring, i.e. TDR sensors and tensiometers are presented along with daily rainfall data from the ILEWS weather station. Unfortunately, no data from position p31 located in the eastern part of the monitoring system was available because this station was only connected to the monitoring system at a very late state. In addition, some monitoring sensors are possibly damaged during installation. Also vandalism, in particular to tensiometers was a problem; in several cases rubber tubes were removed causing tensiometers to run dry until they were repaired and refilled during later maintenance works.

Soil hydrology sensors at p11 are located in the south of the monitoring network, in the garden below the house suffering cracking due to slope movements. Records from the initial phase of monitoring in 2008 show no variations at (see Fig. 6.18). After maintenance work by the project partner IMKO, in which the sensor software was updated, real measurements commence in early 2009. Tensiometer measurements in 8.6 m depth describe positive values (up to >300 hPa) over the entire monitoring period indicating that the sensor was permanently below the groundwater table. Similar conditions are documented by TDR data from 8.8 m depth with constant volumetric water content of around 50%. Tensiometer in 4.5 m depth reflects saturated conditions for most times, and only negative values for summer and autumn 2009. The course of the graph is similar to the deeper tensiometer, however, reaction to rainfall events is quicker. Unfortunately, no TDR data is available from a similar depth because the probe malfunctioned. Also measurements by the tensiometer in 1.75 m depth may be influenced by a bad connection to the soil. From 2009

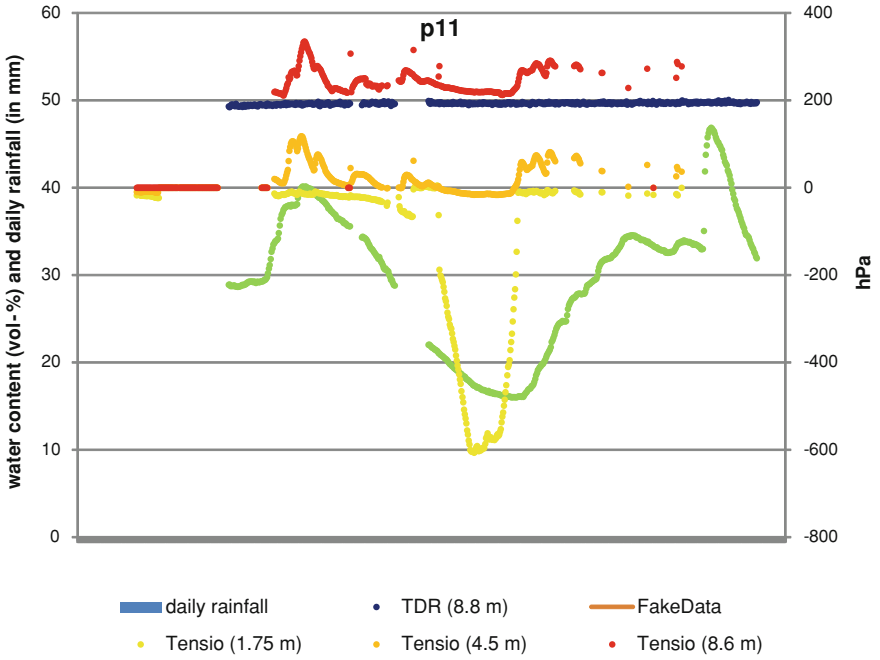

Fig. 6.18 Hydrological monitoring at location p11

on, stable conditions close to saturation were recorded without any significant influence of rainfall events. From August 2009 on, measured pore pressure quickly decrease until October. Similar behaviour can also be observed for some other tensiometers. According to the project partners IMKO who were responsible for the monitoring system, this behaviour is related to drying of the ceramic contact. However, after refilling during maintenance works, in this case around November 2009, records increased again and returned to values similar to the initial conditions. TDR sensor in 1.95 m depth describes a strong increase of water content from below 30 to over 40% between February and April 2009, followed by a decrease until approximately November. For 2010, also water contents of over 45% were recorded indicating full saturation. Strong peaks for deep tensiometers and the shallow TDR sensor can be observed after February 2009. This event is highlighted in more detail later in this chapter. Groundwater conditions for the following spatial interpolation of groundwater and subsequent modelling were determined to vary between 2 and 4.7 m for this location. Highest groundwater positions referred to high saturation values measured at the shallowest tensiometer (1.95 m depth), while lowest water Table referred to minimum levels of 4.5 m tensiometer.

Hydrological sensors at p12 are located at the damaged house, only 2 m away from inclinometer chain in borehole Lic02. The TDR sensor in 9.5 m depth recorded large fluctuations of volumetric water content which varied between approximately 35 and 45% (see Fig. 6.19). The amplitude of this sensor is the

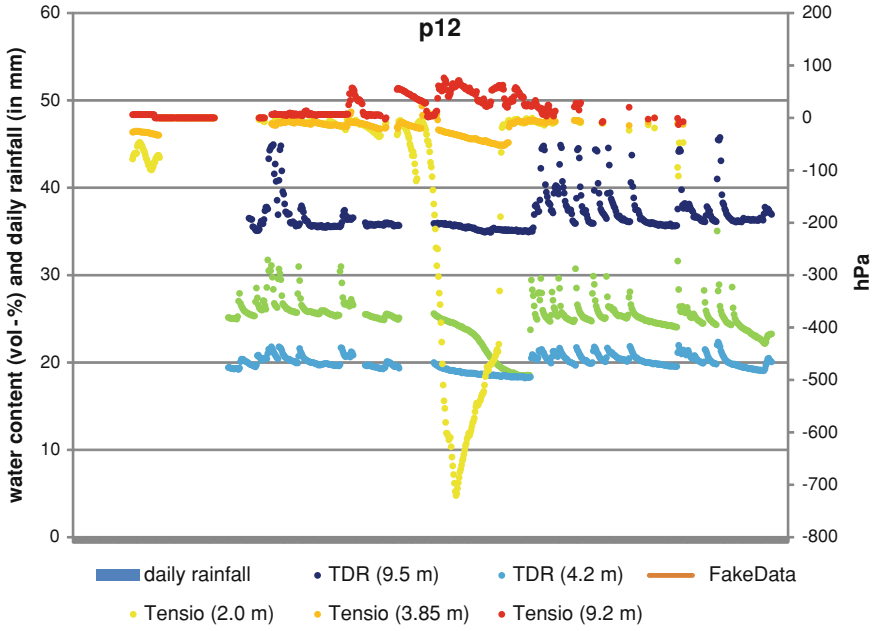

Fig. 6.19 Hydrological monitoring at location p12

highest of all TDR probes installed at this locations. Strong peaks can be observed for February 2009, and from November 2009 on. Tensiometer data from similar depth (9.2 m) illustrates conditions of high saturation but with lower fluctuations. Some stronger rainfall events (e.g., May 2009) caused strong peaks relating to a location below groundwater table. Phreatic conditions were also recorded by the tensiometer in 3.85 m depth for some periods. Response to rainfall events by this sensor is relatively low. Records from tensiometer in 2.0 m depth only show small variations and lower response to rainfall events than the tensiometer in 9.2 m. From August 2009 on massive drop of recorded measurement in 1 month and increase afterwards, which likely to be caused by drying of the tensiometer ceramics and refilling during maintenance works in October 2009. TDR sensors in 2.35 and 4.2 m illustrate clear response of volumetric water content to rainfall events. Both graphs describe similar trends, however, stronger variations can be observed for the shallow TDR which also has higher mean water content ($\sim$25 and $\sim$20%). During late summer and early autumn 2009, TDR in 2.35 m depth recorded quickly decreasing water contents, while the 4.2 m TDR sensor describes more steady conditions. However, after strong rainfall in December 2009, both sensors return to initial value levels. Minimum and maximum groundwater table depths for this location were determined to be 4.5 and 2.0 m, respectively. The high water Table referred to almost saturated conditions at 2.0 m tensiometer. Low water Table definition followed measurements of the tensiometer in 3.85 m, which documents not saturated conditions for some periods.

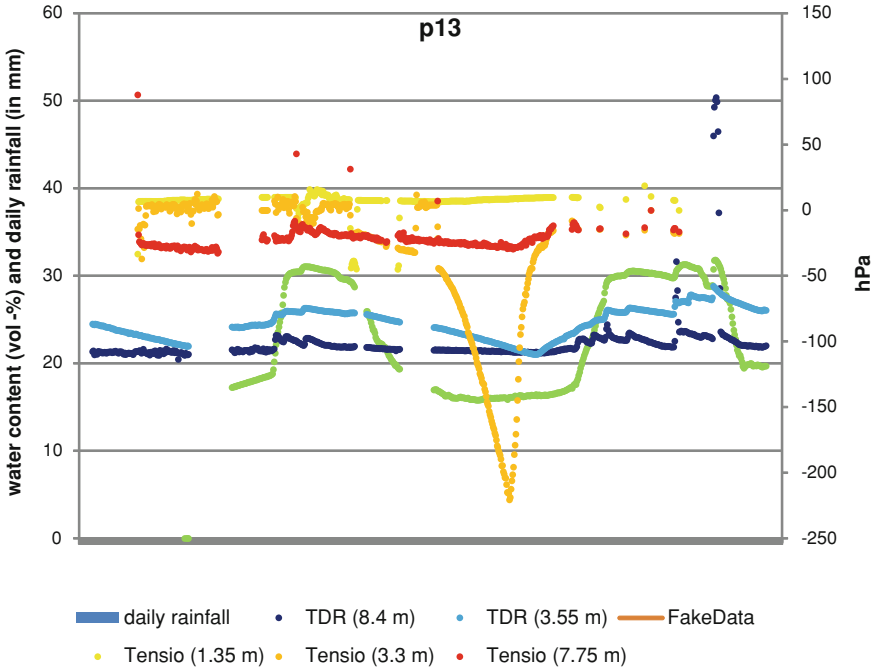

Fig. 6.20 Hydrological monitoring at location p13

Sensors at p13 are located in the centre of the monitoring system at inclinometer Lic05 and the container with monitoring equipment. For the TDR in 8.4 m depth, volumetric water contents between approximately 20 and 25% can be observed (see Fig. 6.20). Strongest peaks occurred in spring 2009 and again in 2010, possibly related to snow melting. However, no direct response to rainfall events can be found throughout the monitoring campaign. Tensiometer in 7.75 m depth recorded no positive values, indicating that full saturation did not occur during monitoring campaign. Reaction to rainfall events is relatively small, with the strongest peak occurring in February 2009. Scattered data close to full saturation was recorded by tensiometer in 3.3 m depth without any significant response to rainfall events. Similar to other tensiometers, records drop in summer 2008, likely to be related to drying of tensiometer ceramics. More stable conditions are documented by tensiometer 1.35 m. Positive values indicate saturation almost for the entire monitoring period. However, data from the shallowest TDR sensor do not indicate fully saturated conditions with water content variation between 15 and more than 30%. For location p13, groundwater minimum levels were determined as 3.7 m, primarily based on 3.55 m tensiometer, which documented unsaturated conditions during the entire monitoring period. A maximum groundwater table was determined to be 1.3 m using high saturation records from 1.35 m tensiometer.

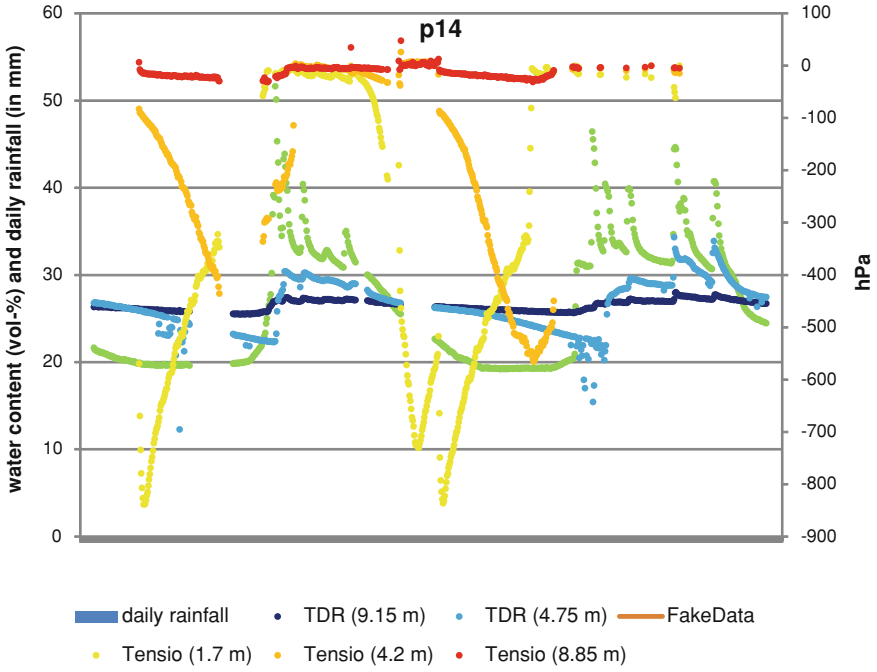

Fig. 6.21 Hydrological monitoring at location p14

The most upslope sensor location is p14, which is positioned in the forest directly neighbouring the geoelectrical monitoring profile. Tensiometer data from 8.85 m illustrates almost saturated conditions for the entire monitoring period, with only little response to rainfall events (see Fig. 6.21). Relatively stable conditions are also documented by the adjacent TDR sensor in 9.15 m depth, with volumetric water contents around 25% and no direct response to rainfall events. Tensiometers in 1.7 and 4.2 m depth recorded diametrical development of pressure measurements in the beginning of monitoring period before documenting conditions close to saturation from February 2009 on. Afterwards, 1.7 m tensiometer reflects sudden drying which is likely to be caused by damaged tensiometers. In August 2009 and October 2009, however, records increase again, possibly due to strong rainfall in August and maintenance works in October. Shallow TDR sensors in 2.0 and 4.75 m depth at p14, document stable conditions without larger changes until February 2009 when water content increases to more than 30 and 40% of volume, respectively. Afterwards, water contents decrease until late 2009, with little response to rainfall events for the deeper sensor. The shallow TDR in 2.0 m depth however reflects strong variations of more than 15% water content for spring periods. A maximum groundwater table of 1.8 m below the surface was determined based on high saturation records of 1.7 m tensiometer. The definition of a minimum water table was difficult due to possible malfunction of tensiometers at

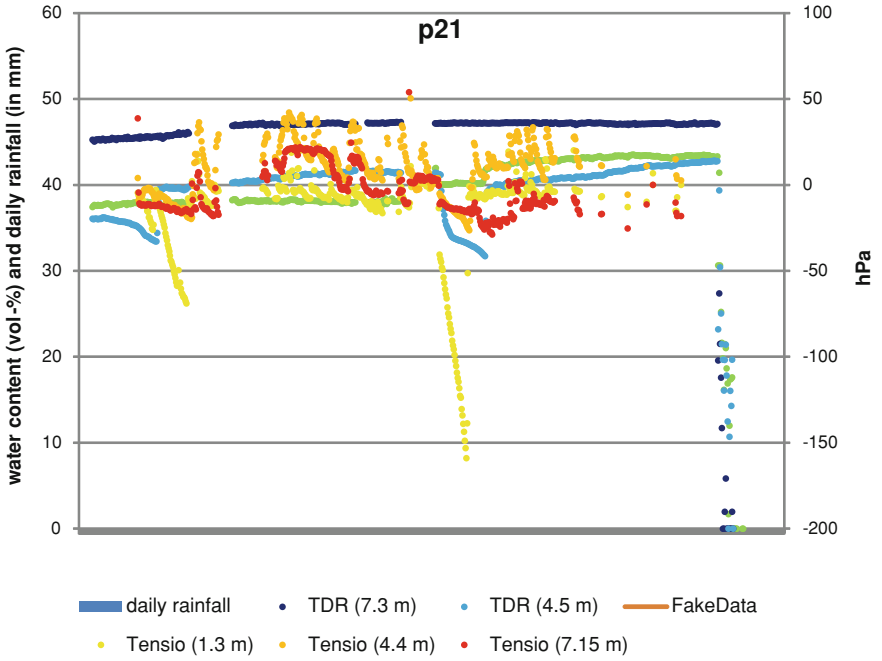

Fig. 6.22 Hydrological monitoring at location p21

this location. However, low water contents of 4.75 m TDR was used to assume a minimum water Table of 6 m.

In the western part of the study area, location p21 is adjacent to inclinometer Lic03. Volumetric water contents of around 48% were recorded by deepest TDR in 7.3 m with no great changes occurring throughout the monitoring campaign (see Fig. 6.22). Phreatic conditions for long periods are also illustrated by tensiometer in a similar depth (7.15 m) with variations in the range of −30 to +54 hPa. Large variations due to rainfall events can be observed for the 4.4 m tensiometer with maximum positive pressures relating to approximately 50 cm of groundwater above the sensor. Very high water contents were also recorded by the adjacent TDR sensor in 4.5 m depth with values above 40%. Driest conditions occurred during October and November 2009. Also TDR sensor located in 1.6 m depth illustrates relatively stable conditions with water contents around 40% and only little response to rainfall events. For this location, minimum and maximum groundwater levels of 4 and 5 m were determined primarily based on the variations of tensiometer data from 4.4 m depth.

The installation of hydrological sensors at p22, located between inclinometer Lic03 and Lic05 directly next to the road was very difficult. Boreholes collapsed several times during installation so that sensors might not be appropriately fixed into the soil. Relatively stable conditions in depth are illustrated by the deepest sensors, with water content around 23% by the TDR sensor in 7.1 m depth, and

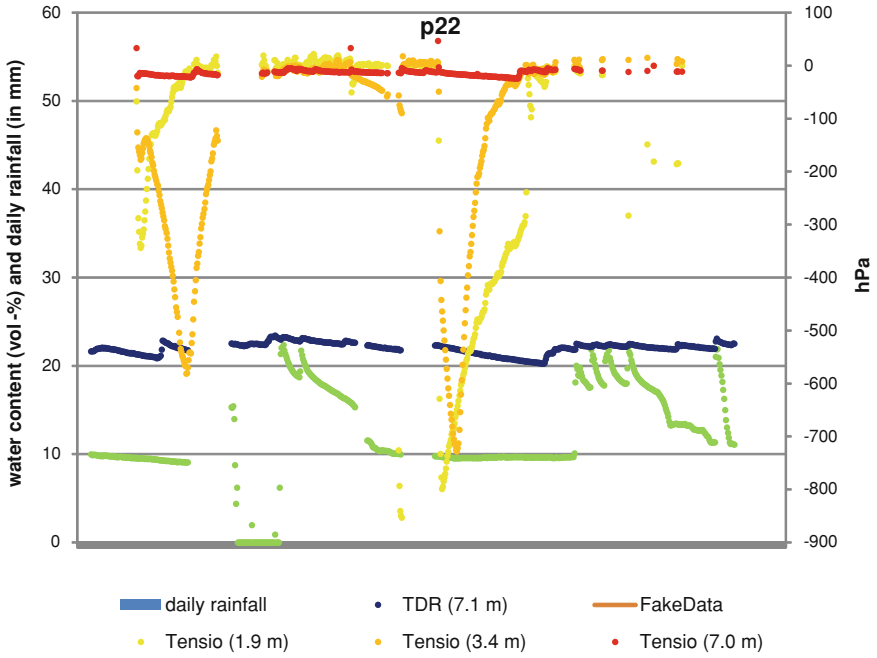

Fig. 6.23 Hydrological monitoring at location p22

almost saturated conditions (tensiometer in 7.0 m) (see Fig. 6.23). Both other tensiometers (in 1.9 and 3.4 m depth) document partly saturated periods during 2009 until August, when records drop to very low values possibly due to drying of tensiometer ceramics. Data from the shallow TDR in 2.1 m depth shows water content of approximately 10% with no variations for two periods in 2008 and August 2009 to January 2010. For some time, water content also drops to 0% which is very likely to be erroneous. More realistic measurements and response to rainfall events were recorded from March 2009 on and again in 2010. Definition of a groundwater levels for this location was difficult due to problematic installation of sensors. However, a maximum groundwater table of 2 m was determined based on high saturation values at the 1.9 m tensiometer. A minimum level of 5 m was assumed using data from the 3.4 m tensiometer for orientation.

Sensors at p24 are located in the eastern part of the study area between inclinometer Lic05, and the lawn with inclinometers Lic01 and Lic04. Saturated conditions are illustrated by deep tensiometer and TDR sensor in 9.35 and 9.5 m, respectively (see Fig. 6.24). Volumetric water content was very constant throughout the monitoring campaign, with values around 48%. Tensiometer data describes positive pressures of up to 100 hPa with some fluctuations. However, tensiometer data also includes measurements of exactly 0 hPa very likely due to malfunction. More shallow tensiometers data has some large scatter and also exhibits drying of tensiometer ceramics until refilling during maintenance works.

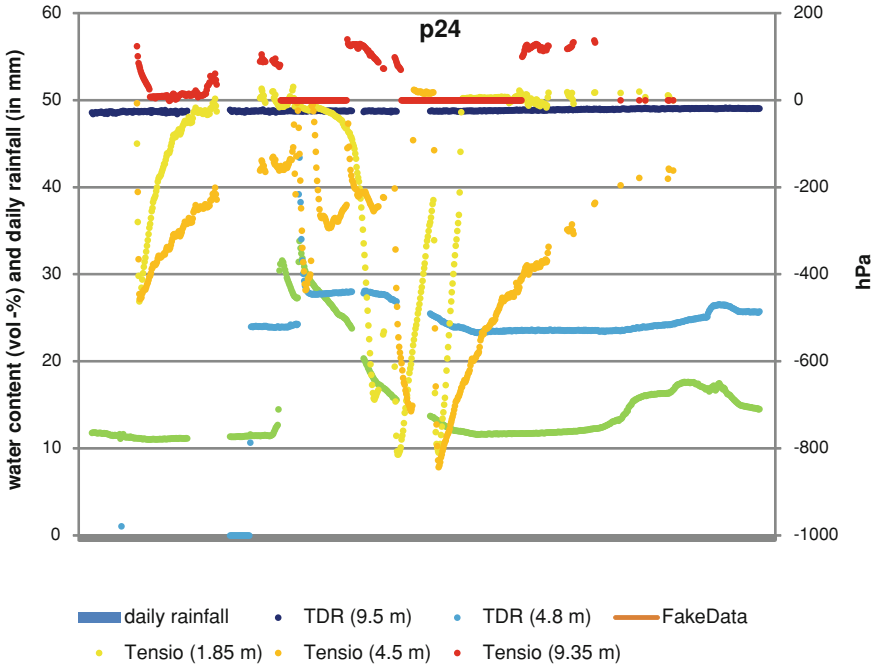

Fig. 6.24 Hydrological monitoring at location p24

Shallow TDR sensors show very little response to rainfall events with relatively dry conditions (mean volumetric water content of 15 for 2.0, and 25% for 4.8 m). Partial saturation of the tensiometer in 1.85 m depth was used to determine a maximum groundwater level as 1.9 m. Lowest groundwater position was assumed to be 6 m based on interpretation of TDR and tensiometer from 4.8 to 4.5 m depth, respectively, which reflect unsaturated conditions for some time.

Hydrological monitoring site p41 is located west of longitudinal geoelectrical monitoring system in the forest. Constantly low volumetric water contents of approximately 13% were measured by the TDR sensor in 7.1 m depth (see Fig. 6.25). The tensiometer 15 cm above recorded some variations of pore water pressure following rainfall events. Saturation was reached during summer 2009 before soil suction drop to lower values around −200 hPa. Tensiometer 1.7 and 3.7 m both show increasing saturation from 2008 on until April 2009, also reaching full saturation for spring 2009 and early 2010. Recorded volumetric water content for the TDR sensors in 3.9 m depth is initially 0% before settling to constant values of 10%. For this sensor it was assumed it was either damaged during installation or not properly fixed into the subsurface. The shallowest TDR sensor in 1.9 m depth also recorded very dry conditions with less than 10% water for long periods. Moreover, no significant response to rainfall events can be observed. For this location, groundwater minimum and maximum levels were determined as 2 and 6 m. Definition of highest water table was based on high

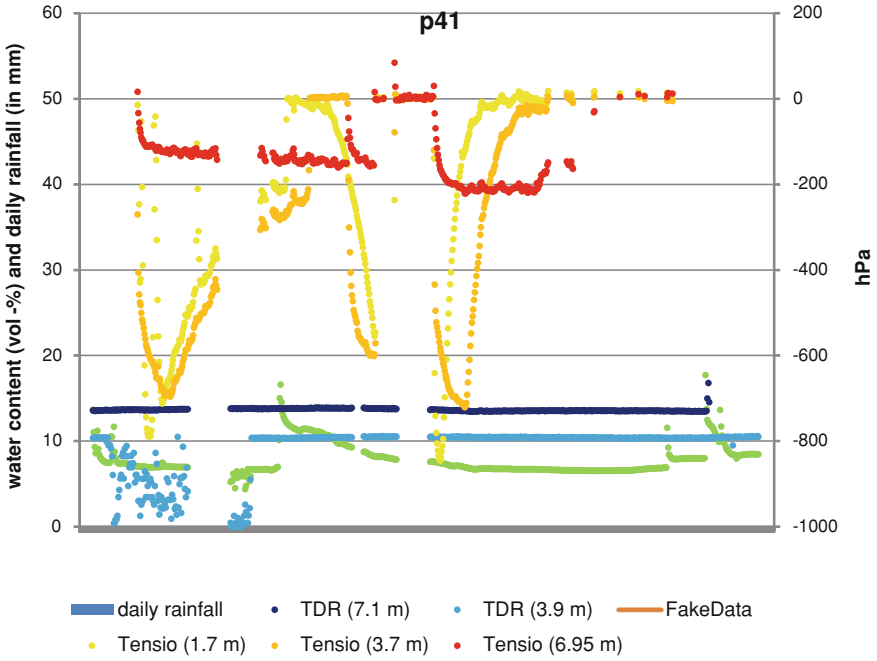

Fig. 6.25 Hydrological monitoring at location p41

saturation of 1.7 m tensiometer. Lowest groundwater levels were primarily assumed by interpretation of data from the deepest hydrological sensors at p41.

A more detailed analysis of hydrological response to rainfall and snow melting was carried out for several shorter periods. Some examples of these will be presented in the following.

The first event analysed in more detail is February 2009, where a strong raise of water content and saturation was documented by several of the hydrological sensors. Climatic data from the ILEWS weather station shows, that in February initially small snow coverage increased to approximately 10 cm until 22nd February, when warmer temperatures led to a quick decline of snow height (Fig. 6.26).

Precipitation records from the unheated rainfall gauge reflect the snow melting process. Peaks in precipitation measurements can be observed for all periods in which the temperatures is above 0°C. Total precipitation in February 2009 cumulates to 77 mm. Snow height data, however, does not follow short-time temperature changes but reflects general trends. The strong decrease of snow height from 22nd February on, however, is only partly documented by precipitation records.

For the February 2009 period, a detailed time-lapse inversion of data from the longitudinal geoelectrical profile was elaborated by Wiebe et al. (2010) which will be presented below. Though data processing was carried out by Wiebe et al. (2010),

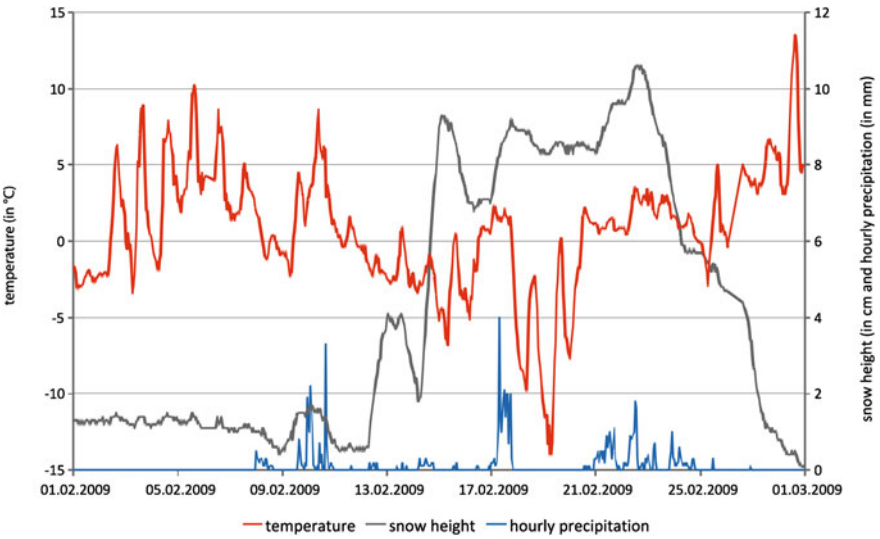

Fig. 6.26 Snow height and temperature in February 2009

the following description and subsequent interpretation are made by the author of this thesis.

Figure 6.27 illustrates the time-lapse inversion, where changes between a reference record and subsequent measurements are described in percent. The time increment between each snapshot is 16 h, and 32 h for the last. The lowest hydrological monitoring site (p11) is located around profile metre 5. The damaged house and p12 are at profile metre 36, Lic05 and p13 at profile metre 55 m. The most upslope hydrological sensors p14 are positioned at profile metre 105.

In the reference model, highest resistivity was measured in the upper sections in the area of the scree slope. Lowest resistivity can be found on around profile metre 35. In the following snapshots, two sections of the profile illustrate some interesting characteristics. For the middle part of the profile, between profile metres 50 and 100, a slow and gradual decrease of resistivity down to approximately 5–8 m throughout the entire time span can be observed. Around profile metre 24 and 48, a similar decrease of resistivity can be noticed in the first plots, however at both points, lowered resistivity quickly reaches depths of about 15 m. Between these areas, approximately at profile metre 36, a superficial area of high resistivity persists in all compared measurements.

To assess, if observed changes in resistivity relate to infiltration of melting snow, TDR sensors along the geoelectrical monitoring profile were analysed. Figure 6.28 displays records from p12 to p13 positioned at profile metres 36 and 55, respectively. Snow melting around 9th February caused increases of soil water content with a magnitude of 3–5% for the sensors in 4.2 and 2.35 m depth at p12, respectively. During the following days, water content slowly decreases. For the TDR sensors at p13, no significant response can be noticed. Further snow melting

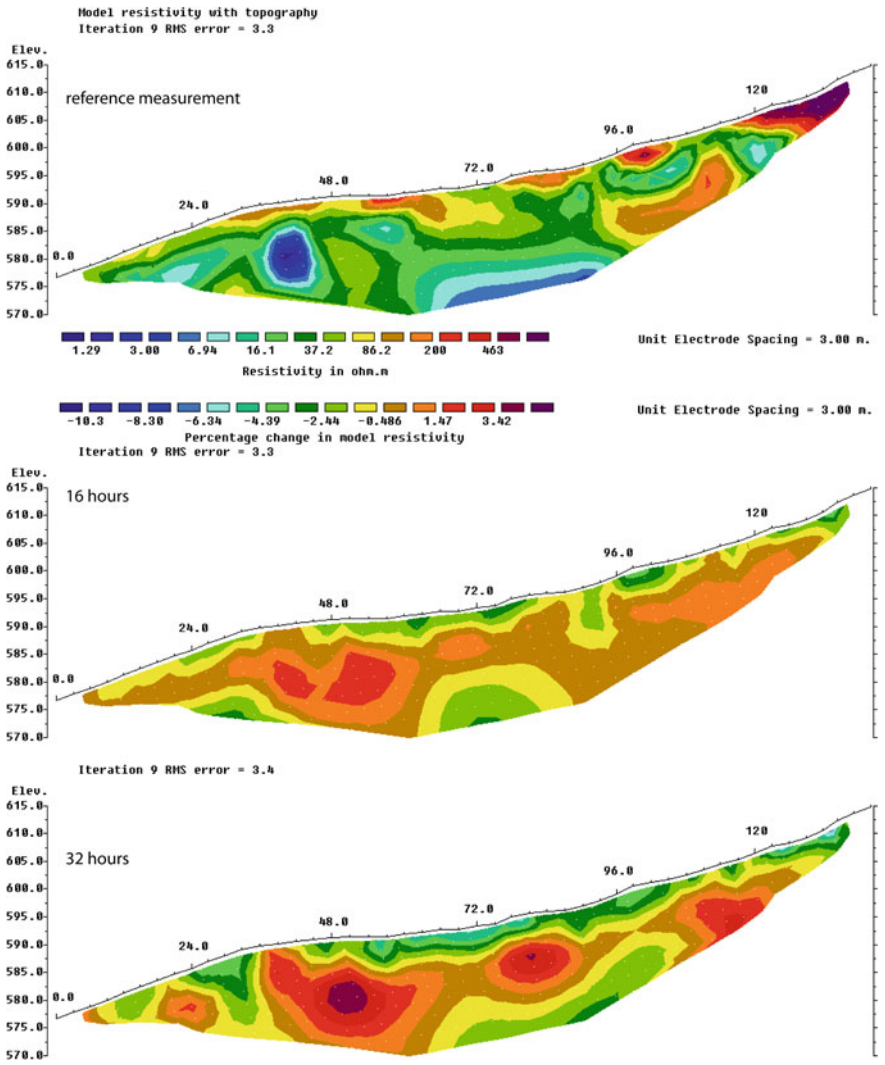

Fig. 6.27 Time-lapse inversion of geoelectrical monitoring data for period of 23rd to 26th of February (after Wiebe et al. 2010)

on the 17th is followed by only smaller deviations of soil moisture, even though more precipitation is documented for this period. More precipitation was recorded from the 21st on, which lead to significant increase in soil water content. The earliest peak can be noticed for the shallowest TDR at p12, approximately 24 h after the precipitation peak. Shortly after, a small increase of water content can be recognized for the 4.2 m deep TDR. The deepest TDR, however, illustrates a very strong soil moisture increase of 6–8% starting on the 25th. Sensors at p13 do not reflect any significant decrease in soil water content over the entire period.

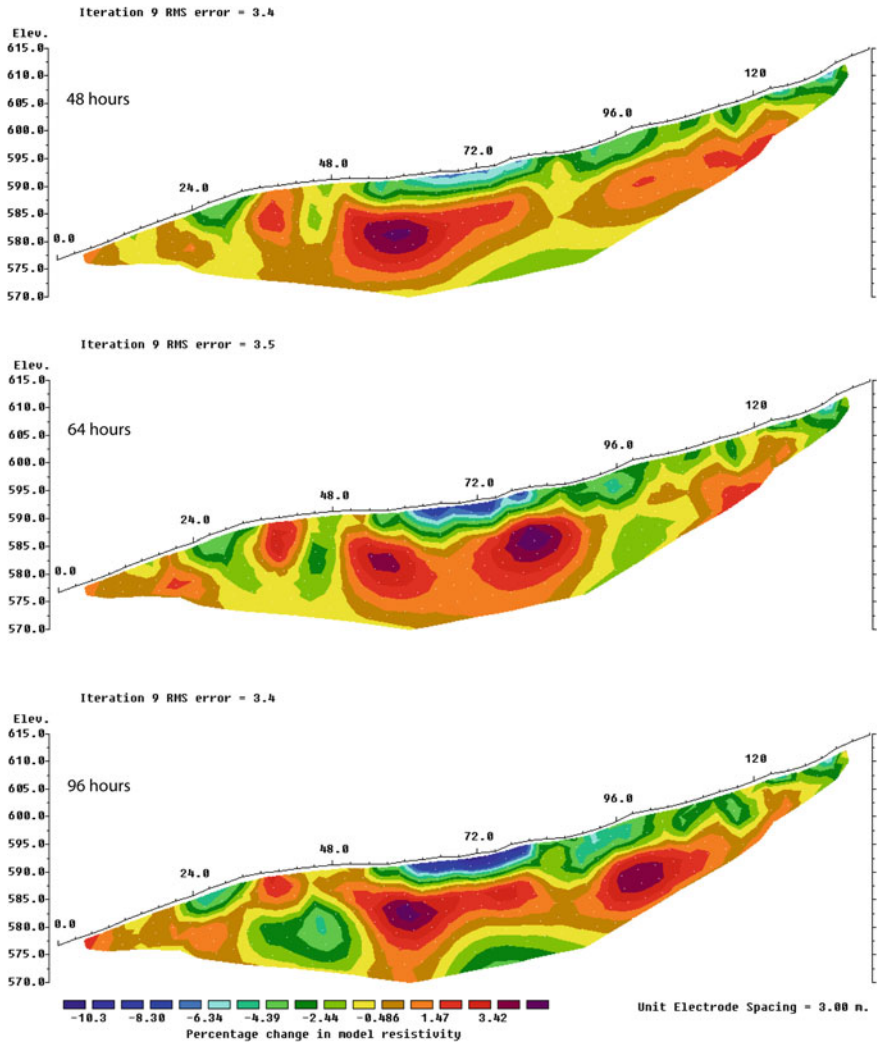

Fig. 6.27 (continued)

The other sensors located along the geoelectrical profile, i.e. p11 and p14, also do not show any sudden increases of soil moisture, except for the TDR probe in 4.2 m at p14.

Here, water content increases starting around 16th February from 20 to over 30% in 9 days, before a further rise to over 50% in only 4 days.

Inclinometer chain data from the same period were analysed to investigate if any increase of movements were recorded during February 2009. After correction of raw data, a total displacement of 0.2–0.5 mm can be observed. Magnitude of displacements varies with installation depth of sensors, with larger movements occurring in shallower locations. However, to carry out manual inclinometer measurements on

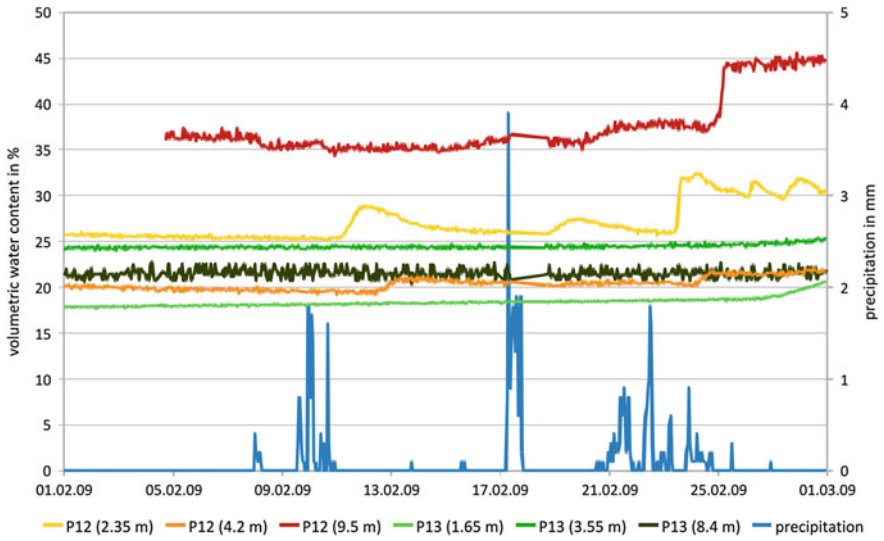

Fig. 6.28 Volumetric water content at location p12 and p13 during February 2009

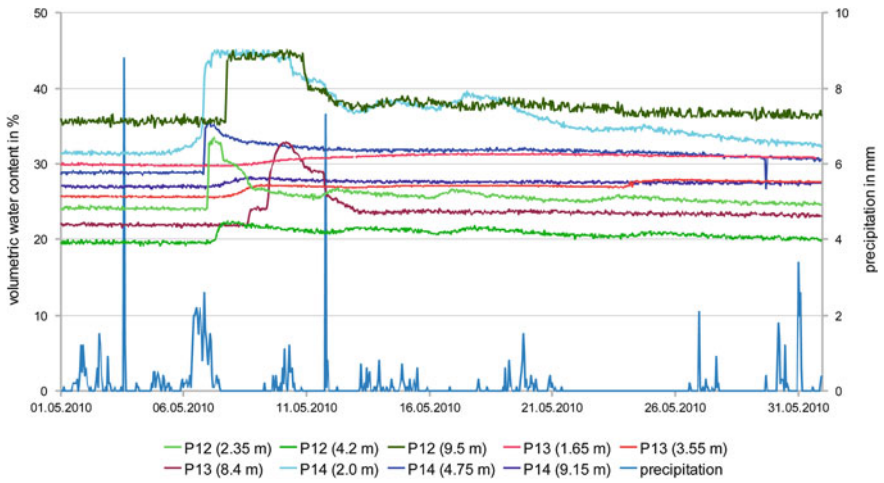

Fig. 6.29 Volumetric water content at location p12, p13 and p14 during May 2010

Lic02 borehole, the chain was extracted and later reinstalled on 12th February. Therefore, it is not possible to assess if displacements describe real slope movements or originate from settling of the inclinometer probes after the extraction from the borehole. Manual measurements show no significant displacements between November 2008 and February 2009. Between February 2009 and the following manual measurement in November 2009, a movement of 1 mm occurring in approximately 15 m was recorded. In addition, the more superficial displacement in approximately 8 m depth also occurred with a total movement of 1.5–2.5 mm.

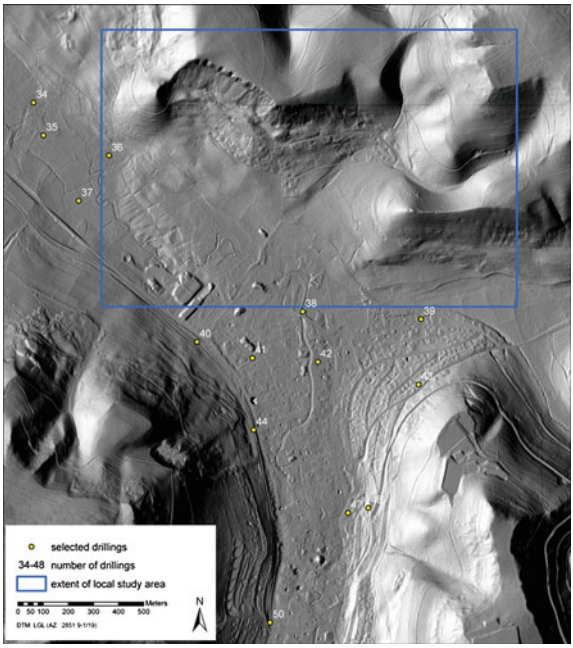

Fig. 6.30 Drillings close to the local study area described in geological map (1:25,000) (after Ohmert et al. 1988)

One of the strongest rainfall events during the period of monitoring occurred in May 2009, with a maximum hourly intensity of 27 mm. During this event, only shallow sensors showed a quick response by increased soil moisture. Sensors located in greater depths do not document significant increases of soil water content, except at p12, where small reaction can be observed. Still, the response of the 9.5 m TDR sensor is larger than the 4.2 m sensor at this location.

Inclinometer chain data from May 2009 shows some movements for the 3 m depth sensor with a maximum displacement of approximately 1 mm, whereas deeper sensors do not display any changes.

Another analysed period was November 2009 for which strong peaks in precipitation records and hydrological data can be noticed. During this entire period, temperatures were above 0°C making an influence of snow unlikely. Within the first 5 days, approaximately 20 mm of precipitation were recorded, however, no signigcant response by TDR sensors can be observed. Similar data was aquired fom tensiometers, which do not reflect any significant changes in soil suctions and pore water pressure, except for the 9.2 m deep sensor at p12 for which an increase from approximately 25 to over 50 hPa was assessed. An increase of this magnitude roughly relates to a rise of the groundwater table by 30 cm.

For November 2009, no significant displacements were recorded by the inclinomter chain.

More than 70 mm rainfall are recorded in the first 10 days of May 2010 which was followed by quick increase of soil water content (Fig. 6.29). At p12, the first sensor the respond to the precipitation event is the shallowest TDR for which a rise

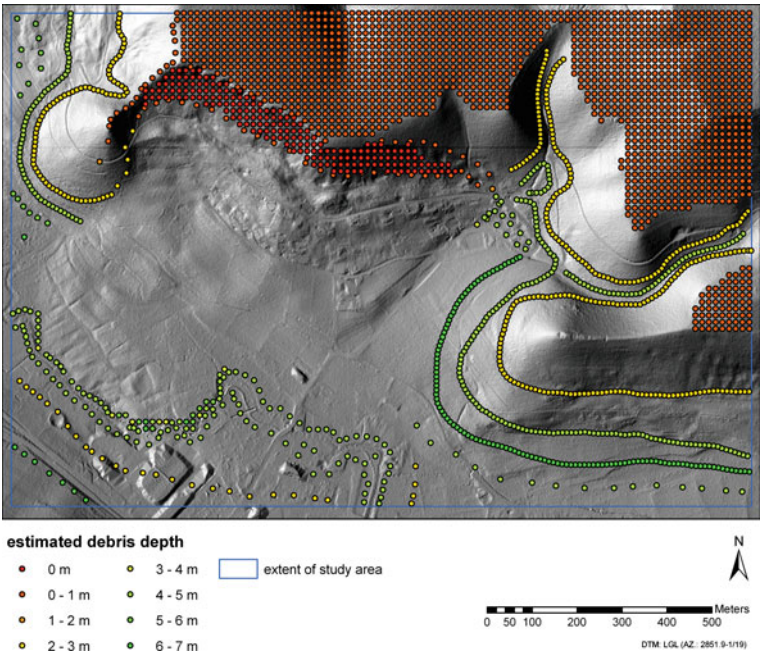

Fig. 6.31 Estimated depth of debris for local study area

of soil moisture of 10% is documented. Shortly after, a response can be observed at the sensor in medium depth, which is again smaller than peak measured by the 9.5 m TDR sensor. Here, water content reaches a maximum of approximately 55%. In contrast, data from shallow TDR probes at p13 only show a slight increase after the rainfall. The deepest TDR probe in 8.4 m depth shows the largest response to rainfall with an increase of soil moisture from 22 to approximately 35% in less than 48 h. TDR sensors at p14 show the strongest increases for the two shallow sensors, and a very smooth and slow rise of soil moisture for the deepest sensor in 9.15 m. However, data from the inclinometer chain for this period does not reflect any significant displacements.

Discussion

In general, hydrological monitoring shows saturated conditions located in greatest depths during the entire monitoring period, and responses to rainfall and snow melting can mainly be observed for sensors in more surficial positions. Yet, for some relatively strong rainfall events, no significant response at all can be noticed. Relatively dry conditions documented for location p41 are likely to be caused by the convergent topography of the monitoring site. Overall, highest groundwater water contents are recorded for spring, while lowest conditions occurred during summer and autumn.

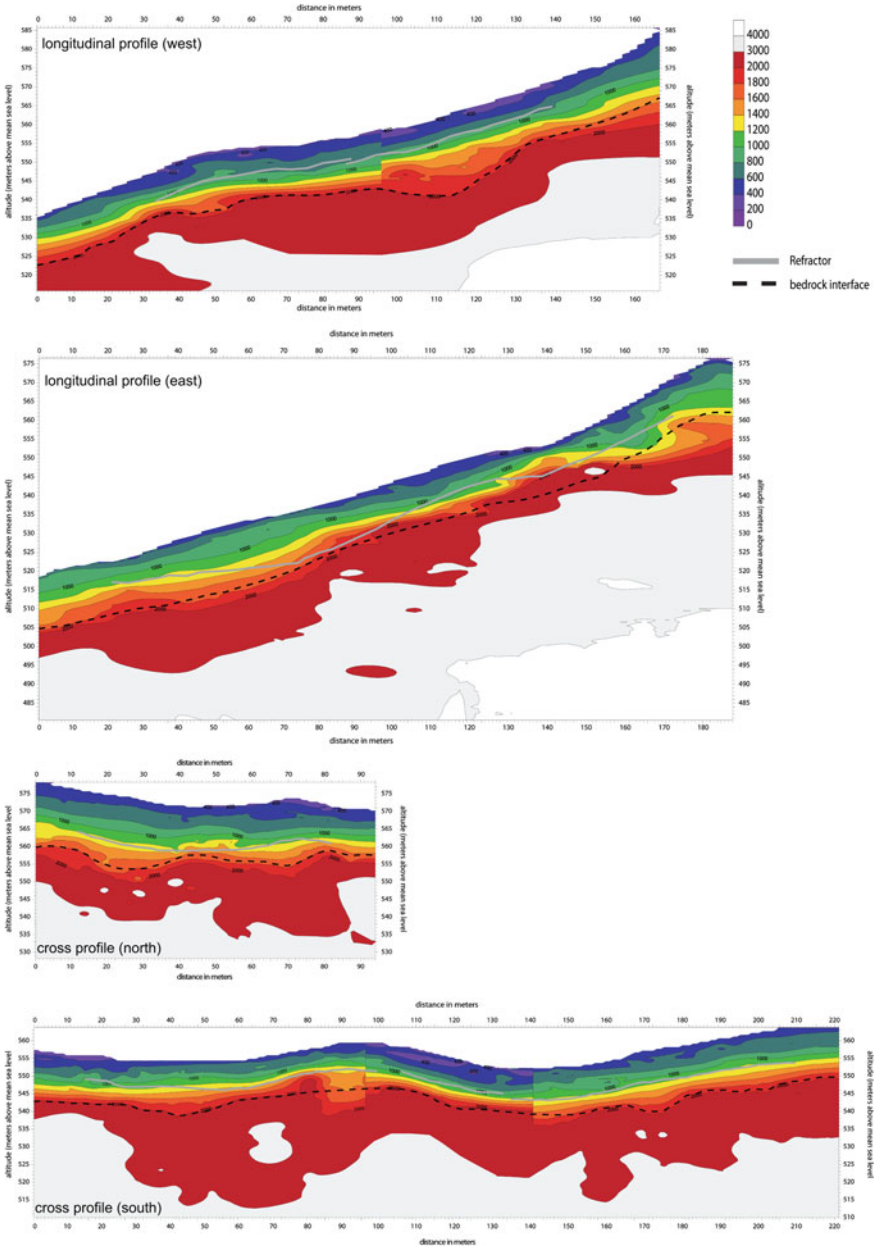

Fig. 6.32 Results of geoseismic prospection and estimated bedrock interface depths (after Bell et al. 2010)

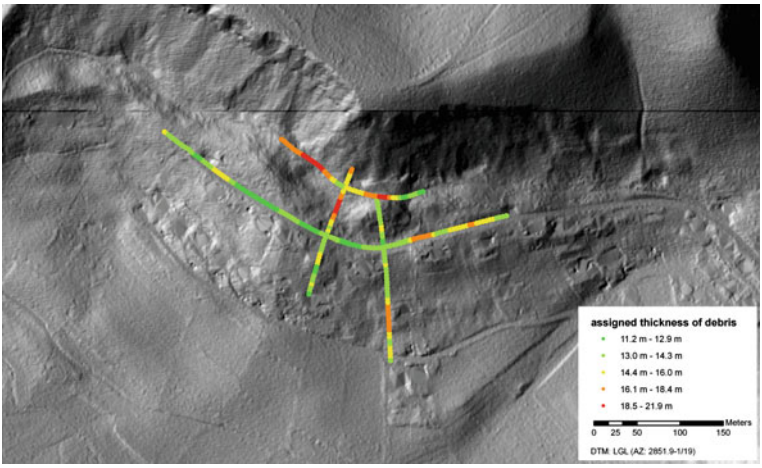

Fig. 6.33 Assigned depth of debris from analysis of seismic prospection data

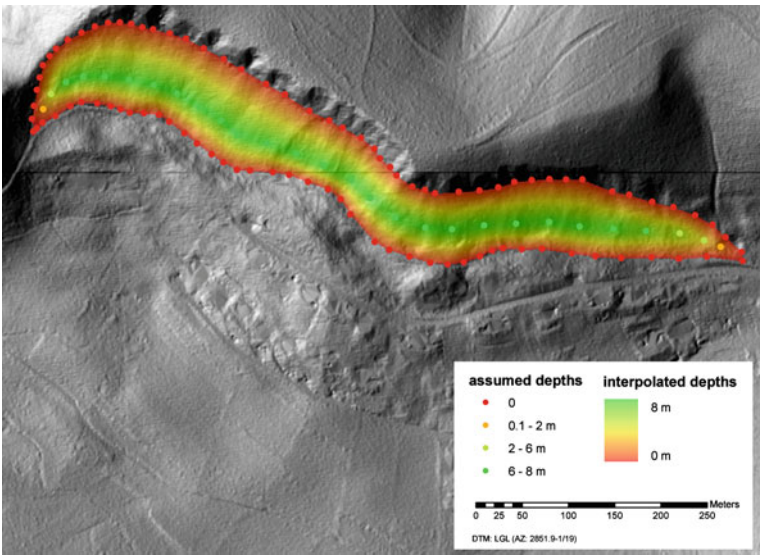

Fig. 6.34 Interpolation of scree thickness

Determination of groundwater positions from hydrological monitoring is also influenced by subjective interpretation of monitoring data, and other experts could estimate different groundwater levels. In theory, tensiometers can be used as piezometers when installed within the phreatic zone, however, measured pressures could not easily be transferred to groundwater positions because of contradicting records. Therefore, uncertainties prevail in the results which could be minimised by installation of additional sensors.

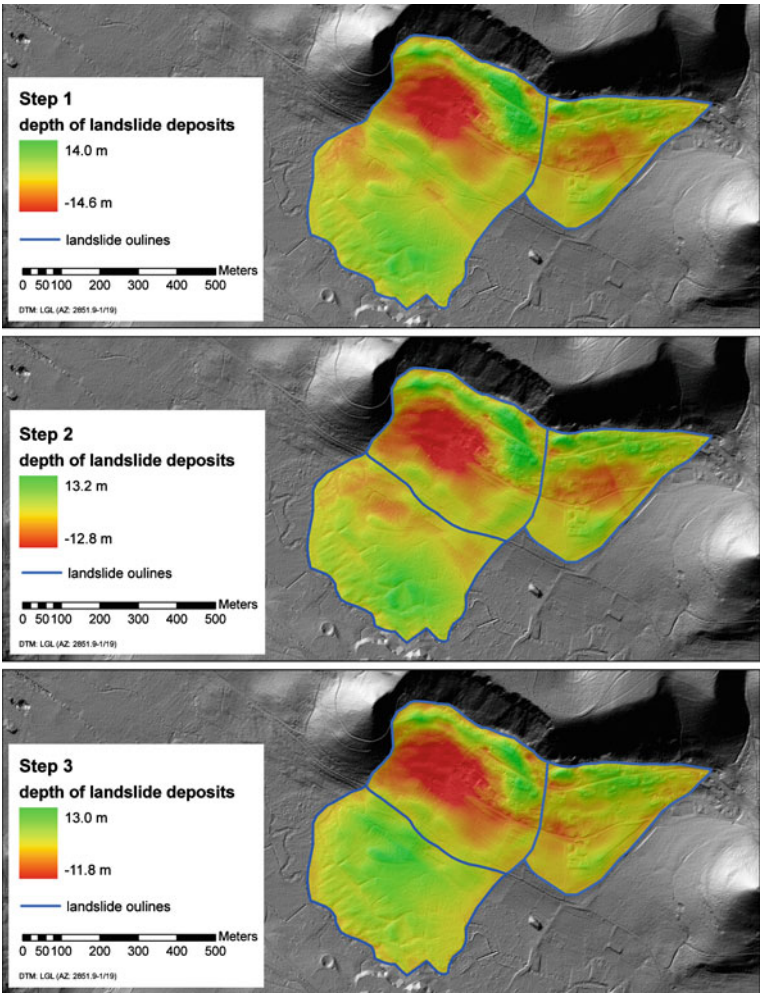

Fig. 6.35 Stepwise interpolation of depth of landslide deposits

Theoretically, the integration of geoelectrical monitoring data could also be used to improve determination of groundwater table positions. Still, investigations of the relation of geoelectrical resistivity and measured soil water content carried out within the ILEWS project (Wiebe et al. 2010) were not able to determine a simple relationship between these parameters. Still, partial correlation were established for certain sensors for relatively dry conditions (>50 ohm or <25% volumetric water content).

The influence of uncertainties due to partly subjective interpretation of hydrological data on subsequent modelling has to be estimated by sensitivity analysis with CHASM, which is described later (Sect. 5.1.3.2).

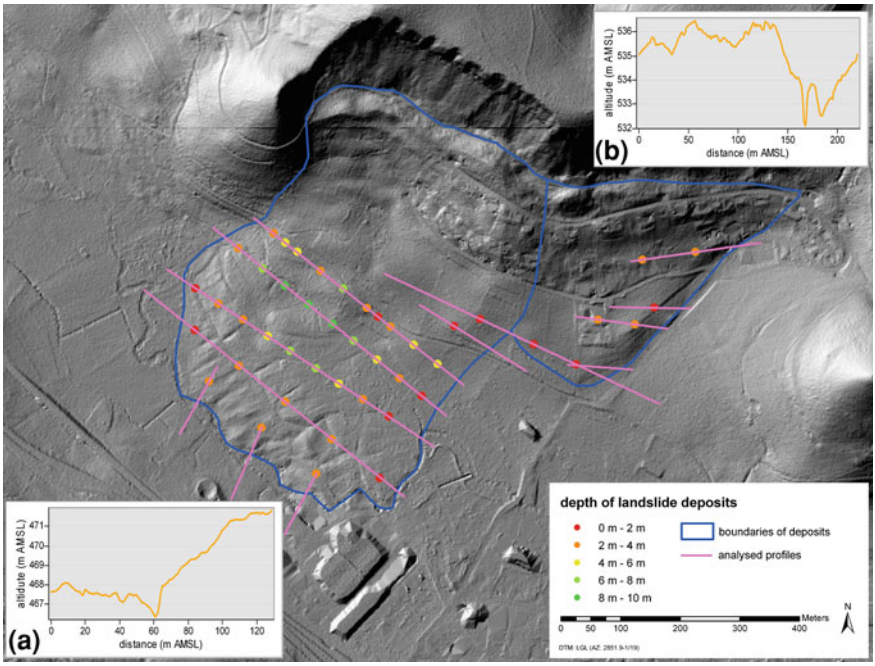

Fig. 6.36 Estimated thickness of landslide deposits by profile analysis

The most interesting results in respect to hydrological response to rainfall and snow melt derive from analysis of single events. In particular hydrological monitoring site p12, located next to the house which frequently suffers crack development due to slope movement, shows insightful characteristics. In general, hydrological sensors in lower depths respond quicker to percolating water than sensors in greater depth. However, at p12 analyses of several single rainfall and snow melt events show a contradicting pattern. Here, the deepest TDR sensor in 9.5 m shows relatively quick and large reactions to rainfall and snow melt, while the water content in medium depth only varies slightly.

The observed variations of soil water content can be interpreted as a result of preferential flow paths by lateral influx of water. This assumption is supported by geoelectrical time-lapse inversions, which illustrate an even decrease of resistivity for most of the measured profile following snow melt. For the area around monitoring site p12 however, low resistivity values in great depth develop without significant increases in shallower depth above. Assuming variations in geoelectrical measurements for this period are primarily related to infiltration and percolation of water, the observed resistivity changes relate to a lateral influx on preferential flow paths.

Without any significant accelerations of slope movement hydrological triggering conditions and thresholds can not be analysed adequately. Similar to the results of Bell (2007) and Bell and Thiebes (2010), no simple correlation between

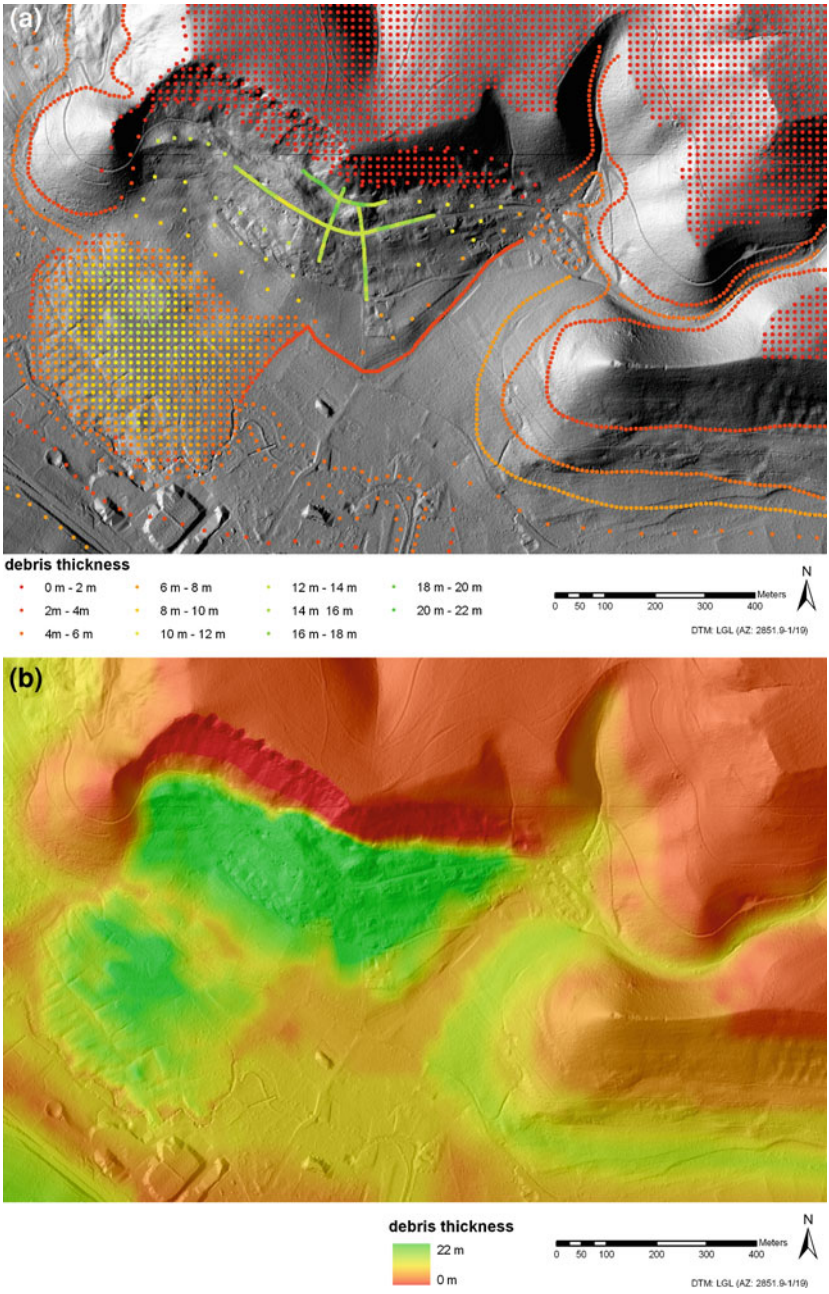

Fig. 6.37 Input data (**a**) and results (**b**) of spatial interpolation of debris cover thickness

rainfall or hydrological conditions and shallow slope displacement can be found. The onset of the deep-seated sliding, however, can be related to snow melting based on the timing of these displacements. Also, deep-seated sliding can be observed for each spring season except for 2007, when snow height in the previous months was relatively small.

Based on the results, it can be noted that tensiometers are of great value to estimate the position of the groundwater table. An advantage of the TDR sensors is the quick response time to rainfall events which make them particularly useful for low depth installations.

Unfortunately, some of the installed tensiometers and TDR sensors seem to either malfunction or may not be properly fixed to the soil. In addition, several tensiometers are likely to have run dry due to low frequency of maintenance works.

Uncertainties of the weather data also have to be noted. Precipitation data from the local weather station is questionable for at least summer 2010. In addition, also in earlier periods, heated and unheated rainfall sensors differ in their records. Therefore, rainfall data has to be interpreted with great care. Snow height data required some correction processes to convert raw measurements into realistic snow depths. Corrected snow height data can be assumed to describe general trends of snow accumulation and melting realistically; however, some uncertainties remain regarding the exact snow height.

6.1.3 Landslide Early Warning Modelling

6.1.3.1 Generation of Input Data

In the following, results of generation of input data for following CHASM modelling and early warning will be presented. These include the development of the general subsurface model, modelling of groundwater scenarios, extraction of rainfall scenarios, and design of an automated shear surface routine.

Subsurface Model

A general subsurface model was generated by a combination of various data sources (Chap. 4) following a complex procedure (Chap. 0) to facilitate subsequent modelling and early warning. Below, the results are presented.

Initially, positions of geological strata as upper limits were extracted from available geological maps (1:25,000 and 1:50,000) including information from described drillings. Both maps contain similar information on positions and thickness for geological strata. However, classification of the uppermost stratum differs between maps. In the 1:25,000 map, this is termed Kimmeridge Massenkalk, while the 1:50,000 map further differentiates into the formations Kimmeridge Massenkalk and Lower Kimmeridge Massenkalk. Table 6.2 shows

Table 6.2 Upper limits of geological strata (based on Ohmert et al. 1988)

Series	Stage	Stratum	Code	Limit (m)
Upper Jurassic	Kimmeridgium	Upper Kimmeridge limestone (Bank- and Felsenkalk)	ki2–3	790
		Lower Kimmeridge marl (Lacunosamergel)	k1	710
	Oxfordian	Oxfordian limestone (Oxfordkalk)	o × 2	670
		Oxfordian marl (Impressamergel)	o × 1	610
Middle Jurassic	Callovian	Callovian clay (Ornatenton)	cl	505
	Bathonian	Bathonian clay (Dentalienton)	bt	475
	Bajocian	Bajocian clay (Hamitenton)	bj3	465
		Bajocian clay and marl (Stephanoceraten- and Ostreenkalk)	bj2+	440
		Bajocian clay (Sonninien-Schichten)	bj1	420

the utilised strata classification of from the larger scale map. Single DTM were created in GIS for each stratum with upper limit altitude as grid cell information. At a later stage, these DTM blocks were merged with debris thickness information to create a general subsurface model (see Fig. 6.38).

Drillings described by Ohmert et al. (1988) were the first source of information for estimation of debris thickness above bedrock.

Figure 6.30 displays drillings selected due to their vicinity to the local study area. Depths of debris material, primarily termed soil, alluvial loam and slope debris by the authors of core descriptions, were extracted, and are summarized in Table 6.3. Holocene calcareous sinter and gravels from periglacial periods found in some drillings, were neglected and therefore add to the geological material which they overly.

Drillings 34–38 are located close to the river and describe a debris cover varying between 3 and almost 6.5 m, under which periglacial gravels and calcareous sinter can be found. Almost 10 m loose material is attested at point 42. Several drillings are in lower slope positions, i.e. 39–50. For these, a debris cover between 4.8 and 13.8 m was measured, with the exception of drilling 41, where over 22 m of fluvial deposits and tufa sand overlie Callovian clay. Drilling 50 is located on landslide deposits and attested a thickness of 24 m of slope debris above clay marl (cl). The drilling located the furthest upslope is positioned at point 48. Here, 8 m of slope debris are overlying Oxfordian marl (ox1).

From drillings 34, 35, 36, 37 and 38, a mean debris cover of 5 m was assumed for areas located close to the river. Estimation of debris thickness for lower and middle slope sections primarily referred to drillings 43 and 44, and 48 for orientation. Debris cover was assumed to vary between 5 and 7 m at similar slope positions. On the plateau area, points were evenly distributed and a depth of bedrock of 1 m was assumed. Variable debris thickness depending on local topography was not included for the plateau area. No debris cover was supposed for the outcropping limestone at the main landslide crown, and the upper scree

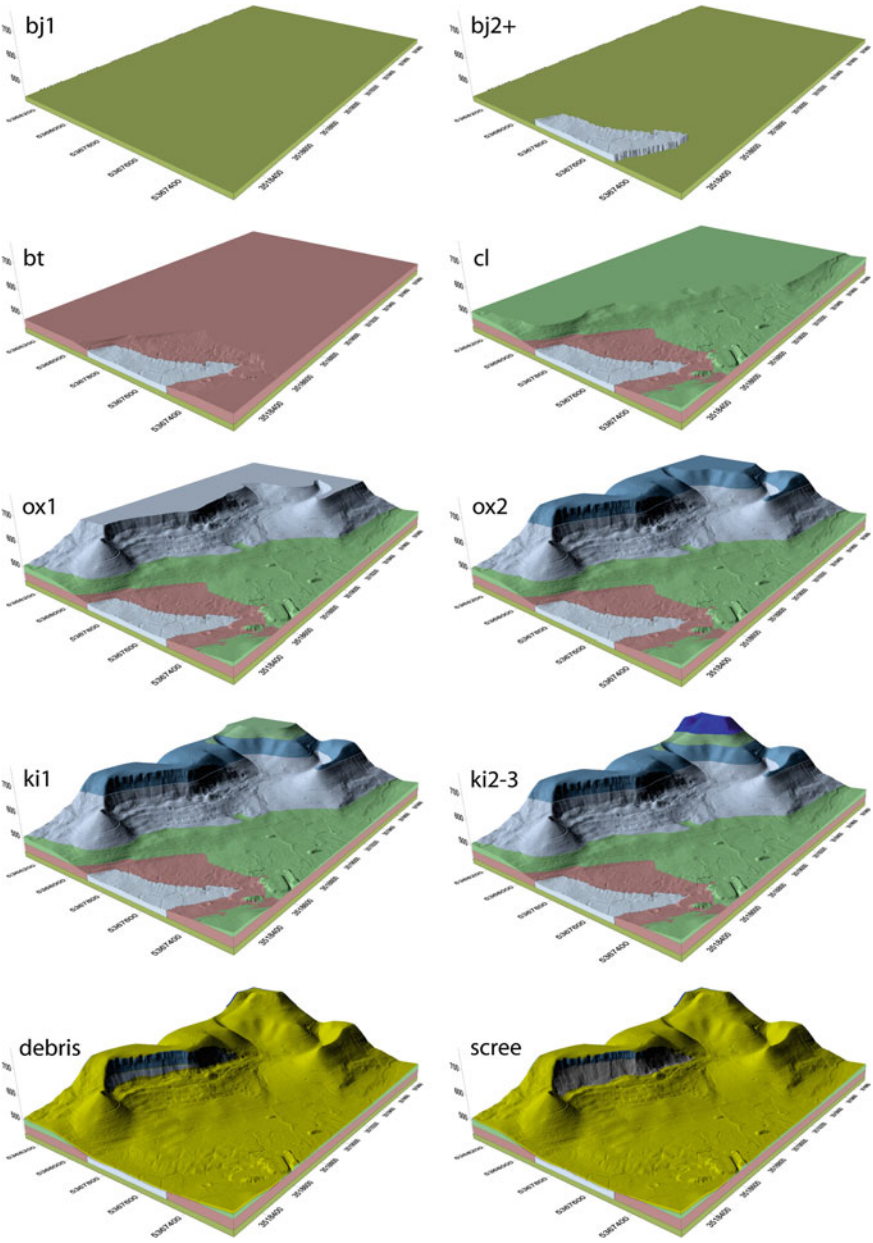

Fig. 6.38 Subsurface model (DTM: LGL AZ: 2851.9-1/19)

slope. However, since evolution of the scree took place after occurrence of the main landslide, debris was assumed to be located underneath for lower sections. A bedrock depth of 1 m was assumed for this area.

Table 6.3 Analysed thickness of debris above bedrock (after Ohmert et al. 1988)

Drilling	Position	Debris thickness (m)	Description
34	River	3.8	Soil, loam
35	River	4.3	Soil, alluvial loam
36	River	6.4	Soil, peat
37	River	3.0	Soil, tufa sand
38	River	6.5	Soil, tufa sand
42	River	9.9	Soil, tufa sand, peat
39	Lower slope	12.0	Soil, tufa sand, slope debris
40	Lower slope	13.8	Soil, tufa sand, slope debris
41	River	21.7	Fill, tufa sand
43	Lower slope	4.8	Slope debris, loam
44	Lower slope	7.2	Fill, slope debris, alluvial loam
47	Lower slope	17.8	Fill, tufa sand, peat
50	Lower slope	24.0	Landslide deposits
48	Middle slope	8.0	Slope debris

According to these findings, the estimated debris thickness for the local study area was stored within GIS as point data and used for subsequent spatial interpolation (Fig. 6.31). In addition to the previously described points, some others were added, e.g. in the western part of the study area, and also for high slope positions, to ensure a smoother interpolation and transition of debris thickness.

In the core area of the local study area, the estimation of debris thickness was based on data from seismic prospection elaborated with Rayfract by the company geoFact (Bell et al. 2010). Processing of seismic data was carried out by the project partner geoFact, following interpretation and deduction of debris thickness is a result of the author of this thesis. Seismic data and estimated depth of bedrock is presented in Fig. 6.32. Since one drilling, i.e. Lic02, penetrated the bedrock, it was used for calibration of seismic results. In addition, the seismic profiles were compared and optimised to each other at four intersections.

The western longitudinal profile intersects with lower and upper cross profiles at 79 and 130 m, respectively. Inclinometers Lic02 and Lic05 are located at 42 and 68 m, respectively. At Lic02, bedrock corresponds to a wave velocity of approximately 2000 m/s, displayed as the transition orange to red, which was subsequently used for interpretation. The plot illustrated in Fig. 6.32 was combined from two single analysed profiles superimposed for interpretation. A refractor computed with plus–minus method was calculated around 900 m/s, relating to a depth between 6 and 8 m. Bell et al. (2010) interpreted the refractor as a weak zone. In general, the 2000 m/s line was interpreted as the bedrock interface, relating to depths between 13 and 16 m for most parts of the profile. Considerable greater depths of over 20 m were estimated for a spoon shaped hollow between profile metre 90 and 130.

The eastern longitudinal seismic prospection survey has a total length of almost 190 m and was acquired in one measurement. At the maximum upslope location, the profile intersects with the northern cross profile. Another intersection is

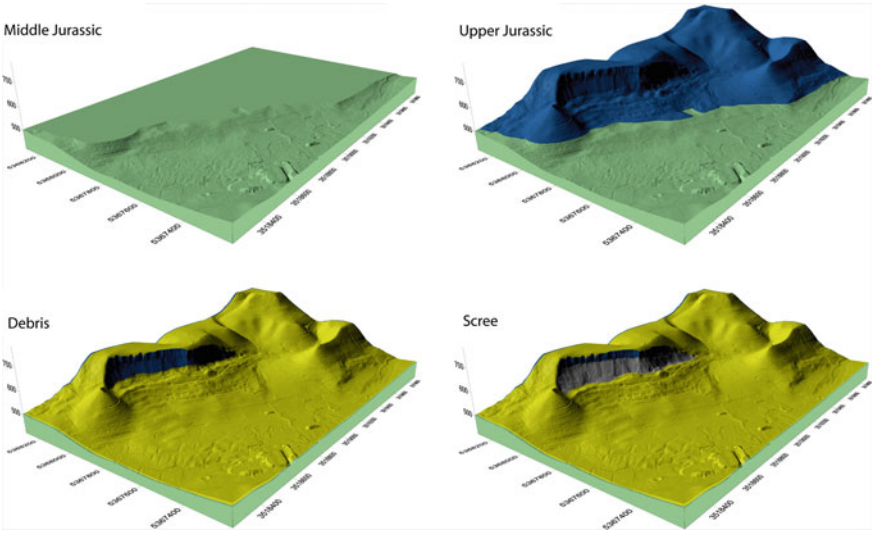

Fig. 6.39 Subsurface model for CHASM (DTM: LGL AZ: 2851.9-1/19)

positioned at profile metre 140. The calculated refractor varies between 8 and 14 m depth, and shows a great variation in terms of wave velocity. For mid and low profile section, depth ranges between 8 and 16 m, respectively. For the upper profile maximum depths of over 20 m were estimated, similar to the northern cross profile.

The northern cross profile has a length of 90 m and intersects with the western and eastern longitudinal profiles at metre 47 and 66, respectively. The calculated refractor is in a depth of approximately 12 m depth, corresponding to a seismic velocity between 1,200 and 1,400 m/s. Estimation of bedrock depth followed the 2,000 m/s line, corresponding to depths of 10 and 15 m for eastern and mid profile sections, respectively. In the western part greater depths over 20 m were estimated in agreement with data from the eastern longitudinal profile.

The southern cross profile was the longest, with a total length of 220 m and was produced by a combination of three single measurements. Intersections with the western and eastern longitudinal profiles are located at metres 113 and 148 m, respectively. The refractor is in the range of 1,000–1,200 m/s, corresponding to a depth of approximately 8 m. For most areas, the 2,000 m/s line was used for estimation of bedrock depth. Still, at around profile metre 90, one larger hollow was interpreted as artefact of data inversion. Depth of bedrock ranges between approximately 16 m in the east, to slightly shallower values around 12 in mid and western profile.

After estimation of bedrock depths in seismic plots, data was transferred to GIS for subsequent spatial interpolation. Depth information was extracted every 4 m, analogue to the distance between the geophones during prospection, and stored within GIS as point data (Fig. 6.33). Greatest debris thickness up to over 20 m was

estimated for the northern profile, especially on the western end, but also in the upper part of the western longitudinal profile. Shallower positioning of bedrock was ascertained for lower slope sections in general, and in particular for the western part.

After analysis of debris depth in the upper landslide area, the depth of material of the scree slope was estimated. In GIS, outlines of scree slope were digitised and converted to point data with scree depth information of zero. From interpretation of geoelectrical monitoring data acquired by Bell (2007) and Kruse (2006), a maximum thickness of 8 m was assumed. Additional data points with the respective depth value were created in GIS, positioned at approximately 60% of horizontal scree length. Further points at the sides were added to ensure smooth spatial interpolation of scree depths. Several interpolation methods (i.e. Kriging, Inverse Distance Weighting, and Nearest Neighbour) were tested, of which the Natural Neighbour method was judged to generate the most realistic results (see Fig. 6.34).

Initial attempts of spatial interpolation of debris cover using the previously described data demonstrated the need to improve representation of lower landslide deposits. Since neither drillings nor geophysical data were available, an iterative GIS based interpolation was carried out (see Fig. 6.35).

In the first interpolation step landslide boundary height information were connected by an ArcGIS TIN creation resulting in a maximum depth of landslide deposits around 13 m for parts of the upper landslide deposits. However, also negative thicknesses up to approximately 14 m were interpolated, e.g. for the landslide head of the western large landslide body. The eastern landslide body illustrates deposit depths between approximately 5 m in the upper part, but also negative depths up to 5 m for some sections. For the lower landslide deposits, depth of material reaches a maximum of around 8 m in the east, but also indicates negative landslide thickness values for the western areas. Overall, results of first interpolation were evaluated to underestimate the overall thickness of landslide for some parts of the landslide, especially in areas with negative values.

For the second interpolation, the western landslide body was separated into a upper and lower part where the lower road is located. TIN interpolation was carried out for these areas and the eastern landslide body separately. For this interpolation, landslide depth was estimated to vary between 13 and −13 m. In comparison to the first interpolation, no changes in landslide depth can be recognised for the smaller eastern landslide body. Some additional material in the order of 2 m was simulated for the western upper landslide body, and up to 3 m for the lower western deposits.

However, lower landslide depths were simulated, too, e.g. for the middle part of the western landslide deposits. Differences add up to over 5 m in some of these areas. Similar to the first interpolation, results of second interpolation were judged to underestimate real landslide deposits with only some centimetres of landslide deposits in the mid section of the lower western landslide. In addition, negative values of landslide thickness were interpolated for some parts of the landslide, indicating an effective hollow instead of additional material.

To further improve spatial interpolation of landslide deposits further details were included. At first, it was aimed to improve interpolation for the eastern and upper

Table 6.4 Elaborated geotechnical parameters (based on Meyenfeld 2010)

		Number of records		Minimum value	Maximum value	Mean value	Standard deviation
Upper Jurassic	Lime	25	c'_{min}	0	10,000	1,436	2,833
	(Kalk)		c'_{max}	0	30,000	3,750	8,269
		30	φ'_{max}	10	0	25	10
			φ'_{max}	10	70	3	5
	Limestone	6	c'_{min}	1,400	4,000	2,467	1,218
	(Kalkstein)		c'_{max}	4,000	8,000	5,333	2,066
		11	φ'_{max}	10	40	29	11
			φ'_{max}	35	70	45	12
	Marl	34	c'_{min}	0	4,000	490	1,044
	(Mergel)		c'_{max}	0	8,000	1,035	2,178
		34	φ'_{max}	10	0	25	8
			φ'_{max}	70	1,111	3	13
	Marlstone	11	c'_{min}	5	1,400	313	542
	(Mergelstein)		c'_{max}	40,000	4,000	823	1,575
		11	φ'_{max}	1	30	24	8
			φ'_{max}	24	45	34	9
Middle Jurrassic	Clay	246	c'_{min}	0	17,000	150	1,106
	(Ton)		c'_{max}	0	23,000	254	1,550
		250	φ'_{max}	0	45	2	9
			φ'_{max}	5	6,533	26	10
	Claystone	69	c'_{min}	0	17,000	365	2,042
	(Tonstein)		c'_{max}	0	23,000	554	2,760
		72	φ'_{max}	8	45	25	8
			φ'_{max}	13	50	31	8
Limestone scree	Debris	4	c'_{min}	0	1	0.3	0.5
	(Schutt)		c'_{max}	0	1	0.3	0.5
		4	φ'_{max}	32.5	33	33	0.3
			φ'_{max}	32.5	3	3	0.3
	Gravel	69	c'_{min}	0	0	0	0
	(Geröll)		c'_{max}	0	0	0	0
		72	φ'_{max}	32.5	40	36	2.3
			φ'_{max}	32.5	45	36	3.1

Note Effective cohesion (c'') in kN/m^2, effective angle of internal friction (φ) in °

western landslide deposits. Altitude information of the points along the boundary of the landslide bodies were lowered by maximum value of 6 m, assumed to be an appropriate depth of landslide deposits for this area. Landslide depth was set to increase linearly and reach its maximum thickness after 2/3 of landslide length.

A second adjustment to the input data used for TIN generation used several profiles placed along the landslide deposit boundaries to estimate thickness by the change of altitude. In Fig. 6.36, results of this procedure are illustrated along with two sample slope profiles. The lower sample profile (A) illustrates a cross-section over the river, which is located at metre 60. While the southern bank is relatively flat, a much quicker increase of altitude can be observed for the landslide deposits on the northern bank. Thickness for the pictured profile was estimated to be at least 4 m for e.g. profile metre 110–120. Similarly, the other sample slope profile (B) shows sharp increase of height of approximately 2 m at the boundary of landslide deposits. In general, estimated depths were found to increase from the boundaries to the mid part of the landslide deposits and reach a maximum of 8–10 m. However, no profiles could be analysed for the upper landslide boundaries since deposits are not visually evaluable.

Results of third interpolation including points of the manipulated landslide boundary between western and eastern landslide bodies, and data points from profile analysis are presented in Fig. 6.35 as step 3. In comparison to the second interpolation, thicker landslide deposits were simulated for most of the landslide areas. Especially for the lower western landslide, the depth of material exceeds 9 m in the mid part. Also for the smaller eastern landslide body, up to 7 m of additional material were calculated. Fewer deposits were interpolated for some parts of the upper western landslide, and for the eastern section of lower western landslide deposits. In this area, material depth was estimated to be around 3 m lower than previously calculated in the second interpolation. Negative values of landslide thickness primarily occur in the upper part of the western landslide. Lower landslide deposits are generally positive, besides some points at the western edge. Still, the upper parts of the western landslide, but also the eastern landslide body were evaluated to be unrealistic; with negative thickness values up to 12 m. For these areas, results were rejected, and subsequent interpolation of debris thickness for the entire local study area was based on data estimated from seismic data and some additional points. Results of the third simulation for the lower landslide deposits of the large western landslide were judged to be an appropriate representation of real landslide deposit depths and were accepted for further analysis. However, to diminish the influence of negative landslide thickness, all values lower than zero were increased to zero.

Interpolation of debris thickness for the entire local study area used all data previously generated. For the upper western and the eastern landslide body thickness was interpolated from results of seismic data analysis. Some additional points were added to ensure a smooth interpolation without large deviations occurring in small distances (see Fig. 6.37a). For lower landslide deposits, regularly spaced points were created in GIS and depth of landslide deposits were extracted from third interpolation. However, since interpolation for this area

Table 6.5 Initial geotechnical values used for CHASM modelling

	Upper jurassic	Middle jurassic	Debris	Scree
Cohesion	300	1,500	20	0
Internal friction	35	15	20	33
K_{sat}	1e−6	1e−9	6,78e−7	1e−1
Moisture Content ($_{sat}$)	40.7	44.7	52.6	48.3
Bulk density($_{sat}$)	25	23	16	16
Bulk density ($_{unsat}$)	23	21	15	15

describes landslide deposits, and not total debris depth, a mean thickness of 4 m for undisturbed material located below was assumed and added to the point data. Similarly, points were added with a depth value of 4 m along the landslide boundaries, assumed to be the mean thickness of debris material for these slope positions if unaffected by landslide processes. For the rest of the study area, point data from previously described analysis of drillings available in the geological map (1:25,000) was used. Some additional points were added to ensure smooth transitions in subsequent interpolation of debris thickness with ArcGIS methods. Several interpolation methods were tested (i.e. Inverse Distance Weighting, Ordinary and Universal Kriging, Spline) of which Tension Spline method was evaluated to produce the most realistic results (see Fig. 6.37b). From the plateau areas into a downslope direction debris thickness smoothly increases from 1 up to 7 m at the foot slope. No debris was interpolated for the outcropping limestone at the landslide crown and the upper part of the scree slope. Calculated debris thickness for the landslide bodies has a maximum of 22 m in the central landslide head area, and decreases to approximately 12 m in the western part. Into downslope direction, debris thickness decreases in the mid part of the landslide to 5–6 m, before increasing in the lower part again. Here, interpolated thickness of debris reaches a maximum of 10–14 m, and levels out to the margins.

With debris depth stored as grid data, the complete subsurface model was created by a series of RASTERCALCULATOR commands in ArcGIS. The scree slope and debris grids were subtracted from the original DTM to derive the surface of geological strata. Results are presented in Fig. 6.38. For the use within CHASM, the subsurface model was simplified since CHASM can only integrate four material layers. The simplified subsurface model contains Middle and Upper Jurassic, debris and scree slope (Fig. 6.39).

Geotechnical Parameters

The estimation of geotechnical parameters of materials present in the local study area utilised the database provided by Meyenfeld (2010, personal communication). Since subsequent modelling of slope stability within CHASM could only accommodate four material layers, geotechnical parameters were elaborated for Upper Jurassic stratum (primarily limestone and marls), Middle Jurassic stratum (primarily clay stones), slope debris covering almost the entire study area, and the

Table 6.6 Water content (in %) derived from SPAW model for suctions (pF) from −10 to −0.1

pF	−10	−8	−6	−4	−3	−2	−1.6	−1.2	−0.8	−0.4	−0.2	−0.1
Scree	0.2	0.3	0.4	0.4	6.9	0.9	1.2	1.53	2.2	4	21.8	35.5
Debris	0	0	0	0	0	0	0	0	0	0	0	0
Upper Jurassic	25.9	26.6	27.6	29.1	30.2	31.8	32.7	34	35.8	39.2	45.7	50
Middle Jurassic	0	0	0	0	0	0	0	0	0	0	0	0

limestone debris located in the scree slope. From the wide range of materials listed within the database, searches for the following terms were carried out: *Kalk* (lime), *Kalkstein* (limestone), *Ton* (clay), *Tonstein* (claystone), *Schutt* (scree material, rubble), and *Geröll* (gravel, debris). A summary of elaborated geotechnical parameters is presented in Table 6.4.

Search for the terms *Kalk* and *Kalkstein*, *Mergel* and *Mergelstein* delivered 30 and 34 records with information on cohesion or friction, respectively. However, some records were excluded from the selection because they were judged inappropriate. Excluded records include records describing for example, materials located in very deep underground conditions (1,000–2,000 m) and weathered debris. The parameter range for both, cohesion and friction is very large. For example, records for *Kalk* contain minimum cohesion values of 0 kN/m^2, and a maximum of 30,000 kN/m^2. The highest number of records was available for *Ton* for and *Tonstein* with 250 and 72 records on cohesion or friction, respectively. Again, the range of geotechnical parameters is very large with cohesion varying between 0 and 23,000 kN/m^2. Only a small number of records were found for *Schutt* and *Geröll*. In controversy to the previously described search terms, parameters are less dispersed. Cohesion is very low for all records, ranging between 0 and 1 kN/m^2, and friction between 33° and 45°. Values of cohesion and internal friction for slope debris could not be elaborated from the database but instead used typical values from literature, which were later checked during sensitivity analysis.

Estimated values for cohesion and friction used for initial CHASM modelling are presented in Table 6.5. For estimation of geotechnical characteristics of the Upper Jurassic layer, *Kalkstein* and *Mergelstein* records were preferred since they focus on intact rock materials. Similar for Middle Jurassic, *Tonstein* was favoured since the Middle Jurassic in the study area is covered by slope debris.

CHASM also required determination of soil suction values and saturated moisture content for materials involved in CHASM modelling. Values for these parameters were elaborated based on the soil database integrated into the SPAW model (Saxton and Rawls 2006). Even though, laboratory analysis provided some initial information on soil suctions and related water contents (Sect. 6.1.2.1), tests only involved a relatively small range of suctions compared to CHASM requirements. Also, laboratory suction analyses concerned only materials from slope debris, but not for the other materials of the subsurface model. For landslide debris, mean values for clay, silt and sand content were calculated from results of

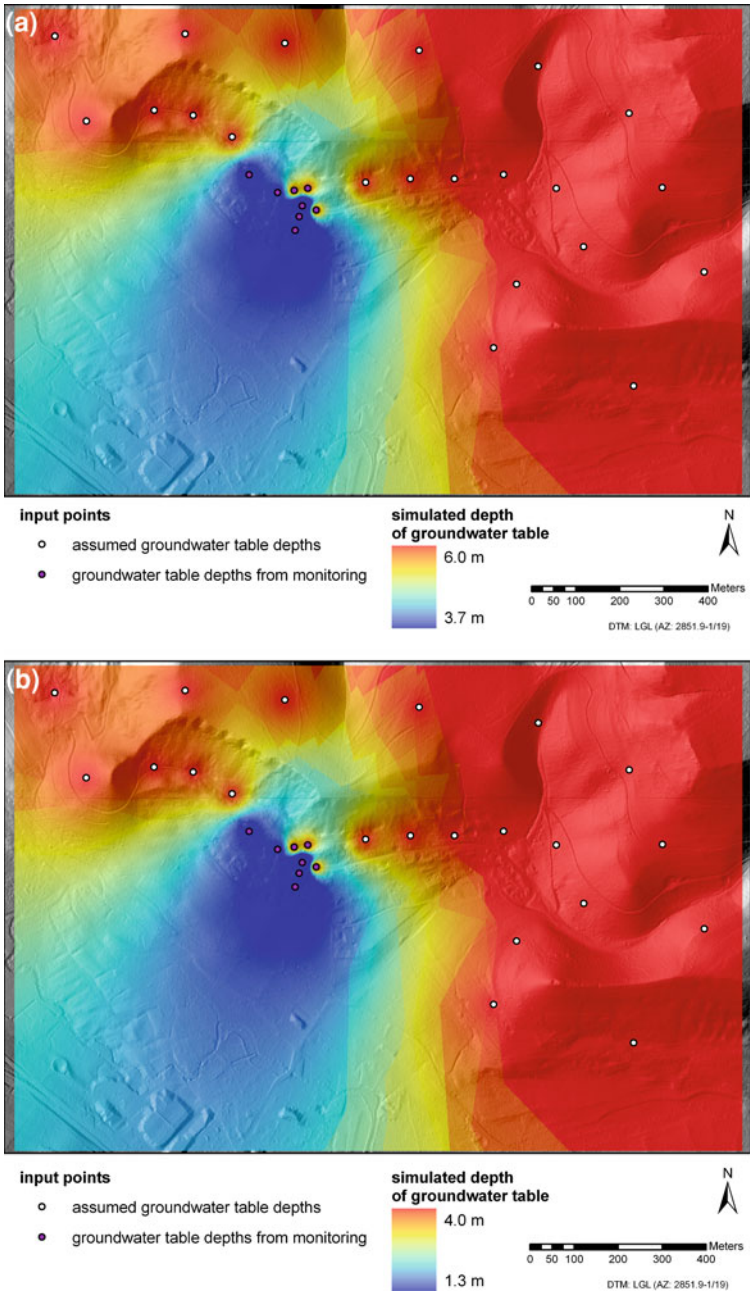

Fig. 6.40 Spatially interpolated groundwater scenarios for dry (**a**) and wet (**b**) conditions

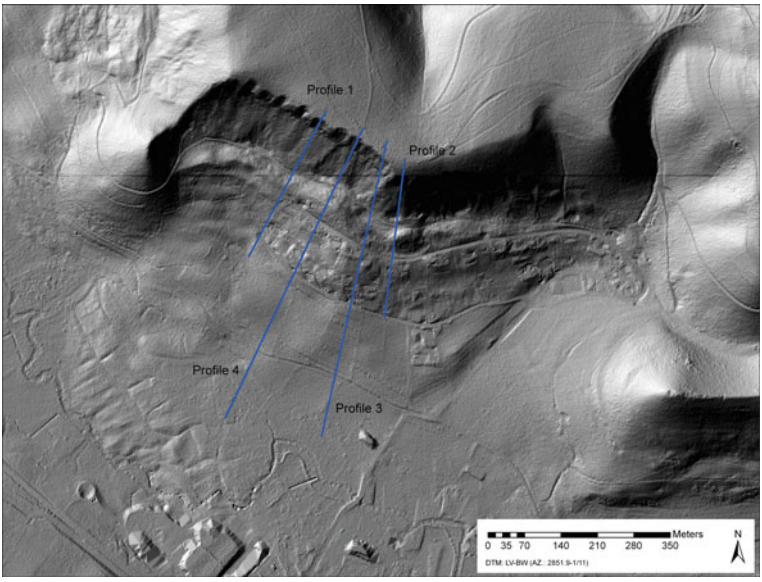

Fig. 6.41 Random slope profiles between 300 and 600 m long

laboratory analysis and used as input for SPAW. In addition, a relatively high gravel content of 40% was assumed, based on experience during drilling and analysis of available borelogs. In comparison to the soil suction data acquired in laboratory analyses, SPAW values describe significantly higher water contents for the entire range of applied suctions. Soil suction behaviour of the limestone scree material was elaborated using assumed values for grain size distribution. High permeability was reflected by 96% sand content and 50% of gravel, as well as a decreased compaction factor of 0.9. In comparison to limestone scree material, Upper Jurassic material was assumed to be denser and less permeable. Soil suction curves were determined using assumed contents of 20% sand, 40% clay, no gravel and dense compaction (1.1). Middle Jurassic materials were assumed to be even less permeable, and soil suction curves were elaborated using 60% clay, 2% sand, no gravel and maximum compaction (1.26). Resulting soil suction points for the described materials are presented in Table 6.6.

Parameter values for hydraulic conductivity (K_{sat}) for the materials involved in CHASM modelling used standard values provided in DIN standard (18130) and literature values (Bear 1972). For limestone scree material, a very high hydraulic conductivity of 10^{-1} m/s was estimated, relating to pervious conditions similar to gravel. The SPAW model was used to establish K_{sat} values for debris material. Hydraulic conductivity of Upper Medium Jurassic materials were determined referring to pervious and semi-pervious materials, respectively. Estimated values for hydraulic conductivity initially used for CHASM simulations are presented along with the other geotechnical parameters in Table 6.5.

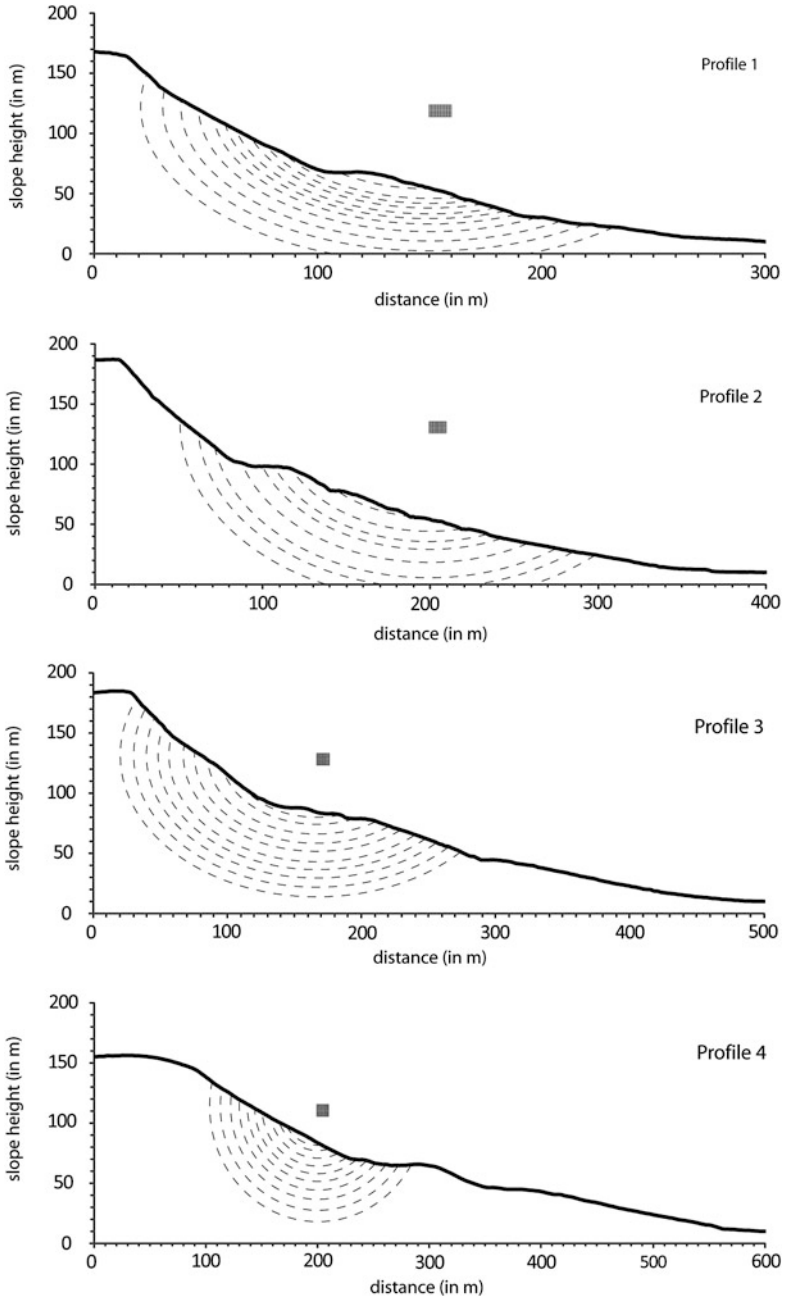

Fig. 6.42 Position of slip search grid and respective possible shear surfaces

Groundwater Scenarios

In Fig. 6.40, results of spatial interpolation of groundwater positions by Inverse Distance Weighting method are illustrated. In addition to the data points describing the positions of hydrological monitoring sensors, several points were included to ensure a smooth and more realistic interpolation of groundwater positions. For these, groundwater table positions had to be assumed since no information was available. Mean groundwater table positions for dry and wet seasons were assumed as 4 and 6 m, respectively.

Results for the dry period (Fig. 6.40a), which relate to the time between approximately October and December, show a spatially varying groundwater table, which is the closest to the surface within the main landslide body. Height of groundwater table was simulated to gradually decrease in a downslope direction to values of approximately 5 m for low slope sections and for areas located close to the river. For steep slope sections, i.e. landslide scree and the western and eastern slopes, drier conditions were simulated, with a groundwater table modelled as 5.8 m below the surface. Lowest groundwater tables were interpolated for the plateau area where a mean position of the water table is about 6 m below the surface. In the area, where hydrological monitoring was carried out, strong variations of groundwater table positions were simulated, relating to the variability of estimated groundwater for each sensor analysed.

Figure 6.40b presents interpolated groundwater table positions for the wet period, which relates to the period between February and April. Compared to the first interpolation (Fig. 6.40a) of groundwater table positions, similar results were computed for the wet season. In general, however, groundwater tables tend to be located closer to the surface with a minimum depth of 1.3–2 m. For the main landslide body, the simulated groundwater table stretches further upslope and reaches minimum values of approximately 3 m for some parts of the plateau area. As in the first interpolation (Fig. 6.40a), groundwater depth decreases in the downslope direction.

Shear Surface Search Routine

A procedure was developed to control the automated CHASM search for circular shear surfaces (Bishop's method) integrated into the web-based decision-support system. A routine provided by Anderson (2009, personal communication) was initially tested, but was judged not well adapted to local slope morphologies since it bound stability calculation to lower slope sections were landslide occurrence is more unlikely. Extensive testing led to a procedure, in which shear surface search varies for each selected profile, depending on profile characteristics and input data (see Appendix V). In the following, the developed routine will be illustrated for four random profiles, which start on the plateau and have a length between 300 and 600 m (Fig. 6.41).

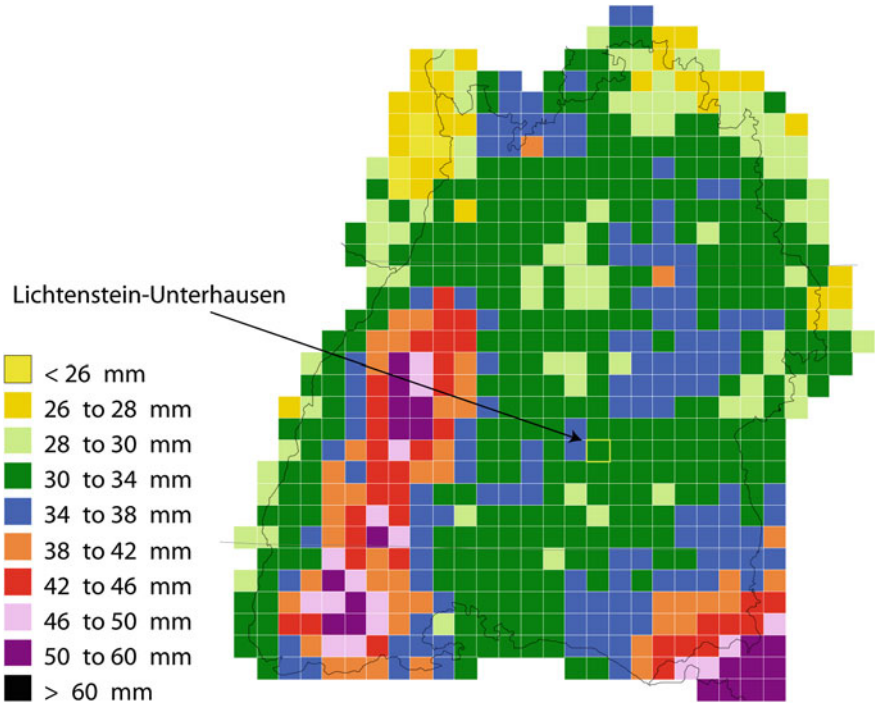

Fig. 6.43 KOSTRA rainfall intensities for 12 h rainstorm with 1/10 year occurrence probability for Baden-Württemberg

Profiles were drawn for areas in which slope failures could occur, i.e. the steep upper slope section either reflecting partial reactivation of landslide deposits, or retrogressive landsliding at the head scarp. Since profiles vary in length, in this case 300–600 m, areas for appropriate shear surface search vary.

Parallel to Andersons procedure, the position of the grid, in which the centres of analysed slip circles are located, were defined by geometrical characteristics of the analysed slope profile (slope length and height). For slope profiles shorter than 450 m, the lower upslope corner of the search grid was defined at two-thirds of slope height and half of slope length. Longer profiles used two-thirds of slope height and one-third of slope length, effectively, moving the grid box further upslope. In Fig. 6.42 the four profiles and the position of grid search box are illustrated along with resulting potential shear surfaces.

For the first two profiles, grid box is positioned at 50% of slope length, for profile 3 and 4, at one-third of profile length. For all profiles, potential shear surfaces reflect slope failures within the head of former landslide deposits or within the steeper upslope area. Retrogressive failure at the plateau can only be analysed when very large radiuses are used.

Apart from position of the grid search box, other settings included its spacing and size, and the incremental increase of the search radius between iterations.

Table 6.7 Cumulative rainfall (in mm) for normal, maximum value and worst case scenarios for return periods between 1 and 100 years and storm duration between 1 and 72 h

Duration in hours	Normal values				Maximum values				Worst case			
	Return period in years											
	1	10	50	100	1	10	50	100	1	10	50	100
1	18	37	50	56	18	38	52	58	20	44	60	70
6	27	48	63	69	29	51	66	73	31	58	76	87
12	32	54	69	75	34	57	73	80	37	66	84	96
24	38	64	82	90	40	70	91	100	44	81	105	120
48	45	73	92	100	50	80	101	110	55	92	116	132
72	55	83	102	110	60	90	111	120	66	104	128	144

The spacing of the grid search box was set to the same dimension as the general mesh, relating to the resolution of the DTM used for profile generation. Since the number of maximum cells in CHASM simulations is limited to 300, maximum profile length is 300 and 600 m for 1 and 2 m DTM, respectively. The size of the grid search box was chosen to be relatively large with 10 by 10 m to increase the number of possible shear surface locations. However, incremental increase of the radius between simulation steps was set to a relatively high value of 1 m to limit the total number of iterations and shorten simulation time.

Rainfall Scenarios

KOSTRA rainfall intensity probabilities were extracted for the grid cell containing the local study area Lichtenstein-Unterhausen and subsequently used to derive CHASM input files. To enhance the understanding of KOSTRA, spatial and temporal variability of rainfall intensities were investigated. KOSTRA data in map format (Fig. 6.43) shows, that the cell directly neighbouring the local study area to the west contains higher rainfall intensities for many scenarios. Higher cumulative rainfall for this area can be observed for all annual probabilities and storm durations. Largest deviations can be identified for rainstorm events of long durations, where cumulative rainfall is over 20% higher.

Comparison of summer (May–September) and winter (October–April) rainfall intensities to the values of the entire year illustrate some interesting features. Summer rainfall intensities are higher than winter rainfalls for almost all rainfall durations and occurrence probabilities, with largest deviations occurring for short storm durations. For these events summer rainfall intensities are up to 400% higher. Only for rainfall events with 72 h duration and bi-annual probability slightly smaller (7%) rainfall intensity is described by KOSTRA. KOSTRA rainfall intensities derived for the entire year are the same as for the summer period for almost all rainfall durations and occurrence probabilities, except for very long durations with high probability of occurrence (>1 per year). Winter rainfall intensities are in all cases lower than values for the entire year, with largest deviations detectable for short duration scenarios (>80%).

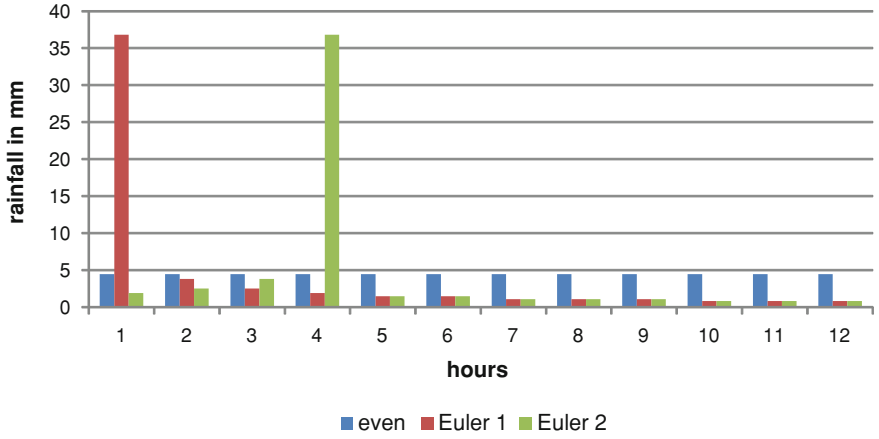

Fig. 6.44 Comparison of even, Euler1 and Euler2 rainfall distributions for a 12 h rainstorm with 1/10 year probability

KOSTRA was used to derive rainfall intensity probabilities for storm durations of 1, 6, 12, 24, 48 and 72 h, and for return periods of 1, 10, 50 and 100 years (Table 6.7). Moreover, standard parameter values within CHASM were altered to derive maximum value scenarios, and uncertainties were integrated as additional rainfall within worst case scenarios. Maximum value scenarios differ from normal value scenarios between approximately 1 and over 11%, with largest deviations occurring for long duration rainstorm events. Worst case scenarios include the fixed uncertainties described within KOSTRA which range between 10 and 20% depending on probability of occurrence. In comparison to normal values maximum values and uncertainties add up to an increased cumulative rainfall of over 30% for long duration and low annual probability scenarios.

Scenarios with varying intensities over the course of a rainfall event were created to describe storm characteristics more realistically. KOSTRA includes Euler1 and Euler2 model rainstorms only for rainfall duration $\leq$12 h; for longer storms, rainfall intensity distributions were computed manually. Fig. 6.44 exemplifies the differences between scenarios of even intensity distributions to Euler1 and Euler2 scenarios. Euler1 scenarios start with a very high rainfall peak which is followed by an even decrease of hourly intensities. In contrast, Euler2 scenarios reach highest hourly intensities after one third of the storm duration.

A total number of 192 rainfall scenarios were created for subsequent use in CHASM and the web-based applications of slope stability assessment. All scenarios were transferred to text-files conform to CHASM requirements. In these files, onset of rainstorm in relation to CHASM simulation length had to be defined. After thorough testing of CHASM (Sect. 6.1.3.2), onset of rainfall was set to hour 10.

Discussion

The subsurface model created for subsequent CHASM modelling exploited a wide range of available data to create a good approximation of real conditions. Yet, at some points of the procedure, subjective interpretations were employed leading to uncertainties.

Data from geological maps provided initial information on strata positions; however, interpolation of few outcrops to the entire study area neglected the slight dipping of approximately 2.5°.

Based on the drillings carried out within this study, it was decided to not further distinguish the slope debris layer. Still, sections of blocky limestones were found in the drill cores which roughly coincided with the refractor computed for seismic profiles. However, no reasonable geomorphological explanation could be found to justify that these limestone block sections occur within the entire study area.

Detailed description of drillings by Ohmert et al. (1988) could be used to estimate thickness of slope debris even though most drillings were carried out outside the local study area. Estimation of debris thickness based on relative slope positions may not provide exact information; however, good approximations could be achieved. For the relatively flat plateau areas, no information on the depth of debris and soil above bedrock was available. Still, these areas do not play an important role in landslide initiation and therefore do not influence subsequent modelling to a high degree.

Seismic prospection data formed the basis for estimation of debris thickness for the main upper landslide body. Only one drilling (Lic02) could be used for calibration since it was the only available which penetrated the bedrock. Geophysical data always requires interpretation because it does not directly display the characteristics analysed, which in this study was position of bedrock, but geophysical conditions which can be used as proxy information. Uncertainties related to the use of seismic data in this study can be estimated preliminarily by comparison of single inversion plots along the same profile. Therein, measured seismic velocity can differ significantly which relates to differences of bedrock position of several meters. Still, at four intersections of the available seismic profiles estimated bedrock depths could be compared and resulted in similar debris thickness. Interpretation of bedrock depths based on seismic data would benefit from additional drillings to exactly determine the depth of bedrock and calibrate measured seismic velocities.

The GIS procedure to assess the thickness of landslide deposits in the lower landslide body was carried out iteratively. Simple TIN creation could not be applied to create a realistic representation of real conditions. Addition of results from topographic analysis of deposits' height significantly improved delineation of the landslide deposits. Though, assessment of landslide deposits' depths is more uncertain for areas further away from the landslide boundaries.

Final interpolation of the slope debris layer resulted in relatively realistic depths for the areas most important for potential landslide initiation.

Geotechnical parameterisation subsurface material required interpretation and subjective judgement since the range of values described in literature sources is very large. Still, the best-fitting parameter settings were also chosen with respect to their influence on slope stability modelling assessed during subsequent sensitivity analysis. Further shear tests could help to minimise uncertainties associated with the use of literature values of geotechnical parameters.

Spatial interpolation of groundwater tables for the entire local study area relied on a limited number of hydrological sensors, which exhibited a great variety even though sensors were located relatively close to each other. For large parts of the local study area, no monitoring data was available and interpolation of groundwater table positions required addition of assumed water Table heights. Since spatial interpolation neglected process simulation but rather relied on general spatial interpolation techniques, results lack a physically based justification. Still, this kind of interpolation would require more detailed information on subsurface conditions, such as material properties and preferential flow paths that would require much more intense field surveys. Estimation of the influence of uncertainties inherent in the applied methodology requires detailed analysis within CHASM. Altogether, the groundwater scenarios can be assumed to be good approximations of real conditions for the area in which hydrological monitoring was carried out, which is also the most important for slope stability analysis. For other areas, estimated groundwater scenarios are more speculative.

The developed shear surface search routine effectively concentrates search procedure to the upper slope areas, which are assumed to be most likely influenced by potential landslide initiation. In order to increase the modelling speed it was necessary to limit the number of potential shear surfaces analysed by the search procedure. The developed procedure reduces the number of possible shear surface positions by a relatively large radius increment of Bishop's shear circles, while at the same time allowing for a large number of possible positions in a horizontal direction. By the current settings, shear surfaces are primarily assumed to be located in the upper slope areas reflecting potential reactivation of at least parts of the landslide deposits. Retrogressive slope failures involving the massive Upper Jurassic limestone can also be modelled, however, they were not given priority in this work. Since only circular shear surfaces are integrated, more complex landslide morphologies can not adequately be recognised by the shear surface search.

The shear surface search procedure is adjusted to the slope morphology in the local study area and can not be transferred to other areas without further modifications. Further improvements of the developed shear surface search procedure could employ additional threshold values, to enhance the positioning of the grid search box depending on profile lengths.

In this study, rainfall events were deduced from the KOSTRA atlas, which represents the most advanced available data source for precipitation intensity probabilities. Still, data is only available for 8.45×8.45 km grid cells and therefore includes simplifications. For example, local topography, which can have a significant influence on rainfall distributions as illustrated in this thesis, is only

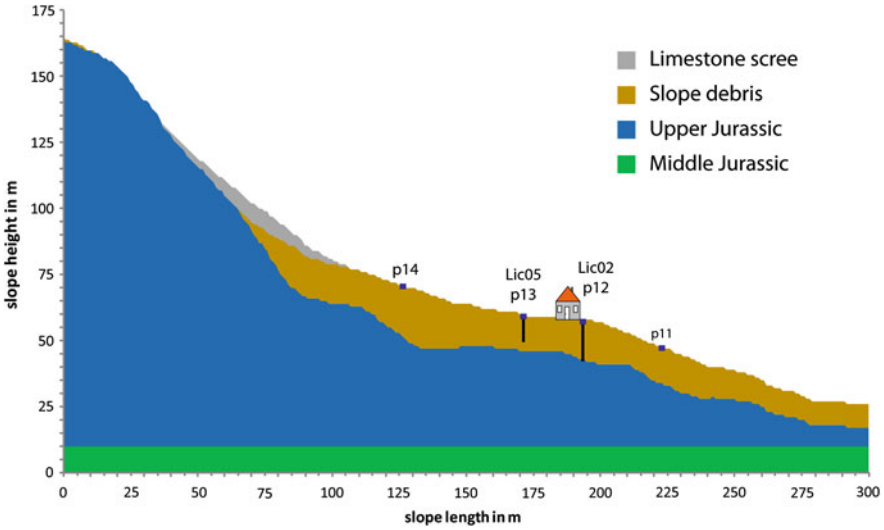

Fig. 6.45 Main slope profile used for CHASM modelling

regarded for the relatively large grid cells. Comparison to neighbouring grid cells shows that rainfall could potentially be higher.

In addition, snow melt is not included in KOSTRA data. However, uncertainties inherent in KOSTRA included as additional precipitation in this study can also be regarded as the effect of snow melting.

Integration of Euler 1 and Euler 2 rainfall scenarios aimed to include more realistic rainfall distributions with distinct peak rainfalls.

6.1.3.2 Model Application

Modelling slope stability with CHASM mostly focussed on the longitudinal slope profile on which four hydrological monitoring sites and geoelectrical monitoring are located. Also, the house experiencing damage due to slope movements is located along the profile. The position of the main profile and its subsurface conditions are illustrated in Fig. 6.45. Other slope profiles were also tested, however, since modelling results did not significantly differ from the main profile, they will not be presented herein.

The main slope profile has a length of 300 m and starts on the plateau. Hydrological monitoring sites are located at approximately 125, 170, 195 and 225 m; inclinometers Lic05 and Lic02 are positioned at profile metres 170 and 225, respectively. Geoelectrical monitoring reaches around 20 m further upslope than hydrological monitoring site p13, and ends at p11.

A sensitivity analysis of CHASM input data was primarily carried out by modifications of parameters for the slope debris layer, which was assumed to be

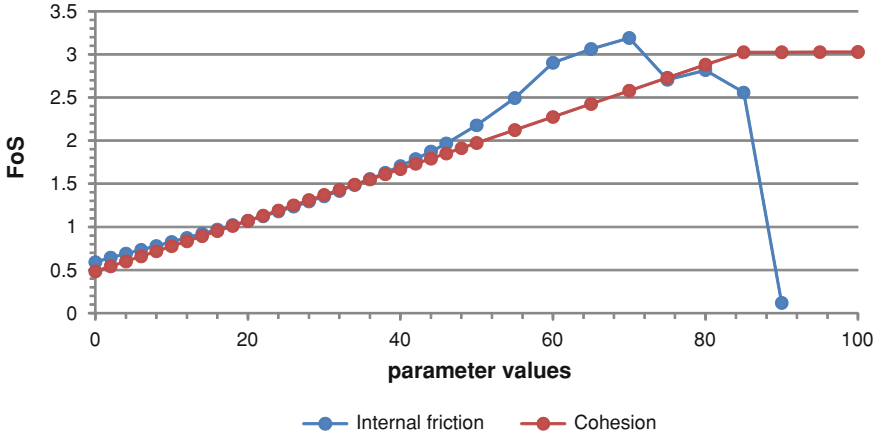

Fig. 6.46 Sensitivity analysis for cohesion and angle of internal friction

the most likely for landslide initiation. For sensitivity analysis for angle of internal friction and cohesion, the 300 m long slope profile illustrated in Fig. 6.45 was used. A 5 h design rainfall with a hourly intensity of 10 mm was used starting at hour 10 of the simulation. Simulation length was set to 20 h to decrease the duration of the simulation. For groundwater position, the previously defined high level water Table was used. Bishop grid search parameters were defined following the procedure previously developed (see Sect. 6.1.3.1). Other settings include soil suction curves as defined in Sect. 6.1.3.1 with Millington-Quirk procedure. Evaporation and upslope recharge were set to zero, and detention capacity was adjusted to 0.1, as in the CHASM standard settings. Internal friction and cohesion of the debris layer, which was assumed to be the most likely to be influenced by instability were changed step-wise to investigate their influence on the calculation of the FoS (Fig. 6.46). For both, cohesion and angle of internal friction, a similar increase of the FoS can be observed for low values. As internal friction approaches values of approximately 45°, the FoS increases quicker to a peak value reached at 70°. Higher values lead to decreased FoS. The linear rise of the FoS with increasing cohesion values continues until values of 85, and larger values do not influence the FoS.

CHASM sensitivity to changed hydraulic conductivity values could not be tested the same way as for cohesion and internal friction, since not only K_{sat} values of the potentially unstable debris layer influences the results, but also the hydraulic conductivity of the other material layers. In addition, hydraulic conductivity parameter values stretch over several orders of magnitudes, leading to an infinite number of possible combinations of K_{sat} values for all materials involved in modelling. Several combinations of hydraulic conductivity values for debris and the Upper Jurassic material below were tested with a wide range of rainfall scenarios and groundwater scenarios. In Table 6.8, a selection of hydraulic conductivity scenarios modelled is presented. In all these scenarios except for the first

Table 6.8 K_{sat} scenarios used for sensitivity analysis

	Limestone scree	Slope debris	Upper Jurassic	Middle Jurassic
Scenario 1	1e−1	6.78e−7	1e−6	1e−9
Scenario 2	1e−1	6.78e−6	1e−7	1e−9
Scenario 3	1e−1	6.78e−5	1e−6	1e−9
Scenario 4	1e−1	6.78e−5	1e−7	1e−9
Scenario 5	1e−1	6.78e−7	1e−8	1e−9
Scenario 6	1e−1	6.78e−6	1e−8	1e−9

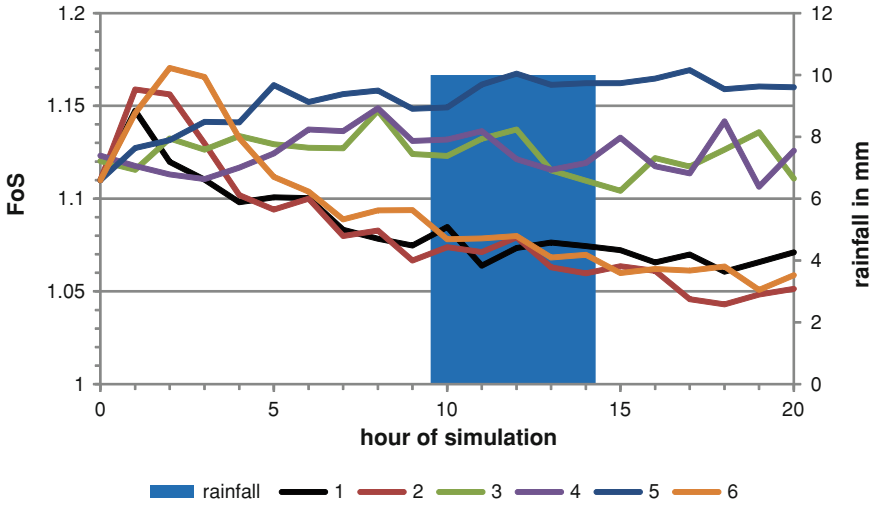

Fig. 6.47 Sensitivity analysis for K_{sat} scenarios

one, the Upper Jurassic layer has a lower hydraulic conductivity than for the slope debris layer to allow for an increase of pore water pressures above the bedrock. For the other settings of CHASM, the same values were applied as in the previous model run. CHASM results using a range of hydraulic conductivity scenarios are presented in Fig. 6.47.

In all scenarios, the FoS is on a similar level of approximately 1.12 at the beginning of the simulation run. From hour 5 on, general trends can be observed. For scenarios 1, 2 and 6, the FoS gradually decreases until the end of the simulation. Scenario 5 however, shows an increase of stability with and no destabilising effect of the rainfall event. Results of scenario 3 and 4 show an increasing FoS for the initial hours of the simulation which then drops during the rainfall event. For further modelling and subsequent early warning modelling, K_{sat} values from scenario 2 were selected.

Since soil moisture curve points used for CHASM modelling were not determined by detailed laboratory analysis but by the SPAW model, the influence of this input parameter on stability calculation was examined. The limited number of

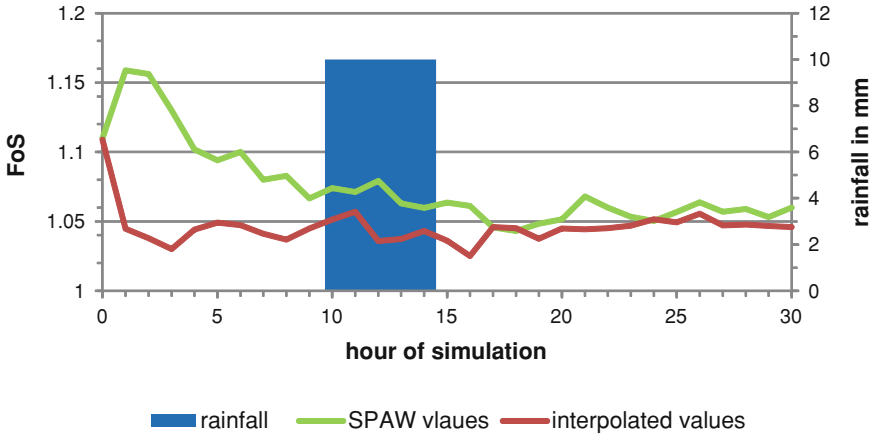

Fig. 6.48 Comparison of modelled FoS using soil suction curves estimated from SPAW model and interpolated laboratory values

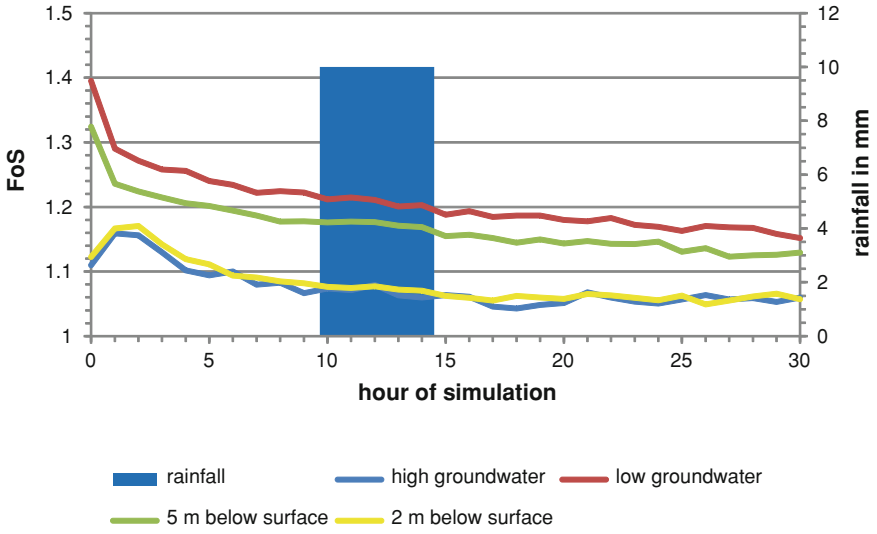

Fig. 6.49 Comparison of modelled FoS using high and low groundwater table scenarios

records on pressures and related water content from laboratory analysis were interpolated to the range required for CHASM analysis, and then used for modelling. These values are significantly lower with water contents approximately 40–50% lower than estimated from SPAW. Estimated values are presented in the appendix VII and results of CHASM simulation are illustrated in Fig. 6.48. The largest differences between the model runs can be observed in the initial hours of

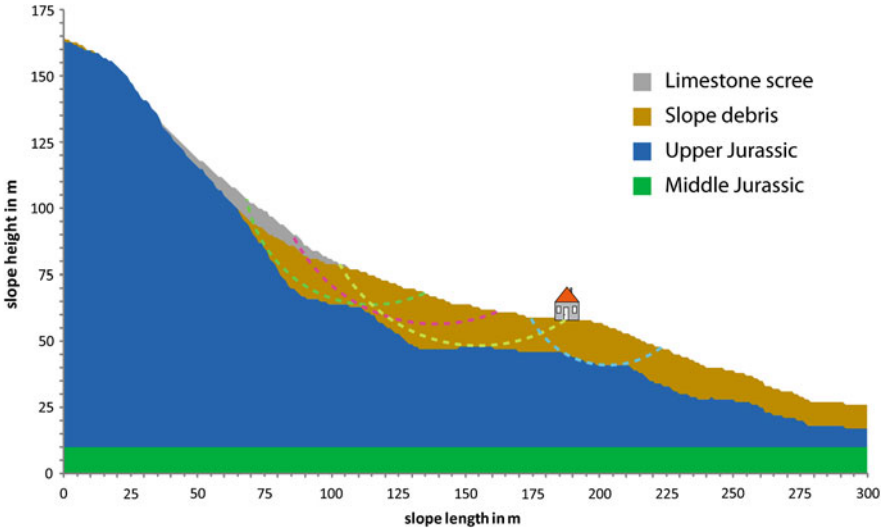

Fig. 6.50 Locations of selected potential shear surfaces

the simulations. Over the course of the simulation, the graphs gradually converge and reach a similar FoS level of approximately 1.05 towards the end. During the initial three hours of the rainfall event the FoS slightly increases, before dropping to lower values for approximately 10 h.

The influence of groundwater positions on CHASM stability calculation was tested for the elaborated high and low groundwater scenarios (see Sect. 6.1.3.1), and also for various designed scenarios in which groundwater was assumed to be located at an equal depth below the surface. Results of CHASM modelling using high and low groundwater table scenarios, and artificial groundwater positions of 2 and 5 m below the surface are presented Fig. 6.49. These simulations were carried out with all other settings being the same as in the previous simulations. The high groundwater scenario and the even 2 m below surface setting both result in very similar FoS of approximately 1.1 in the beginning of the simulation, and gradually decreasing to values of 1.06 towards the end. Lower groundwater tables, i.e. low groundwater scenario and the designed groundwater scenario with an equal depth of groundwater of 5 m below the surface, result in higher FoS which decrease during the entire the simulation. No significant accelerated decrease of the FoS can be observed during the rainfall event.

Several potential shear surface positions were investigated within this study. In Fig. 6.50, a selection of four analysed slip surfaces is presented in which the Bishop method integrated in CHASM was used. For the upper most shear surface (green), indicating a initiation of a slope failure below the scree slope a FoS of 0.78 and 0.75 with low and high groundwater table scenarios was calculated, respectively. The slip surface located further downslope (pink), starting at the lower end of the scree slope, resulted in a FoS of 1.52 and 1.4 for low and high groundwater scenarios,

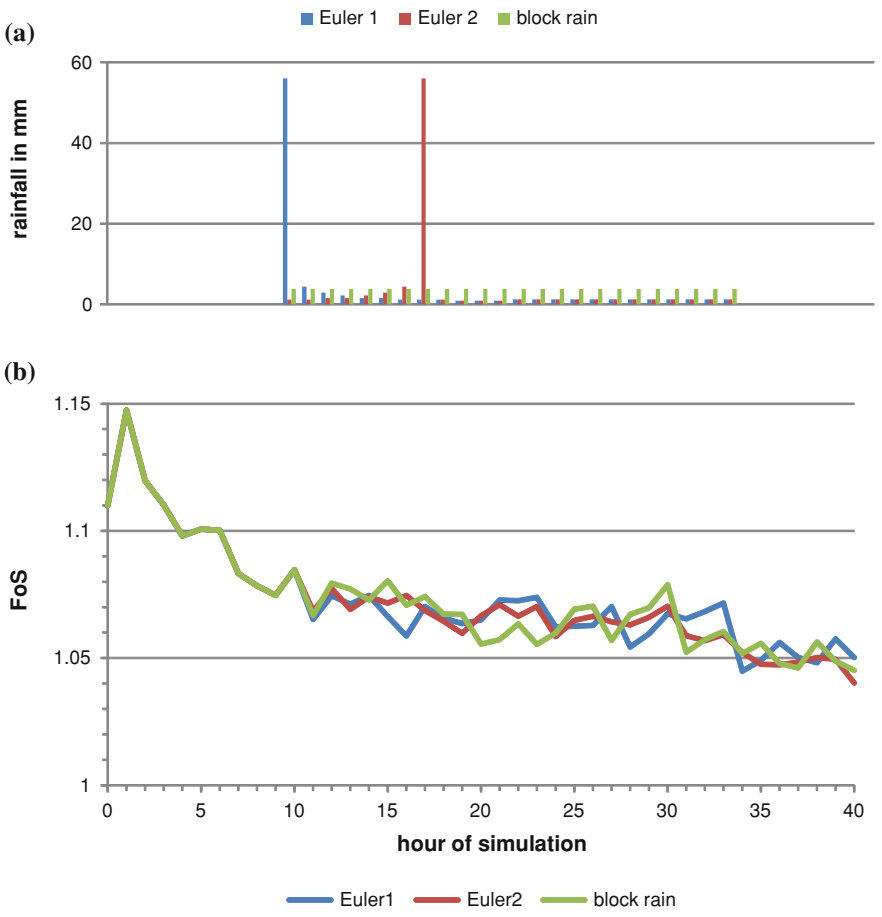

Fig. 6.51 Rainfall distribution for Euler 1, Euler 2 and block rainfall events (**a**) and resulting FoS (**b**)

respectively. For the third slip surface (yellow), with a shear plane affecting the house at its lower end, a FoS of 1.15 for low groundwater conditions, and 1.05 using the high groundwater positions was simulated. This shear surface was also the same, which was used for previous CHASM simulations and is the result of shear surface definitions described in Sect. 6.1.3.1. The highest FoS was calculated for the potential shear surface located below the damaged house (teal). For low groundwater conditions, the FoS was simulated as 1.78, and 1.61 using the high groundwater scenario. Other shear surfaces not displayed here were also tested, including failures comprising bedrock. However, the FoS for such shear surfaces was significantly higher with FoS values between 3.0 and over 6.0.

The influence of rainfall events on slope stability was tested with several rainfall distribution and intensities. In the following, results of three rainfall events with different distributions of rainfall intensities will be presented (Fig. 6.51).

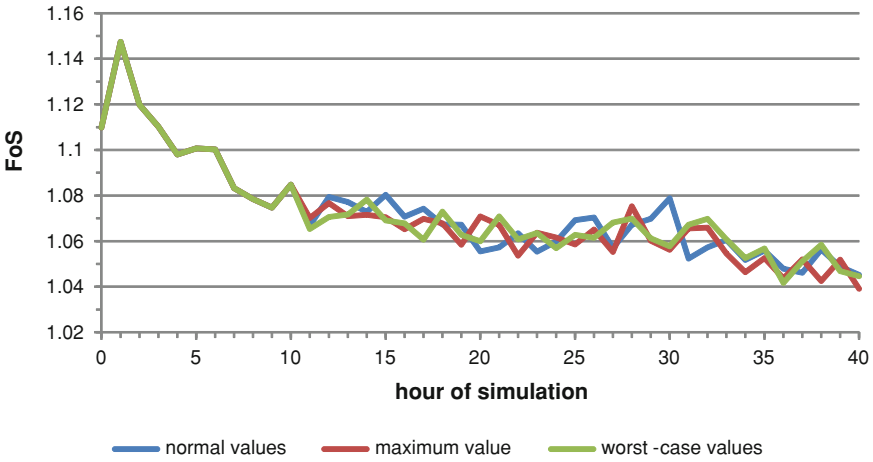

Fig. 6.52 Comparison of modelled FoS using normal, maximum and worst-case scenario rainfall events

Therein, Euler 1 and 2 rainfall events are compared to a block rainfall using previous CHASM setting and the high groundwater scenario. All rainfall scenarios comprise the same sum and only differ in their hourly distribution. For this comparison, the 24 h rainfall was used with an annual occurrence probability of 100 years. In all scenarios, rainfall commenced at hour 10 of simulation and lasted until hour 34. The block rainfall has a steady precipitation intensity of 3.8 mm/h. The Euler 1 scenario has a hourly maximum intensities of 56 and 44 mm in the first and second hours of the rainfall event, respectively. Afterwards, rainfall continues with relatively low hourly intensities of 1.25 mm/h for the rest of the simulation. Similarly, the Euler 2 rainfall has distinct precipitation peaks, however, these occurs in hour 7 and 8.

The course of the graphs is identical until hour 10 of the simulation, when the rainstorm commences. Euler 1 rainfall (blue line) shows the lowest FoS at hour 16 of the simulation caused by the high intensity rainfall occurring in the first 2 hours of the rainfall event. A similar drop of FoS can not be observed for the Euler 2 (red line) which has its maximum intensity at hour seven to eight. Between hour 20 and 24, the lowest FoS can be observed for the block rain with constant hourly rainfall intensity. For the later simulation time, all tested rainfall distributions result in similar FoS of approximately 1.05. Overall, only very small deviations of the FoS between the simulation runs using different rainfall distributions can be observed documenting to a relatively low sensitivity to rainfall distributions.

Normal, maximum value and worst-case rainfall scenarios derived from KOSTRA were also tested for their influence on slope stability calculation in CHASM. Fig. 6.52 shows the CHASM results using a 24 h duration rainfall with annual occurrence probability of 100 years beginning at hour 10 of the simulation.

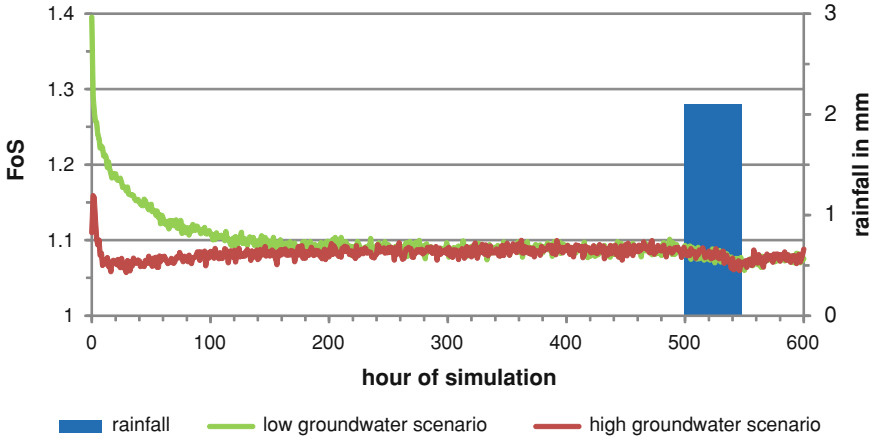

Fig. 6.53 Long duration simulation of slope stability using high and low groundwater scenarios and a 1 in 100 years rainfall with 48 h duration

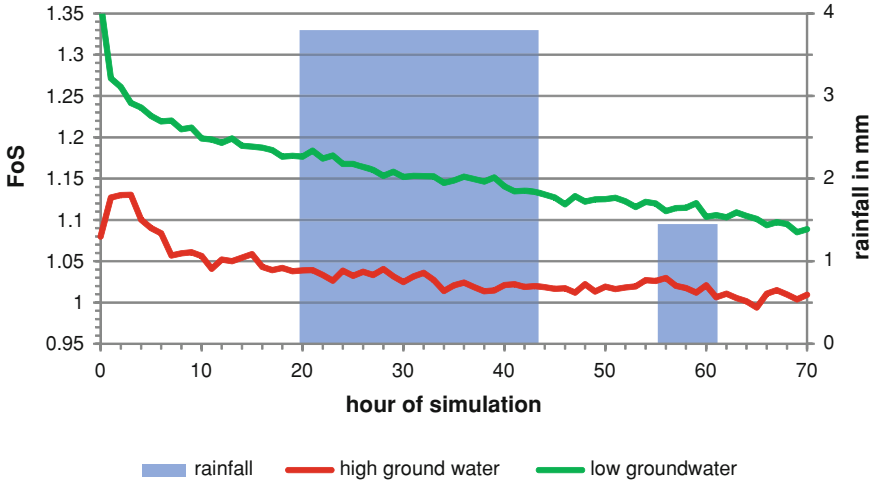

Fig. 6.54 Comparison of modelled FoS using high and low groundwater scenarios and two consecutive rainfall events

Total rainfall for these scenarios is 91.2, 100.8 and 120 mm for normal, maximum value and worst-case rainfall scenarios, respectively.

Until hour 10 of the simulation, when rainfall commences, FoS for all model runs is the same in all simulations. Afterwards, the worst-case scenario shows slightly lower FoS values for the following 7 h; however, the difference between the model runs is very small with FoS deviations of approximately 0.05. For the rest of the CHASM simulation, all three simulations produced very similar FoS

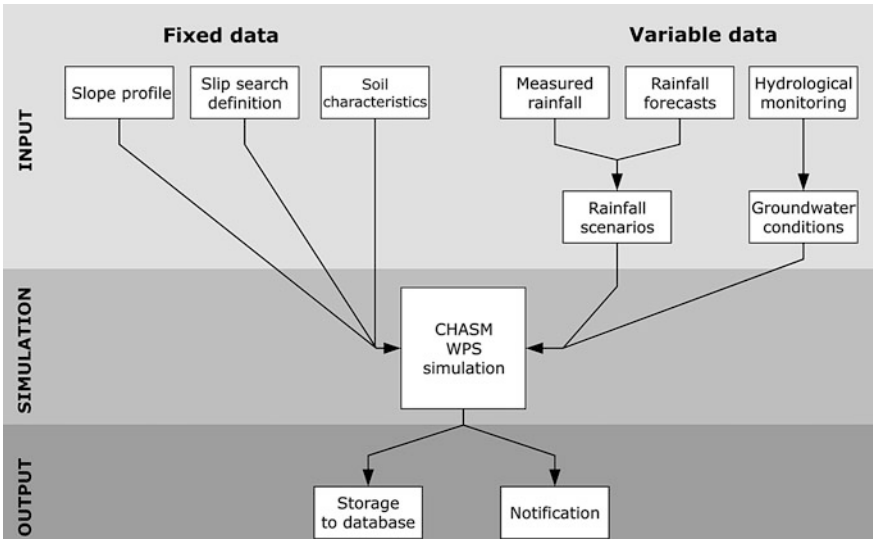

Fig. 6.55 Overview on the CHASM landslide early warning model

values with only minor deviations. Towards the end of the model run, FoS values of all three simulations converge to an equal level of approximately 1.04.

The previously presented CHASM simulation had a maximum duration of 40 h. An example of a long simulation is presented in Fig. 6.53. In this model run high and low groundwater scenarios were used without any precipitation for the first 500 h of simulation followed by a 48 h rainfall event with an annual occurrence probability of 100 years.

The relatively high FoS of 1.4 for the low groundwater scenario gradually decreases over time and reaches the same level as the high groundwater simulation after approximately 200 h of simulation. Between hour 200 and 500, both graphs show a similar course, with mean FoS of 1.08. When rainfall commences, the FoS is lowered to a minimum value of approximately 1.05 reached at the end of the rainfall event and then gradually increases again.

Additional modelling using the previously described CHASM settings and various combinations KOSTRA derived rainfall events showed, that no FoS below 1.0 could be modelled. Lower than unity FoS could only be achieved by either increasing the rainfall intensity five to ten-fold, or adjustment of geotechnical parameters. In Fig. 6.54, the modelling results using high and low groundwater scenarios and consecutive precipitation events are illustrated. For these simulations, the cohesion value for slope debris was decreased from 20 to 19 effectively lowering the general level of the FoS. Rainfall events comprise a 24 h rainfall (1 in 100 year occurrence probability), followed by 6 h worst-case scenario rainfall (1 in 100 year occurrence probability).

In both simulations, the FoS decreases until the first rainfall event commences. This trend continues for the low groundwater scenario until the end of the simulation.

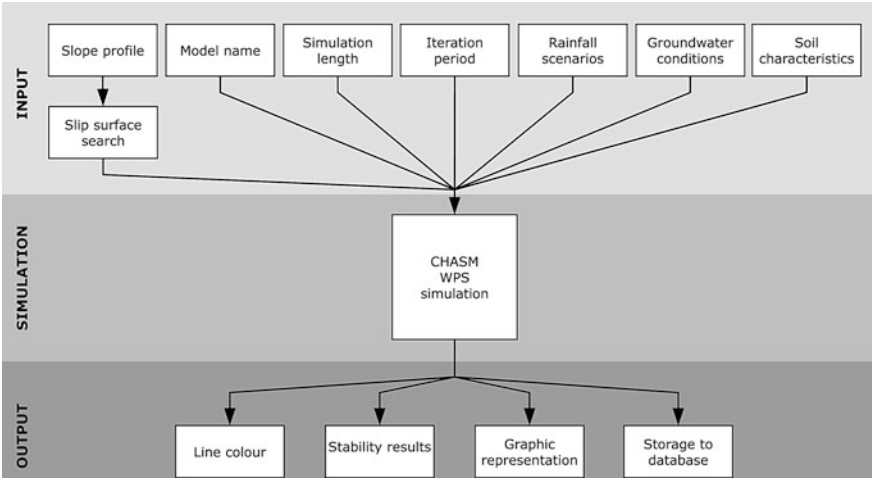

Fig. 6.56 Overview on the CHASM decision-support application

For high water conditions, the FoS slightly increases after the first rainfall, and then decreases during the second, reaching a minimum of 0.99 four after the precipitation ceases.

To allow for possible FoS values below unity, the cohesion value of the soil debris layer was lowered to 19 for all following CHASM simulations and subsequent CHASM early warning modelling.

All previously described CHASM simulations employed a two-dimensional topography. Three-dimensional topography in the form of varying cell width was applied in several model runs but was found to have no significant effect on stability calculation as described by the FoS.

For most simulations, only the FoS as the prime output of CHASM simulation was analysed. However, CHASM also provides hydrological results, i.e. soil moisture content and pore water pressures for each cell, which can be exported for single-time steps as graphic or text files. Since analysis of hydrological results for long slope profiles is very time-intensive, this was only done for few simulations. Hydrological results for most modelled CHASM scenarios illustrate fully saturated conditions for all but the top cells, for which the saturation gradually increases during rainfall events.

Discussion

Sensitivity analysis of geotechnical parameters yielded some interesting results which help to estimate the influence of the respective factors. Cohesion and angle of internal friction have a similarly strong linear influence on CHASM stability calculation. Hydraulic conductivity (K_{sat}) is an important factor which strongly controls simulation of the FoS. If these values are not carefully chosen,

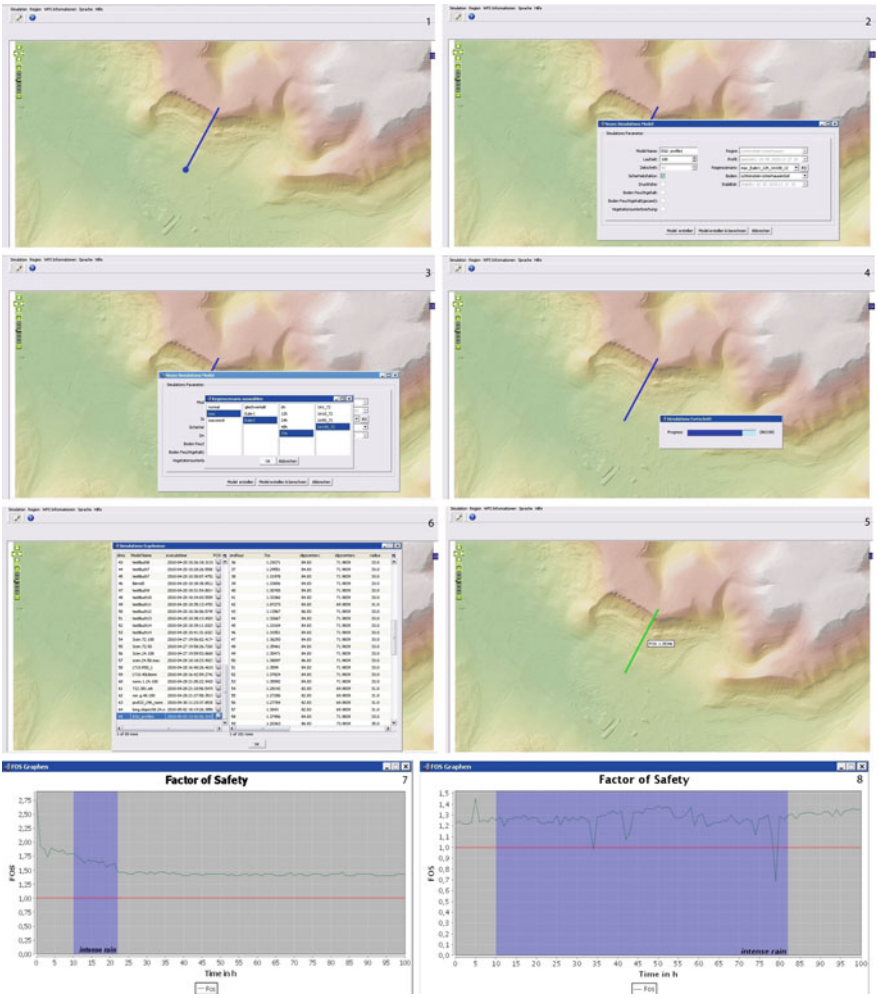

Fig. 6.57 Screenshots of the web-based implementation of the CHASM decision-support application (DTM: LGL AZ: 2851.9-1/19)

hydrological simulations can not result in positive pore pressures essential for destabilisation. Soil moisture curves and groundwater table positions have a strong effect on stability calculation, however, during long duration simulations the differences gradually level out.

All modelled slope profiles and shear surface positions show low FoS values illustrating potential slope failure. The lowest stability was calculated for the upper slope area. CHASM results demonstrate that potential shear surfaces are most likely located at the interface of slope debris and the underlying bedrock. Shear surfaces also including bedrock material have a significantly higher FoS and no CHASM simulation produced shear surfaces within the debris material. CHASM

simulations therefore reflect deep-seated sliding slope movements as monitored in Lic02 inclinometer, which have a depth of approximately 15.5 m at this point. The shallower displacements recorded in approximately 8.5 m depth, which shows characteristics of a flowing movements and possibly the progressive development of a shear surface, is not detected by CHASM simulations. Still, limit-equilibrium analysis can only be used to simulate failure processes, in which a rigid body slides along a shear surface, so progressive failure, flow processes and slow creep of material can not be modelled.

A very low influence of rainfall in general, and specifically for rainfall distributions and intensities is documented by the CHASM simulation results. Even very high precipitation events do not significantly lower the FoS. A possible explanation for the low influence of rainfall on CHASM stability calculation might be that the model is often used in tropical and sub-tropical environments and is possibly optimised for exceptionally strong rainfall. FoS values lower than 1.0, which in theory represent the initiation of slope movements, can only be simulated by modified geotechnical parameters, high groundwater conditions, and strong consecutive rainfall events.

6.1.3.3 CHASM Early Warning Model

In the following, the general procedure and technical implementation of the web-processing service application of CHASM for local landslide early warning is presented. The CHASM early warning model is a result of the work presented before, and the technical implementation carried out by the ILEWS project partner Geomer (Jäger et al. 2010).

The developed CHASM landslide early warning system uses a combination of fixed and variable data inputs to simulate hydrological processes and their influence on slope stability for one profile every 24 h. An overview on the CHASM early warning procedure is presented in Fig. 6.55. Fixed input data include a slope profile, definition of shear surface search parameters and soil characteristics. The slope profile along the damaged house, which was used for most CHASM model runs, was also chosen for modelling early warning. The shear surface relating to a potential failure in the upper slope area and also affecting the already damaged house was selected. Soil characteristics were chosen according to settings judged to be the most appropriate during CHASM sensitivity analysis (Sect. 6.1.3.2).

Variable data include recorded precipitation, rainfall forecasts and groundwater conditions. Measured rainfall from ILEWS weather station and rainfall forecasts from COSMO-DE are combined to one rainfall scenario file adapted to CHASM requirements. In the current setting, this file comprises a total simulation length of 560 h and includes 480 h of recorded rainfall, 20 h of forecasted rainfall, and 10 h without any precipitation. A relatively long simulation length was selected to decrease the influence of pre-defined groundwater scenarios, and to allow for a larger variation of slope stability calculations.

Groundwater scenarios are chosen depending on current hydrological conditions recorded by the monitoring system. For this, the TDR sensor in 9.5 m depth located at the damaged house (monitoring site p12) was selected and a threshold of 40% volumetric water content was determined. If current soil moisture is higher than the thresholds value, the high groundwater table scenario is chosen; a lower soil water content results in the integration of the low groundwater table scenario.

Fixed and stable input data are both integrated into the web-processing service of CHASM implemented by the project partner Geomer (Jäger et al. 2010). Results of the simulation are stored in the database for later access. CHASM early warning modelling is connected to an alarm sensor on the ILEWS website which changes its status depending on the results of the simulation and provides notification to involved experts. More detailed information on ILEWS alarm sensors and subsequent issuing of early warnings is provided in Chap. 7. However, since no real-time data is available on rainfall forecasts the connection to the alarm sensor is currently disabled.

Discussion

The developed prototypic CHASM early warning model applies the program fixed settings found to be the most appropriate during earlier model application and sensitivity analysis. Variable input data for early warning modelling combines measured and forecasted rainfall into one CHASM readable scenario file.

Groundwater scenarios depend on hydrological monitoring data, however, in a simplified form of minimum and maximum scenarios. Direct integration of each hydrological sensors' measurements are hindered by CHASM structure, which can only accommodate simplified groundwater conditions. Complex groundwater conditions, for example increasing groundwater positions in a downslope direction, and preferential flow paths can not be represented. Still, determination of an exact groundwater table position based on hydrological monitoring is difficult and can not be carried out without subjective interpretation (see Sect. 6.1.2.3). Without further modifications of CHASM, improvements of the integration of groundwater conditions can mainly be achieved by the addition of more groundwater scenarios and respective threshold determination. To decrease the influence of simplified groundwater conditions, a long duration for early warning modelling was selected.

The developed CHASM early warning model procedure represents a prototypic development, which at the moment can only provide theoretical early warnings. However, if local stakeholders demand realistic early warning, the technical system can be adjusted with little efforts.

The notification service set-up by Jäger et al. (2010) to inform the involved experts on potentially dangerous slope stability changes is based on CHASM modelling results. Still, without the possibility to validate CHASM simulation with real slope displacement events, the notification thresholds can only be determined hypothetically.

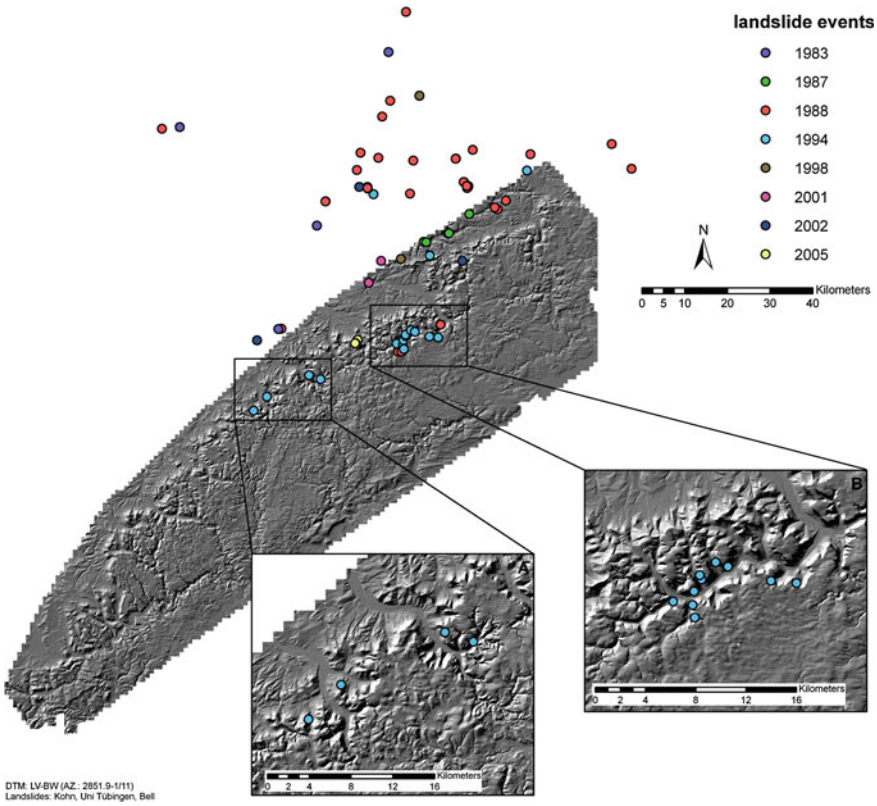

Fig. 6.58 Selected landslide events with known date of occurrence. Magnified areas show **a** April 1994 events from Tübingen University inventory, and **b** April 1994 Filstal events

6.1.3.4 CHASM Decision-Support Tool

The web-based CHASM decision-support tool was developed to be able to quickly assess slope stability for freely selecTable profiles using a variety of input parameters.

The general procedure is a results of this work, technical implementation, however, was carried out by the ILEWS project partner Geomer (Jäger et al. 2010). A graphical overview on the developed CHASM decision-support web-processing service application is presented in Fig. 6.56. Screenshots of each step of the web-based CHASM simulation are presented in Fig. 6.57.

The slope profile for which stability is to be calculated can be selected by clicking on the DTM of the local study area (1). Automatically, the CHASM slope file is produced taking into account the simplified subsurface model with a two metre resolution. According to profile length, the slip surface search (Sect. 6.1.3.1) is selected. In the next step (2), the user can enter a name for the simulation and set model parameters, i.e. simulation length and iteration period. All rainfall scenarios

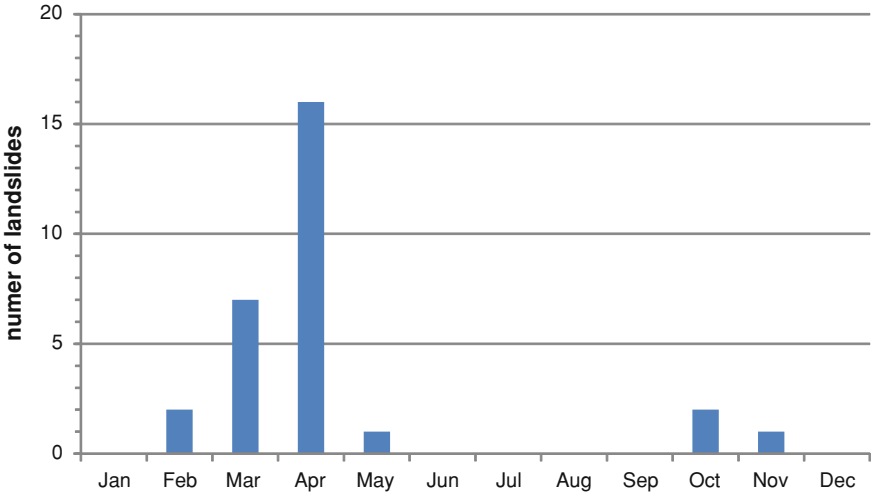

Fig. 6.59 Monthly distribution of selected landslide events

derived from KOSTRA can be selected for slope stability calculation from a drop down menu (3). Currently, all rainfall events start at the hour 10 of the simulation. High and low groundwater scenarios are available as input data. For soil characteristics, either the CHASM standard parameter or the parameter values developed in this study can be chosen. CHASM is executed on the ILEWS server and takes approximately 1 min for most simulations (4). The selected slope profile is colour-coded according to the simulated FoS of the last hour of the simulation, with green for FoS larger than 1.3, orange for FoS between 1.0 and 1.3, and red for FoS lower than 1.0 (5). Further information, for example, the course of the FoS throughout the simulation or the position of the shear surface can be accessed (6). In addition, all previous simulations are stored in the database can be selected for analysis. Sample results are presented in screenshots 7 and 8. Therein, rainfall is marked as a blue area and the course of the FoS can be viewed. While in the first of these figures, the FoS decreases during rainfall and stabilises afterwards, the second graph drops to much lower values for some steps of the simulation. This was found to be related to a changed position of shear surfaces parameters in the respective time-steps of the simulation.

The CHASM decision-support application is available in German and English language. In addition, a bilingual step-by-step tutorial explaining the functionality of the service and basic terms of slope stability calculation were developed to increase usability (see Appendix VIII and Appendix IX).

Discussion

The aim of the CHASM decision-support system was to allow quick calculation of slope stability without the need to elaborate slope profile and shear

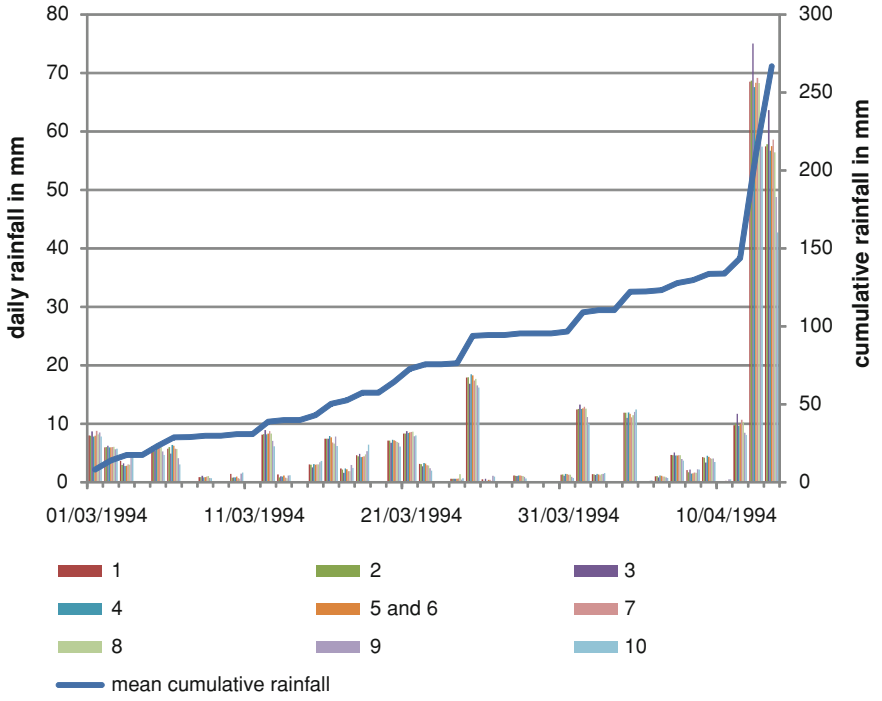

Fig. 6.60 Daily rainfall and mean cumulative rainfall for April 1994 in Fils valley landslide locations (1–10)

surface definition files. It was not the goal to convert the entire CHASM stability software into a web-based simulation program; however, if this is demanded by the CHASM developers, further works could be based on the work described in this thesis. In addition to the previously described uncertainties inherent in CHASM modelling, the developed CHASM decision-support system is subject to uncertainties arising from automated shear surface search which causes the slip search to be located at different positions for some hours of the simulation.

Concluding the results of this work, it can be noted, that the developed CHASM decision-support system enables quick judgement on slope stability for various slope profiles and variable input data. This can be potentially of great help to stakeholders that require assessing slope stability situation for larger areas in a short amount of time.

However, the slope under investigation did not show any significant phase of increased movement speed and CHASM simulations could not be sufficiently validated. Application of the decision-support system in more active study areas could improve the overall performance and aid to assess its value in the context of landslide risk management and early warning.

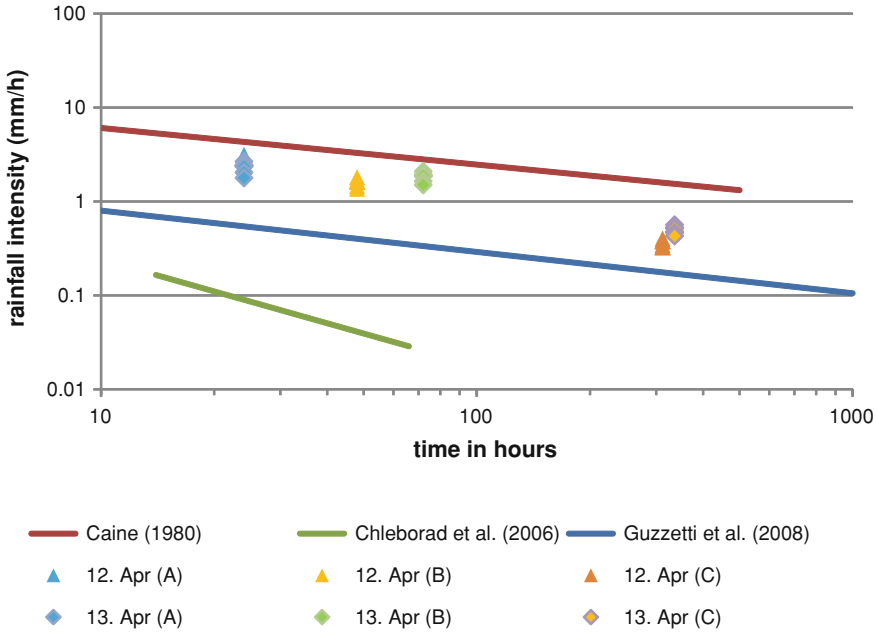

Fig. 6.61 Comparison of 1994 Fils valley landslides to intensity-duration rainfall threshold accounting for two potential triggering dates and three potential triggering rainfalls (**a**–**c**)

6.2 Regional Scale

6.2.1 Inventory Analysis

Not all landslide inventories available for the Swabian Alb could be employed for verification of rainfall thresholds because they did not meet the defined criteria.

The general landslide map by Kallinich (1999) provides extensive information on the spatial distribution of slope failures, but does not contain information on the date of occurrence.

The Tübingen University inventory contains over 600 landslide events and information about geological and geomorphological characteristics of slope failure sites. However, only for a fraction of 36 events the date of occurrence is acknowledged. Earliest records date back to 1851; still, the majority of landslide took place in the last 50 years. Information on timing of slope failures varies between exact dates, year, or rough information like "approximately 15 years ago". From all dated events, only four landslides could be used for further investigations, since only these occurred during the period for which rainfall data is available. The selected landslide events describe the "second half of April 1994" as triggering date. To be able to investigate if these landslides followed the exceedance of rainfall thresholds, further analyses of rainfall events during this period were required.

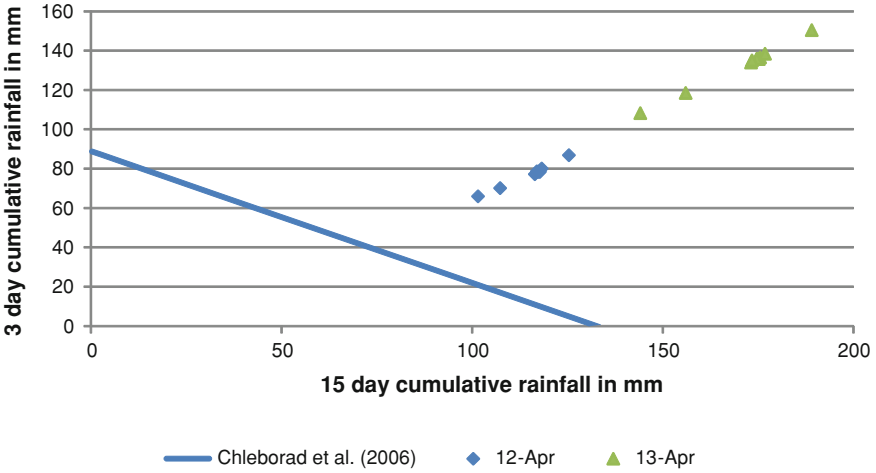

Fig. 6.62 Comparison of April 1994 Fils valley landslides to cumulative rainfall threshold accounting for two potentials triggering dates

The landslide inventory created by analysis of historic documents within the InterRISK and ILEWS projects (Röhrs and Dix 2010) includes a total number of 216 events, of which the earliest date to the year 1416. The majority of events, however, took place within the last 200 years. For most slope failures date of occurrence is only acknowledgements in terms of years. No events from this inventory could be employed for subsequent threshold analysis.

The landslide event inventory provided by Bell (2010, personal communication) lists 10 slope failures that occurred after strong rainfalls in April 1994 in the Fils valley. Since rainfall data in the form of regionalised climate data is available for this period, the entire inventory could be used for threshold verification.

Another inventory for the Fils valley produced by Brennecke (2006) only includes relative information of landslide age, making threshold verification for these events impossible.

The most detailed information on temporal occurrence of landslides is available in the inventory of the Department of Transportation of the administrative district Stuttgart created by Kohn (2006). A total number of 389 landslides are included, of which 250 were localised in GIS. However, many landslides are not located in the Swabian Alb but can still be used to ensure recorded landslides were not singular slope failures but the result of rainfall threshold exceedance. Altogether, 10 events of increased landslide activity between 1 and 44 days long were determined, in which a total number 62 landslides occurred. However, only 15 of these took place within the Swabian Alb.

In total, 29 landslides were judged to be adequate for the use within rainfall threshold verification for the Swabian Alb. An overview on these landslide events is presented in Fig. 6.58. Therein, not only the 29 selected events, but also the other slope failures outside the Swabian Alb are displayed.

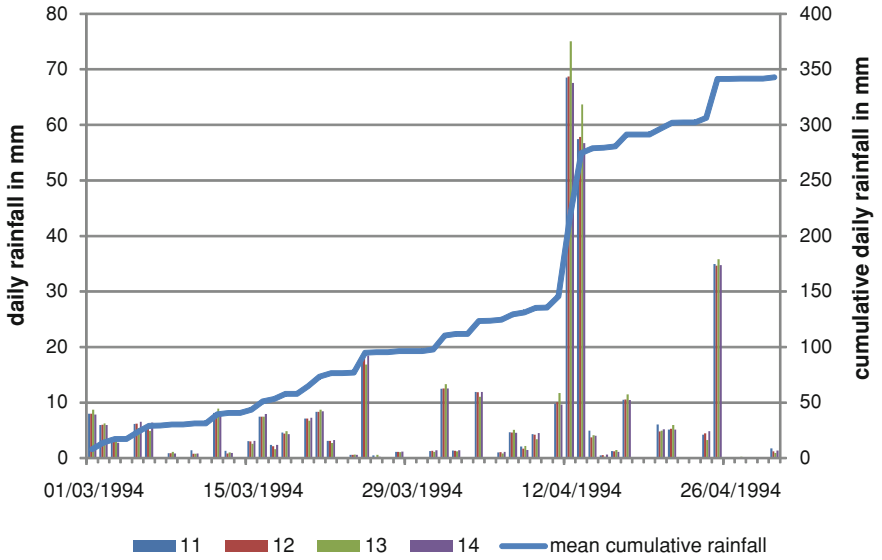

Fig. 6.63 Daily rainfall and mean cumulative rainfall for April 1994 landslide locations (11–14)

The monthly distribution of the selected 29 slope failures shows a strong peak in April, primarily due to the event inventories by Bell (2010, personal communication) and Tübingen University (Fig. 6.59).

6.2.1.1 Discussion

Results of inventory analysis illustrate some general problems associated with rainfall thresholds, i.e. the availability of information on temporal and spatial occurrence of slope failures. In most cases, the exact date of landslide triggering is not acknowledged and can not easily be ascertained by analysis of potential triggering rainfall events. From all available data sources, the inventory of the Department of Transportation of the administrative district Stuttgart (Kohn 2006) provides the most reliable data on temporal landslide occurrence, since road damage can be expected to be reported shortly after slope failures. However, these failures are often associated with bank failures and therefore may not reflect the conditions which lead to failures of natural slopes.

In addition, the triggering agents are not always recorded in the inventories and uncertainties remain whether landslides are initiated by for example rainfall, earthquakes or inadequate construction works. The integration of landslides which are located outside the Swabian Alb aimed to reduce these uncertainties.

Since the availability of rainfall data with a high temporal resolution was limited, not all landslide failures available in inventories could be used for the verification of rainfall thresholds. If additional data became available, more landslides events could be integrated into threshold verification.

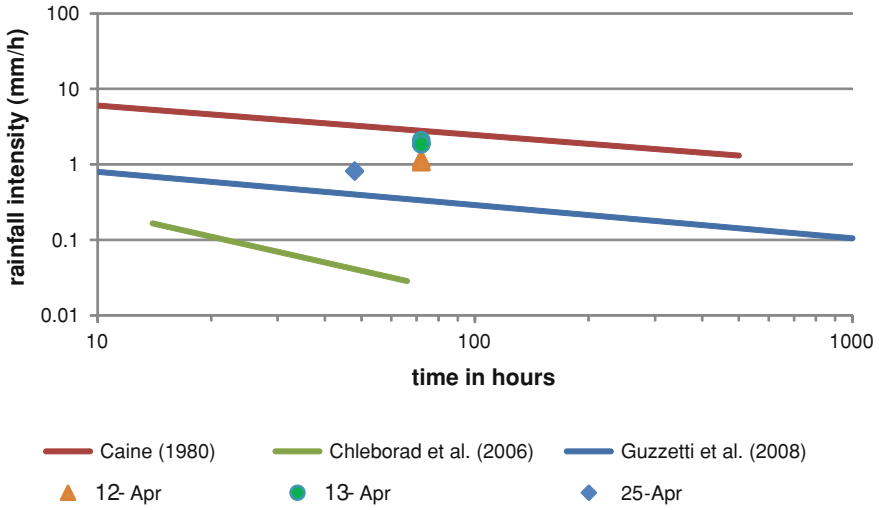

Fig. 6.64 Comparison of 1994 Tübingen University landslide events to intensity-duration rainfall threshold for three potential triggering dates

6.2.2 Threshold Verification

For two landslide events comprising 14 landslide failures in total, the exact date of occurrence is unknown. These include 10 landslides in the Fils valley triggered on 12th or 13th February 1994, and four slope failures acknowledged to have occurred in the "second half of April 1994". To estimate rainfall thresholds, rainfall data was analysed and different potential dates of slope failures were assumed based on rainfall records. Fig. 6.60 illustrates daily rainfall for each landslide location in the 6 weeks preceding landslide failures in Fils valley.

Several rainfall events exceeding 10 mm/day occurred during March and April. Strongest peaks were recorded for 12 and 13th April, for which a total of approximately 120 mm was measured. According to KOSTRA rainfall intensity atlas, rainfall intensities of this magnitude have recurrence intervals of 50–100 years.

Since it is unsure on which day landslides were triggered, rainfalls for both potential dates were analysed. Comparison to intensity-duration thresholds also required identification of the landslide triggering rainfall event. Fig. 6.61 displays Fils valley landslides with three assumed triggering rainfall events, beginning (a) on the day of potential slope failure, (b) after a day with low precipitation of less than 1 mm, and (c) after the last day with no precipitation. For all potential triggering dates and assumed triggering rainfall events, precipitation exceeded the thresholds of Guzzetti et al. (2008) and Chleborad et al. (2006), Caines' (1980) threshold however, is not reached by the records.

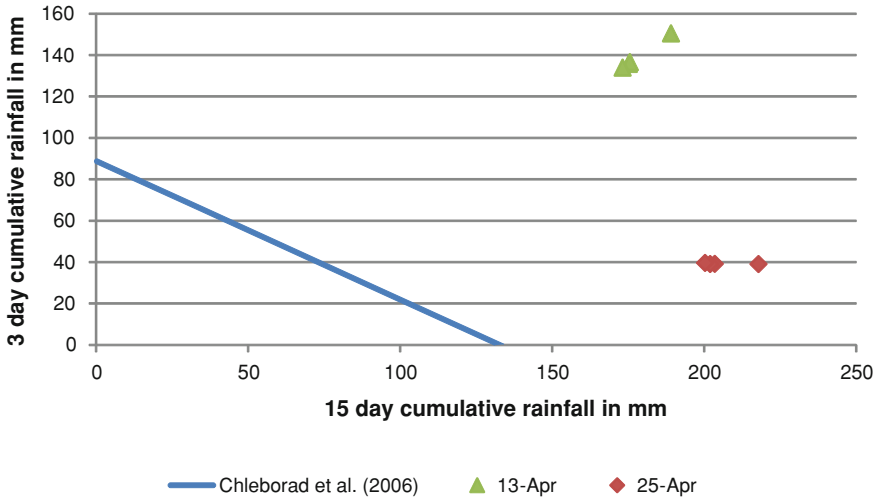

Fig. 6.65 Comparison of April 1994 Tübingen inventory landslides with cumulative rainfall threshold accounting for two potentials triggering dates

A comparison of rainfall records for the Fils valley landslides to the cumulative rainfall threshold by Chleborad et al. (2006) is illustrated in Fig. 6.62. For this, both potential dates of landslide occurrence, i.e. 12th and 13th April were considered. Cumulative rainfall was higher for all landslides than threshold values, independent from date of occurrence.

For the four landsides from Tübingen University inventory, the exact date of slope failure was also unknown. Rainfall records for April 1994 (see Fig. 6.63) show a strong rainfall peak on the 12 and 13th April, similar to that in the Fils valley that had triggered multiple landslides. A second rainfall peak can be observed on the 25th April; however, rainfall intensities on that day are about 50% lower than the previous peaks. Both dates were assumed to be potential dates of landslide occurrences and were used to verify rainfall threshold values.

For comparison of rainfall records for the four landslides from Tübingen University inventory, two potential dates of slope failures were analysed to be the most likely, i.e. 12/13th April and 25th April. For this analysis, triggering rainfall event was determined to begin on the day following low precipitation record of less than 0.1 mm/day. Results are presented in Fig. 6.64 and show that for all tested potential dates of landslide occurrence thresholds of Chleborad et al. (2006) and Guzzetti et al. (2008) are exceeded, while Caines' (1980) threshold is not reached. Similar results were elaborated when taking into account only the rainfall on the days of potential slope failures.

Cumulative rainfall thresholds (Chleborad et al. 2006) were exceeded using 13th and 25th April as potential landslide failures (Fig. 6.65). For the 25th April, threshold exceedance is primarily influenced by 15-day cumulative rainfall, while for the 13th the 3-day cumulative rainfall has a greater influence.

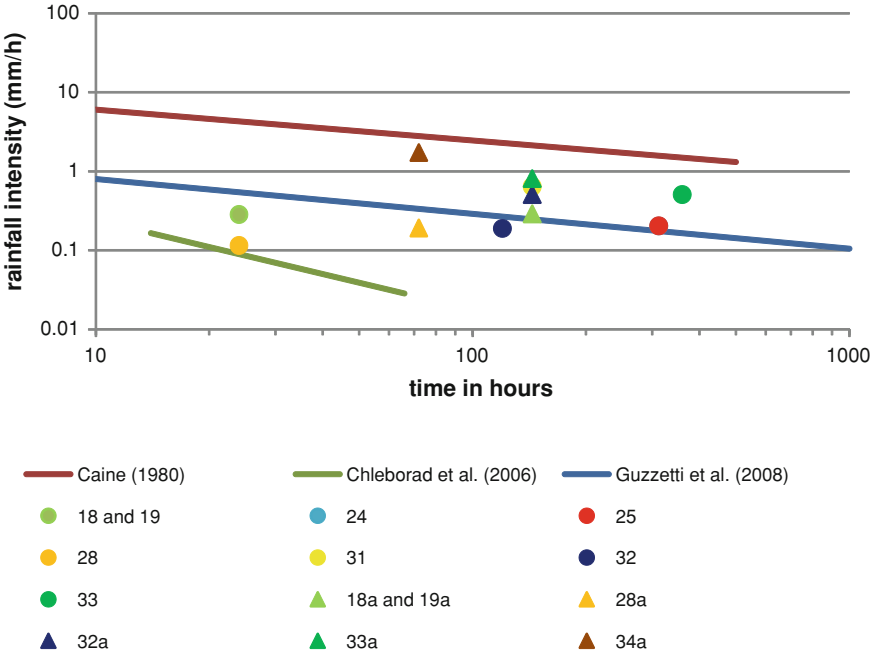

Fig. 6.66 Comparison of presumably rainfall triggered landslides (18–34) to intensity-duration thresholds accounting for alternative triggering dates (18–34a)

For the April 1994 landslides the triggering factor was known to be strong rainfall. This is however not the case for the other selected landslide events which could also be initiated by for example snow melting. Regionalised climate data including snow water equivalent and temperature records were integrated into threshold analysis for all landslides where data was available. Slope failure records without data on snow cover changes and temperature include seven events with a total number of nine landslides which had occurred in the Swabian Alb.

Two landslides (ID 18 and 19) were triggered on 30th July 1987 close to Schwäbisch Gmünd. According to inventory information the landslides were both triggered on a day with only 6.8 mm precipitation, a total sum occurring very often. However, rainfall events up to four times stronger occurred some days earlier and later. Since the recorded triggering date may be inaccurate, alternative triggering dates were considered.

Two more landslides (ID 24 and 25) were triggered in the same area on the 15th October 1988.

Between 26th May and 9th June 1983, seven landslides are listed in the inventory, of which one (ID 31) is located in the northern Swabian Alb. Even though snow data was available for this period, no snow was recorded.

Four landslides were recorded between 11th and 22nd April 1994 of which one is located in the study area (ID 32). The total size of the landslide was 625 m^2 and it was triggered on a day with relatively low precipitation of only 8.5 mm.

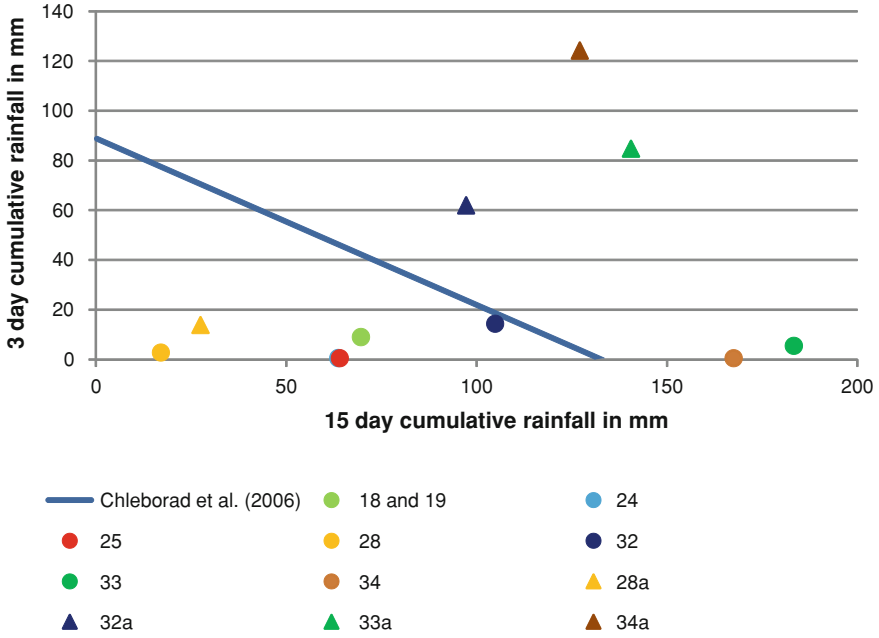

Fig. 6.67 Comparison of presumably rainfall triggered landslides (18–34) to cumulative thresholds accounting for alternative triggering dates (28–34a)

However, a much stronger rainfall event (>50 mm) occurred 1 day later, and was considered as a potentially more accurate triggering date.

For late March 2002, the inventory contains four landslides of which one (ID 34) is in the Swabian Alb. The slope failure covered an area of 450 m^2 and had a depth of 3 m. No rainfall was recorded for the day of landslide initiation or the day before. An extremely strong rainfall event of almost 70 mm occurred 6 days earlier and was checked as an alternative triggering date.

The inventory contains one record (ID 28) for the 29th August 1990 on which several landslides had occurred close to Neidlingen; though, only one coordinate is provided. Rainfall data describes only 2.8 mm of precipitation for the day of landslide occurrence. As an alternative triggering date, the subsequent day was considered, on which more than 11 mm precipitation were recorded.

At the boundary of the Swabian Alb, close to Kirchheim, one landslide (ID 33) was recorded for the 6th November 1998. Two more landslides occurred outside the study area on the preceding day.

A low total precipitation of only 1 mm was recorded for the triggering day; however, a very strong rainfall event with over 70 mm 6 days earlier might have been the correct initiation day and was therefore considered as an alternative.

Results of intensity-duration threshold analysis of landslides for which only rainfall data was available are presented in Fig. 6.66.

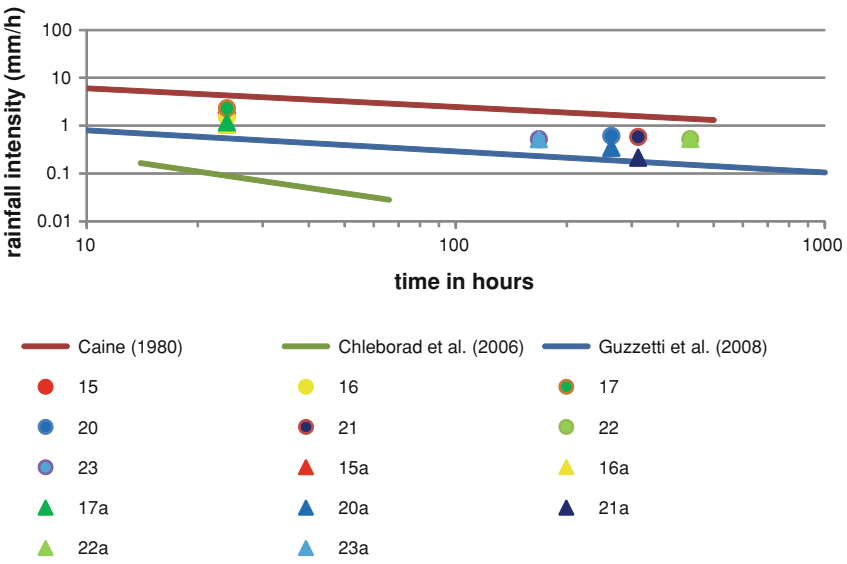

Fig. 6.68 Comparison of presumably snow-melt triggered landslides (15–23) to intensity-duration thresholds including alternative triggering dates (15a–23a)

All landslides are above the intensity-duration threshold used in the Seattle landslide early warning system. From the landslides for which the recorded triggering date was used four lie below Guzzetti et al. (2008) threshold. Caines' threshold was not exceeded by any of the slope failures. Alternative triggering dates generally increased intensity-duration values and led to two landslides being raised above Guzzetti et al. (2008) threshold; however, slope failures of the Neidlingen event (ID 28) remain below.

Results of cumulative threshold analysis of landslides for which only rainfall data was available are presented in Fig. 6.67. Therein, recorded and alternative landslide triggering dates were considered.

When using recorded triggering dates, five of seven landslides analysed were located below threshold values. Generally, these show relatively low values for 3-day cumulative precipitation. Only landslides 33 and 34 exceed the threshold due to high cumulative rainfall of more than 150 mm. Alternative triggering dates generally have higher cumulative rainfall values, however, only for landslide 31 the threshold was thereby exceeded.

Landslide events, for which also snow data was available, include three events in March 1987, March and April 1988 and February 2005.

On 27th March 1987 three landslides (ID 15–17) occurred at the border of the Swabian Alb close to Ellwangen. Slope failures were between 20 and 40 m and had a maximum depth of 4.5 m.

The highest number of landslides occurred in March and April 1988. However, of 33 landslides listed in the inventory, only four were triggered in the study area.

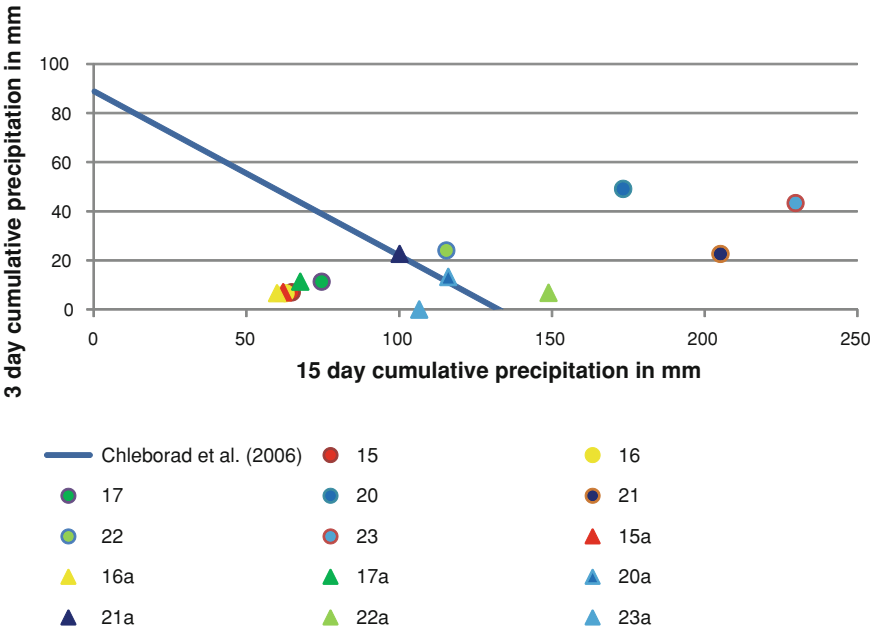

Fig. 6.69 Comparison of presumably snow melt triggered landslides (15–23) to cumulative rainfall threshold including alternative triggering date (15a–23a)

Three of these landslides (ID 20–23) were classified as failures in natural slopes, and one as rockfall. The largest of the landslides had a total size of 2,500 m^2 and required concrete injection for stabilisation. In the days preceding the described slope failures snow height quickly decreased by approximately 60 cm occurred.

Two failures in embankments (ID 29 and 30) are listed for 17th February 2005. Even though data on snow cover and temperature were available, no threshold analysis could be performed. According to weather data, temperature was below zero throughout the triggering period, and all precipitation was stored as snow.

Results of intensity-duration and cumulative threshold analysis of landslides for which snow height data was integrated are presented in Figs. 6.68 and 6.69, respectively.

All landslides analysed have intensity-duration values lying between the thresholds by Guzzetti et al. (2008) and Caine (1980). In general, longer duration precipitation events were considered since snow melting occurred over periods up to 18 days. When neglecting additional rainfall while using the same precipitation event durations, results show slightly lower intensity-duration values; however, these are still above the values of Guzzetti et al. (2008).

Results of cumulative rainfall threshold analysis show that four landslides are above, and three below the threshold by Chleborad et al. (2006). In general, threshold exceedance is strongly influenced by long term 15-day cumulative precipitation and only to a lower extent by 3-day cumulative precipitation.

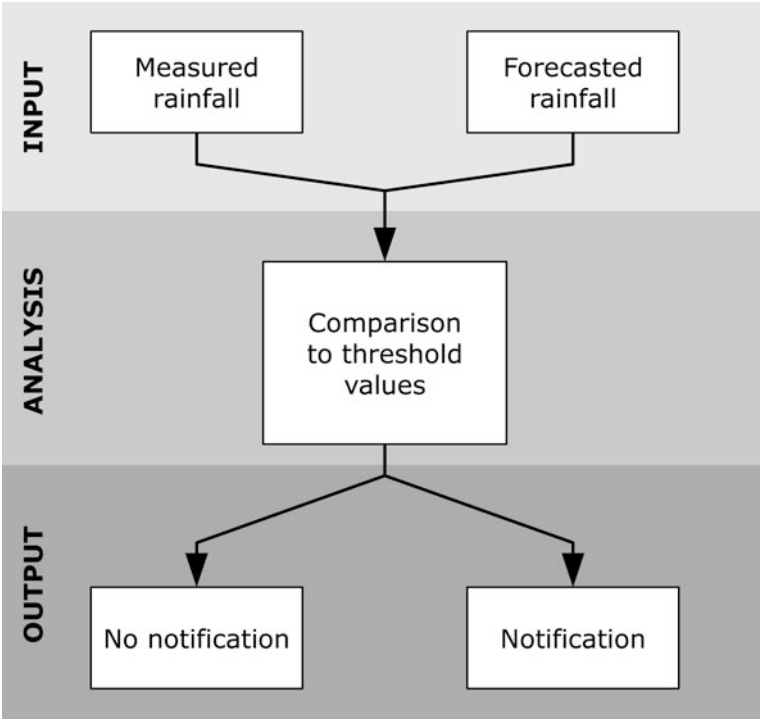

Fig. 6.70 Overview on the regional landslide early warning model

Integration of snow data generally raised cumulative rainfall values. When snow melting is not considered only one landslide (22a) is clearly above threshold values, and two others (20a and 21a) are very close to threshold line.

Some interesting characteristics can be observed for landslide 23, which shows a significant difference depending on the integration of snow melting. When snow melting is considered, it results in the highest cumulative precipitation values of all landslides. When only measured precipitation is used, no 3-day cumulative precipitation can be observed resulting in values below the threshold.

Most landslides occurred between intensity-duration values between thresholds by Caine (1980), which was never exceeded by landslides analysed, and Guzzetti et al. (2008), which was exceeded by a large proportion of the landslides. The lowest intensity-duration threshold from the Seattle landslide early warning system was exceeded by all analysed landslides. Similarly, the cumulative rainfall threshold by Chleborad et al. (2006) was exceeded in most cases; still some landslides occurred below.

For some cases, the recorded landslide triggering date did not coincide with highest rainfall intensities and alternative dates were considered. In general, this resulted in higher index values and more landslides being above threshold levels.

Table 6.9 Preliminary rainfall threhsolds used for regional landslide early warning

Antecedent rainfall (in mm)	Forecasted rainfall (in mm)
130	0
90	30
50	50
20	70
0	80

6.2.2.1 Discussion

Limited availability of data on landslide occurrences and related initiating rainfall events hindered the establishment of rainfall thresholds specifically for the Swabian Alb. Tested rainfall intensity and duration thresholds proposed in the literature, however, performed satisfactorily. In general, Caines' (1980) threshold seems too high for the Swabian Alb, since no landslide exceeded its critical values. In contrast, the threshold proposed by Chleborad et al. (2006) appears to be too low, since most landslides triggering rainfall events significantly exceeded critical values. Still, further analysis integrating rainfall events that did not cause landslides should be tested to verify this assumption. From all tested intensity duration thresholds, the one proposed by Guzzetti et al. (2008) performed most satisfactorily, with a high number of landslides exceeding critical values.

Cumulative rainfall thresholds tested in this study (Chleborad et al. 2006) can be considered adequate since a large number of landslides occurred above threshold values. In comparison to intensity-duration thresholds, a slightly higher number of landslides occurred below threshold rainfall.

Still, some uncertainties remain in the results. The exact date of landslide triggering is not known for all landslides. Analysis of additional potential triggering dates, as carried out in this thesis, can help to ascertain these, however validation can not be carried out. Similarly, triggering rainfall events are difficult to determine but can have a significant influence on threshold verification.

Results illustrate the need to integrate data on snow melting into thresholds determination, especially due to the frequent landslide occurrence in spring.

Regionalised climate data used within this study is subject to uncertainties. In particular snow melt does not represent real measurements but results of modelling. Integration of real snow height measurements could significantly improve the results and make threshold verification more reliable.

6.2.3 Early Warning

The regional early warning system was designed in cooperation with the company of Geomer which was also responsible for technical implementation (QUOTE). In the following, the design of the regional early warning system will be presented.

Detailed information on the technical implementation is provided by Jäger et al. (2010). Additional information on the warning procedure initiated once a threshold is exceeded is described in Chap. 7.

The early warning scheme of the developed prototypic regional system integrates measured precipitation, rainfall forecasts and thresholds. Since only historic rainfall forecasts were available, the system represents a technical solution without realistic early warning capabilities at this stage. However, the regional landslide early warning system was planned to be modifiable and extendable when additional data becomes available.

The regional landslide early warning system for the Swabian Alb was designed as a spatially distributed system where rainfall thresholds and warning levels may vary throughout the focus area. In the current state of the system technical implementation, only the area of Lichtenstein-Unterhausen is integrated, which is also the local project area in this study. An overview on the early warning procedure is presented in Fig. 6.70.

Precipitation recorded by the ILEWS weather station is utilised to describe antecedent rainfall conditions of the past 15 days. Rainfall forecasts for the next 20 h are extracted from regionalised climate modelling results of COSMO-DE for the grid cell containing Lichtenstein-Unterhausen. The combination of antecedent precipitation and forecasted rainfall is then compared to defined threshold values. Five preliminary thresholds values were determined (Table 6.9) using Chleborad et al. (2006) as a reference.

The regional early warning system is also connected to alarm sensors on the web-based ILEWS early warning platform. If any threshold is exceeded, an alarm sensor is activated and a notification is sent to the involved experts for evaluation of the current situation. More information on the actual early warning procedure is provided in chapter. However, since no real-time rainfall forecasts were available for this study, early warnings only have a hypothetical character and the alarm sensor is currently disabled.

6.2.3.1 Discussion

The developed regional landslide early warning system represents a prototype application which can not issue realistic warning at the current state due to the lack of real-time rainfall forecasts. The technical system however, can be used for realistic early warnings, once real-time rainfall forecasts become available.

Rainfall thresholds currently implemented in the regional early warning model are determined in reference to the values proposed by Chleborad et al. (2006). However, threshold values can easily be modified in the web-based warning platform (see Chap. 7) once more results become available.

In its current layout, the regional warning system accounts for the Lichtenstein-Unterhausen area. Extension of the system to the entire Swabian Alb region as a fully-fledged regionalised early warning model can be based upon the prototype developed in this thesis. Further developments could also include spatially varying rainfall thresholds once these are investigated in more detail.

References

Aslan AM, Burghaus S, Li L, Schauerte, W, Kuhlmann H (2010) Bewegungen an der Oberfläche. In: Bell R, Pohl J, Glade T, Mayer J, Greiving S (eds) Integrative Frühwarnsysteme für gravitative Massenbewegungen (ILEWS) Monitoring, Modellierung, Implementierung. Klartext, Essen, Germany, p 74

Bear J (1972) Dynamics of fluids in porous media. Dover, New York

Bell R (2007) Lokale und regionale Gefahren- und Risikoanalyse gravitativer Massenbewegungen an der Schwäbischen Alb. University of Bonn, Germany

Bell R, Thiebes B (2010) Untergrundbewegungen. In: Bell R, Pohl J, Glade T, Mayer J, Greiving S (eds) Integrative Frühwarnsysteme für gravitative Massenbewegungen (ILEWS) Monitoring, Modellierung, Implementierung. Klartext, Essen, Germany, p 84

Bell R, Wiebe H, Krummel H (2010) Vorerkundung. In: Bell R, Pohl J, Glade T, Mayer J, Greiving S (eds) Integrative Frühwarnsysteme für gravitative Massenbewegungen (ILEWS) Monitoring, Modellierung, Implementierung. Klartext, Essen, Germany, p 62

Brennecke M (2006) Erstellung einer Inventarkarte gravitativer Massenbewegungen an der Schwäbischen Alb—Kartierung aus Luftbildern und einem digitalen Höhenmodell. University of Bonn, Germany

Caine N (1980) The rainfall intensity: duration control of shallow landslides and debris flows. Geografiska Annaler. Ser A Phys Geogr 62(1/2):23–27. Accessed 18 Oct 2010

Chleborad AF, Baum RL, Godt JW (2006) Rainfall thresholds for forecasting landslide in the seattle. Area—exceedance and probability. U.S. Geological Survey Open File Report, Washington, pp 2006–1064

Guzzetti F, Peruccacci S, Rossi M, Stark CP (2008) The rainfall intensity–duration control of shallow landslides and debris flows: an update. Landslides 5(1):3–17

Jäger S, Paulsen H, Mayer C, Huber B, Dietz R, Greve K, Camek T (2010) Informationstechnik in der Frühwarnmodellierung. In: Bell R, Pohl J, Glade T, Mayer J, Greiving S (eds) Integrative Frühwarnsysteme für gravitative Massenbewegungen (ILEWS) Monitoring, Modellierung, Implementierung. Klartext, Essen, Germany, pp 155–179

Kallinich J (1999) Verbreitung, Alter und Ursachen von Massenverlagerungen an der Schwäbischen Alb auf der Grundlage von geomorphologischen Kartierungen. In: Bibus E, Terhorst B (eds) Angewandte Studien zu Massenbewegungen. Tübinger Geowissenschaftliche Arbeiten. pp 59–82

Kohn J-C (2006) Potenzial der Auswertung des Archivs der Straßenbauverwaltung für die Risikoforschung—Nutzung des Archivs der Baustoff und Bodenprüfstelle Ludwigsburg als historische Quelle. University of Bonn, Germany

Kruse JE (2006) Untergrunderkundung und Monitoring von gravitativen Massenbewegungen mit Gleichstromgeoelektrik und Radiomagnetotellurik. University of Bonn, Germany

Ohmert W, Von Koenigswald W, Münzing K, Villinger E (1988) Erläuterungen zu Blatt 7521 Reutlingen (Geologische Karte 1:25.000 von Baden Württemberg). Geologisches Landesamt Baden-Württemberg

Röhrs M, Dix H (2010) Rekonstruktion historischer Ereignisse. In: Bell R, Pohl J, Glade T, Mayer J, Greiving S (eds) Integrative Frühwarnsysteme für gravitative Massenbewegungen (ILEWS) Monitoring, Modellierung, Implementierung. Klartext, Essen, pp 46–61

Saxton KE, Rawls WJ (2006) Soil water characteristic estimates by texture and organic matter for hydrologic solutions. Soil Sci Soc Am J 5(70):1569–1578

Scheffer F, Schachtschabel P (2009) Lehrbuch der Bodenkunde, 15th edn. Spektrum Akademischer Verlag, Stuttgart, Germany

Wiebe H, Krummel H, Camek T, Thiebes B (2010) Kombinierte Auswertung der Bodenfeuchte. In: Bell R, Pohl J, Glade T, Mayer J, Greiving S (eds) Integrative Frühwarnsysteme für gravitative Massenbewegungen (ILEWS) Monitoring, Modellierung, Implementierung. Klartext, Essen, pp 116–129

Chapter 7
Integrative Early Warning

Local and regional early warning models developed in this thesis forecast future landslide behaviour and are embedded into the integrative landslide early warning system elaborated by the ILEWS project. In the following, the web-based information and warning platform, as well as the process of transformation of alarm notifications into early warnings are presented. More detailed descriptions are provided by (Jäger et al. 2010; Mayer and Pohl 2010), respectively. Since the developed early warning chain is a result of the cooperative risk management and communication carried out in the ILEWS project, additional information on the challenges of the integration of early warning systems into the social and administrative framework and decision making processes are summarized.

The main goal of the web-based platform is to store and visualise monitoring and modelling results based on standardised geo-data services to ensure interoperability. In addition, notifications to experts are provided in case pre-defined alarm thresholds are exceeded, which then can lead to an early warning. The GIS-based visualisation of real-time monitoring data is managed by a complex geodata infrastructure described in detail by (Jäger et al. 2010). Latest measurements can be viewed by hovering the mouse over the sensor on a map (Fig. 7.1).

Several settings can be changed for data analysis. For the automated inclinometer, these include analysed time-frame, scale of visualised data, and also direct comparison to hydrological monitoring results.

Similar visualisation capabilities are implemented for all continuously and periodically measured monitoring data. Single and groups of hydrological sensor records can be visualised and directly compared to climate data from the ILEWS weather station. Geoelectrical monitoring data can be displayed for single or groups of measurement points. In addition, resistivity pseudo-sections with a time-lapse function can be computed. Movement data from periodic tachymetry and inclinometer measurements in the form of interactive maps but can also be downloaded for further analysis. Furthermore, the CHASM early warning and decision-support systems are implemented on the ILEWS platform. For quick evaluation of the current situation, a status control system was set-up illustrated in Fig. 7.2.

B. Thiebes, *Landslide Analysis and Early Warning Systems*, Springer Theses,
DOI: 10.1007/978-3-642-27526-5_7, © Springer-Verlag Berlin Heidelberg 2012

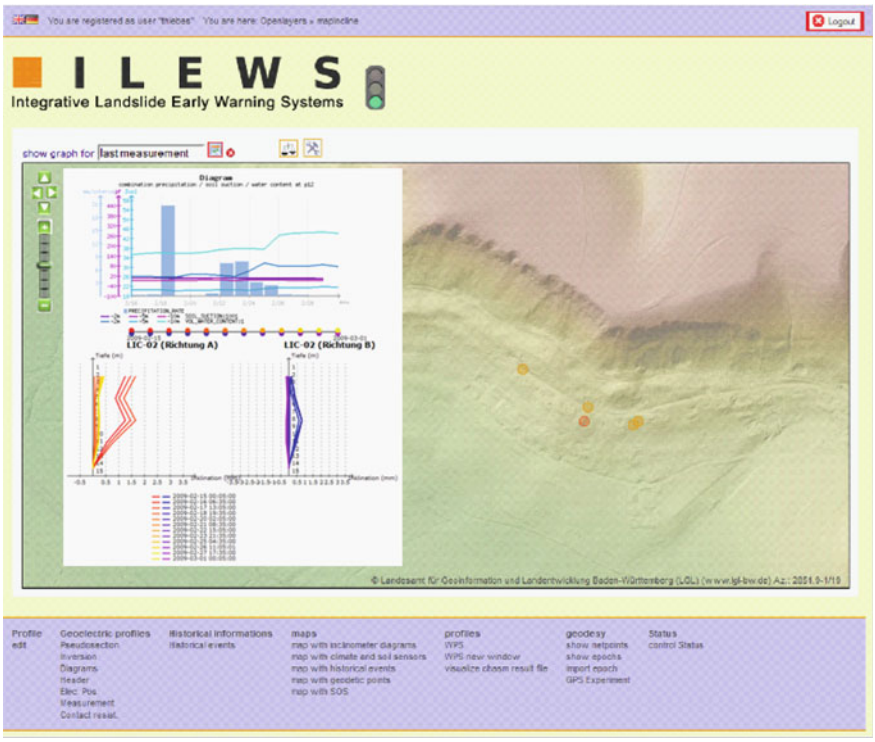

Fig. 7.1 Web-based visualisation of real-time inclinometer monitoring data and comparison to monitoring results

Alarm thresholds are implemented for each continuously measuring sensor in the field, accounting for changes of measurement values for varying time periods (Fig. 7.2a). Additional alarm thresholds are implemented for the CHASM early warning model, and regional rainfall thresholds. Latest measurements are compared to threshold values and displayed as an alert level (Fig. 7.2b). In addition, the current status of the alarm thresholds is visualised as coloured alert lights (Fig. 7.2c), which change from green to yellow if a pre-defined threshold is exceeded. Ultimately, the alarm thresholds influence the three-coloured early warning signal light (Fig. 7.2d).

The ILEWS landslide early warning system was set up as an expert system, in which registered users can only view the data, but only experts can edit the system and for example modify thresholds values, adjust frequency of measurements and change the early warning level. The current early warning level of the signal light is controlled by a procedure illustrated in Fig. 7.3.

As long as real-time measurements are below alarm thresholds, the signal light is on a green level, indicating that no critical situation is expected. Once an alarm threshold is exceeded, respective alarm senor and the early warning signal light

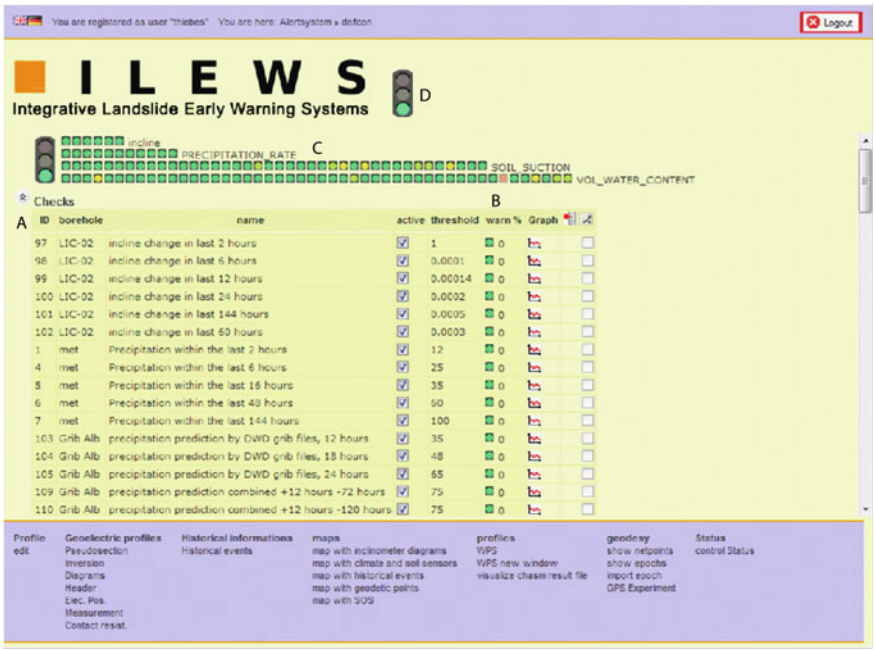

Fig. 7.2 Status control of real-time measurements with alarm thresholds (**a**), alert level (**b**), alert sensors (**c**) and early warning signal (**d**)

change to yellow. Simultaneously, SMS and emails are sent to the involved experts (e.g. scientists) and registered users (e.g. local and regional administration, local population, media), informing that a pre-defined monitoring or modelling threshold has been exceeded. Experts are requested to check the situation and decide whether the situation is potentially dangerous or a false alarm. Depending on the experts' decision, the early warning signal light is either set back to green, or upgraded to red. Red early warning level is directly followed by automated messages with action advises to registered users and emergency forces are informed by the experts.

The ILEWS early warning chain is the result of cooperative risk assessment and communication with local and regional stakeholders and was developed during several discussions and round-table meetings to ensure the early warning system is optimised to the end-users (Mayer and Pohl 2010). The local community represented by the local administration and the mayor were the first potential end-user interviewed about the demands towards a landslide early warning system. On a local level however, landslide hazards and early warning are of low interest partly due to the administrative framework which regulates the responsibilities between local, regional and national political entities. At the current state, the situation in the local study is not regarded an imminent hazard but only as potentially dangerous (*Gefahrenverdacht*) for which the political framework does not foresee any

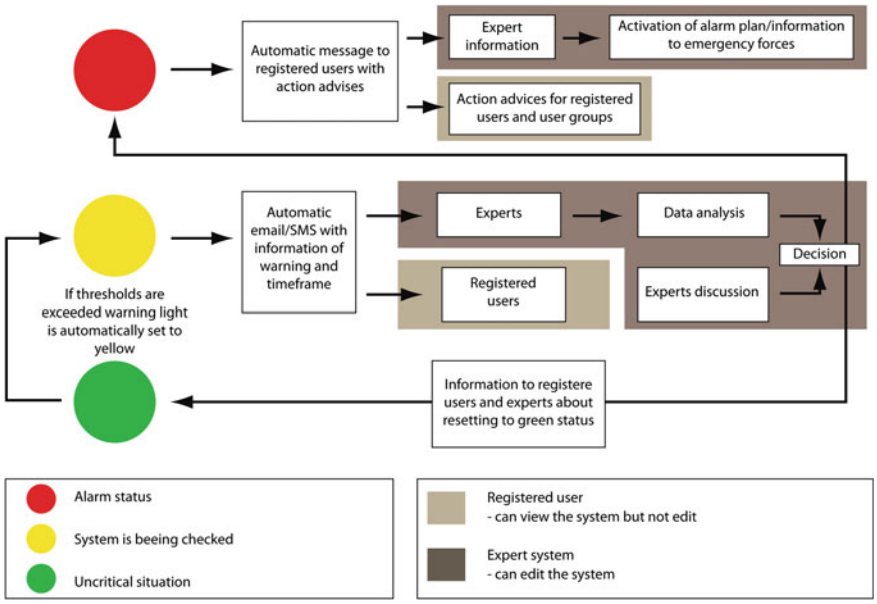

Fig. 7.3 Signal light (after Mayer and Pohl 2010)

compulsory actions. The local administration has no interest in detailed visualisation of monitoring data and other scientific products. Instead, only short information is required in case any emergency actions have to be initiated. Therefore, management of the landslide early warning system can not be undertaken by local administration, but has to be embedded into higher-level institution responsible for civil protection.

Round-table meetings with regional decision-makers included three administrative levels which share responsibilities for risk management of natural hazards including landslides. Early warning however, is not directly integrated into the federal system of Baden-Württemberg and the other federal states of Germany. On the lowest regional level of civil protection (*Untere Katastrophenschutzbehörde*) the district office (*Landratsamt*) is factually responsible and carries out measures in cooperation with specialist authorities (*Fachämter*), e.g. geological survey. The local community only acts as a connecting authority between local population and regional decision-makers. On the medium level (*Obere Katastrophenschutzbehörde*) the regional councils (*Regierungspräsidien*) deals with civil protection issues affecting technical infrastructure and for affairs which exceed the lowest level responsibilities. On the highest level (*Oberste Katastrophenschutzbehörde*), the Ministry of Interior of the federal state Baden-Württemberg is responsible for planning of civil protection measures; localised phenomena such landslides however, do not play an important role for this agency. None of the regional stakeholders responsible for civil protection and risk management of natural hazards wanted to be in charge of the developed early warning system and act as the managing expert. However, each authority named

other agencies, which to their position were dedicated to fulfil the role of the expert. These results show that the inexplicit administrative and political structures of responsibilities hinder an effective application of landslide early warning systems. Successful integration of landslide early warning into the decision-making process therefore requires modifications of the political framework in Baden-Württemberg to ensure responsibilities are clearly defined.

References

Jäger S, Paulsen H, Mayer C, Huber B, Dietz R, Greve K, Camek T (2010) Informationstechnik in der Frühwarnmodellierung. In: Bell R, Pohl J, Glade T, Mayer J, Greiving S (eds) Integrative Frühwarnsysteme für gravitative Massenbewegungen (ILEWS) Monitoring, Modellierung, Implementierung. Klartext, Essen, pp 155–179

Mayer J, Pohl W (2010) Risikokommunikation. In: Bell R, Pohl J, Glade T, Mayer J,Greiving S (eds) Integrative Frühwarnsysteme für gravitative Massenbewegungen (ILEWS) Monitoring, Modellierung, Implementierung. Klartext, Essen, pp 180–202

Chapter 8
Discussion

During the monitoring campaign, small slope movements have been recorded by surface and subsurface measurements which are extremely-slow according to the definition by Cruden and Varnes (1996). In particular with regard to inclinometer Lic02, these displacements can be interpreted as a continuation of the displacement previously described by Bell (2007). In contrast to this earlier study, the research described in this thesis could employ geodetic measurements carried out by Aslan et al. (2010a) for interpretation of large scale movement trends.

According to geodetic monitoring, three blocks of similar movement trends can be distinguished: relatively large downslope movements in the eastern part, relatively low displacements rates in the middle part, and alternating movement directions in the western part. These movement trends are partly affirmed by inclinometer measurements. Exact boundaries of current landslide displacement, however, can not be determined. Still, geodetic measurements lack fixed points outside the potential landslide which limits their informative power.

Most important landslide movement data was recorded at inclinometer Lic02, and in particular by manual measurements. Two depths of seasonally varying slope displacements can be observed: a deep seated sliding occurring in 15.5 m depth in spring, and a flow-like movement in 8.5 m depth in summer and autumn. The latter movements are also recorded by other inclinometers, however, deep-seated sliding can not be assessed due to the positioning above stable bedrock. When taking into account all manual measurements of inclinometer Lic02, it seems as the shallower displacement gradually transformed into a more slide-like movement, possibly indicating the progressive development of a shear surface.

While manual inclinometer measurements provide superior data on spatial distribution of movements, temporal resolution is higher for the automated inclinometer chain. However, the deep-seated movement is not appropriately detectable with the inclinometer chain due to the position of the lowest sensor. During the monitoring campaign, no distinct accelerations phases could be observed. Such continuous low displacements rates can possibly be interpreted as secondary creep as described by Okamoto et al. (2004) and Petley et al. (2005a, b, 2008), in which

B. Thiebes, *Landslide Analysis and Early Warning Systems*, Springer Theses,
DOI: 10.1007/978-3-642-27526-5_8, © Springer-Verlag Berlin Heidelberg 2012

diffuse micro-cracks develop. Therefore, an increase of movement speed during a tertiary creep phase is a potential future scenario, which should be controlled by continued monitoring. In particular, the inclinometer chain is of great value for this task since notifications by the ILEWS early warning system are provided if displacement thresholds are exceeded. In addition, continued monitoring could provide the data required to improve definition of triggering conditions.

The hydrological monitoring by tensiometers, TDR and geoelectrical monitoring provided indications for preferential flow paths leading to a quick rise of water content in great depths at the damaged house, i.e. monitoring site p12. This is not surprising given the heterogenic subsurface conditions documented by the drillings. Even though no direct contribution of preferential flow to slope instability can be appointed, it is likely that some effect is present given the recorded displacements in inclinometer Lic02 and the crack development at the house. Further investigations are necessary to assess the influence of preferential flow paths since they are important for slope stability and should be integrated into early warning (Uchida 2004). In particular, geoelectrical monitoring could aid to estimate the complex subsurface hydrological processes. Unfortunately, hydrological monitoring data could not be analysed in full detail by Wiebe and Krummel (2010) and Wiebe et al. (2010) due to limited resources.

With regard to these results, the first research question, *How does slope hydrology contribute to the reactivation of landslide movements*?, can not easily be answered. Without any periods of pronounced slope movement, preferably larger than error margin of the monitoring equipment, no exact triggering conditions can be determined. Instead, only broad statements on hydrological influence on slope stability can be made, for example that some correlation between snow melting in spring and deep-seated sliding exist.

The generation of a subsurface model aimed to describe real surface and subsurface conditions as realistic as possible to facilitate slope stability and early warning modelling with CHASM. In general, a good approximation of real conditions could be achieved even though subjective interpretation was required at some points of the applied methodology. For estimation of slope debris thickness, for example, the drillings by Ohmert (1988) provided accurate data for some points and were interpolated to the entire study area based on relative slope positions. Similarly, estimation of landslide deposit thickness from seismic prospection data included personal judgment but greatly enhanced representation of real conditions. Topographic analysis for the lower landslide deposits significantly improved the subsurface model. Geotechnical parameters estimated from literature sources provided good initial information on the possible range of real values. Subsequent sensitivity analysis helped to assess the influence of the parameters and allowed for calibration of CHASM stability calculation.

Based on the available information from drillings and the interpretation of seismic prospection data, the slope debris layer could not further be distinguished. Still, drill demonstrated heterogenic subsurface conditions which in reality can not be assumed to behave uniformly. In particular in terms of hydrological conditions, this is a significant simplification of real conditions. Still, preferential flow paths as

indicated by hydrological monitoring data, for example, cannot be accommodated within the current simulation approach implemented in CHASM.

Results of CHASM analysis show a generally low stability for the entire slope profile along the damaged house, with the lowest stability occurring in the upper slope sections, thus indicating a potential slope failure similar to the medium-age landslide located in the western part of the study area. Drill cores from borehole Lic05 provided some indication for the existence of a potential shear surface in the upper slope area; however, to verify this assumption, continued monitoring or the installation of additional inclinometers, preferably stably fixed into the bedrock is required. Still, it should also be questioned if additional costly installations are justified in regard to the extremely-slow displacement recorded over the last 6.5 years. From a scientific point of view, an extended monitoring system could not only facilitate the understanding of the processes occurring at the slope under investigation in this thesis, but also provide important information regarding slow moving slopes in the Swabian Alb in general.

According to CHASM simulations, shear surfaces are most likely positioned at the boundary of slope debris and the bedrock below. In contrast, shear surfaces also including the bedrock material have a significantly higher FoS and are therefore less probable. A shear surface position at the bedrock interface reflects a deep-seated sliding, similar to the movements recorded in approximately 15.5 m at inclinometer Lic02. The shallower displacement measured at this location, which also shows characteristics of a flowing movement, cannot be simulated by CHASM due to the limitations of the limit-equilibrium method. Future applications of dedicated simulation models, for example finite-element software, could provide more insights into the displacement process. Some promising initial tests have already been carried out by Aslan et al. (2010b) and further research is currently being performed.

Two CHASM-based applications were developed to address the second research question: *How can physically-based slope stability models be applied in landslide early warning*?

With the CHASM early warning model slope stability is continuously simulated based on current groundwater conditions and measured and forecasted rainfall. Sensitivity analysis of CHASM provided some interesting results regarding the influence of rainfall events which is also important for subsequent modelling of early warning. Surprisingly, rainfall distribution and rainfall intensity have a very low influence on slope stability calculation which limits the predictive power of the CHASM early warning model. Possibly, further adjustment of CHASM parameters could increase the sensitivity to rainfall; however, this would preferably require a distinct onset of displacement to be able to appropriately validate the input data. In its current state of development, the notification service can only issue hypothetic early warnings since real-time rainfall forecasts are not available. However, if these became accessible, the technical system could easily be adjusted. Nevertheless, the developed CHASM early warning application is a prototype with a high potential for the further applications.

The second CHASM application for the use in the context of early warning is a decision-support tool for quick calculation of slope stability without time-consuming elaboration of a slope profile and the respective shear surface parameters. In addition, the effect of a variety of input data can be tested which is a significant improvement in comparison to the standard single profile analysis. The integrated shear surface search routine effectively concentrates search procedure to the upper slope areas which are the most landslide prone areas according to CHASM simulations. However, the decision-support system represents a prototype development which does not include all capabilities of CHASM and cannot replace more detailed investigations. Overall, the ability to quickly initiate CHASM simulations for freely-selectable slope profiles has great potential for future applications.

Available landslide inventories for the Swabian Alb contain several hundred landslide events with the earliest records dating back to the Fifteenth century. However, estimation and verification of rainfall thresholds can not in all cases benefit from this data since the exact day of initiation and the triggering agents are not accounted for. Still, landslide inventories are essential data sources for other research objectives besides early warning, for example determination of geomorphological activity, landslide hazard and risk management, and spatial planning in general. Therefore, efforts for recording of landslide events and investigation of available data sources should be continued and increased in the future.

With the limited number of dated landslide events it was not tried to determine rainfall thresholds for the Swabian Alb, but to verify the applicability of thresholds proposed in the literature. Comparison of landslide events to intensity-duration and cumulative rainfall thresholds was carried out for all events for which the date of initiation was recorded, and regionalised climate data was available. For some landslide events, the exact date of occurrence was unknown but could be ascertained by assuming potential triggering dates. In general, tested intensity-duration and cumulative rainfall threshold performed satisfactorily and affirm the applicability of such an approach in the Swabian Alb. Still, not all landslides can be explained by the applied rainfall thresholds and subsequently early warning cannot be expected to be able to predict all future slope failures.

The importance of snow melting for the initiation of slope failures in the Swabian Alb is demonstrated by the temporal clustering of landslide events in spring. In addition, the integration of snow melting into verification of rainfall thresholds was able to explain some of the landslide events, which could not have been predicted by rainfall alone.

The technical regional early warning system implemented by Jäger et al. (2010) employs preliminary rainfall thresholds which can be expected to be able to predict the majority of landslide events. Once more appropriate threshold values become available alarm levels can easily be modified on the web-based warning platform. In its current state, early warnings are only hypothetical since no real-time rainfall forecasts are available; still, from a technical point of view, the

system is capable of providing notifications to the experts in charge. However, before realistic early warnings can be issued, decision-makers have to define the desired warning levels in regard to possible false alarms and missed warnings. The regional early warning system has a great potential for a transfer to larger areas. By relatively small modifications, the early warning system could be developed into a fully-fledged regional system accounting for spatially varying threshold values, similar to the system in Hong Kong.

Based on the presented threshold verification and the implemented regional landslide early warning prototype, the research question raised in the beginning—*Are landslide triggering rainfall thresholds applicable to regional early warning in the Swabian Alb*?—can be answered in the affirmative.

References

Aslan AM, Burghaus S, Li L, Schauerte W, Kuhlmann H (2010a) Bewegungen an der Oberfläche. In: Bell R, Pohl J, Glade T, Mayer J, Greiving S (eds) Integrative Frühwarnsysteme für gravitative Massenbewegungen (ILEWS) Monitoring, Modellierung, Implementierung. Klartext, Essen, Germany, pp 74–84

Aslan AM, Schauerte W, Kuhlmann H (2010b) Empirisches Frühwarnmodell. In: Bell R, Pohl J, Glade T, Mayer J, Greiving S (eds) Integrative Frühwarnsysteme für gravitative Massenbewegungen (ILEWS) Monitoring, Modellierung, Implementierung. Klartext, Essen, pp 140–150

Bell R (2007) Lokale und regionale Gefahren- und Risikoanalyse gravitativer Massenbewegungen an der Schwäbischen Alb. University of Bonn, Germany

Cruden DM, Varnes DJ (1996) Landslide types and processes. In: Turner AK, Schuster RL (eds) Landslides: Investigation and mitigation (Special Report). Washington, D.C., USA: National Research Council, Transportation and Research Board Special Report 247, Washington, D.C., USA, pp 36–75

Jäger S, Paulsen H, Mayer C, Huber B, Dietz R, Greve K, Camek T (2010) Informationstechnik in der Frühwarnmodellierung. In: Bell R, Pohl J, Glade T, Mayer J, Greiving S (eds) Integrative Frühwarnsysteme für gravitative Massenbewegungen (ILEWS) Monitoring, Modellierung, Implementierung. Klartext, Essen, pp 155–179

Ohmert W, Von Koenigswald W, Münzing K, Villinger E (1988) Erläuterungen zu Blatt 7521 Reutlingen (Geologische Karte 1:25.000 von Baden Württemberg). Geologisches Landesamt Baden-Württemberg

Okamoto T, Larsen JO, Matsuura S, Asano S, Takeuchi Y, Grande L (2004) Displacement properties of landslide masses at the initiation of failure in quick clay deposits and the effects of meteorological and hydrological factors. Eng Geol 72(3–4):233–251

Petley DN, Higuchi T, Dunning S, Rosser NJ, Petley DJ, Bulmer MH, Carey J (2005a) A new model for the development of movement in progressive landslides. In: Hungr O, Fell R, Couture R, Eberhardt E (eds) International conference on landslide risk management. Taylor & Francis, Vancouver, pp 350–358

Petley DN, Higuchi T, Petley DJ, Bulmer MH, Carey J (2005b) Development of progressive landslide failure in cohesive materials. Geology 33(3):201–204

Petley DN, Petley DJ, Allison RJ (2008) Temporal prediction in landslides–understanding the Saito effect. In: Chen Z, Zhang J-M, Ho K, Wu F-Q, Li Z-K (eds) Landslides and engineered slopes: from the past to the future. Taylor & Francis, Xi'an, pp 794–800

Uchida T (2004) Clarifying the role of pipe flow on shallow landslide initiation. Hydrol Process 18(2):375–378

Wiebe H, Krummel H (2010) Bodenfeuchte (Geoelektrik). In: Bell R, Pohl J, Glade T, Mayer J, Greiving S (eds) Integrative Frühwarnsysteme für gravitative Massenbewegungen (ILEWS) Monitoring, Modellierung, Implementierung. Klartext, Essen, pp 100–116

Wiebe H, Krummel H, Camek T, Thiebes B (2010) Kombinierte Auswertung der Bodenfeuchte. In: Bell R, Pohl J, Glade T, Mayer J, Greiving S (eds) Integrative Frühwarnsysteme für gravitative Massenbewegungen (ILEWS) Monitoring, Modellierung, Implementierung. Klartext, Essen, pp 116–129

Chapter 9
Perspectives

The results of this thesis raise new questions for future investigations in the Swabian Alb in general and in particular for the landslide in Lichtenstein-Unterhausen. In addition, some refinements could improve local and regional early warning applications and their landslide forecasting capabilities. In the following, potential improvements are presented, and the prospects for a transfer of the developed early warning applications and the ILEWS warning system in general are discussed.

On a local scale, a continuation and expansion of the slope monitoring system could improve the understanding of slope hydrology and the process of landslide reactivation. In particular additional inclinometers installed into stable bedrock could help to define the boundaries of measured slope displacements and enhance the subsurface model. The integration of fixed points outside the landslide area in tachymetry measurements could enable a more accurate interpretation of large scale movement trends and the verification of possible deep-seated displacement for inclinometers Lic04 and Lic05. Definition of distinct triggering condition requires the continuation of measurements, in particular by the automated inclinometer. Results of hydrological monitoring indicate preferential flow paths in the area of the damaged house. Future research could install additional hydrological sensors to assess the characteristics of subsurface hydrology and the contribution to slope instability. Furthermore, geoelectrical monitoring data has not been analysed in full detail and could aid understanding of subsurface hydrology. Moreover, the application of hydrological simulation software could improve the interpolation of groundwater conditions for subsequent stability modelling. Possibly, analysis of chemical properties of groundwater composition could provide interesting insights and help to predict future accelerations.

Early warning modelling with CHASM could benefit from an improved subsurface representation and more detailed study in groundwater table positions. The application of designated models, for example the Sloping Local base Level approach (Jaboyedoff et al. 2004) could improve the approximation of the subsurface morphology. Hydrological simulation models could be used to create more realistic and sophisticated groundwater scenarios for subsequent modelling.

B. Thiebes, *Landslide Analysis and Early Warning Systems*, Springer Theses,
DOI: 10.1007/978-3-642-27526-5_9, © Springer-Verlag Berlin Heidelberg 2012

In addition, shear tests and more complex hydrological laboratory tests of soil samples could improve the overall performance of slope stability simulation. CHASM capabilities not tested in this study, such as Janbu's non-circular shear surface methodology could potentially enhance simulation of landslide behaviour. Furthermore, other physically-based landslide simulation models could be applied on the slope in Lichtenstein-Unterhausen. In particular finite-elements models could help to understand the processes of landslide movement reactivation. It would also be interesting to see how other landslide simulation models perform in early warning systems.

The CHASM early warning procedure would benefit from the integration of real-time rainfall forecasts instead of historic records so that real warnings can be issued. In addition, the integration of snow melting could increase the accuracy of slope stability predictions.

The transfer of the developed CHASM decision-support and early warning applications to other study areas are attractive prospects. Appropriate study areas should include deep-seated landslides with a known shear surface depth. Ideally, hydrological monitoring should be available to be able to estimate groundwater tables. However, the monitoring system could be significantly smaller if subsurface conditions are more homogeneous. To take full advantage of quick slope stability calculation capabilities of the developed CHASM decision-support system, an ideal study area would comprise similar slope morphologies within the focus area. For example slopes along roads or railway lines would be suitable for an effective application.

For future regional scale research on landslides, an improvement of the landslide inventory by further exploration of data sources currently not available to science is desirable. Therefore, ongoing recording of landslide events in addition to continued research in historic archives and media reports is required. The application of hydrological models could help to define triggering dates for landslides for which the exact date is unknown and thus provide the data needed for more sophisticated verification of rainfall thresholds.

In this work, a limited number of landslide triggering rainfall thresholds was analysed. Future investigations could possibly benefit from an examination of other threshold concepts; in particular approaches in which long-term conditions are integrated, for example taking into account mean annual precipitation or the antecedent soil water status. Also, deterministic models could be used to enhance determination of landslide triggering rainfall threshold, since these approaches have lower requirements regarding landslide inventory data (Terlien 1998).

The regional landslide early warning system would benefit from real-time weather forecasts which would enable to issue real early warnings. Prediction of landslide events could be enhanced by an automated integration of snow melting data into the regional early warning model. One of the most promising improvements of the regional landslide early warning application could be achieved by further development into a spatially distributed system similar to the system implemented in Hong Kong. Such a system could accommodate both regional and

local landslide triggering rainfall thresholds for which additional research is required.

A transfer of the developed regional landslide early warning procedure could be carried out with very little technical modifications. In particular the availability of rainfall forecasts with a high spatial and temporal resolution in the form COSMO-DE simulations could be used as the basis for further implementation of regional landslide early warning systems in central Europe. However, without additional studies on landside initiating rainfall thresholds, only generic alarm levels could be employed. In addition, warning thresholds had to be determined by cooperative discussions to meet the end-users requirements towards the early warning system.

Even though the technical feasibility of local and regional landslide early warning system in the Swabian Alb has been confirmed, effective early warning also requires integration into political and social structures. In the federal system of Germany, competences are currently not clearly defined and local and regional decision-makers are reluctant to overtake responsibilities for early warnings. It is therefore essential to inform policy makers about the benefits of early warning systems within integrative risk management strategies.

References

Jaboyedoff M, Baillifard F, Couture R, Locat J, Locat P, Rouiller J-D (2004) Toward preliminary hazard assessment using DEM topographic analysis and simple mechanic modeling. In: Lacerda W, Ehrlich M, Fontoura SAB, Sayao AS (eds) Landslides: evaluation and stabilization. Nineth International symposium on landslides. Balkema Publishers, Rio de Janeiro, Leiden, pp 191–197

Terlien MT (1998) The determination of statistical and deterministic hydrological landslide-triggering thresholds. Env Geol 35(2):124–130

Chapter 10
Summary

Landslides are among the most hazardous natural hazards and can have disastrous effects on society as demonstrated by recent large slope failures for example in China. In places, where landslide prone areas cannot be avoided or slopes cannot be stabilised, early warning systems can be a useful counter-measure to effectively protect the local population and also act as an integral element of risk management. Despite the common use of slope stability simulation software for landslide analysis and forecasting in geotechnical practice, landslide early warning systems rarely take full advantage of these models. Moreover, regional landslide early warning systems are mostly implemented as prototype applications even though necessary input data like quantitative rainfall forecasts and rainfall thresholds are widely available.

The main objectives of this thesis are the analysis of landslide characteristics and the subsequent development and implementation of local and regional early warning models in the Swabian Alb. In the local study area, a reactivated deep-seated landslide is equipped with an extensive monitoring system to investigate the contribution of slope hydrology to the process of displacement reactivation. A physically-based slope stability model is applied to simulate and forecast landslide behaviour and subsequently implemented as a decision—support and early warning model. On the regional scale, available landslide inventories are analysed and dated mass movements are compared to rainfall thresholds elaborated in other studies. Consequently, a prototypic early warning application is implemented based on the results.

The work is embedded in the ILEWS project, in which the entire early warning chain from the sensors in the field to user-optimised action advises is addressed.

Forecasting of slope failures, and in particular slow moving landslides is extremely difficult. For such processes, long phases of slow and steady displacements, frequently termed creep, can be observed prior to final failure. Changes of displacement rates may occur due to variations of hydrological conditions and progressive weakening of the soil material. Difficulties of landslide forecasting also arise from the complex nature of landslide processes, in which feedback

B. Thiebes, *Landslide Analysis and Early Warning Systems*, Springer Theses,
DOI: 10.1007/978-3-642-27526-5_10,

processes and non-linear behaviour hamper predictions. Landslide prediction usually employs thresholds of triggering factors such as rainfall. In particular thresholds accounting for rainfall characteristics such as intensity-duration have frequently been applied on a regional scale. A wide range of methods can be applied for landslide investigation and monitoring of hydrology and slope displacements and several simulation models are available for landslide modelling of which limit-equilibrium methods are possibly the most frequently applied. Effective early warning of landslides is not only a technical challenge but also requires integration into the society's political framework and processes of decision-making. A review on landslide early warning systems worldwide shows that most systems have prototypic character and that no simple best-practice approach is available. Landslide early warning systems for single slopes generally apply extensive monitoring systems of displacement and potential triggering factors to predict slope failure; or are implemented as post-event systems which issue an alarm once a landslide process has been initiated. In most cases, regional landslide early warning systems rely on rainfall measurement and forecasts which are compared to pre-defined threshold values.

The study area of this thesis is the lower mountain range of the Swabian Alb in southwest Germany, an area which is frequently affected by landslides. The region's geology consists of Jurassic, clays, marls and limestones, of which the latter form a steep escarpment (*Albftrauf*). In the local study area Lichtenstein-Unterhausen, a reactivated landslide body which has also been investigated in previous research projects, regularly causes cracking to a house.

A wide range of data was used in this study. On the local scale these include geological maps and drillings, geotechnical parameters from literature values, slope hydrology and movement monitoring data acquired within the ILEWS project. For regional scale analysis climate data and landslide inventories are the most important data sources.

Extensive field work including drillings, drill core extraction, and the installation of inclinometers and hydrological sensors were an essential part for the research carried out in this thesis, as well as for the ILEWS project. Data analysis included comparative examination of movement monitoring records in the form of tachymetry measurements, manual and automated inclinometers records. Hydrological data was analysed to investigate the response of slope hydrology to rainfall events. The deterministic limit-equilibrium software was CHASM used to simulate slope behaviour, and forecast future behaviour. Subsequently, two novel applications were developed for landslide decision-support and early warning. To facilitate landslide modelling, a general subsurface model combining geological data, drillings, results of geophysical prospection and geotechnical parameters was created by a step-wise and iterative GIS procedure. Groundwater scenarios were elaborated based on analysis of hydrological data and spatially interpolated for subsequent CHASM modelling. In addition, rainfall scenarios were generated using the KOSTRA atlas. Furthermore, a procedure was developed to control the automated shear surface search implemented within CHASM. Simulation of slope behaviour with CHASM investigated the influence of a variety of input parameters including

rainfall, groundwater, and geotechnical parameters during a sensitivity analysis. CHASM was subsequently implemented as an early warning model to continuously calculated slope stability. A CHASM decision-support system allowing for quick calculation of slope stability for freely selectable slope profiles was developed based on previously generated input data. On the regional scale, the applied methodology focussed on analysis of landslide inventories in the Swabian Alb to select slope failures appropriate for the verification of landslide initiating rainfall thresholds. Three intensity-duration and one cumulative rainfall thresholds were tested for their applicability in the Swabian Alb, based on regionalised climate data reflecting daily rainfall intensities and snow height. Subsequently, a regional early warning concept was developed, which was then technically implemented by Jäger et al. (2010).

Results of drill core analysis illustrate heterogenic subsurface conditions with an alternation of dense clays and sections of large limestone blocks. A hydrological monitoring system was installed including a total number of 27 tensiometers and TDR sensors located at nine locations in three different depths. In addition, two inclinometer pipes were installed and one automated inclinometer chain was put into an existing borehole. Tachymetry measurements carried out by Aslan et al. (2010) illustrate a maximum downslope movement of up to 8 mm, and variations of geodetic height of up to 1.2 cm. Extremely slow slope movements are also documented by inclinometer measurements; however, displacements are for most inclinometers still in the error margin. Inclinometer Lic02, which is fixed into stable bedrock recorded a total downslope displacement of approximately 1.5 cm in 6.5 years. Two displacement patterns can be observed: a sliding movement in 15.5 m depth in spring, and a flowing movement in 8.5 m depth occurring in late summer and autumn. Single dates or short periods of accelerated displacement cannot be determined based on the inclinometer chain data. Hydrological data illustrate seasonal variation of groundwater conditions and were estimated to vary between 1.3 and 6 m depending on location and season. In general, only small fluctuations and little response to rainfall events can be observed for the deepest hydrological sensors. However, at the monitoring site located at the damaged house strong peaks in hydrological data demonstrate quick percolation of precipitation. Similarly, geoelectrical data describes anomalous characteristics for this site during a period of strong snow melting. The subsurface model created combines several geological strata, limestone scree and mixed slope debris. Based on drillings and interpretation of seismic data, the thickness of the slope debris layer was estimated to reach maximum values of over 20 m for the landslide head area, and approximately 8 m for the lower deposits. Analysis of geotechnical parameter values in the literature for the materials present in the study area illustrates a very large range which was later partly tested during CHASM sensitivity analysis. The developed grid search routine is based on slope geometry and effectively focuses slope stability calculation on the upper slope areas. Rainfall scenarios created from KOSTRA account for normal, maximum and worst-case scenarios. Rainfall events have annual exceedance probabilities between 1 and 100 years and cover durations from 1 to 72 h. CHASM sensitivity analysis documents a linear influence of angle

of friction and cohesion for lower value range. Groundwater conditions have a strong influence on slope stability calculation. In contrast, rainfall intensities and rainfall distributions do only slightly affect the Factor of Safety (FoS). According to the results, a potential slope failure is most likely in the upper slope area where the FoS only slightly above unity. Computed shear surfaces are located at the interface of slope debris and the bedrock below. The developed CHASM early warning model combines monitored groundwater conditions with measured and forecasted rainfall to forecast future landslide behaviour. The CHASM decision-support represents an entirely web-based application based on the input data generated in this thesis. The user can chose a profile and select from various rainfall and groundwater conditions for calculation of slope stability. A total number of 29 appropriate landslide events were selected for regional verification of rainfall thresholds. Most landslide events exceeded two of the three tested intensity-duration and the cumulative rainfall threshold. The regional early warning procedure developed in this thesis and technically implemented by Jäger et al. (2010) employs rainfall threshold values in reference to the cumulative rainfall thresholds proposed by Chleborad et al. (2006).

The developed local and regional early warning applications are integrated into the web-based information and early warning platform implemented within the ILEWS project (Jäger et al. 2010). An early warning chain was elaborated (Mayer and Pohl 2010) in which experts can issue an early warning after being notified about the exceedance of pre-defined thresholds. However, the topic of early warning is not explicitly regulated in the political framework of Baden-Württemberg and responsibilities are not clearly defined, thus hindering the effective application of the developed system.

The installed monitoring system provides essential information on slope hydrology and also indicates the occurrence of preferential flow in the area of the damaged house. However, extremely slow slope movements showed no acceleration phase during the monitoring campaign which could be attributed to hydrological conditions. Continuous manual inclinometer measurements supply evidence for the transition from a flowing slope movement to a sliding process along a progressively developing shear surface.

Physically-based modelling of slope behaviour with CHASM based on a detailed representation of subsurface conditions showed only little response to rainfall events hindering forecasting of landslide prediction. Nevertheless, the developed CHASM early warning application represents a novel approach to landslide early warning in which a physically-based model is directly incorporated. In addition, the CHASM decision-support tool is a major advancement to the simulation model and allows quick assessment of stability for various slope profiles.

With the limited information available on landslide occurrences, only a small number of landslides events could be compared to rainfall threshold values. Still, tested rainfall thresholds performed satisfactorily and forecasting landslides can be expected to predict a large proportion of future landslide events. The developed regional landslide early warning application represents a prototype but demonstrates the feasibility of threshold-based early warning in the Swabian Alb.

Future research should include continuation of local slope monitoring and recording of landslide occurrences on a regional scale. Additional investigations are required to assess the contribution of preferential flow on slope instability and landslide reactivation in Lichtenstein-Unterhausen. The regional early warning system could be extended to a fully distributed regional system with very little efforts. Both landslide early warning applications developed in this thesis offer a great potential for a transfer to other study areas. In particular the CHASM decision-support system could be effectively used for landslide risk management for example along linear traffic lines such as roads and railway lines.

References

Aslan AM, Burghaus S, Li L, Schauerte W, Kuhlmann H (2010) Bewegungen an der Oberfläche. In: Bell R, Pohl J, Glade T, Mayer J, Greiving S (eds) Integrative Frühwarnsysteme für gravitative Massenbewegungen (ILEWS) Monitoring, Modellierung, Implementierung. Klartext, Essen, Germany, pp 74–84

Chleborad AF, Baum RL, Godt JW (2006) Rainfall thresholds for forecasting landslide in the Seattle. Washington, area—exceedance and probability. U.S. Geological Survey Open File Report 2006–1064

Jäger S, Paulsen H, Mayer C, Huber B, Dietz R, Greve K, Camek T (2010) Informationstechnik in der Frühwarnmodellierung. In: Bell R, Pohl J, Glade T, Mayer J, Greiving S (eds) Integrative Frühwarnsysteme für gravitative Massenbewegungen (ILEWS) Monitoring, Modellierung, Implementierung. Klartext, Essen, Germany, pp 155–179

Mayer J, Pohl W (2010) Risikokommunikation. In: Bell R, Pohl J, Glade T, Mayer J, Greiving S (eds) Integrative Frühwarnsysteme für gravitative Massenbewegungen (ILEWS) Monitoring, Modellierung, Implementierung. Klartext, Essen, Germany, pp 180–202

Erratum to: Landslide Analysis and Early Warning Systems

Benni Thiebes

Errata	Item or line	Corrections
Chapter 6	Fig. 6.7, p. 136	Replace Old Fig. 6.7 with New Fig. 6.7
Chapter 6	Fig. 6.18, p. 148	Replace Old Fig. 6.18 with New Fig. 6.18
Chapter 6	Fig. 6.19, p. 149	Replace Old Fig. 6.19 with New Fig. 6.19
Chapter 6	Fig. 6.20, p. 150	Replace Old Fig. 6.20 with New Fig. 6.20
Chapter 6	Fig. 6.21, p. 151	Replace Old Fig. 6.21 with New Fig. 6.21
Chapter 6	Fig. 6.22, p. 152	Replace Old Fig. 6.22 with New Fig. 6.22
Chapter 6	Fig. 6.23, p. 153	Replace Old Fig. 6.23 with New Fig. 6.23
Chapter 6	Fig. 6.24, p. 154	Replace Old Fig. 6.24 with New Fig. 6.24
Chapter 6	Fig. 6.25, p. 155	Replace Old Fig. 6.25 with New Fig. 6.25

B. Thiebes (✉)
Department of Geography and Regional Research, University of Vienna,
Universitaetsstrasse 7, 1010, Vienna, Austria

B. Thiebes, *Landslide Analysis and Early Warning Systems*, Springer Theses,
DOI: 10.1007/978-3-642-27526-5_11,

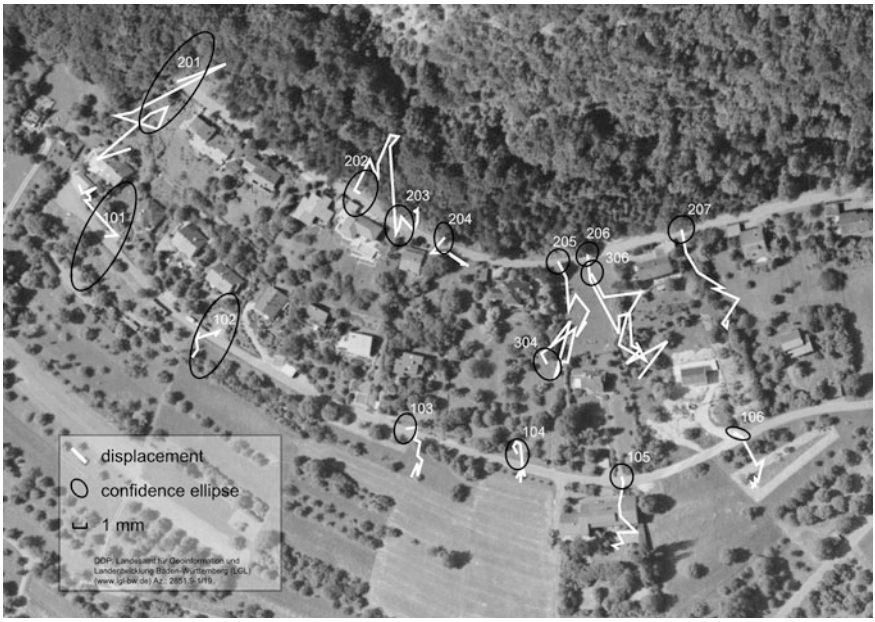

Fig. 6.7 Cumulative geodetic displacement measurement from nine epochs (after Aslan et al. 2010)

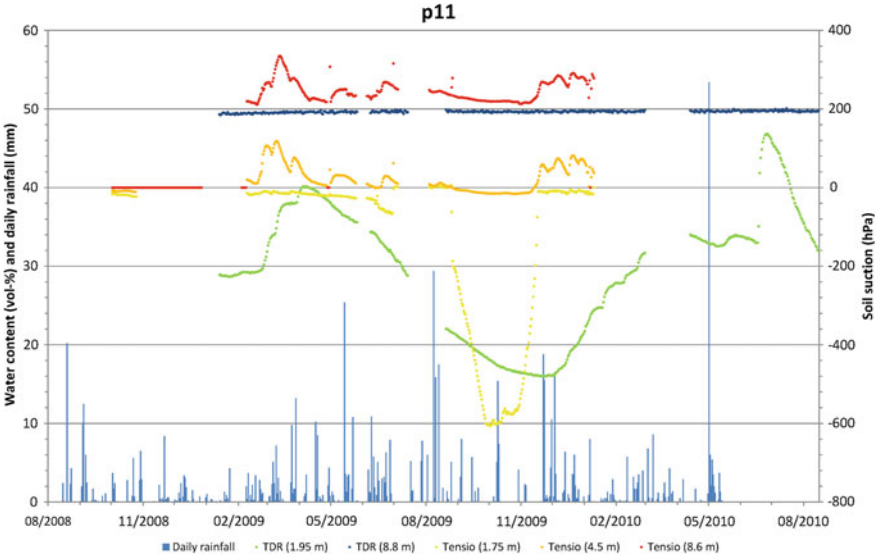

Fig. 6.18 Hydrological monitoring at location p11

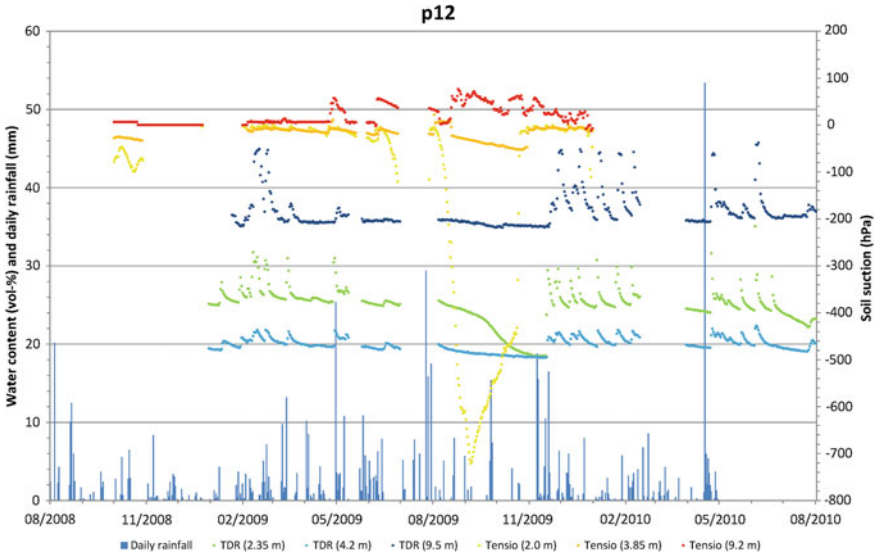

Fig. 6.19 Hydrological monitoring at location p12

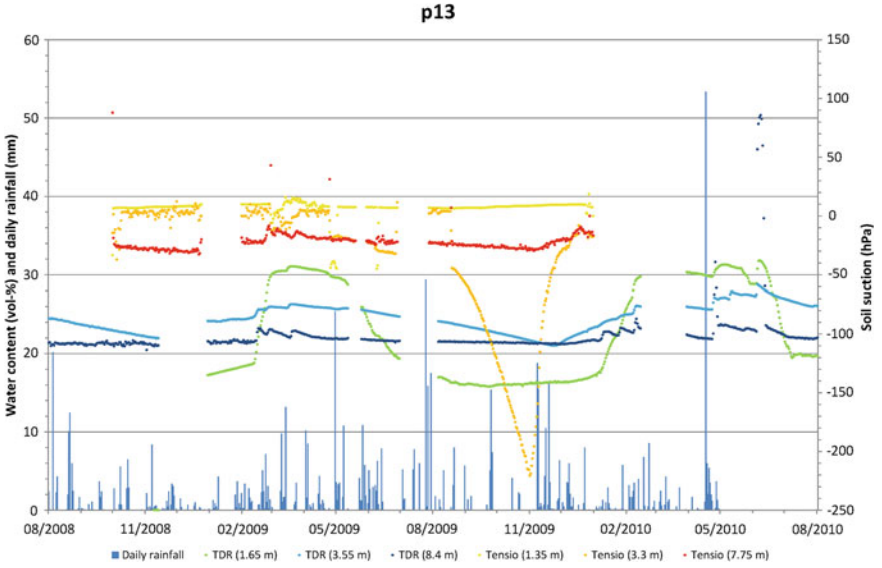

Fig. 6.20 Hydrological monitoring at location p13

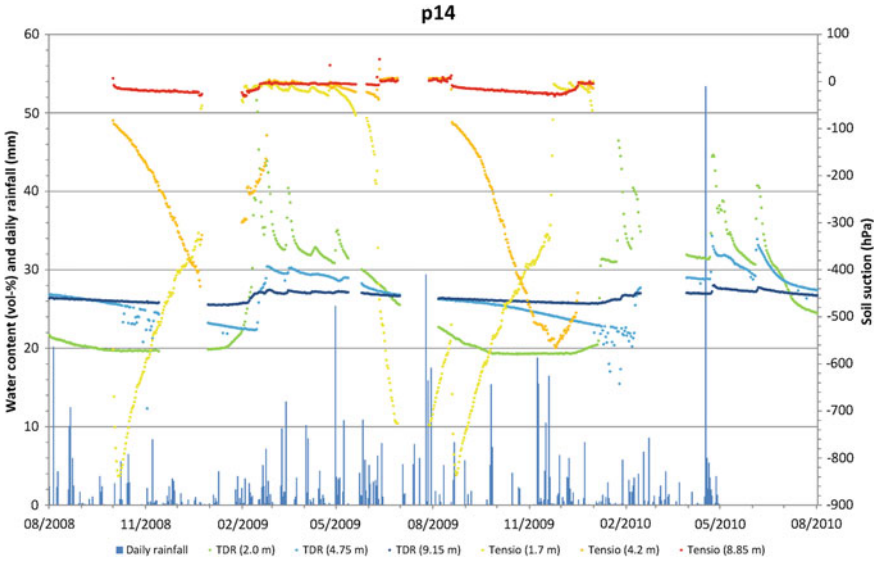

Fig. 6.21 Hydrological monitoring at location p14

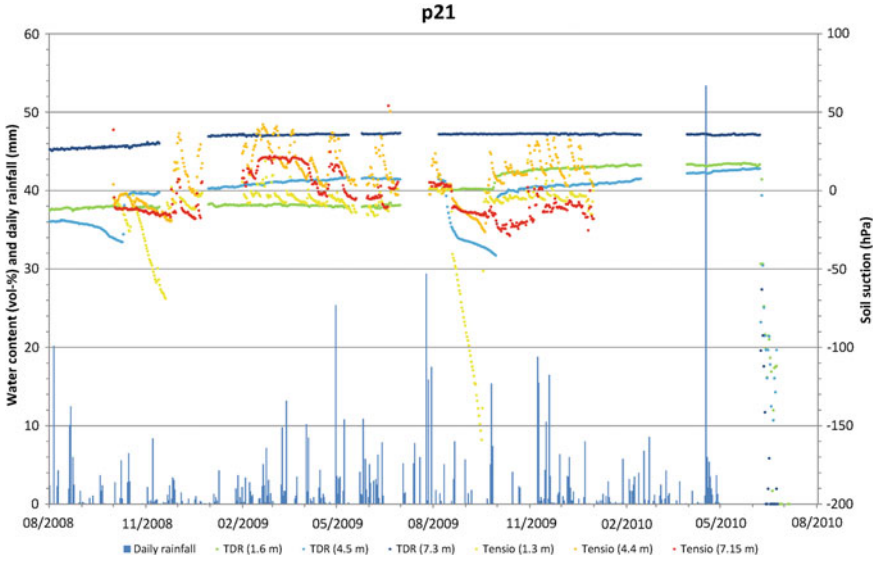

Fig. 6.22 Hydrological monitoring at location p21

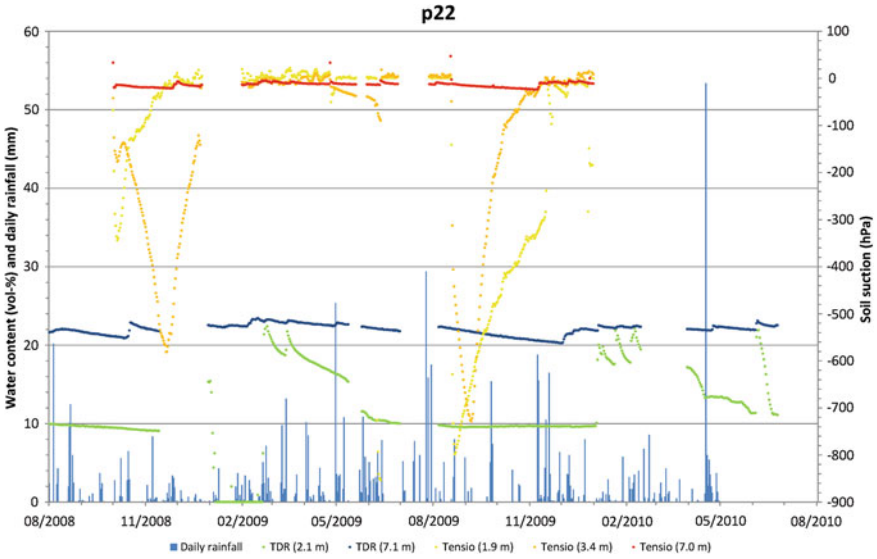

Fig. 6.23 Hydrological monitoring at location p22

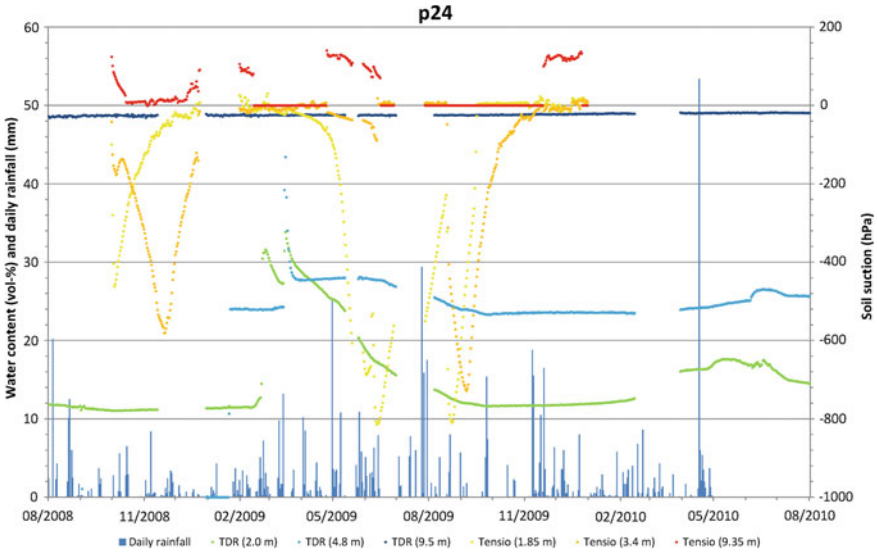

Fig. 6.24 Hydrological monitoring at location p24

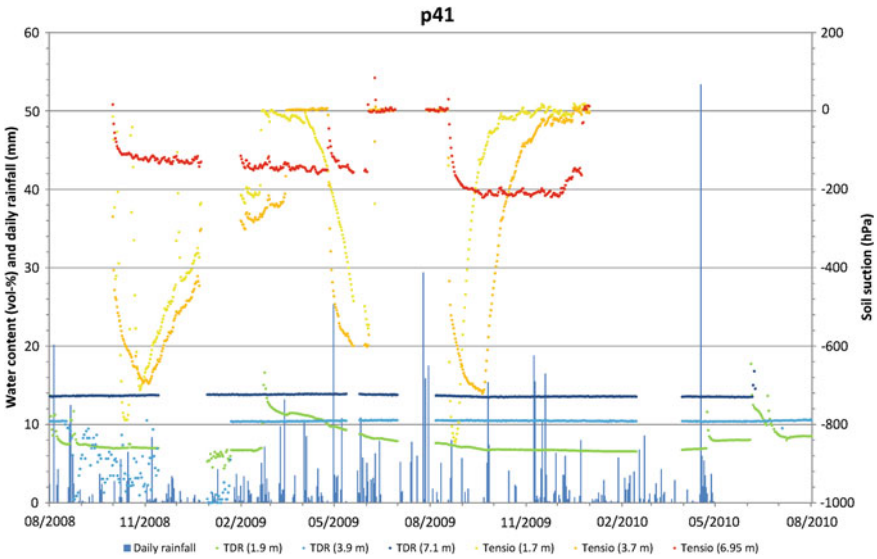

Fig. 6.25 Hydrological monitoring at location p41

Reference

Aslan AM, Burghaus S, Li L, Schauerte, W, Kuhlmann H (2010) Bewegungen an der Oberfläche. In: Bell R, Pohl J, Glade T, Mayer J, Greiving S (eds) Integrative Frühwarnsysteme für gravitative Massenbewegungen (ILEWS) Monitoring, Modellierung, Implementierung. Klartext, Essen, Germany, p 74

Appendix I
Borehole Plots for Lic04 and Lic05 Drillings

B. Thiebes, *Landslide Analysis and Early Warning Systems*, Springer Theses,
DOI: 10.1007/978-3-642-27526-5, © Springer-Verlag Berlin Heidelberg 2012

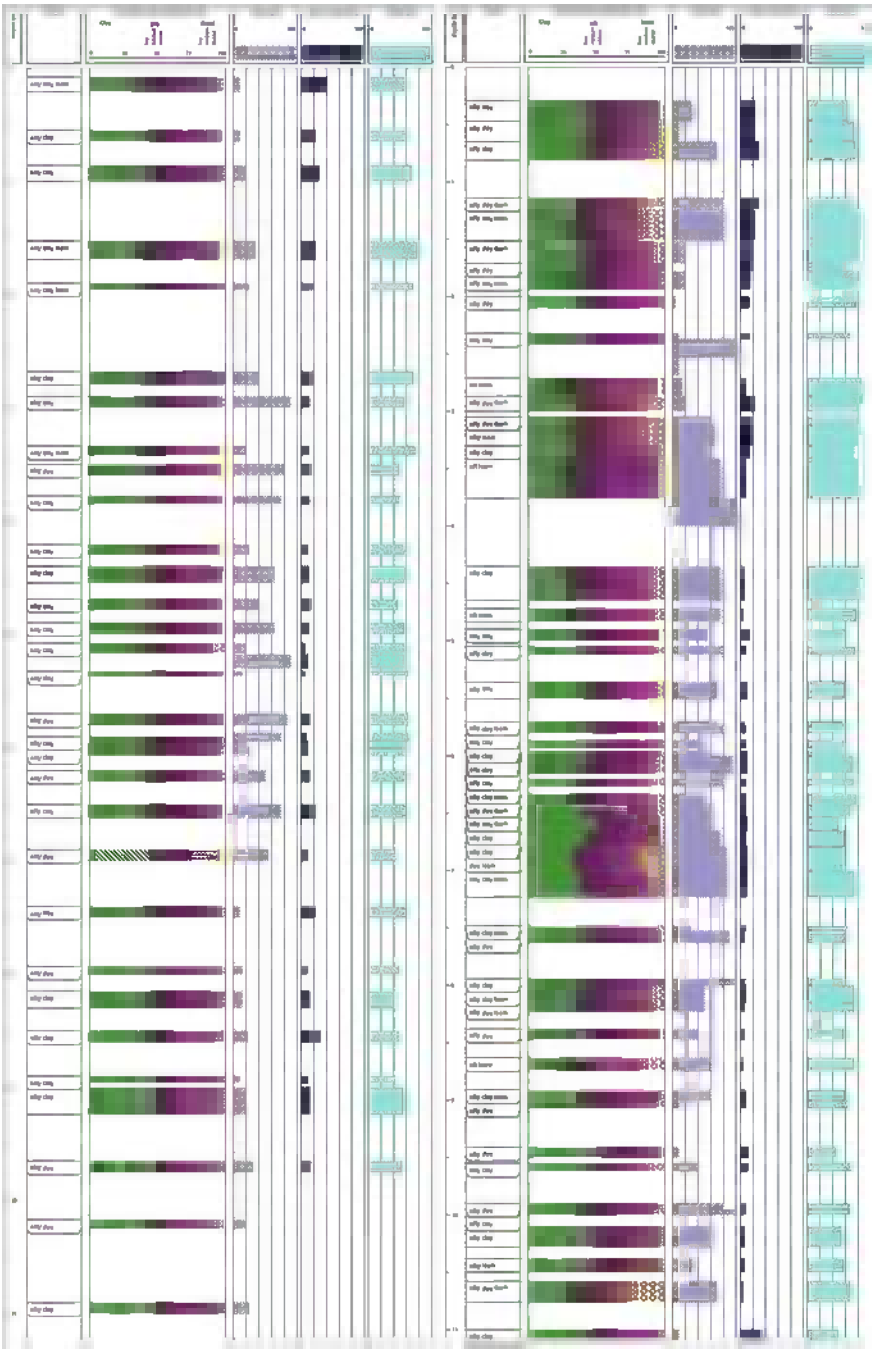

Appendix II
Inclinometer Measurements for Lic01

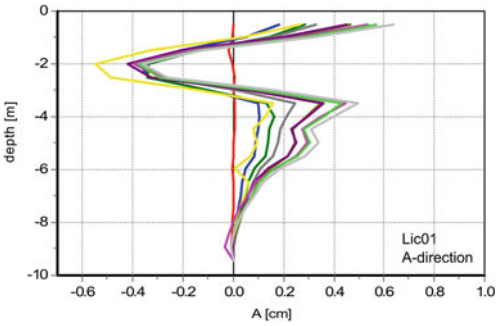

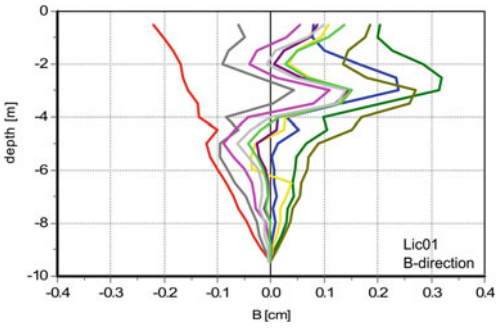

line	compared records	interval (days)
	05.08.2004 - 11.06.2004	56
	21.09.2005 - 11.06.2004	468
	30.03.2006 - 11.06.2004	658
	26.09.2006 - 11.06.2004	838
	19.12.2007 - 11.06.2004	1287
	06.05.2008 - 11.06.2004	1426
	09.11.2008 - 11.06.2004	1613
	18.11.2009 - 11.06.2004	1987
	02.03.2010 - 11.06.2004	2091
	07.01.2011 - 11.06.2004	2401

B. Thiebes, *Landslide Analysis and Early Warning Systems*, Springer Theses,
DOI: 10.1007/978-3-642-27526-5, © Springer-Verlag Berlin Heidelberg 2012

Appendix III
Inclinometer Measurements for Lic04

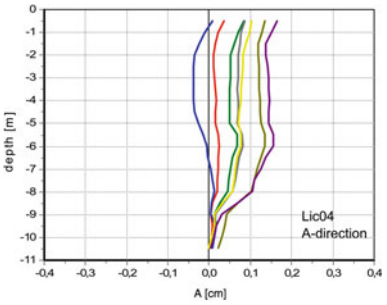

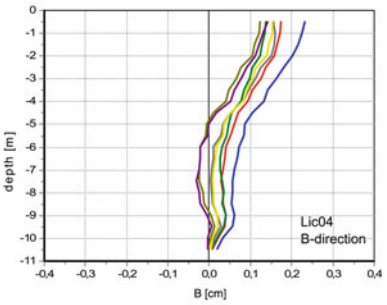

line	compared records	interval (days)
	09.11.2008 - 06.05.2008	187
	12.02.2009 - 06.05.2008	282
	01.06.2009 - 06.05.2008	391
	03.08.2009 - 06.05.2008	454
	18.11.2009 - 06.05.2008	561
	02.03.2010 - 06.05.2008	665
	07.01.2011 - 06.05.2008	976

B. Thiebes, *Landslide Analysis and Early Warning Systems*, Springer Theses,
DOI: 10.1007/978-3-642-27526-5, © Springer-Verlag Berlin Heidelberg 2012

Appendix IV
Inclinometer Measurements for Lic03

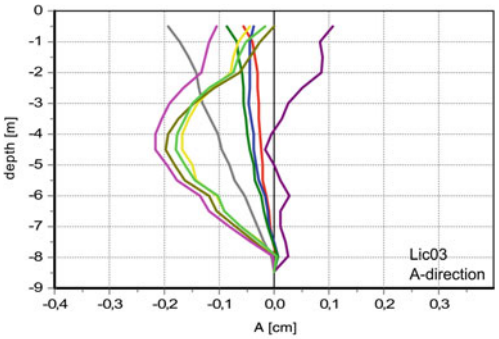

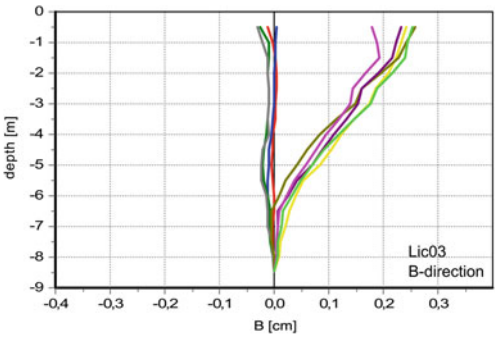

line	compared records	interval (days)
	21.06.2005 - 15.04.2005	67
	09.03.2006 - 15.04.2005	328
	11.07.2006 - 15.04.2005	452
	07.05.2007 - 15.04.2005	752
	19.12.2007 - 15.04.2005	978
	06.05.2008 - 15.04.2005	1117
	12.02.2009 - 15.04.2005	1399
	03.08.2009 - 15.04.2005	1571
	02.03.2010 - 15.04.2005	1782

B. Thiebes, *Landslide Analysis and Early Warning Systems*, Springer Theses,
DOI: 10.1007/978-3-642-27526-5, © Springer-Verlag Berlin Heidelberg 2012

Appendix V
Slip Search Grid Location Definition

Slip Search Grid Location

1.1. Define coordinates of the lower left hand corner of the grid: at one-third of the profile length and at two-thirds height for profiles longer than 450 m; half the height and two-thirds of length
1.2. If grid overlaps with slope surface, move right 1 mesh coordinate
1.3. Define grid spacing as the same as mesh size, and grid dimensions as 10 by 10
1.4. Set minimum radius as 10 m and radius increment as the same as mesh size

B. Thiebes, *Landslide Analysis and Early Warning Systems*, Springer Theses,
DOI: 10.1007/978-3-642-27526-5,

Appendix VI
ArcGIS RASTERCALCULATOR Commands for Computation of the Subsurface Model

Command to create DTM segments for geological strata in ESRI ArcGIS RASTERCALCULATOR based on maximum elevation. The procedure involves two commands to be executed in RASTERCALCULATOR. In this example nine segments are created, of which the lowest is below the level of the DTM

Step 1:

```
step1_elevation2 = con([DTM] > elevation3, [DTM])
step1_elevation3 = con([DTM] > elevation4, [DTM])
step1_elevation4 = con([DTM] > elevation5, [DTM])
step1_elevation5 = con([DTM] > elevation6, [DTM])
step1_elevation6 = con([DTM] > elevation7, [DTM])
step1_elevation7 = con([DTM] > elevation8, [DTM])
```

Step 2:

```
step2_elevation1 = con([DTM] > elevation2, [DTM])
step2_elevation2 = con([elevation2_1] >= elevation2, elevation2, [elevation2_1])
step2_elevation3 = con([elevation3_1] >= elevation3, elevation3, [elevation3_1])
step2_elevation4 = con([elevation4_1] >= elevation4, elevation4, [elevation4_1])
step2_elevation5 = con([elevation5_1] >= elevation5, elevation5, [elevation5_1])
step2_elevation6 = con([elevation6_1] >= elevation6, elevation6, [elevation6_1])
step2_elevation7 = con([elevation7_1] >= elevation7, elevation7, [elevation7_1])
step2_elevation8 = con([DTM] < elevation8, [DTM])
step2_elevation9 = con([DTM] > elevation9, elevation9)
```

B. Thiebes, *Landslide Analysis and Early Warning Systems*, Springer Theses,
DOI: 10.1007/978-3-642-27526-5, © Springer-Verlag Berlin Heidelberg 2012

Appendix VII
Soil Suction Curves Defined by Spaw Model in Comparison to Laboratory Measurements with Interpolated Values

Pf	Laboratory values	SPAW values	Interpolated values
15	0.13486667	0.245	0.13486667
10		0.259	0.14915
8	0.15643333	0.266	0.15643333
6		0.276	0.16625416
4		0.291	0.176075
3		0.302	0.18589583
2		0.318	0.19571667
1.6		0.327	0.2055375
1.2		0.34	0.21535833
0.8		0.358	0.22517917
0.4		0.392	0.235
0.3	0.235		0.235
0.2		0.457	0.24
0.1	0.2587	0.5	0.2587
0.06	0.26413333		0.26413333
0.03	0.27656667		0.27656667

B. Thiebes, *Landslide Analysis and Early Warning Systems*, Springer Theses,
DOI: 10.1007/978-3-642-27526-5, © Springer-Verlag Berlin Heidelberg 2012

Appendix VIII
English Tutorial for Web-Based Chasm Decision-Support System

1. Welcome to the web-processing service by the ILEWS project! On this website you can calculate slope stabiltiy for our test slope in Lichtenstein-Unterhausen at the Swabian Alb, Germany. To start please activate the pencil symbol in the upper left corner and create a slope profile for the calculation by clicking on the map.
2. Please select a name for your chosen profile. You can change some model parameters like the length of the simulation and the timesteps. Please select the output information that you would like to receive. Please select the rainfall scenarios by clicking on RS.
3. Please select a rainfall scenario for you simulation.

   - Scenario type: normal, worst case and maximal worst case
   - Rainfall distribution pattern: equally distributed rainfall distribution, Euler 1 and Euler
   - Rainfall duration: 6, 12, 24, 48 and 72h.
   - Likelihood of occurence: 1 in 1, 1 in 10, 1 in 50, 1 in 100 and click OK.

4. Click on "Create model" to save the your simulation settings to the database, or click "create model and calculate" to also start the simulation.
5. Your simulation is beeing processed on the server. Please wait until calculation is finished.
6. The slope profile is calculated with respect to your settings and the profile is coloured regarding the calculated stability. The FoS of the last simulation step is shown next to the profile. Please select Simulation>model resuls>show results for further information for your simulation.
7. Please select your simulation or any other simulation created before.
8. Clicking on the curve symbol behind your simulation opens a graphical presention of the FoS in the course of the simulation.
9. Congratulation! You have completed a CHASM WPS simulation!

B. Thiebes, *Landslide Analysis and Early Warning Systems*, Springer Theses,
DOI: 10.1007/978-3-642-27526-5, © Springer-Verlag Berlin Heidelberg 2012

Appendix IX
English Frequently Asked Questions (FAQ)

General information

The web-processing service of CHASM enables the user to calculate slope stability for the study area of the project ILEWS. For further information please read the FAQ and visit the websites.

CHASM

CHASM is an integrated slope hydrology/slope stability software package. The software has been written to assist in the estimation of controls on slope stability and to be of value to a wide range of potential users ranging from pre-site investigation engineering applications to evaluations concerned with the impact of bioengineering on slope stability. Source and additional information:
http://chasm.info/

WPS

A Web Processing Service (WPS) is designed to standardize the way that GIS calculations are made available to the Internet. WPS can describe any calculation (i.e. process) including all of its inputs and outputs, and trigger its execution as a Web Service. Source and additional information:
http://en.wikipedia.org/wiki/Web_Processing_Service

CHASM-WPS

The CHASM WPS is a pivotal development in the ILEWS project as has been jointly designed by the company Geomer (Germany) and the Workgroup on Geomorphological Systems and Risk Research (ENGAGE), Institute of Geography and Regional Research, University of Vienna (Austria). For further information:
http://www.geomer.de/ and http:// geomorph.univie.ac.at/?L=2

B. Thiebes, *Landslide Analysis and Early Warning Systems*, Springer Theses,
DOI: 10.1007/978-3-642-27526-5, © Springer-Verlag Berlin Heidelberg 2012

KOSTRA

Kostra (also KOSTRA-2000-DWD) is a storm rainfall event catalogue published by the Deutscher Wetter Dienst (DWD) (German Weather Service). Source and additional information:
http://de.wikipedia.org/wiki/Kostra and http://www.itwh.de/S_kostra.htm

Factor of Safety (FoS)

A measure of slope stability. With FoS > 1 a slope is defined stable and FoS < 1 as unstable. For more information:
http://en.wikipedia.org/wiki/Factor_of_safety

ILEWS

The ILEWS project is is concerned with the development and implementation of modular and transferable landslide early warning systems for local and regional scales which can also be adapted to other localities and processes. Within ILEWS early warning systems are regarded as a chain starting from the sensor in field as the pivotal part of a robust monitoring system, reliable data transmission, innovative modelling and communication of possible actions with stakeholders. For more information:
http://www.ilews.eu

Rainfall scenarios

Rainfall scenarios are based on the KOSTRA atlas. From the statistical modelling of the rainfall intensities performed within KOSTRA three types of scenarios were created for.

Normal: These scenario are based on the standard intensities given by KOSTRA
Maximum: As KOSTRA rainfall events are based on probability calculation upper and lower limits are given. Max scenarios are bases on the upper limit given in KOSTRA.
Max-worst: Rainfall intensities given in KOSTRA are subject to uncertainties and these are also quantified (up to 20%). In max-worst scenarios the uncertainties are added to the maximum rainfall intensities.

Rainfall distributions

Three kinds of rainfall distributions are available:

Equally distributed: same intensities for the entire course of the rainfall event

Euler 1: a statistically derived rainfall distribution used within drainage planning. Euler 1 events have the highest rainfall intensities in the beginning of the rainfall event and decreasing intensities afterwards
Euler 2: similar to Euler 1 scenarios but the highest intensities occur after one third of the duration of the rainfall.

Disclaimer

Slope stability calculation presented here is for informational use only. Calculations are based on simplified models and no recommendations for possible actions should be deduced of the CHASM WPS without the consultancy of experts. Neither the project ILEWS nor the owner of the website are responsible for inappropriate use of the CHASM WPS.

Contact

For questions regarding the implementation of CHASM as WPS please contact info@geomer.de For questions concerning the calculation of slope stability, data used and other model parameters please contact benni.thiebes@univie.ac.at For questions on CHASM please contact chasmenv@bristol.ac.uk

Index

B. Thiebes, *Landslide Analysis and Early Warning Systems*, Springer Theses,
DOI: 10.1007/978-3-642-27526-5,